Performance of a Transcritical Carbon Dioxide Heat Pump for Simultaneous Refrigeration and Water Heating

A thesis presented in partial fulfilment of the requirements for the degree of Master of Technology at Massey University.

Michael George Yarrall
B.Tech. (Hon)

1998

ABSTRACT

Many industrial processes require both refrigeration to less than 0°C and water heating to greater than 60°C. Traditional independent refrigeration and boiler systems have relatively poor energy efficiency, whilst conventional heat pumps can provide both cooling and heating but are limited in terms of the temperature lift that can be achieved. A novel heat pump using CO_2 as the refrigerant in a transcritical cycle has been proposed as a new technology that can overcome these disadvantages. The use of CO_2 as a refrigerant has many advantages. It is environmentally benign, safe, and has good thermodynamic properties, especially compared with fluorocarbons. The transcritical cycle involves evaporation of CO_2 at constant temperature and pressure below the critical point to provide refrigeration, while cooling of the CO_2 occurs at temperatures and pressures above the critical point to provide heating of water. The objective of this project was to design and construct a prototype transcritical CO_2 heat pump to simultaneously provide refrigeration and water heating, and to test its performance over a wide range of operating conditions.

The prototype CO_2 heat pump had a nominal cooling capacity of 90 kW at –6°C and nominal water heating capacity of 127 kW from 10°C to 90°C. The prototype was designed to operate with a suction pressure of 30 bar and discharge pressure of 130 bar. The major components were a gas cooler, recuperator, flooded evaporator, low pressure separator/receiver, compressor, expansion valve, connecting piping and a control system. All components were standard high pressure equipment used by the natural gas processing industry. The gas cooler had a reasonably unique design to ensure close to pure counter-current heat exchange between the cooling CO_2 gas and the water being heated, both of which had relatively low flowrates. The compressor used was an open crankcase, reciprocating type with special gas seals on the piston rod to prevent CO_2 leakage. Refrigeration capacity (suction pressure) was controlled by varying the compressor speed. Water heating capacity was controlled by both using the expansion valve to control the CO_2 discharge pressure and varying the water flowrate through the gas cooler.

The main problem encountered during commissioning of the prototype was CO_2 leakage through the compressor piston rod seals. Alternative sealing systems were tried, but the leakage remained an on-going problem that prevented prolonged operation of the prototype, such as would be necessary in industrial applications.

Performance of the prototype was determined by energy balances based on measurements of CO_2 and water flowrate and temperature when it operated at steady-state. The energy balances generally agreed to within 6%. Trials were performed with suction pressures from 29.6 to 35.5 bar, discharge pressures from 80 to 130 bar, with hot water outlet temperatures from 65°C to 90°C, and evaporator water inlet temperatures from 11°C to 21°C.

When heating water to 90°C and providing refrigeration at 1°C (35.5 bar suction pressure), the maximum overall Coefficient of Performance (COP) achieved was 5.4 at a discharge pressure of 114 bar. Below this optimum discharge pressure, the COP

declined due to gas cooler heat transfer limitations (lower compressor discharge temperature led to lower temperature difference in the gas cooler and high CO_2 outlet temperature). Above the optimum, the decline in thermodynamic and compressor efficiency as pressure ratio increased caused the COP to decrease. The maximum heating and cooling capacities were about 13% less than the design values. This was attributed to the lower than expected volumetric efficiency of the compressor. The performance of the heat exchangers were generally close to the design values when allowances for lower than design water flowrates were taken into account.

As expected, when suction pressure was reduced to 29.6 bar (-6°C), there was up to a 10% decrease in optimum COP as well as reduced heating and cooling capacity. When heating water to 65°C rather than 90°C, the optimum COP was about 20% higher. When suction pressure or hot water outlet temperature was decreased, the optimum discharge pressure became slightly lower due to the gas cooler heat transfer being less of a limitation on overall system performance.

Addition of oil to the CO_2 did not reduce the CO_2 leakage sufficiently to allow long-term operation without recharging, and had minimum impact on the performance of the gas cooler, recuperator and compressor. However, oil fouling caused a significant drop in heat transfer performance of the evaporator.

The measured prototype performance agreed well with process simulations of the equipment and with results for similar laboratory scale equipment reported in the literature. Therefore, simulations could be used to optimise component and system design with a reasonable level of confidence. It was shown that the biggest increase in COP could be achieved by improving compressor isentropic efficiency rather than increased heat exchanger size.

Overall, the concept of the transcritical CO_2 heat pump for simultaneous refrigeration and water heating was proven and the required energy efficiency was sufficiently high that the heat pump is likely to be economically competitive with traditional heating and cooling systems. Further work should concentrate on improving compressor design to eliminate CO_2 leakage and to improve both isentropic and volumetric efficiency.

ACKNOWLEDGEMENTS

Thanks to all those who have helped me during the course of my degree, especially:

My supervisors, Don Cleland and Stephen White for all their help and for guiding me through the tough times.

Thanks to everyone at Flotech, including Chris Beh, Richard Hedley, Brett Rumble, Stephen Broadbent, Rodney Stephenson who helped me with my project.

Rodger Kallu for his help and advice.

My parents for their encouragement and support.

Finally, thank you to all those whom I may have inconvenienced by my misjudgement of when I was going to finish.

I also wish to acknowledge the help I received from the following foundations and scholarships:

Graduate Research in Industry Fellowship (Foundation for Research, Science and Technology)
IPENZ Craven Scholarship
Massey Masterate Scholarship

TABLE OF CONTENTS

List of Figures

List of Tables

1 INTRODUCTION

The provision of heating and cooling is a very important function in many industrial processes. In New Zealand an estimated 4700 TJ of energy is used for heating to less than 100°C, and 4500 TJ of energy is used for refrigeration by the food processing industry each year (Kallu and Cleland, 1996). A large proportion of the heating is used to generate hot water for cleaning, sterilisation and other general process heating duties. Often the water needs to be at greater than 80°C due to food safety regulations and other process constraints. Most of the refrigeration is required at temperatures less than 10°C for preservation of food and other perishable products.

Traditionally, heating and refrigeration have been provided separately. This has several advantages. In particular, the amount of heating or refrigeration is easily controlled, and neither is dependent on the other. If only heating or cooling is required at any one time, separate systems are generally more cost efficient.

Cooling is usually provided by vapour compression refrigeration cycles, in which heat is usefully extracted at low temperatures and is rejected to the environment at higher temperatures. Refrigeration cycles at about 0°C typically provide about four times as much cooling as the energy required to drive the compressor.

Heating has been traditionally supplied by boilers. This can be quite cost effective when the price of the fuel for the boiler is low and temperatures greater than 80°C are required. The energy efficiency of boiler systems is typically between 50 and 80%.

An alternative to the use of boilers is passive heat recovery. This is only feasible when an existing process stream is available at sufficiently high temperature. For example, desuperheating of refrigerants after compression in refrigeration systems can provide high temperature heat, but the total heat available at high temperature is usually less than 15% of the total heat rejected from the refrigeration system (White *et al*, 1997). At most sites, there is a large number of options for heat recovery to achieve low temperatures (eg. less than 60°C), but relatively few for higher temperatures.

Another alternative are heat pumps which use the same cycle as refrigeration systems except that waste heat is extracted from the environment and it is the heat of rejection at higher temperatures that is useful. Traditional heat pumps can be energy efficient, typically giving two to six times as much heat as energy consumed (Hewitt *et al*, 1997). However they generally have a high capital cost, and are restricted in the temperatures they can deliver due to loss of efficiency at large temperature lifts and the pressure limitations of commonly available equipment. Conventional heat pumps often use fluorocarbons as the refrigerant, which are currently being phased out due to their ozone depleting and global warming effects.

The use of heat pumps enables the possibility of providing simultaneous heating and cooling. If the heat extracted by the heat pump system is also utilised for refrigeration, much greater overall energy efficiency is obtained. In addition, a single, integrated system requires less space and maintenance than the two separate systems.

Unfortunately, with most conventional heat pump and refrigeration systems, the large temperature split required to provide simultaneous heating and cooling at useful temperatures cannot be achieved without a large loss in efficiency.

Lorentzen (1994) proposed the transcritical carbon dioxide heat pump as a system which is able to efficiently provide high temperature process heat as well as simultaneous cooling. This technology has the potential to be more efficient and cost effective than present systems and also has the advantage of using CO_2 which is naturally occurring and environmentally friendly compared with fluorocarbon refrigerants.

The general objective for this project is to investigate the feasibility of utilising the transcritical CO_2 heat pump cycle for industrial heating and cooling. The project has been organised as part a joint venture between Flotech Ltd, Electricity Corporation of New Zealand Ltd (ECNZ), and Massey University.

2 LITERATURE REVIEW

2.1 Heat Pumps

Industrial heating is usually provided by either boilers, or heat recovery from a heat source.

Heat recovery is more energy efficient than boilers as it utilises an existing low grade heat source, and does not rely completely on a high grade heat source. There are two main methods of heat recovery available: passive heat recovery and heat pumping. Passive heat recovery essentially consists of a heat exchanger to transfer heat from a hot stream to a colder one. For example waste heat from desuperheaters, condensers and oil coolers in traditional refrigeration systems can be used to preheat other streams (Kallu and Cleland, 1996). Passive heat recovery is restricted by the temperature of the hot stream. So to achieve higher temperatures with a low temperature heat source, a heat pump must be used.

Currently, there are several important barriers to the implementation of heat pumps into heating markets. These include low fossil fuel cost, high first cost of equipment, unfamiliarity, and the overall effect of new working fluids (Bouma, 1995). As heat pumps are typically more efficient than conventional forms of heating, the application of heat pump technology would greatly reduce energy usage and therefore operating costs. Rush and Carrington (1984) calculated that there was a potential to save 21% of the energy used in non-transport applications in New Zealand through the use of heat pumps.

2.1.1 Conventional cycle

The heat pump cycle and refrigeration cycle are essentially the same, but usually the heat pump cycle operates with higher temperatures at the condenser and evaporator than refrigeration systems because the desired outcome is heating rather than cooling. In the conventional cycle (Figure 2.1), working fluid as a vapour is compressed (1), increasing

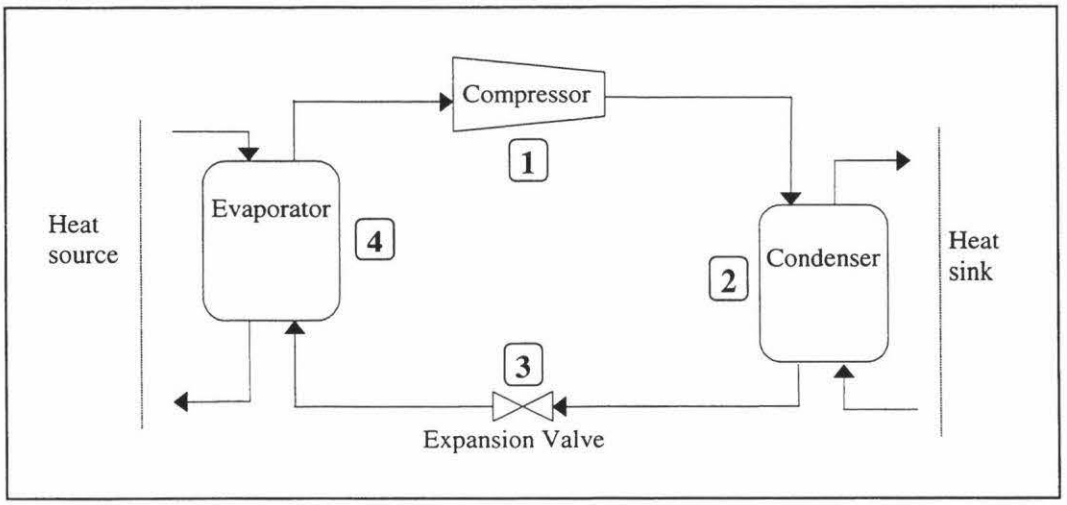

Figure 2.1: Conventional Refrigeration / Heat Pump Cycle

its pressure and hence boiling point. The hot, high pressure vapour is condensed (2) in a heat exchanger (the condenser), transferring heat to the heat sink. The pressure is then reduced as the liquid passes through an expansion valve (3), resulting in a much colder liquid-vapour mixture. The liquid is evaporated (4) in a heat exchanger (evaporator) with heat being transferred to the working fluid, resulting in the cooling of the heat source. The vapour then passes back to the compressor. In the overall process, heat enters the system from the compressor and evaporator, and is rejected via the condenser. The expansion valve is effectively adiabatic.

Conventional heat pump and refrigeration systems operate with relatively low pressures. For example, for an evaporation temperature of -6°C, an R22 system operates with a 4 bar low side pressure, while a R134a system has a pressure of 2.3 bar. As the aim of conventional refrigeration cycles is refrigeration, they usually operate with relatively low condensing temperatures. At a typical condensing temperature of 40°C the pressure is 15.3 bar for R22 and 10.2 bar for R134a (ASHRAE, 1993).

In refrigeration, only the heat source (cold side) is utilised, with the heat sink (hot side) being wasted. With a heat pump, the opposite usually occurs. However, if a large enough temperature split could be obtained, both the heat sink and source could be used to simultaneously provide heating and refrigeration. This would lead to a greatly increased overall efficiency. Unfortunately, with traditional heat pumps, high temperature splits usually lead to poor system efficiency due to the very large pressure ratios. For example, if R134a is used with an evaporation temperature of 0°C and a condensing temperature of 90°C (32 bar pressure - ASHRAE, 1993) the pressure ratio is 11. Conventional heat pump systems are also constrained to temperatures below about 70°C (21 bar for R134a) because of equipment pressure limitations. Because of these reasons, fossil fuel fired boilers are generally used to supply heat above about 40°C unless other significant heat recovery options are available.

High pressure ammonia heat pumps are one option to obtain water at higher temperatures. Kristensen (1993) tested a Sabroe high pressure ammonia heat pump at various industrial installations. This used a conventional cycle with condensing temperatures up to 63°C (with a corresponding pressure of 28 bar). Desuperheaters in high temperature heat pumps may also be used to provide a small amount of heating at even higher temperatures (Edwards and Kallu, 1997).

The coefficient of performance (COP) is a measure of the energy efficiency of a heat pump. It is the ratio of the energy output (in terms of usable heating and/or refrigeration) to the energy input from the compressor. Conventional heat pumps typically have COPs between two and six times (Hewitt *et al*, 1997). The COP is a function of several factors, including evaporation temperature, condensation temperature, refrigerant type and compressor efficiency.

2.2 Environmental Aspects

Recently, there has been much concern about the use of chlorofluorocarbon (CFC) refrigerants, as they both destroy ozone and contribute to the greenhouse effect. Because of this, alternatives to CFCs have to be found. Hydrochlorofluorocarbons

(HCFCs) can be used but, although better than CFCs, these are also quite harmful to the environment.

Carbon Dioxide (CO_2) is a sensible alternative as it is already found in high quantities in the atmosphere. Therefore using it as a refrigerant will not have any unexpected detrimental effects on the environment.

2.2.1 Fluorocarbons

The first fluorocarbon refrigerant, R12 (a CFC), was introduced in the 1930's. Important factors influencing market penetration were the heavy advertising, an effective system of technical information and a well organised effort by the manufacturers to solve the various operating problems as they occurred. Other motives for change included the possibility of using simple and cheap construction methods, copper tubing, light screw or solder fittings, cheap automatic control equipment, hermetic motors, etc. (Lorentzen, 1995).

The traditional refrigerants used were R12 and R22 in cooling applications, while R502 and R22 were used in low temperature applications. R114 was used for heat pump applications (Eggen and Røsvik, 1995).

2.2.1.1 Ozone Layer

CFCs are extremely stable chemicals. If emitted to the atmosphere, they will have a high atmospheric lifetime, and therefore are able to reach the stratosphere.

In 1974, Molina and Rowland proposed a theory that UV radiation breaks down the CFCs in the stratosphere forming chlorine radicals. Later, a hole (area of low concentration) in the ozone "layer" over Antarctica was observed. Ozone (O_3) is produced by the photodissociation of oxygen (O_2) by short wavelength (200 nm) UV radiation. Chlorine radicals are the main destroyers of ozone. Chlorine radicals occur naturally (eg. from sea water), but significant amounts are produced in the photodecomposition of CFCs. These radicals act as catalysts in the destruction of ozone (Lucas, 1993). The ozone depletion potential (ODP) relative to CFC11 or CFC12 is used to quantify this destructive effect. HCFCs also photodecompose to form chlorine radicals but, because they have shorter atmospheric lifetimes, their ODP is lower.

Ozone is the main filter for UV radiation from 290 to 325 nm. As radiation of this wavelength is harmful to living things, a reduced ozone layer will have serious consequences for the Earth's ecosystem.

Because of the concern about the destruction of the Ozone layer by CFCs and HCFCs, the "Montreal Protocol on Substances that Deplete the Ozone Layer" was signed by twenty four nations in September 1987. Amendments to the Montreal Protocol were made in London (1990) and Copenhagen (1992). The result of this is that all CFC production should have ceased by the end of 1995, and HCFC production will end by 2030 (Riffat *et al*, 1997). Currently most nations world-wide have ratified the Montreal protocol.

2.2.1.2 Greenhouse Effect

Another issue with CFC and HCFC refrigerants is the contribution they make to the Greenhouse effect. The Greenhouse Effect is due to the heat trapping effect of CO_2, water vapour, methane, NO_x and other substances (including fluorocarbons in the atmosphere). This leads to a significantly raised temperature on Earth. Since the industrial revolution, there has been a sudden rise in temperature. There is an obvious link with human activity, especially with the consumption of fossil fuels (Lucas, 1993).

Two factors used to measure the impact of a greenhouse gas are (Lucas, 1993):

- GWP (Global Warming Potential) - Usually given with CO_2 as a reference. Calculation must allow for the lifespan of the molecule in the atmosphere. CFCs have a very high global warming impact. One molecule of R11 has a heat absorption capacity about 10,000 times greater than CO_2.
- TEWI (Total Equivalent Warming Impact) - This takes into account the direct global warming effect (GWP) as well as the indirect global warming effect which depends on the energy used in the process, and therefore how much CO_2 is produced by the production of electricity to run the equipment over its life. This obviously depends on how the electricity is generated, so it will vary from region to region.

If current trends continue, the consequences of the Greenhouse effect could include a 3 to 5 °C rise in temperature by the year 2050, a rise in ocean level, and changes in climate (Lucas, 1993).

2.2.2 Fluorocarbon Alternatives

The main arguments put forward for CFCs was their safety, and their harmlessness to the environment. Both these claims have turned out to be wrong, as many people have suffocated from CFCs, and CFCs have had a huge effect on the ozone layer and greenhouse effect (Lorentzen, 1994b).

At present, much research is going into finding replacements for CFCs and also HCFCs. However, a single ideal refrigerant does not exist as all available compounds have their weak points (Lorentzen, 1994b). Many other halocarbon refrigerants have been researched and proposed as alternatives (mainly hydroflourocarbons - HFCs). There is a possibility that if a multitude of replacement products are found, refrigeration will be unnecessarily complicated (Lorentzen, 1994b). Also, the alternative refrigerants from the HFC group are often either flammable, have a significantly lower efficiency, or a very high global warming potential (Hesse and Kruse, 1993).

2.2.2.1 Natural Refrigerants

In the past, many synthetic chemicals, foreign to nature, have caused unexpected problems when released into the environment (eg. DDT, PCB, etc). It would be an obvious advantage to use suitable natural substances which are present in abundance in the environment and proven to be harmless (Lorentzen, 1994b).

The main refrigerants in use in the first 30-40 years of this century were natural refrigerants: ammonia, sulfur dioxide, and carbon dioxide. Since the introduction of fluorocarbons, only ammonia has remained in wide use. However, ammonia, propane

(and mixtures with other hydrocarbons), and carbon dioxide are suitable to cover all practical applications in the conventional refrigeration range (Lorentzen, 1994b).

As CFCs and HCFCs are phased out, ammonia could become more widely used. It was widely used in the past, and is still commonly used in large refrigeration systems at present. It has excellent thermodynamic and heat transfer properties. Ammonia is poisonous and flammable, although accidents are rare (Lorentzen, 1993). Its characteristic smell can act as a warning signal, although it may also cause panic. Ammonia is also cheap compared with the fluorocarbons (Halozan, 1996).

Hydrocarbons are another attractive alternative to CFCs and HCFCs. They have been used in large refrigeration plants in the chemical process industries for many years. Propane has excellent thermodynamic properties approaching those of ammonia (its efficiency is higher than R-22 systems), but the explosion and fire hazard is much greater. Because of this propane and other hydrocarbons are probably ruled out for many larger systems. Propane has a high potential for use in household refrigeration and freezing because the charge only has to be about 50g, which is less than the charge used as a propellant in aerosol cans (Lorentzen, 1993). Propane can be used as a drop in substitute for R-12 and R-22, although the expansion device and lubricant may need to be changed. Hydrocarbons are also favoured by Greenpeace as a substitute for halocarbons. Regulations (perhaps over restricting) governing propane may hinder its implementation in residential and commercial buildings, especially in the U.S. due to liability concerns (Halozan, 1996).

Water vapour (Mechanical Vapour Recompression systems) is extensively used as a refrigerant in industry when evaporating water. Air can also be used as a refrigerant for either heating or cooling, but suffers from relatively low energy efficiency (Stene, 1996).

As discussed in Section 2.3, carbon dioxide is another promising alternative. It has many properties that could make it an excellent refrigerant in the right application.

2.3 Carbon Dioxide as a Refrigerant

Carbon Dioxide (R-774) is a colourless, odourless gas that is plentiful in the atmosphere. Many authors have mentioned the benefits of using CO_2 as a working fluid in heat pumps, including Eggen and Røsvik (1995), Halozan (1996), Hesse and Krusse (1993), Pettersen (1995), Protsenko *et al* (1992), Riffat *et al* (1997), and especially Lorentzen (1993, 1994, 1995).

CO_2 has been widely used in maritime refrigeration in the past, and is still used in some low temperature applications (Halozan, 1996). CO_2 was overtaken by fluorocarbons due to the rapid loss of cooling capacity at high cooling water temperatures in the tropics and the failure of manufacturers to follow modern trends in compressor design towards more compact and high speed types (Lorentzen, 1993).

Table 2.1 compares the characteristics of CO2 with a few commonly used refrigerants.

Table 2.1: Characteristics and Properties of Some Refrigerants (Lorentzen, 1994a)

Refrigerant	CFC-12	HCFC-22	HFC-134a	NH_3 (R-717)	C_3H_8 (R-290)	CO_2
Natural substance	No	No	No	Yes	Yes	Yes
ODP	1.0	0.05(1)	0	0	0	0
GWP(2): 100 yrs	7100	1500	1200	0	0	1(0)(3)
20 yrs	7100	4100	3100			1(0)
$TLV_{(8hr)}$ (ppm)	1000	1000	1000(4)	25	1000	5000
IDLH(5) (ppm)	50,000	-	-	500	20,000	50,000
Amount per room volume(6) (vol. % / kg/m3)	4.0 / 0.2	4.2 / 0.15	-	-	0.44 / 0.008	5.5 / 0.1
Flammable or explosive	No	No(7)	No(7)	Yes	Yes	No
Flammability limits in air (vol. %)	-	-	-	15.5 - 27	2.2 - 9.5	-
Toxic/irritating decomposition products	Yes	Yes	Yes	No	No	No
Approx. relative price	1	1	3 – 5	0.2	0.1	0.1
Molar mass	120.92	86.48	102.03	17.03	44.1	44.01
Volumetric(8) refrigerating capacity at 0°C (kJ/m^3)	2740	4344	2860	4360	3870	22,600

(1) Somewhat higher values have been suggested by recent studies.
(2) Global warming potential in relation to CO_2, with 20 and 100 years integration time (IPCC 1990, 1992).
(3) Abundant amounts of CO_2 are recovered from waste gas. Thus the effective GWP of commercial carbon dioxide, for instance used as a refrigerant, is 0.
(4) Suggested by ICI etc.
(5) Maximum level from which one could escape within 30 minutes without any escape-impairing symptoms or any irreversible health effects.
(6) Maximum refrigerant charge in relation to refrigerated room volume, as suggested in ANSI/ASHRAE 15-1989: Safety Code for Mechanical Refrigeration.
(7) Although considered to be non-flammable, both R-22 and R-134a are combustible in certain mixtures with air at elevated pressures, but ignition may be difficult.
(8) Enthalpy of evaporation divided by saturated vapour volume.

2.3.1 Advantages

Using CO_2 as a refrigerant has many advantages.

(i) Safety:
In terms of safety, CO_2 is at least as good as the best of the fluorocarbons. It is non flammable or explosive, non toxic, and thermally stable (Hesse and Kruse, 1993). Further toxicity testing is not required (Pettersen, 1995). If released from the liquid form, about half will evaporate with the remainder becoming a solid which can be removed or left to sublimate (Lorentzen 1993). Flammable refrigerants like propane or butane may not be suitable for passenger car air-conditioning because of the safety risk for passengers and people outside the car. The use of CO_2 will obviously not have such risks (Gentner, 1998).

(ii) Environmental Aspects:
As can be seen in Table 2.1, the effect of CO_2 as a greenhouse gas is minute compared with the fluorocarbons. CO_2 has zero ozone depletion potential and essentially zero global warming potential (Hesse and Kruse, 1993). CO_2 used in heat pumps will probably come from the atmosphere originally, so there will be essentially no contribution to the greenhouse effect. The amount of CO_2 emitted from these heat pumps through leakage or accidental release of charge will be insignificant compared to major sources of CO_2. Ironically, even though a heat pump could use CO_2, it could reduce the amount of CO_2 emitted to the atmosphere as it can replace combustion technologies currently in use that create vast amounts of CO_2.

(iii) Cost:
CO_2 for industrial processes is readily available in all parts of the world so production capacity and distribution does not need to be developed (Lorentzen and Pettersen, 1993). This leads to low cost and good availability. The capital cost of equipment may also be less due to reduced tube dimensions because of the smaller volume required as a result of the high pressures used.

(iv) Thermodynamic Properties:
Figure 2.2 shows the pressure-enthalpy diagrams for CO_2 and R12. The most notable differences between CO_2 and other common refrigerants are the higher saturation pressures for a given temperature, the potential for rejecting heat at temperatures above the critical point, the influence of pressure on specific enthalpy in the supercritical region, and the higher evaporation enthalpy of CO_2 (shown by the greater distance between each side of the envelope).

The properties and characteristics of CO_2 are well known and documented. CO_2 has a relatively low critical temperature and pressure which is ideally suited for application in a transcritical cycle rejecting heat at temperatures above ambient temperature. CO_2 generally offers better refrigerant characteristics than the hydrocarbons (in terms of specific heat, evaporation enthalpy, thermal conductivity and viscosity), but is generally slightly inferior to ammonia, except for the very low viscosity of CO_2 (Lorentzen and Pettersen, 1993). These thermodynamic properties lead to CO_2 having advantages over R12 including improved heat transfer characteristics (Lorentzen and Pettersen, 1993).

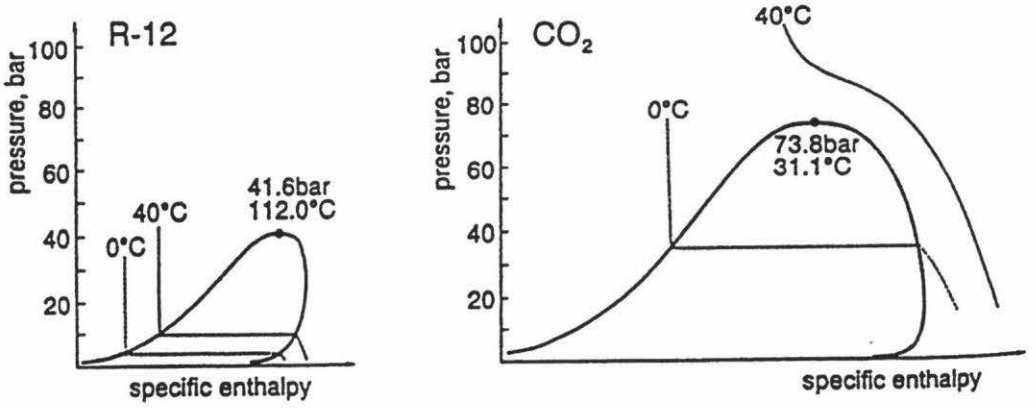

Figure 2.2: Pressure - Enthalpy diagrams for CO_2 and R12 (Pettersen, 1995)

(v) Operation:
CO_2 is completely compatible with normal lubricants and common machine construction materials. It only requires simple operation and servicing, and it is not necessary to recover CO_2 from the system for maintenance work (Lorentzen, 1995). No corrosion has been reported with the use of CO_2 in industrial processes, although there is the potential for corrosion to occur if high moisture levels are allowed (Stene, 1996). However, nickel-plated tubes should be avoided. Cavitation in pumps has not been reported when operated under normal conditions. There is no formation of acid compounds during welding.

CO_2 also has potential as a secondary refrigerant. The ideal secondary refrigerant would be a dense, non-toxic liquid having a high thermal conductivity, a high specific heat, and low viscosity. Liquid CO_2 fulfils most of these requirements, but its thermal conductivity is low and it has to be operated at high pressure (Pearson, 1993).

2.3.2 Disadvantages

As mentioned before, ammonia, as well as some other fluorocarbon refrigerants, offer better general refrigerant characteristics than CO_2. In a conventional (subcritical) cycle, the low critical temperature of CO_2 would lead to a poor energy efficiency (Protsenko *et al*, 1992). Some sealing materials may also be a problem since CO_2 is non-polar (Stene, 1996).

While many of the advantages associated with CO_2 are due to its safety, there are also some hazards to overcome. The main hazards related to the accidental release of CO_2 are (Berghmans 1996):

- Freezing due to bodily contact;
- Asphyxiation due to lack of oxygen;
- Wounding, death or material damage due to blast waves following pressure vessel rupture.

Suffocation from CO_2 probably presents the greatest risk. Even though CO_2 is not actually toxic, it still can be potentially lethal as it displaces oxygen and thus can suffocate people. CO_2 has no colour or odour and is heavier than air so it could accumulate without a person knowing it. The safety aspects of CO_2 are very similar to the fluorocarbons. In Norway, as many deaths from refrigerants have been caused by fluorocarbons as by ammonia, which is toxic (Lunde and Lorentzen, 1994). The densities of the fluorocarbon refrigerants are approximately twice the density of CO_2 (Eggen and Røsvik, 1995), so fluorocarbons are potentially even more dangerous as they displace air more readily. Also, many fluorocarbons can decompose to harmful products when in contact with an open flame (Lorentzen, 1994a).

A good ventilation system would be required to eliminate any risk of suffocation. Some kind of CO_2 sensor could also be provided to further reduce risk. In general, such sensors are relatively cheap compared with sensors to detect fluorocarbons.

In the case of a pressure vessel rupturing, the energy release is proportional to the charge. Due the high volumetric refrigeration effect, the charge in a CO_2 system will be

small so the amount of damage would be small (Lorentzen, 1993). Equipment based on CO_2 should be designed and operated with the same safety requirements as current systems (eg. with high-pressure cut out switch, high and low side pressure relief devices, and minimum burst pressure 2.5 to 3 times higher than the pressure relief settings (Pettersen, 1995).

Loss of refrigerant to the atmosphere is a common occurrence, and normally quite undramatic (Lunde and Lorentzen, 1994). This is probably due to the slightly careless attitude taken with CFCs as they were assumed to be perfectly safe. The hazards of CO_2 could be amplified if it is treated as a completely harmless substance. The dangers of CO_2 need to be made clear, especially with respect to asphyxiation.

2.4 Transcritical CO_2 Process

The efficiency of any reversible process is independent of the working medium used. This follows the second law of thermodynamics. There has been much comparison between refrigerants when they are used in the traditional reference process, the Evans-Perkins (E-P) process. However, a compound that does not show up well on the basis of an E-P process may actually give superior performance in a suitably designed plant (Lorentzen, 1994b).

In an Evans-Perkins cycle, without superheating or subcooling, at an evaporation temperature of 5°C, the theoretical COP of CO_2 is generally less than half that for R12. Internal heat exchange improves this to between 55% and 75% of R12 values (Lorentzen and Pettersen, 1993). The differences in performance are only partially compensated by factors such as compressor efficiency, heat transfer efficiency, and the effects of pressure losses on system performance (Pettersen, 1995).

Rather than trying to develop a chemical compound to satisfy the requirements of a particular cycle, Pettersen (1995) suggested that the cycle should be adapted to the properties of the substance.

Angelino and Invernizzi (1994) found that the transcritical heat pump cycle gives improved efficiency when the critical temperature of the working fluid is close to ambient. Hence, the transcritical cycle appears to be well suited for use with carbon dioxide as the refrigerant.

2.4.1 Transcritical Heat Pump Cycle Description

In conventional cycles, compression, condensation, expansion and evaporation of the fluid take place below the critical point in the sub-critical region. In transcritical cycles, evaporation is subcritical, but compression and expansion are transcritical, and refrigerant cooling is in the supercritical region. Above the critical pressure, a fluid no longer exists as either a liquid or gas but as a supercritical fluid. As long as this fluid is kept above the critical pressure, it will not condense or evaporate.

Ordinary CFC refrigerants are unsuited for use in transcritical cycles because their critical temperature is too high (above 100°C), and because, owing to their chlorine

atoms, thermal stability is far below the temperature range where transcritical cycles are attractive (Angelino and Invernizzi, 1994). The low critical temperature and good thermal stability of CO_2 mean it is well suited to this process.

Figure 2.3 shows the transcritical cycle to be investigated in this project. CO_2 vapour is compressed to a pressure higher than the critical pressure of CO_2. This supercritical CO_2 fluid is cooled by water in a counter-current heat exchanger. This results in hot water at a useful temperature. As the pressure is above the critical pressure, the CO_2 can not condense, so sensible heat is removed rather than latent heat. The CO_2 is further cooled in the recuperator. It is then expanded to a pressure below the critical pressure where the CO_2 becomes a saturated vapour - liquid mixture. This cold CO_2 enters the separator/surge drum. The liquid at the bottom circulates through the evaporator and back to the separator/surge drum. A fraction of the CO_2 liquid boils as it absorbs heat from the water side and the water passing through the evaporator is thus cooled. The low pressure CO_2 vapour exiting the separator/surge drum is superheated by the recuperator. The vapour then returns to the compressor.

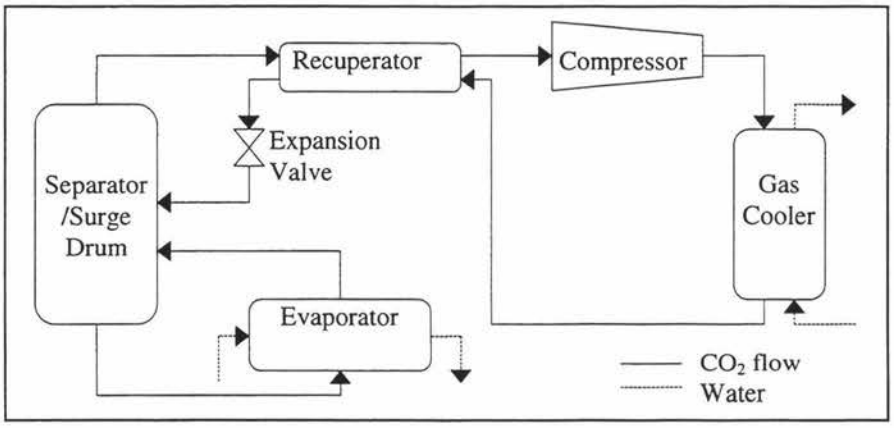

Figure 2.3: Transcritical CO_2 Heat Pump General Set-up for Project

The differences between the conventional and transcritical cycles are illustrated by the following pressure-enthalpy (P-h) diagrams (Figure 2.4 and Figure 2.5). The cycles are described in Table 2.2.

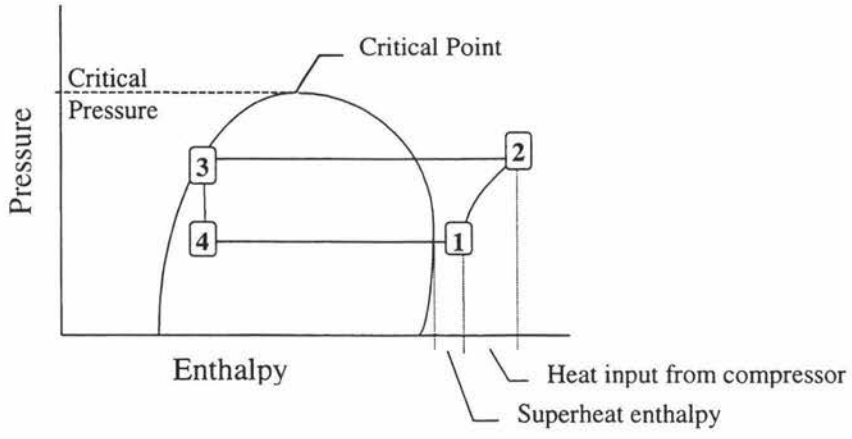

Figure 2.4: Pressure - Enthalpy Diagram for a Conventional Cycle

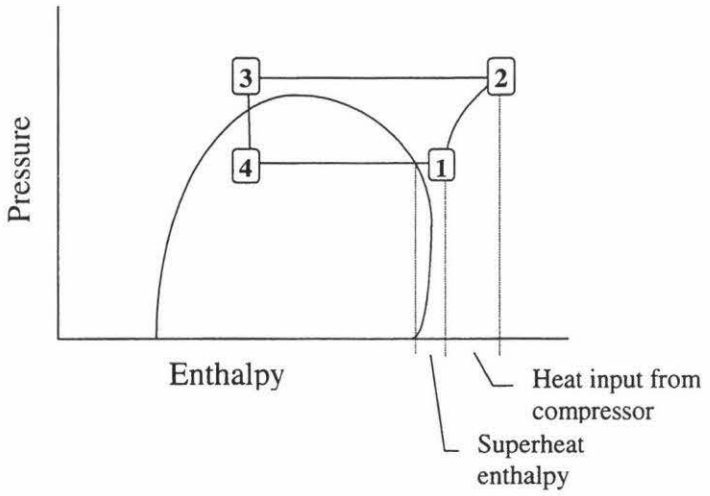

Figure 2.5: Pressure - Enthalpy Diagram for a Transcritical Cycle

Table 2.2: Explanation of cycles on pressure-enthalpy diagrams

Point on P-h diagram	Conventional Cycle	Transcritical Cycle
(1)	Low pressure superheated vapour. The superheat enthalpy is shown as the distance from the envelope to point 1	
(1) to (2)	(Ideally isentropic) Compression	
(2)	Superheated vapour	Supercritical fluid, as the fluid has been compressed to a pressure higher than its critical pressure
(2) to (3)	Cooling of liquid by heat exchange with heat sink. The vapour desuperheats until it reaches the envelope on the diagram (saturation), then condenses to form a liquid (the other side of the envelope)	Cooling of fluid by heat exchange with heat sink. The supercritical fluid cools without phase change. The last part of the cooling may be carried out in the recuperator.
(3)	Liquid	Supercritical fluid
(3) to (4)	Pressure is reduced across a valve to reduce temperature.	
(4)	Vapour - Liquid mixture	
(4) to (1)	Heating of liquid by heat exchange with heat source until pure vapour exists (opposite side of envelope), plus some superheating of vapour (carried out by recuperator)	

An internal heat exchanger (called the recuperator in this project) may be used to protect the compressor from liquid carryover and to increase efficiency. The recuperator transfers heat between the exit of the gas cooler and the compressor suction. This

increases the compressor suction temperature, and therefore the discharge temperature. This can result in a better temperature match in the gas cooler leading to increased efficiency. As well as preheating the suction vapour, it also acts as a precooler for the refrigerant before it is expanded in to the evaporator (White *et al*, 1997).

2.4.1.1 Advantages

The transcritical cycle has many features that make it attractive for simultaneous heating and cooling.

A potential application of supercritical heat pump cycles, in general, is the generation of high-temperature process heat. In ordinary compression cycles featuring isothermal vaporisation and condensation the overall pressure ratio is directly linked to the phase change temperatures and becomes impracticably large as the cycle temperature range increases. Supercritical cycles are intrinsically free of this correlation between temperature and pressure, so a large temperature lift does not imply a large pressure ratio and the heat production temperature is not limited by the fluid critical temperature as in conventional cycles (Angelino and Invernizzi, 1994). The lower pressure ratios also lead to considerably improved compressor efficiency compared with R12 (Lorentzen and Pettersen, 1993).

Supercritical cycles require a relatively simple configuration for achieving a large temperature lift compared to a conventional cycle. A conventional cycle requires multiple stages to achieve good efficiency for large temperature lifts, whereas a supercritical cycle only requires one stage for good efficiency due to the moderate pressure ratios (Angelino and Invernizzi, 1994). If both heating and cooling are utilised, the practical COP will be much greater than a conventional cycle. The transcritical cycle achieves a big enough temperature difference between the hot and cold sides to make both usable.

The CO_2 transcritical process operates at much higher pressures than conventional processes. This offers many advantages. It results in small component dimensions, low compression ratios (due to the higher suction pressure), and higher volumetric heating capacity (Nekså, 1994). The high volumetric heating capacity reduces equipment dimensions and cost. A relatively low pressure ratio allows a one stage compressor to be used, so it will not have to be very complex (Protsenko *et al*, 1992). The capacity for a given compressor volume is in general 5 - 10 times higher for CO_2 than for other common refrigerants (Pettersen, 1995). High pressure also allows greater pressure drops to be tolerated, allowing for smaller inner tube diameters, which give greater velocity and therefore better heat transfer (Manzione, 1998).

Having relatively high pressures on the low pressure side also has advantages. For example, R-134a has a normal boiling point of –26.4°C, and during operation at very low temperature, the low side pressure may be lower than atmospheric. The pressure may also drop below atmospheric at very low ambient temperature, leading to problems with the ingress of moisture and air (Hafner *et al*, 1998). The higher pressures required on the low side of the transcritical process for a given temperature will avoid this problem.

The volumetric heating capacity varies less with heat source temperature than a conventional system. For air-conditioning systems, this can give a higher seasonal performance factor if not operating at design conditions (Nekså, 1994).

The transcritical CO_2 cycle is best suited to the case of an unlimited heat source and limited heat sink with high temperature glides, as would be found with traditional refrigeration and hot water production (Halozan, 1996). Figure 2.6 (a) shows the temperature profile for the heating of water by a conventional cycle. The vapour condenses to a liquid at a constant temperature, giving a very large temperature difference as the water enters the heat exchanger, and a very small one as the water leaves. For improved efficiency, a cycle with a gliding temperature output is required. As illustrated in Figure 2.6 (b), the CO_2 transcritical cycle approaches this cycle. The transcritical CO_2 does not condense, therefore its temperature decreases as it loses heat, maintaining a much more constant temperature difference. This leads to more efficient heat transfer.

However, the heat capacity of CO_2 near the critical point is not constant, and this can lead to a pinch effect in the middle of the refrigerant cooler (ie. the region of low temperature difference driving force in Figure 2.6). This results in reduced heat transfer in this region. The effect of this pinch point can be reduced by increasing the discharge pressure, or by increasing the suction temperature by a recuperator. A higher discharge temperature (the dashed line in Figure 2.6 b) leads to the pinch point being found closer to the end of the cooler.

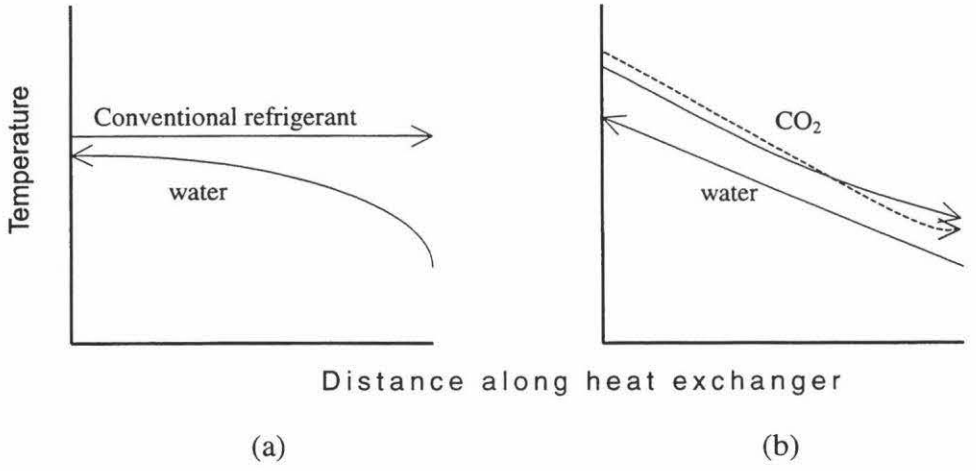

Figure 2.6: Differences in condenser / cooler profiles for conventional and transcritical CO_2 processes.

Pettersen (1995) showed that the COP of the CO_2 system was 10 - 20% higher than a similar heat pump based on HFC-134a. Similarly, Lorentzen (1995) found that the single stage system is most suitable when the required temperature glide is higher than 40-50°C. In such cases it may reduce specific power consumption by up to 40% compared to conventional processes, improving the COP correspondingly.

2.4.1.2 Disadvantages

Even though the transcritical system has many benefits, there are also several drawbacks.

If the heat pump is used with a heat sink with no temperature glide (eg. in space heating), the efficiency of the process is reduced as the temperature profiles will no longer match as closely. If only heating or cooling is used with the other side going to waste, the efficiency will be much lower than heat pump systems that simultaneously provide heating and cooling.

There has been a desire to operate well below the critical point with conventional refrigeration and heat pump systems. For most currently used refrigerants the critical pressure is between 30 - 50 bar, so standard compressors on the market therefore have a maximum pressure rating of about 25 bar. The technology to operate at much higher pressures is available, but is not widely used in heat pumps at present (Lorentzen, 1993). The high pressures involved also require a stricter standard of construction compared with conventional refrigeration systems. The increased installation costs due to the high pressures could be offset by the reduced volume requirement due to the pressure (Pettersen, 1995).

2.4.2 Control

With the transcritical cycle, the high side pressure can be optimised either with regard to COP or capacity (Aarlien and Frivik, 1998). At a certain high side pressure, the COP reaches a maximum, above which the added refrigerating capacity no longer fully compensates for the additional work of compression (Pettersen, 1994). This leads to an optimal high side pressure for efficiency (Figure 2.7).

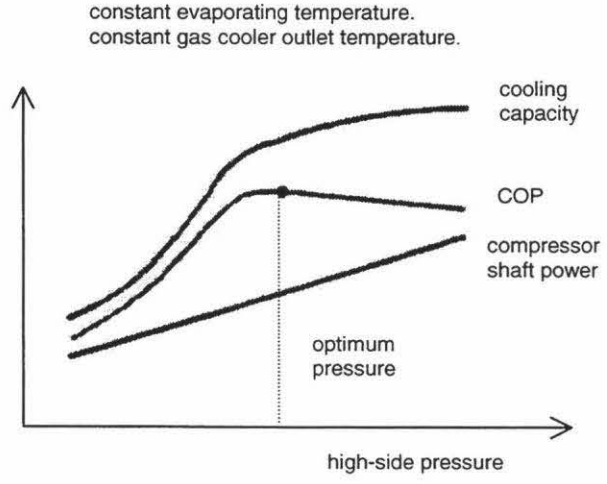

Figure 2.7: Optimum High Side Pressure for COP (Nekså *et al*, 1997)

Alternatively, Pettersen and Skaugen (1994) suggest that high side pressure can be used for capacity control. At supercritical pressures, pressure is independent of temperature, and has a strong independent effect on enthalpy. Therefore capacity can be controlled by varying the high side pressure, since the specific refrigerating capacity is determined by the enthalpy and therefore by the pressure at the throttling valve inlet. Since the gas cooler exit temperature will still be about the same, the enthalpy before the expansion valve will decrease, and both the heating and refrigerating capacity increase (Aarlien and Frivik, 1998). This enables the CO_2 system to maintain its heating capacity at low evaporating temperatures (Hafner *et al*, 1998).

As it is very difficult to control heating and refrigeration capacity independently, one generally has to be chosen to be controlled. It is usual to control that with the smallest capacity, and make up the other with supplementary heating or cooling. If both are similar the refrigeration capacity is often controlled, as it is cheaper to store heat (eg. hot water tank) than cold (eg. ice bank).

In order to get a close fit to the temperature curve of the heat absorbing medium (water), the discharge pressure should be well above the critical pressure. The discharge pressure and suction gas condition can be varied to control the discharge temperature (higher discharge pressure and more superheat in the suction leads to higher discharge temperature). The flexibility for temperature reduction is rather limited, though. Lowering the discharge pressure too much will lead to an internal pinch in the heat exchanger, while reducing the enthalpy at the compressor suction could lead to a wet suction condition, which rapidly leads to poor compressor performance (Lorentzen, 1995).

To achieve hot water at a certain temperature, the CO_2 discharge pressure needs to be high enough to obtain an adequate discharge temperature. The temperature of the water can then be controlled by varying the water flowrate through the gas coolers (Hwang and Radermacher, 1998).

Skaugen and Svensson (1998) created a dynamic model of the transcritical CO_2 system to investigate control aspects. The system modelled had a recuperator and the hot water temperature was fixed. The system operated at pressures between the critical pressure and 120 bar. As the evaporator water flow and temperature were constant, it assumed the cold side inlet conditions to the recuperator were constant.

The dynamic model was tested against experimental data (results shown in Table 2.3). Skaugen and Svensson (1998) believe the model gave good qualitative agreement with the experimental data, but the quantitative agreement was not so good possibly due to a mismatch between the simulated and measured mass flowrate.

Table 2.3: Simulated and Measured Response of the Transcritical CO_2 System (Skaugen and Svensson, 1998)

		Simulation			Experiment		
		Initial Value	Steady State Value	Time to Steady State	Initial Value	Steady State Value	Time to Steady State
Step Increase in Gas Cooler Water Flowrate	Hot Water Temperature	65°C	37°C	300 s	60°C	40°C	140 s
	High Side Pressure	82 bar	81.5 bar	400 s	80 bar	80 bar	600 s
Step Decrease in Control Valve Opening	Hot Water Temperature	64.2°C	64.9°C	600 s	61.5°C	71°C	600 s*
	High Side Pressure	82 bar	112 bar	30 s	83 bar	110 bar	700 s

*still not completely at steady state

2.5 Applications and Performance Testing

The transcritical CO_2 process has been investigated both using simulations and actual experiments.

2.5.1 Process Performance - Simulated

Dynamic modelling of the system provides a number of benefits over experimental testing (Skaugen and Svensson, 1998). These include:

- It is cheaper to use computer models of the transcritical CO_2 heat pump to simulate the effect of varying the size of individual components than to build several different sized plants.
- It is easier to develop control strategies with a simulation than to experiment with a real system.
- It is possible to extrapolate performance to new situations.

The thermophysical property data of pure CO_2 is reasonably well known, except in the critical region. This may lead to some uncertainty and difference in the results.

2.5.1.1 Heating Only Applications

The transcritical CO_2 cycle is ideally suited to water heating, but can also be used for other heating applications such as space heating.

Numerous authors have shown that the CO_2 transcritical heat pump has a better heating COP than conventional Evans Perkins cycles when a high temperature split between the heat source and sink is required. Protsenko *et al* (1990) found that for a 45°C to 55°C temperature split, the COP of the transcritical CO_2 system was 12% to 28% higher than the R12 system and 27% to 44% higher than the ammonia system. Nekså (1994) found that for a temperature split of about 70°C, the R134a process (without a subcooler) was only about 70% of the CO_2 process COP. The R134a process was worse than the CO_2 process for all hot water temperatures above 55°C. Hwang and Radermacher (1998)

found the transcritical CO_2 process had a 10% higher simulated COP than R-22 for a temperature split of around 60°C.

While the COP of the CO_2 system increases when the temperature split decreases, the difference between the two cycles becomes less significant. The decrease in temperature split could be caused by decreasing the required hot water temperature. Nekså (1994) found that below a hot water temperature of 55°C the R134a process outperformed the CO_2 process. It can also be caused by increasing the heat source temperature (Protsenko *et al*, 1992; Nekså, 1994; Enkemann and Kruse, 1997). Protsenko *et al* (1992) found that for producing 65°C hot water, when the heat sink inlet temperature was above 15°C, the R12 process was better than the CO_2 process.

Several conditions have been found to affect the optimum discharge pressure for COP. Increasing heat source temperature (Nekså, 1994; Enkemann and Kruse, 1997; Hwang and Radermacher, 1998), increasing heat sink inlet temperature, and increasing hot water temperature (Nekså, 1994) all lead to the optimum discharge pressure increasing. The use of a real compressor (with less than ideal efficiencies) led to a shorter range of optimum pressures compared to using an ideal compressor (Enkemann and Kruse, 1997). Typical values obtained for the optimum discharge pressure were about 114 bar for producing 90°C hot water (Nekså, 1994), 100 bar when for heating water from 10°C to 60°C (Hwang and Radermacher, 1998), and 100 bar when heating water from 34°C to 66°C (Enkemann and Kruse, 1997).

Some authors have tried varying the cycle to try to improve performance. Protsenko *et al* (1992) modelled the CO_2 cycle both with and without a recuperator placed after the gas cooler. When heating water to temperatures between 50°C and 70°C, the recuperator gave an average COP increase of 5% over the system without a recuperator. Chumak *et al* (1996) modelled the transcritical system with superheating carried out with a recuperator placed in the middle of the gas coolers (as illustrated in Figure 2.8). The reason for this was to try to avoid the internal pinch point in the gas coolers. With this system, the COP increased with the amount of superheating by the recuperator, and also increased with decreasing discharge pressure.

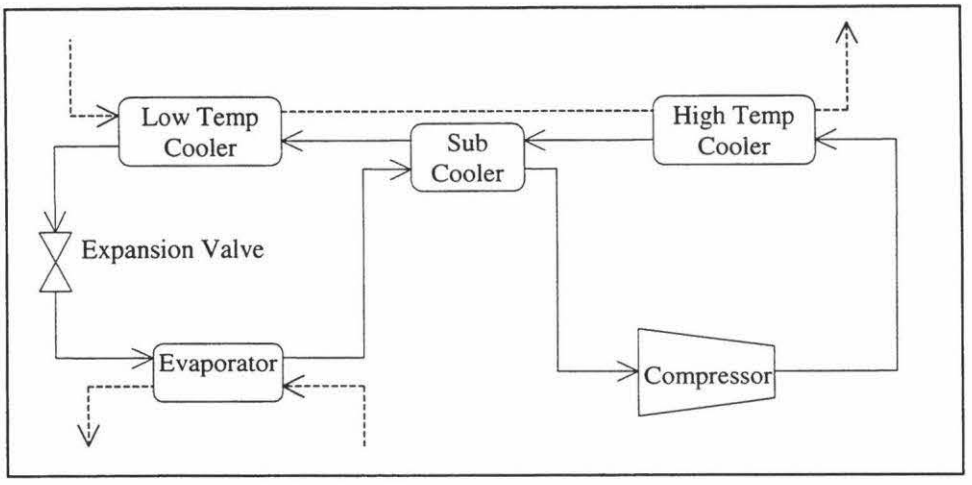

Figure 2.8: Flow circuit of the Transcritical CO_2 Heat Pump used by Chumak *et al* (1996)

2.5.1.2 Cooling Only Applications

While the transcritical CO_2 cycle would not normally be considered for traditional cooling only applications due to its low efficiency, it has potential in some applications, especially in car air-conditioning where safety is an important issue.

Several authors have shown an optimum discharge pressure exists for COP (Pettersen and Skaugen, 1994; Liao and Jakobsen, 1998; Robinson and Groll, 1998). Pettersen and Skaugen (1994) showed that the optimum discharge pressure increases with increasing gas cooler exit temperature and increasing the evaporation temperature was found to lead to a very small decrease in the optimum discharge pressure. With non-ideal compression (with volumetric losses and increased power requirements) the optimum pressure was lower, and the drop in COP with increasing pressure was more pronounced. Robinson and Groll (1998) found the optimum pressure reached a maximum for a given evaporator temperature, although the overall variation in optimum pressure was less than 4 bar over a 45°C range in evaporation temperature.

Pettersen and Skaugen (1994) developed a computer simulation of a CO_2 system for vehicle air conditioning. It showed that moving away from the optimum did not have a large effect on COP and capacity, particularly when at higher than optimum pressures. For example, at a cooler outlet temperature of 35°C, operation at high side pressures between 82 and 101 bar gave a difference in COP and capacity of less than 5%.

Pettersen and Skaugen (1994) found that a recuperator after the gas cooler led to lower optimum pressures, especially at higher gas cooler exit temperatures. The recuperator reduces optimum pressures as it lowers the expansion valve inlet temperature. At these lower temperatures any increase in discharge pressure has little effect on specific refrigeration capacity (the enthalpy does not decrease much). Robinson and Groll (1998) found the use of a recuperator increased the cooling COP by an average of 7%.

Liao and Jakobsen (1998) found that increasing the evaporation temperature led to a rapid increase in cooling COP, and there was a negligible effect of superheat on cooling COP. The COP can therefore be given as a function of high side pressure, gas cooler exit temperature, and evaporator temperature. Equations for the optimum high side pressure were based on curve fits to the simulation data. The range of gas cooler exit temperatures used in the simulations for the curve fit was between 30 and 44°C. The equations used are limited to refrigeration, as they do not take the desired hot water temperature into account.

2.5.1.3 Heating and Cooling Applications

A residential transcritical CO_2 air-conditioning system providing either heating or cooling was simulated by Aarlien *et al* (1996). An equal capacity R22 reversible circuit with equal compressor efficiency was used as a reference. The CO_2 system had a better cooling COP at ambient temperatures less than 27.8°C. The CO_2 system had a reduced drop in heating capacity at low ambient temperatures.

White *et al* (1997) used a computer simulation to test the performance of a transcritical CO_2 cycle for both simultaneous refrigeration and water heating. A –5°C evaporation temperature was used. The heating COP was slightly greater than 3 when heating water

from 15°C to 90°C. Lowering the hot water exit temperature from 90°C to 65°C lead to a 10% and 15% increase in COP and refrigeration capacity respectively. Simulations were also carried out for the case when a recuperator was used. This only gave a small increase in refrigeration capacity and COP. The recuperator did not seem to be justified on the grounds of improved COP when the compressor discharge pressures were well above the critical pressure. However, the small cost of including the recuperator may be justified by the flexibility of operating efficiently over a wider range of compressor discharge pressures and protection from liquid carryover into the compressor.

White *et al* (1997) found that the refrigeration capacity increased with increasing compressor discharge pressure. For discharge pressures below 130 bar, the increased capacity was accompanied by an increase in COP, but above 130 bar the COP was relatively constant. This was explained by the location of the minimum temperature difference (pinch point) between the refrigerant and water in the refrigerant cooler heat exchanger. At pressures below 130 bar, the pinch point was predicted to be in the middle of the cooler, causing poor performance because the CO_2 vapour can not be cooled below about 40°C. For discharge pressures above 130 bar, the pinch point was found to be at the cold end of the cooler, leading to improved performance. The optimum compressor discharge pressure for a single stage cycle was found to be between 130 and 150 bar.

Hafner *et al* (1998) simulated a transcritical CO_2 automobile heating and cooling system. A reversible cycle with a recuperator was used. Both the engine coolant circuit (after the radiator) and a variable mixture of ambient and passenger compartment exit air were used as a heat sink (for cooling of the passenger compartment) or a heat source (for heating). In heating mode, both the COP and capacity were found to increase with increasing ambient and engine coolant temperature (heat source). In cooling mode the COP decreased with increasing ambient temperature (heat sink). The same effects were obtained by Aarlien *et al* (1996). The optimum high side pressure for the cooling operation of the system was found to be between 110 to 120 bar.

Nekså *et al* (1998) modelled a CO_2 system that provided refrigeration, and heating either directly to air using a subcritical cycle or to a brine waste heat loop using a transcritical cycle. Simulations showed that the lowest energy consumption when using the brine loop was obtained at 30°C maximum brine return temperature, and a temperature glide of 10°C. The highest energy consumption occurred at a maximum temperature glide of 30°C. The high temperature glide increased the heating capacity of the system, and the heat can be used for tap water if the space heating is not required. The power consumption of the system was similar to that of a R22 system. They also simulated two transcritical CO_2 refrigeration units with the heat being rejected to a closed water/glycol recirculation loop that provided tap water heating and/or space heating. Excess heat was rejected to ambient air and, if necessary, by an auxiliary chiller. Calculated energy savings in the refrigeration and space/water heating ranged from 25% to 45% compared to the baseline R22 system. The optimum brine return temperature depends on the energy price for alternative heating, the amount of hot tap water needed, and the efficiency of the CO_2 systems, the auxiliary chiller and the R22 baseline system (Nekså *et al*, 1998).

2.5.2 Process Performance - Experimental

Theoretical calculations can give some indication of process performance, but assumptions and simplifications in the problem formulation may limit the applicability of simulated results. Experimental results give more reliable performance data for the given system. Most performance testing has been carried out with smaller heat pumps that would have limited industrial application. For most systems tested, the receiver was almost invariably placed after the evaporator.

2.5.2.1 Heating Only Applications

Nekså *et al* (1997) tested a prototype CO_2 heat pump producing hot water, with a nominal heat output of 50 kW. The maximum operating pressure of the plant was 130 bar. The compressor used was a prototype open crankcase reciprocating compressor with one cylinder. It had isentropic and volumetric efficiencies of 0.84 and 0.86 at design conditions. The heating COP was found to decrease with increasing hot water temperature and to increase with increasing evaporator temperature.

The measured data (Figure 2.9) showed that the high side pressure optima for a given hot water temperature were reasonably flat. Nekså *et al* (1997) believed that the recuperator influences how flat these optima were, with small heat exchangers leading to a more pronounced optimum. The optimum pressure increased with increasing hot water temperature. The optimum heating COP for production of 80°C hot water was found to be about 3.75 at a high side pressure of 110 bar, while for 60°C hot water, the maximum COP was 4.4 at 88 bar.

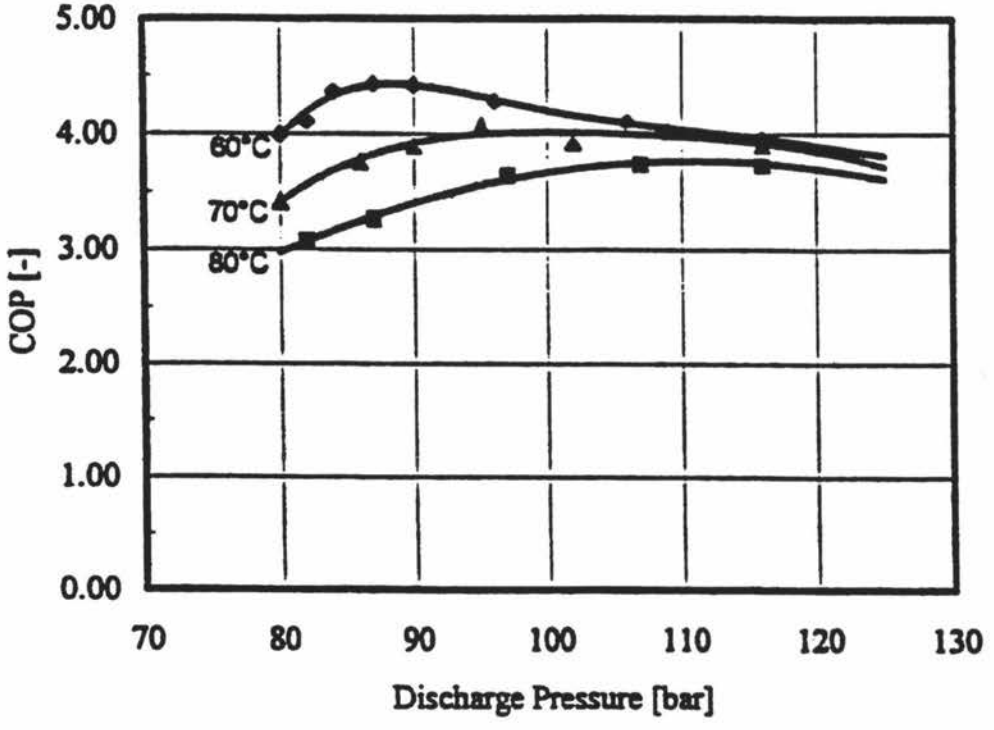

Figure 2.9: Optimum discharge Pressures for Various Hot Water Temperatures (Nekså *et al*, 1997)

Hwang & Radermacher (1998) tested a transcritical CO_2 system for water heating. A prototype positive displacement, hermetic compressor was used with a capacity of 11 kW. The compressor discharge was limited to a maximum temperature of 100°C. Lowering the hot water temperature (by increasing the gas cooler water flowrate) was found to increase capacity and COP. A maximum COP of 3.2 was obtained when heating water from 13°C to 62°C. A 26°C water inlet temperature to both the cooler and evaporator gave better performance (both in terms of capacity and COP) than 8°C inlet temperature. Higher water inlet temperatures decreased gas cooler performance (as the gas cannot be cooled as far), but they enabled the evaporator to operate at a higher temperature. A higher evaporator temperature leads to a smaller pressure ratio, and hence reduced compressor power consumption. A higher cooler water temperature did not affect the high side pressure.

2.5.2.2 Cooling Only Applications

Lorentzen and Pettersen (1993) built a car air-conditioning system with CO_2 as its working fluid. The system used a 3-cylinder wobble plate compressor with a swept volume of 26 cm^3, a tube-in-fin evaporator (with 4.6 mm diameter tubes), a tube-in-fin cooler, and a recuperator. The maximum cooling capacity achieved during testing was 4.9 kW. It was found that the CO_2 system was at least as good as the standard R12 system, and generally performed better. The relative performance of the CO_2 system was even better at high ambient temperature and low compressor speed (idling). The COPs decreased with increasing air temperature.

Pettersen and Skaugen (1994) also ran tests on the prototype car air-conditioning CO_2 system used by Lorentzen and Pettersen (1993). The compressor used did not have piston rings so it suffered from internal leakage. Clear maxima were obtained for both COP and capacity with respect to high side pressure. For a gas cooler exit and evaporator temperature of 35°C and 10°C respectively, the optimum pressure for COP was at about 90 bar, and the optimum for capacity only slightly higher. At a 50°C gas cooler exit temperature the optimum was at 114 bar.

Kaiser (1996) used a prototype two-cylinder reciprocating compressor with a swept volume of 30 cm^3 to test the transcritical CO_2 system. Using a gas cooler exit temperature of 50°C the CO_2 system was compared to R134a, R290, and R600a systems. CO_2 had the lowest cooling COP for a given evaporation temperature and increased the most slowly with increasing evaporation temperature. There were problems with getting the valves to close completely, so the compressor was not optimised. However, the volumetric efficiency of the CO_2 compressor was still more than 10% higher than any of the other compressors for a given pressure ratio. Higher gas cooler CO_2 exit temperatures led to a decrease in optimum COP and an increase in optimum discharge pressure.

Yin *et al* (1998) carried out experimental tests comparing automobile air-conditioning units using R134a and CO_2. The CO_2 system was a transcritical cycle with a recuperator, and a suction accumulator between the evaporator and the cold side inlet to the recuperator. A prototype 10.5 kW open reciprocating compressor was used to enable direct comparison with the R134a system which had a 10.5 kW reciprocating

compressor. The R134a system was a standard system currently in use. The CO_2 system was sized to provide approximately equal capacity at the extreme high temperature of 54.4°C at idling, but its COP fell 10% short of the R134a system at this point. However, at outdoor temperatures below 40°C where most air-conditioning occurs, the CO_2 system performance exceeded the R134a system by 40% or more. The COP of both systems decreased with increasing ambient temperature. The capacity of the CO_2 system was greater for almost the entire range of operating conditions, except at high ambient temperatures. The R134a system was optimised for cost and compactness. If it was optimised for efficiency (eg. with a thermostatic expansion valve or variable displacement compressor), it may have yielded better results. The CO_2 system relied on prototype components because optimised systems did not exist.

Lorentzen and Pettersen (1993) found that the performance of the CO_2 system was better than that of a R12 system at higher ambient temperatures. Yin *et al* (1998) found the opposite happened with R134a, and at high ambient temperatures the performance of the CO_2 system was worse. This is consistent with Kaiser (1996), who found the performance of the CO_2 system to be less than R134a, R290, and R600 at high ambient temperatures, indicating that the difference in relative performance may be due to the reference process refrigerant.

Gentner (1998) tested the transcritical CO_2 system with a recuperator in a car air-conditioning system. The compressor used was a reciprocating machine with a swept volume of 26 cm^3. Special development was required for the shaft seal which had to work against a pressure difference of 50 bar and a speed range from 800 to 8000 rpm. By varying the gas cooler outlet temperature from 35°C to 50°C, the optimum high side pressure increased from 85 to 120 bar.

2.5.2.3 Heating and Cooling Applications

Aarlien and Frivik (1998) tested a reversible transcritical CO_2 air-conditioning system. A prototype seven-cylinder wobble-plate, reciprocating, open compressor, with a swept volume of 30 cm^3 was used. Maximum pressure was 140 bar and maximum temperature was 200°C. Extruded micro-tube, parallel flow heat exchangers were used for the evaporator and condenser. A recuperator was used. The reference unit used R22 as its working fluid. It had a rated cooling capacity of 7.8 kW when in cooling mode and heating capacity of 7.9 kW when in heating mode. The indoor and outdoor temperatures and relative humidities were held constant for both systems. In cooling mode, the cooling COP of the CO_2 system was lower than that of the R22 system possibly due to the CO_2 evaporation temperature being lower than the R-22 system. The temperature approach in the gas coolers was between 1.5 and 2°C. In heating mode, the CO_2 system had higher heating COPs, the temperature approach was between 7.2 and 15°C, and the CO_2 heating evaporation temperature was generally higher than for R22. The lower evaporation temperatures in cooling mode indicate that there were inefficiencies in the evaporator. This may be due to water retention between the heat exchanger fins. In heating mode there were inefficiencies caused by insufficient gas cooler heat exchange area. As expected, increasing the outdoor (heat sink) temperature decreased the COP in cooling mode. In contrast, increasing the outdoor (heat source) temperature increased the COP in heating mode. This was consistent with other studies.

Nekså *et al* (1998) tested a transcritical CO_2 system for refrigeration and water or space heating. Water was heated from 10 to 70°C in the gas cooler and the expansion valve controlled the high side pressure at 95 bar. An optional recuperator was used. The cooling capacity of the system was about 6 kW with an evaporation temperature of –10°C, and 2 kW at –35°C. Increasing the gas cooler water inlet temperature decreased the cooling COP from 2.15 with a gas cooler water inlet temperature of 10°C, to 1.8 with an inlet temperature of 26°C. These results were lower than the simulations by 15% and 10% respectively. This was mainly caused by poor compressor efficiency. Decreasing the evaporation temperature to –35°C reduced the COP to about 0.9 with 10°C gas cooler inlet water. This was 30% lower than simulations, although the optimum suction pressure was unable to be obtained due to insufficient insulation. The recuperator was found to increase the COP by 5%, compared with 0.3% suggested by simulations.

2.5.3 Process Performance Summary

The simulated results show that transcritical CO_2 system performs as well as or better than traditional refrigerants in conventional cycles. However, the relative performance of the transcritical CO_2 system may decrease at lower temperature splits. The experimental results show that the transcritical CO_2 system had higher COPs than the conventional systems for heating applications, but the results were mixed for cooling applications. The CO_2 system was outperformed by conventional refrigeration systems in two studies: by R22 in one (Aarlien and Frivik, 1998) and by R134a, R290, and R600a in the other (Kaiser, 1996), although the cause for the former application was the evaporator being undersized.

Simulated and experimental results universally showed that elevated hot water temperatures (higher heat sink temperature) could be obtained at the expense of lower heating and refrigeration COPs. This was because the discharge pressure must be increased to achieve the desired temperatures. Increasing the hot water temperature also increased the optimum discharge pressure.

The simulated performance of the recuperator was varied. Protsenko *et al* (1992) and Robinson and Groll (1998) found that it would increase performance, while White *et al* (1997) found it would have negligible effect. This may be due to the first two systems operating at slightly lower discharge temperatures and pressures, and the first system having a higher heat source inlet temperature. Nekså *et al* (1998) performed simulations which showed that there would be negligible effect from the recuperator. However, experiments with the inclusion of the recuperator gave a 5% increase in performance. The recuperator was also found to lower the optimum pressure.

Higher evaporation temperatures (higher heat source temperatures) gave higher COPs and a higher optimum pressure. Increasing the heat source temperature or the CO_2 temperature at the gas cooler exit were both found to increase the optimum pressure.

In general, the simulated predictions of heating COPs in water heating applications range from about 3 to 4.7, with the higher COP achieved at an evaporation temperature of 10°C. Experimental results gave similar values ranging from 3.2 to 4.3 (with the latter at a 60°C hot water discharge temperature). Work to date has concentrated on

small domestic applications. The largest system tested has a maximum heating capacity of 50 kW.

2.5.4 Equipment Performance

The ideal thermodynamic performance of the CO_2 transcritical cycle appears to be good compared with traditional technology. However, the performance of the system will be strongly influenced by the performance of the equipment component parts. Factors influencing the performance of component parts are discussed below.

2.5.4.1 Compressor

Sealing is particularly important due to the large pressure differential which could lead to internal leakage losses through valves and piston or piston rod blow-by. Leakage losses could cause compressor inefficiency and loss of charge from the system. As long as there is effective sealing to prevent leakage, either past the piston rings or down the piston rod, other loss factors should be of minor significance. The high volumetric refrigerating effect means the pressure loss through valves will be much smaller. Cylinder friction losses are also likely to be lower due to reduced cylinder dimensions (Lorentzen and Pettersen, 1993). Also, compressor efficiencies tend to be very competitive in CO_2 compressors, as the pressure ratio is smaller than in conventional machines (Aarlien and Frivik, 1998).

Suß and Kruse (1998) measured and modelled the heat flow between the compressor cylinder and CO_2 in the cylinder, to determine its effect on compressor efficiency. It was determined that the effects were negligible (as they are for CFC and HCFC compressors).

Lorentzen and Pettersen (1993) found the pressure ratios in the CO_2 system ranged from 2.5 to 3.5, while a R12 compressor works at between 5 and 7. As the isentropic efficiency of practical compressors decreases with increasing pressure ratio, the CO_2 machine was expected to have better performance. Experiments found the efficiency of the CO_2 compressor to be 70% (pressure ratio 3.8), compared to 50% for the R12 machine (pressure ratio 6.5).

Aarlien and Frivik (1998) tested a reciprocating compressor in a CO_2 heat pump. The compressor volumetric efficiency ranged from 0.52 to 0.76, while the isentropic efficiency varied between 0.58 and 0.74. This was lower than expected, but this was attributed to worn bearings, and a leak through the stuffing box.

Eggen and Aflekt (1998) further tested the prototype CO_2 compressor used by Nekså *et al* (1997). The isentropic efficiency was 5-10% higher than that obtained in commercial compressors for the traditional working fluids. This is due to the high energy transfer for the small CO_2 compressor volume compared with other refrigerants.

The isentropic efficiency for the CO_2 compressor used by Yin *et al* (1998) ranged from 0.70 to 0.79, compared with 0.53 to 0.60 for the R134a compressor. The volumetric efficiency was 0.72 to 0.80 for the CO_2 compressor and 0.45 to 0.59 for the R134a compressor.

Enkemann and Kruse (1997) developed a model for a real compressor derived from measurements of a prototype (Figure 2.10). The isentropic efficiency reached a maximum of 0.75 at a compression ratio of 2.5. The steepness of the volumetric efficiency curves increased with decreasing compressor speed.

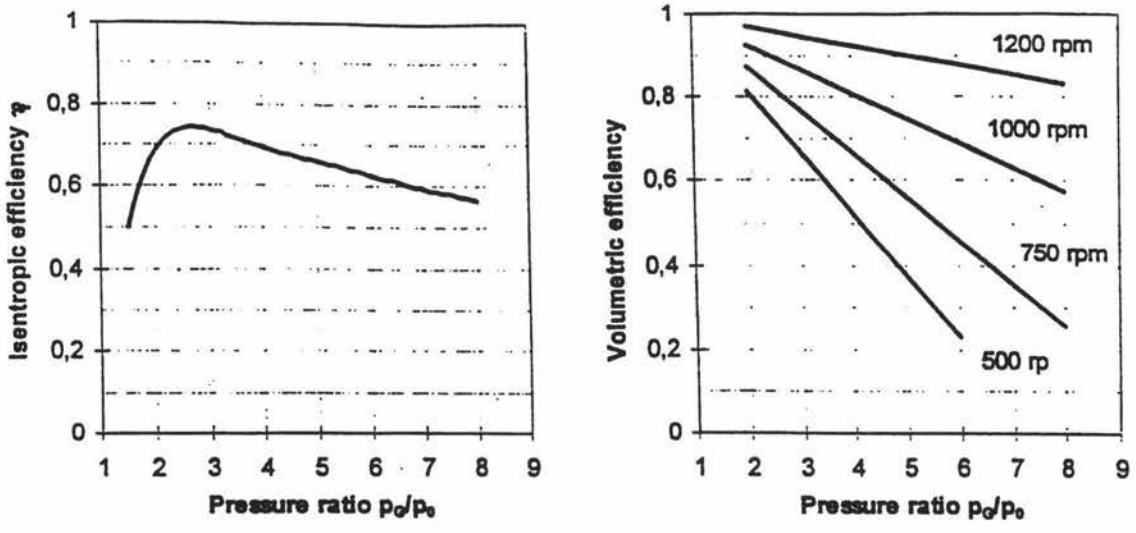

Figure 2.10: Compressor Model Based on Prototype Measurements (Enkemann and Kruse, 1997)

Compressor speed can be used to control the capacity of the system, but in order to provide the necessary capacity, simulations by Enkemann and Kruse (1997) showed the compressor would have to run between 10% and 100% of maximum speed. This low speed may cause a problem with bearings in the compressor as the oil pump is often driven by the compressor. It may be possible to change the design to allow this range in speed, either by using different bearings, or by having a variable stroke.

Fagerli (1996) investigated the use of a single cylinder hermetic CO_2 compressor. The design suction and discharge pressures were 30 bar and 100 bar. The gas was superheated by 10°C at the compressor suction. The swept volume was about 2.6 cm^3 with a mass flow of 0.007 kg/s at 2880 rpm and a pressure ratio of 4. Reed valves were used. Naphthenic mineral oil was used for lubrication. The volumetric efficiency decreased from 0.85 at a pressure ratio of 1.3 to 0.5 at a pressure ratio of 4. Fagerli (1996) suggested the major challenge would be the connection between the piston and connecting rod, as substantial wear may be caused by the high load.

Fagerli (1998) investigated the use of scroll compressors in the transcritical CO_2 process using a theoretical analysis. Fagerli concluded that it should be possible to design a competitive scroll compressor. However, gas leakage is the main challenge. The compressor could be similar to the R134a baseline compressors except that the CO_2 leakage clearance gap would need to be significantly smaller.

2.5.4.2 Expanders

Heyl *et al* (1998) simulated the transcritical process with an expander-compressor unit in place of a separate expansion valve and compressor. They found that for outlet temperatures from the gas cooler between 35 and 45°C, the thermodynamic efficiency could be improved by the addition of this unit. It consisted of a piston engine with the gas to be compressed on one side, and the gas to be expanded on the other. A 78% overall efficiency was achieved.

Taniguchi *et al* (1988) investigated a screw expander using R12 both theoretically and experimentally. They found that the internal efficiency approaches a maximum of 80% with increasing rotor diameter, while the power output increases in proportion to the square of the rotor diameter. The internal efficiency increases as the rotor speed increases due a decrease in leakage.

Robinson and Groll (1998) predicted that the COP of the CO_2 cycle with an 60% isentropic efficiency turbine is on average 25% higher than the COP of a valve expansion cycle with internal heat exchange and 34% higher than a cycle without internal heat exchange. If an expander was used, the optimum heat rejection pressure would decrease and, the more efficient the expander, the lower the optimum pressure would be. The use of a recuperator in conjunction with a work recovery device (expander) decreased the COP.

2.5.4.3 Heat Exchangers

An important factor in obtaining an efficient gas cooler is that the temperature approach (the temperature difference between the refrigerant exiting, and the heat sink entering) is as small as possible. Properly designed heat exchangers may offer a temperature approach as low as 1°C (Aarlien and Frivik, 1998).

Hafner *et al* (1998) calculated the heat transfer for round tube and brazed microchannel CO_2 gas coolers for different approach temperatures. Brazed all-aluminium microchannel heat exchangers gave the best overall performance.

Schönfeld and Krauss (1997) created a model of a gas cooler for CO_2, with water on the shell side. The heat exchanger consisted of three parts each three meters long. The heat exchanger contained 45 8mm OD (6mm ID) tubes, and baffles every 45.4 mm. CO_2 entered at 138°C and 89.7 bar, while water was heated from 10°C to 63.5°C. The capacity of the system was about 25 kW. The overall heat transfer coefficient ranged from about 250 W/m^2K to 450 W/m^2K. The water-side heat transfer coefficient (3100 W/m^2K to 4100 W/m^2K) was far higher than the CO_2 side heat transfer coefficient (300 W/m^2K increasing to a peak of 700 W/m^2K at the critical point).

Hwang and Radermacher (1997) also created a CO_2 gas cooler model. This had CO_2 in the tubes (4×9.842m, OD = 9.52mm, wt = 1.65mm) and water in the shell (OD = 31.8 mm). A constant CO_2 mass flow of 0.6 kg/s and water volumetric flow of 0.2 L/s were used. The Ghajar-Asadi correlation was used for the refrigerant side heat transfer coefficient. When the gas cooler water inlet temperature was less than the critical temperature of CO_2, the heat transfer coefficient increased with gas cooler water inlet temperature. Lower pressures also lead to higher heat transfer coefficients. For a gas

cooler inlet water temperature of 20°C, the heat transfer coefficients based on inside area ranged from 3900 W/m^{2}K at 110 bar gas cooler pressure (2550 W/m^{2}K based on outside area) to 5600 W/m^{2}K at 80 bar (3650 W/m^{2}K based on outside area).

A large difference exists between the calculated CO_2 heat transfer coefficients of Hwang and Radermacher (1997) and Schönfeld and Krauss (1997). This difference may be explained by a difference in mass flux. The gas cooler tested by Hwang and Radermacher (1997) had a large mass flux of 4937 kg/m^2/s, while the mass flux for the Schönfeld and Krauss (1997) gas cooler was unspecified. Different CO_2 property estimation methods were also used, and Schönfeld and Krauss (1997) used an overall heat transfer coefficient based on outside surface area, while Hwang and Radermacher (1997) based theirs on inside surface area.

Protsenko *et al* (1990) suggested that the metal content of the gas cooler can be greatly reduced if individual, series connected, single pass gas cooler heat exchangers are used instead of multiple pass heat exchangers. Using chemical cleans for the heat transfer surfaces and moving the heat carrier at high velocity will ensure good heat transfer, thus possibly reducing heat exchanger area. Keeping a high CO_2 velocity will not add any costs, as there is a large reserve of pressure gradient from the compressor that is usually expended needlessly on throttling.

Eggen and Aflekt (1998) compared a CO_2 evaporator with 4 parallel tubes of 28.8m to a R22 evaporator with 8 parallel tubes of 14.4 m (both with the same area). Finned tubes were used, with CO_2 inside and a 2.8 m/s air velocity outside. The CO_2 evaporator had superior capacity and overall heat transfer coefficient for all log mean temperature differences.

Bredesen *et al* (1997) measured the heat transfer and pressure drop for in-tube evaporation of CO_2. The test section consisted of two 1250 mm horizontal tubes connected by a 180° bend. The tube had an inside diameter of 7 mm, and a wall thickness of 1.5 mm. Electrical heating was used to provide a specified heat flow. The CO_2 was lubricant free. Increasing the mass or heat flux initially lead to little change in heat transfer coefficient, but at higher values, the heat transfer coefficient increased. Initially, increasing the evaporation temperature increased the heat transfer coefficients, especially at high vapour fractions. At high evaporation temperature (5°C) very high heat transfer coefficients were obtained at low vapour fractions, and at high vapour fractions the coefficient was lower than at any of the other temperatures. This reversal in trends was explained by the high pressure and low liquid/high vapour density ratio near the critical point negating the effects of convection.

The highest heat transfer coefficient was about 15000 W/m^{2}K at –10°C evaporation temperature, 400 kg/m^2/s mass flux and at 3000 W/K heat flux at a vapour fraction of 1. The lowest was just over 4000 W/m^{2}K for the same conditions, but with a vapour fraction of 0.

Increasing the heat flux had very little effect on pressure drop but increasing the evaporation temperature decreased the pressure drop especially at high vapour fractions due to the decrease in the liquid-vapour density ratio. The maximum pressure drop was

just under 5000 Pa/m at –10°C evaporation temperature, 400 kg/m^2/s mass flux, 6000 W/K heat flux at a vapour fraction of about 0.8.

Hwang *et al* (1997) found that the Bennett-Chen correlations were closest to the experimental data by Bredesen *et al* (1997), but the mean deviation was still 25%. When the Bennett-Chen correlation was modified for CO_2 it had a mean deviation of 14%.

Zhao *et al* (1997) measured the evaporation heat transfer coefficient of CO_2 inside a smooth tube 1.78m long. Water flowed on the outside of the inner tube. The water was heated by a heating wire to give a constant heat flux. The inner tube had a diameter of 7.94 mm OD and a wall thickness of 1.27 mm. The inlet vapour quality was 0.04 to 0.08, and the pressure was 50 bar (15°C). The heat transfer coefficient of CO_2 increased with mass flowrate and heat flux. The heat transfer coefficients obtained were significantly lower than achieved by Bredesen *et al* (1997). The highest heat transfer coefficient achieved was almost 8900 W/m^{2}K at a mass flux of 440 kg/m^2/s and heat flux of 30000 W/m^2. The heat transfer coefficient at a heat flux of about 6000 W/m^2 was between 2000 and 3000 W/m^{2}K for the range of mass fluxes (140 to 440 kg/m^2/s). Bredesen *et al* (1997) achieved a heat transfer coefficient of 14000 W/m^{2}K at 5°C evaporation temperature, 200 kg/m^2/s and 6000 W/m^2 at a 0.15 vapour fraction.

2.5.4.4 Separator

Since there is no liquid present at supercritical conditions on the high pressure side of a transcritical cycle, the receiver can be combined with the liquid separator in the suction line (Lorentzen, 1994c). Most CO_2 systems in the literature had the receiver after the evaporator, with a liquid-vapour mixture entering the evaporator and superheated vapour exiting.

2.6 Conclusions

Carbon dioxide is a naturally occurring compound which can be used as an environmentally benign refrigerant to replace existing refrigerants which have been shown to damage the ozone layer and contribute to global warming. The heat transfer properties and volumetric refrigeration capacity of CO_2 are very attractive. The safety aspects of CO_2 are also as good as the best of the fluorocarbon refrigerants.

While the low critical temperature of CO_2 would normally lead to poor performance in a conventional refrigeration process, CO_2 appears to be ideally suited for application in a transcritical cycle. The transcritical cycle is similar to a conventional cycle except that the refrigerant is compressed to a supercritical pressure where it cannot condense. Therefore, cooling instead of condensation occurs. As pressure and temperature are independent of each other at supercritical conditions, high temperature process heat can be obtained without the problems of high pressure ratios. This, along with the gliding temperature in the coolers, means the cycle is ideal for heating water.

The performance of the transcritical CO_2 cycle has been shown to be very good both theoretically and in practice, especially when the transcritical cycle is used for both the

heating and cooling. Heating COPs generally range from 3 to 4 when heating water to 90°C. The cycle has been shown to outperform conventional refrigerants in many applications, such as water heating, space heating, and car air-conditioning.

There has been very little work on large scale transcritical CO_2 systems. Most work carried out has been on smaller systems, such as for car air-conditioning. Also, most work carried out has been for refrigeration or heating only, thus negating the major potential advantage of high energy efficiency if simultaneous cooling and heating can be achieved.

3 OBJECTIVES

The overall aims of this project are to develop an industrial scale prototype transcritical CO_2 heat pump system, and to assess its feasibility for simultaneously supplying refrigeration and water heating for the processing industries. The specific objectives of this project are to:

1. Design or select the major components of the transcritical CO_2 heat pump. These are the:
   - Gas cooler / Water heater
   - Evaporator / Water Chiller
   - Recuperator
   - Compressor
   - Separator / Receiver
   - Control system

2. Construct the full scale prototype;

3. Commission the prototype and, if necessary, carry out improvements;

4. Test the prototype's performance across the full range of likely operating conditions;

5. Compare the prototype performance to results predicted by theoretical cycle analysis;

6. Assess the economic viability of the prototype compared with traditional refrigeration and water heating technologies.

4 PROTOTYPE DESCRIPTION

4.1 General Description

Figure 4.1 shows the general arrangement for the CO_2 heat pump. The skid mounted CO_2 heat pump package was 3.5 m long, 1.95 m wide, and 2.735 m high (to the top of the pipework). It consisted of a large steel frame to which the components and interconnecting pipework of the system were attached. The main components of the heat pump were the compressor, electric motor and variable speed drive to drive the compressor, separator / receiver vessel, three gas cooler units, a recuperator and the evaporator. All the components used were standard industrial products, except for the separator which had to be designed specifically for this project.

The heat pump was designed to give a nominal water heating capacity of about 130 kW from 10°C to 90°C and a nominal cooling capacity of about 90 kW at -6°C, with a compressor power consumption of approximately 40 kW.

4.2 Process Description

Figure 4.2 shows the process flow diagram (PFD) for the system at nominal design conditions. At design conditions, CO_2 vapour is compressed from 30 bar to 130 bar raising the temperature from 10°C to about 140°C. At this discharge pressure and temperature, CO_2 exists as a supercritical fluid (ie. above the critical point where the properties of vapour and liquid become identical). The CO_2 flows to the gas cooler where it is cooled by counter-current heat exchange with water. The gas cooler consists of three identical heat exchangers in series. As the CO_2 is a supercritical fluid, it cannot condense, so unlike conventional heat pumps, the CO_2 temperature drops as the water is heated. This results in a close temperature profile match between the CO_2 being cooled and water being heated, leading to reduced thermodynamic losses. The CO_2 is cooled from 140°C to 25°C and the water is heated from 10°C to 90°C.

At the exit from the gas coolers, the CO_2 passes into the recuperator. Here the supercritical CO_2 is further cooled from 25°C to 15°C by counter-current heat exchange with cold CO_2 vapour flowing from the separator to the compressor.

The CO_2 pressure is then reduced through the expansion valve from 130 to 30 bar as the CO_2 enters the separator. The CO_2 becomes liquid as it is throttled below the supercritical pressure, and then it begins to vaporise at the lower pressure which results in the temperature dropping from about 15°C to -6°C. The resultant mixture of saturated liquid and vapour separates in the separator (receiver).

Liquid CO_2 in the bottom of the separator flows by gravity to the evaporator, where CO_2 boils to provide the refrigeration necessary to cool another water stream from 10°C to 3°C.

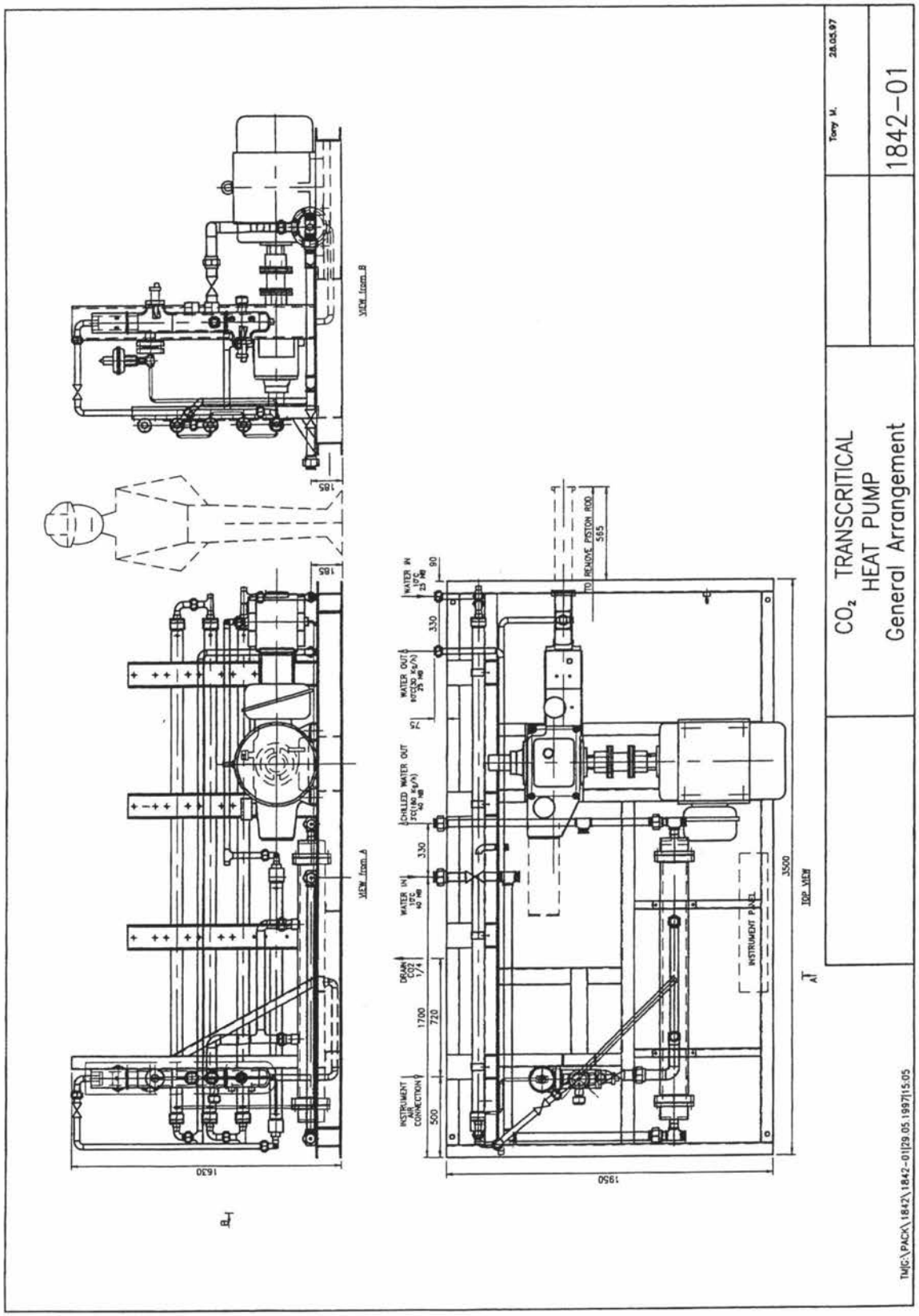

Figure 4.1: General Arrangement for Prototype Transcritical CO_2 Heat Pump

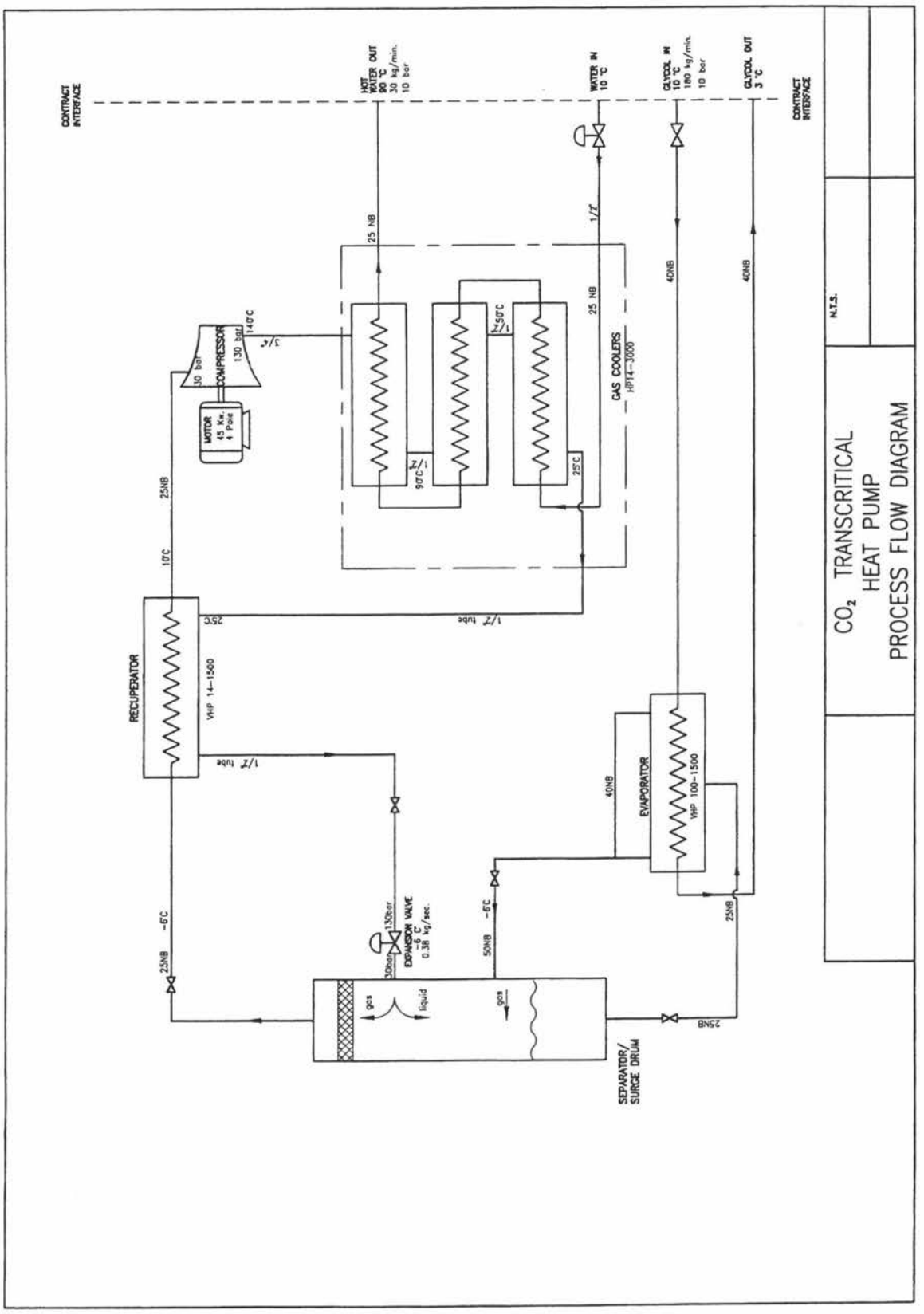

Figure 4.2: Process Flow Diagram

A proportion of the CO_2 is vaporised at –6°C, with negligible temperature increase and the two-phase mixture then circulates back into the separator, entering just above the liquid level. The driving force for flow through the evaporator is a thermosiphon effect, caused by the difference in density between the liquid entering and the vapour-liquid mixture leaving the evaporator. The separator provides separation of the liquid and vapour as well as acting as a surge vessel.

The saturated CO_2 vapour at the top of the separator passes to the recuperator where the temperature is increased from -6°C to 10°C (superheating the vapour).

Finally, the superheated, low pressure CO_2 vapour is compressed back to 130 bar to complete the cycle.

The prototype was originally designed to operate oil free, but an oil return system was later retrofitted between the evaporator and the compressor so that trials with oil circulating with the CO_2 in the system could be undertaken.

4.3 Component Description

4.3.1 Design Pressures

All vessels and piping on the low pressure side (evaporator, separator / receiver, recuperator tubes) were designed for a maximum of 100 bar (achieved when the heat pump is at rest at an ambient temperature of 40°C, compared with a normal operating pressure of 30 bar). A mechanical design pressure of 150 bar was used.

The vessels and piping on the high pressure side were designed to operate at a maximum of 140 bar (compared with an nominal operating pressure of 130 bar). This led to a mechanical design pressure of 210 bar being used. If a high pressure fault occurs on the high pressure side, the system will stop, and the pressure will naturally decrease due to heat transfer from the high side CO_2 to the surroundings.

The design pressures are all quite high compared with normal refrigerants (typically 25 bar maximum). Therefore, it was desirable for the components to be small in size so that mechanical design requirements could be achieved with relatively small wall thicknesses.

4.3.2 Design Procedures

The heat exchangers were sized using the correlations given in Perry's Chemical Engineers' Handbook (1984), with equations (10-120) to (10-135) used to estimate convective heat transfer coefficients and equations (10-136) to (10-138) used to estimate pressure drops. CO_2 thermal properties were calculated using the methods described in Section 5.3.1. Mechanical design for all components was based on ASME VIII Div 1.

4.3.3 Gas Coolers

Objective of Unit: The objective of the gas coolers is to transfer heat from the CO_2 discharged from the compressor to water, resulting in hot water being produced at a useful temperature. Simultaneously, the CO_2 must be cooled to as low a temperature as possible to maximise the energy efficiency of the system.

Special Design Features / Criteria: The large temperature lift in the water stream coupled with a relatively small CO_2 to water temperature difference means that the heat exchanger must have close to perfect counter-current flow. The water and CO_2 flowrates need to be low to give the required temperature change, but the conditions must give a high rate of heat transfer. The solution was to use three very long, small diameter, horizontal heat exchangers. Shell and tube heat exchangers were used due to the high operating pressures of the CO_2. Small diameter heat exchangers were used because they allowed economic design for high pressure service, and the small number of tubes contained in the small diameter shell gave high fluid velocities and good heat transfer. As the specific heat capacity of supercritical CO_2 is not constant, the log-mean temperature difference could not be assumed in the gas cooler, so an actual mean temperature difference had to be used. This was calculated using the methodology discussed in Section 5.3.2.2. However, for ease of comparisons, the gas cooler heat transfer rating was expressed on a log mean temperature difference basis.

Figure 4.3 shows the mechanical drawings of an individual heat exchanger in the gas cooler. The detailed specifications are given in Table 4.1.

Table 4.1: Detailed Gas Cooler Specifications

	Shell	Tubes (14 / unit)
Model	Flotech HP14	
Passes	1	1
Contents	CO_2	Water
Length	3×2.958 m	3×3 m
Outside Diameter	73 mm (65 NB)	9.52 mm (3/8")
Wall Thickness	7 mm	1.2 mm
Inside Diameter	66 mm	7.12 mm
Baffles	28/unit (57 mm OD, 3 mm thick)	
Weight (empty)	70 kg	
Design Pressure	140 bar	10 bar
Operating Pressure	130 bar	4 bar
Hydrostatic Test Pressure	210 bar	150 bar
Mechanical Design Temp (max/min)	150°C/-20°C	150°C/-20°C
Design Inlet Temperature	140°C	10°C
Design Outlet Temperature	25°C	90°C
Design Flowrate	0.436 kg/s	0.384 kg/s
Charge Volume	3×5.05 L	
Design Heat Flow	129 kW	
Design Pressure Drop	37.9 kPa	3.5 kPa
Heat Transfer Area	3×1.256 m^2	3×0.939 m^2
Heat Transfer Coefficient	1990 W/m^{2}K	4700 W/m^{2}K
Overall HTC (outside tube)	1175 W/m^{2}K	

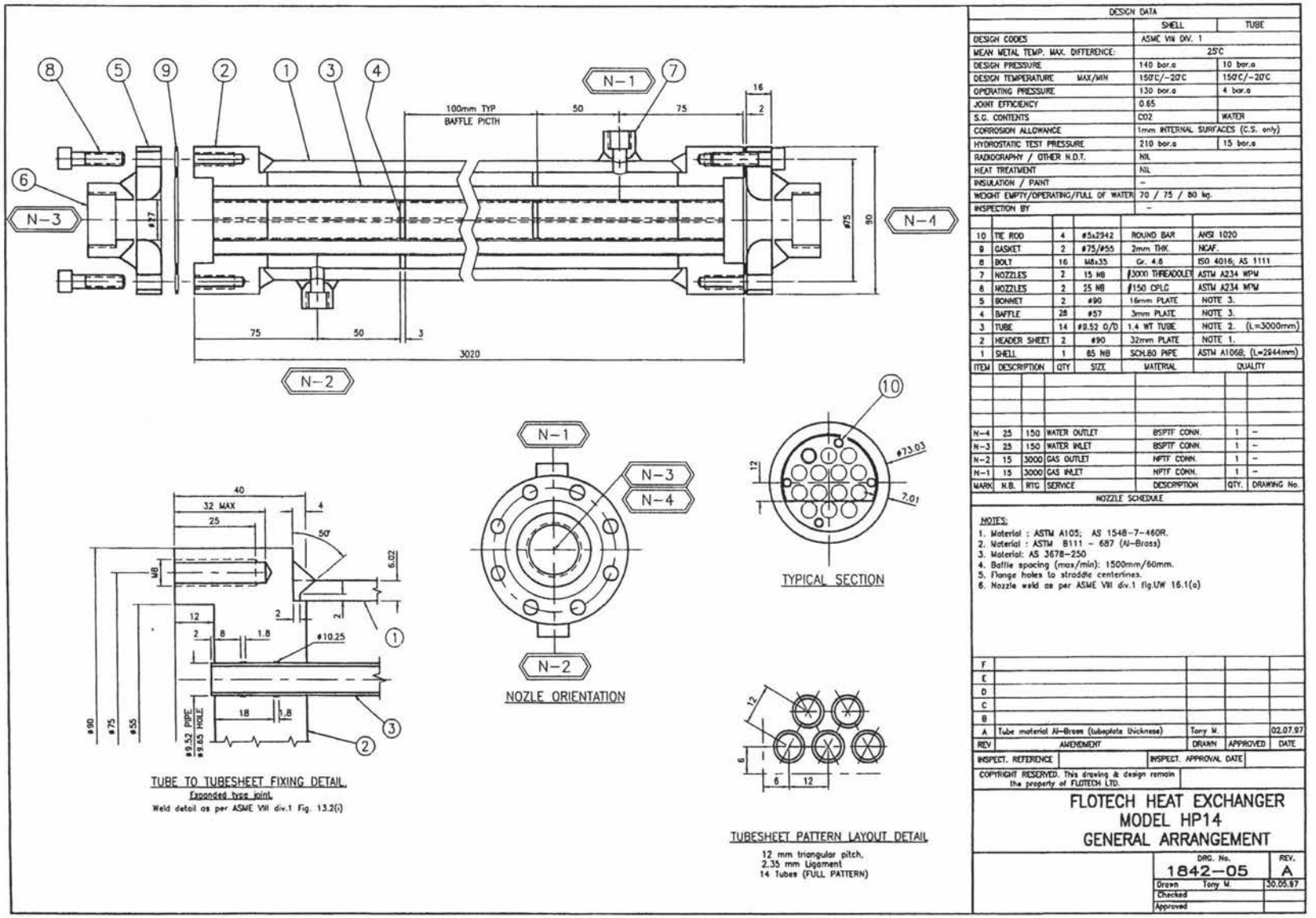

Figure 4.3: Mechanical Drawings for Gas Cooler Heat Exchanger

4.3.4 Evaporator

Objective of Unit: This heat exchanger removes heat from the chilled water stream by boiling low pressure CO_2 flowing through the evaporator.

Special Design Features / Criteria: A horizontal shell and tube heat exchanger was used, with the CO_2 on the shell side. The liquid CO_2 was fed into the bottom via a single 25 mm (1") tube, and the gas-liquid mixture exited at the top via two 38 mm (1.5") pipes. A natural gravity circulation of CO_2 from the separator to the evaporator (the thermosiphon effect described in Section 4.3.7.1) was used to avoid the need for liquid pumps or sophisticated refrigerant control equipment.

Figure 4.4 shows the mechanical drawings for the evaporator. The detailed specifications are given in Table 4.2.

From the initial commissioning trials, it was found the evaporator was under performing. To rectify this, the evaporator was converted from a 1 tube pass unit to a 2 tube pass unit. This greatly improved the water velocity through the heat exchanger and thus the heat transfer coefficients for the same total water flowrate.

Table 4.2: Detailed Evaporator Specifications

	Shell	Tubes (109 / unit)
Model	Flotech VHP100	
Passes	1	1
Contents	CO2	Water
Length	1.446 m	1.5 m
Outside Diameter	168.3 mm (150 NB)	9.52 mm (3/8")
Wall Thickness	11 mm	0.9 mm
Inside Diameter	157.3 mm	7.72 mm
Baffles	20 (145 mm OD, 3mm thick)	
Weight (empty)	145 kg	
Design Pressure	100 BAR	10 bar
Operating Pressure	30 bar	4 bar
Hydrostatic Test Pressure	150 bar	15 bar
Mechanical Design Temperature (max/min)	50°C/-20°C	50°C/-20°C
Design Inlet Temperature	-6°C (pure liquid)	10°C
Design Outlet Temperature	-6°C (vapour-liquid mixture)	3°C
Design Flowrate	2 × Overfeed	3.0 kg/s
Charge Volume	13.10 L	
Design Heat Flow	88 kW	
Design Pressure Drop	9.1 kPa	2.117 kPa
Heat Transfer Area	4.890 m^2	3.965 m^2
Heat Transfer Coefficient	3490 W/m^2K	3280 W/m^2K
Overall HTC (outside tube)	1490 W/m^2K	

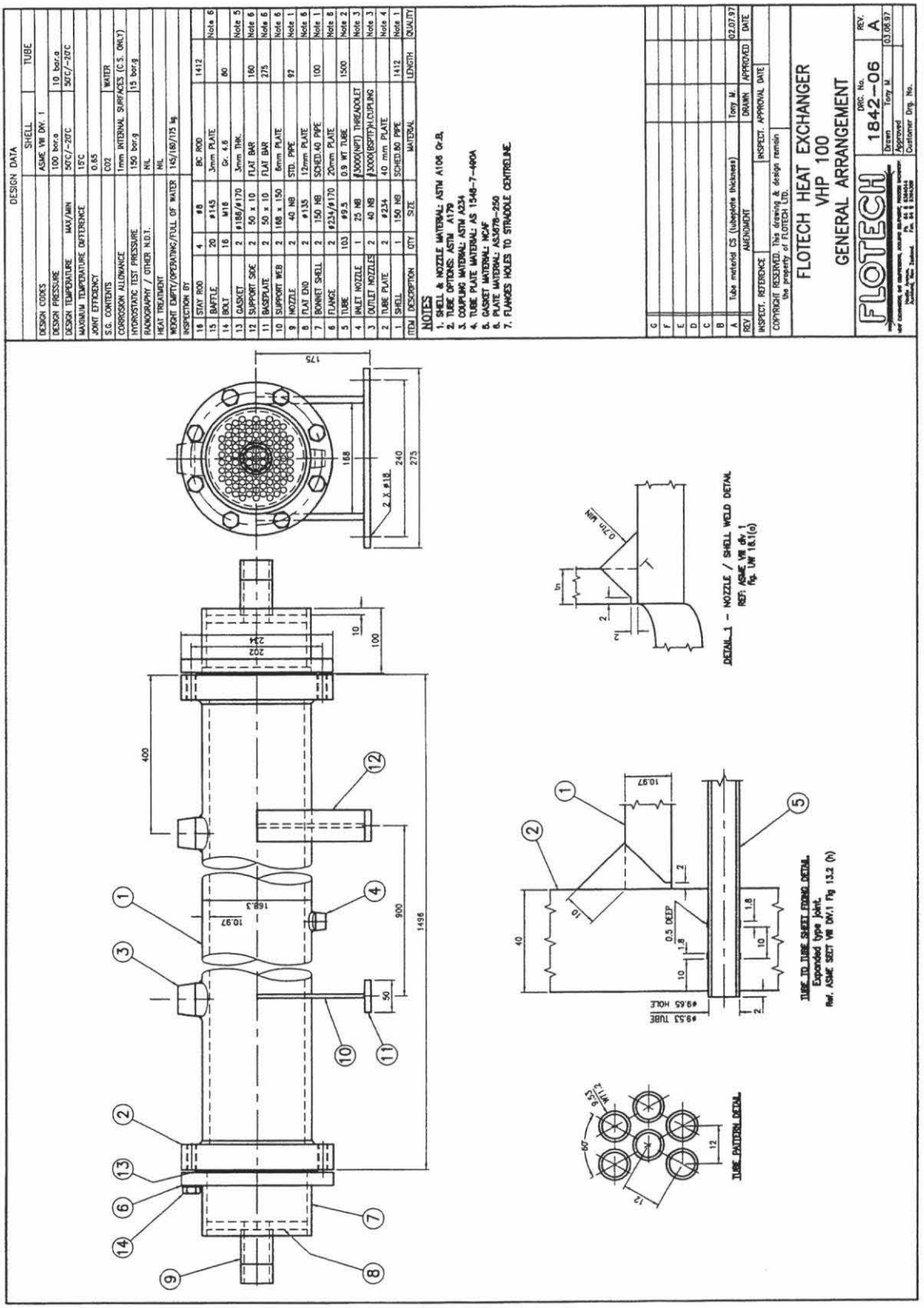

Figure 4.4: Mechanical Drawings for Evaporator

4.3.5 Recuperator (Internal Heat Exchanger)

Objective of Unit: The objective of this heat exchanger is to transfer the remaining heat in the high side CO_2 after the gas coolers to heat the CO_2 exiting the separator. This superheats the saturated vapour going to the compressor (providing increased security against liquid entering the compressor), and further cools the supercritical fluid entering the expansion valve, thus increasing the overall energy efficiency of the whole system.

Special Design Features / Criteria: This heat exchanger is similar to the gas cooler except that there is CO_2 on the tube side as well as the shell side. It is physically quite small to maximise the benefits obtained for the capital cost involved. The possibility of locating this heat exchanger in alternative positions in the process was also desired. For example, possibilities included putting the recuperator between the 3 parts of the gas cooler as suggested by Chumak *et al* (1996), or using it as an extra gas cooler by using water instead of CO_2 on the shell side.

Figure 4.5shows the mechanical drawings of the recuperator. The detailed specifications are given in Table 4.3.

Table 4.3: Detailed Recuperator Specifications

	Shell	Tubes (14 / unit)
Model	Flotech VHP14	
Passes	1	1
Contents	CO_2	CO_2
Length	1.460 m	1.5 m
Outside Diameter	73 mm (65 NB)	9.52 mm (3/8")
Wall Thickness	7 mm	1.2 mm
Inside Diameter	66 mm	7.12 mm
Baffles	14 (57 mm OD, 3mm thick)	
Weight (empty)	40 kg	
Design Pressure	140 bar	100 bar
Operating Pressure	130 BAR	30 bar
Hydrostatic Test Pressure	210 bar	150 bar
Mechanical Design Temp (max/min)	150°C/-20°C	150°C/-20°C
Design Inlet Temperature	25°C	-6°C
Design Outlet Temperature	15°C	10°C
Design Flowrate	0.38 kg/s	0.38 kg/s
Charge Volume	2.49 L	0.89 L
Design Heat Flow	10 kW	
Design Pressure Drop	0.69 kPa	0.21 kPa
Heat Transfer Area	0.628 m^2	0.470 m^2
Heat Transfer Coefficient	1970 W/m^2K	2378 W/m^2K
Overall HTC (outside tube)	860 W/m^2K	

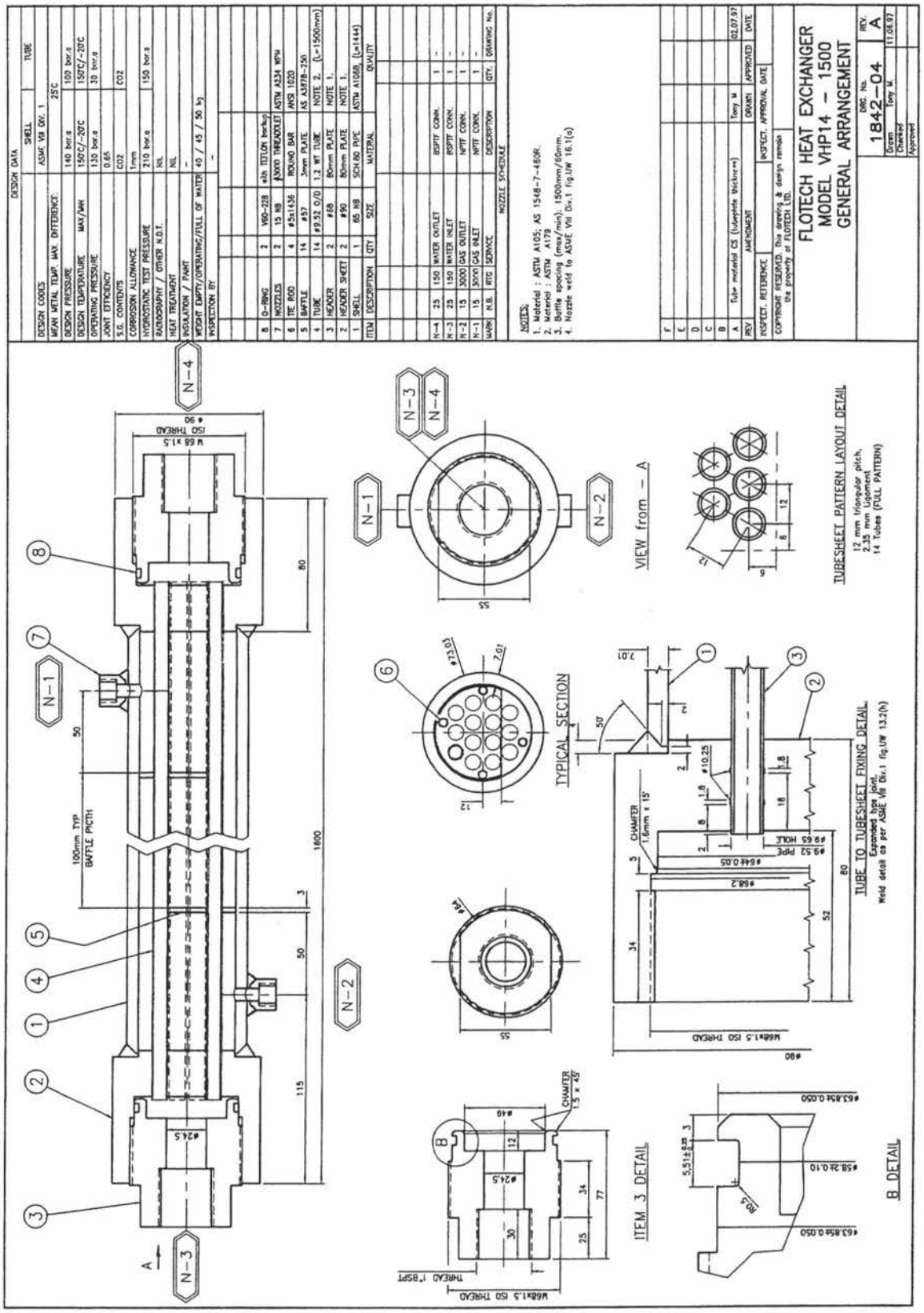

Figure 4.5: Mechanical Drawings for Recuperator

4.3.6 Separator (Receiver)

Objective of Unit: The separator vessel has multiple functions:

- It separates the saturated liquid and vapour mixtures that enter the vessel from both the expansion valve and the evaporator. This protects the compressor from liquid slugs if proper separation occurs.
- It acts as a surge vessel. Changes in high and low side pressures, water flowrates, and charge will vary the amount of CO_2 held in the rest of the system and hence the liquid in the separator. The separator must have sufficient volume to cope with the resulting level fluctuations without compromising its ability to perform its other functions.
- It provides a reservoir of liquid CO_2 to ensure there is adequate head for the thermosiphon.
- It provides a buffer volume so that continuous charging is not required. If there is some leakage from the system, extra CO_2 needs to be added to the system eventually. The buffer volume dictates the length of time between recharging.
- The separator can also be used for recovering oil if oil is used in system.

Special Design Features / Criteria: The separator diameter was designed to provide a low enough vapour velocity so that the liquid droplets being carried by the vapour can separate out under gravity. A vertical separator was used to provide a more stable thermosiphon effect. The saturated CO_2 vapour at the top of the separator passes through a wire mesh, which assists in the coalescence and separation of liquid droplets. Four 25 mm (1") sight glasses were placed on the separator to assist in determining the CO_2 liquid level. These were PresSure Products, Bull's Eye sight glasses.

Figure 4.6 shows the mechanical drawings for the separator. The detailed specifications are given in Table 4.4.

Table 4.4: Detailed Separator Specifications

Contents	CO_2
Height	1.882 m
Outside Diameter	219.1 mm (200 NB)
Wall Thickness	12.7 mm
Inside Diameter	193.7 mm
Volume	55 L
Design Pressure	100 bar
Operating Pressure	30 bar
Hydrostatic Test Pressure	150 bar
Design Temperature (max/min)	50°C / 0°C
Separation Velocity	0.180 m/s
Separation Distance	0.6 m
Charge Volume (min)	18.1 kg (15 L liquid)
Charge Volume (max)	21.3 kg (19 L liquid)

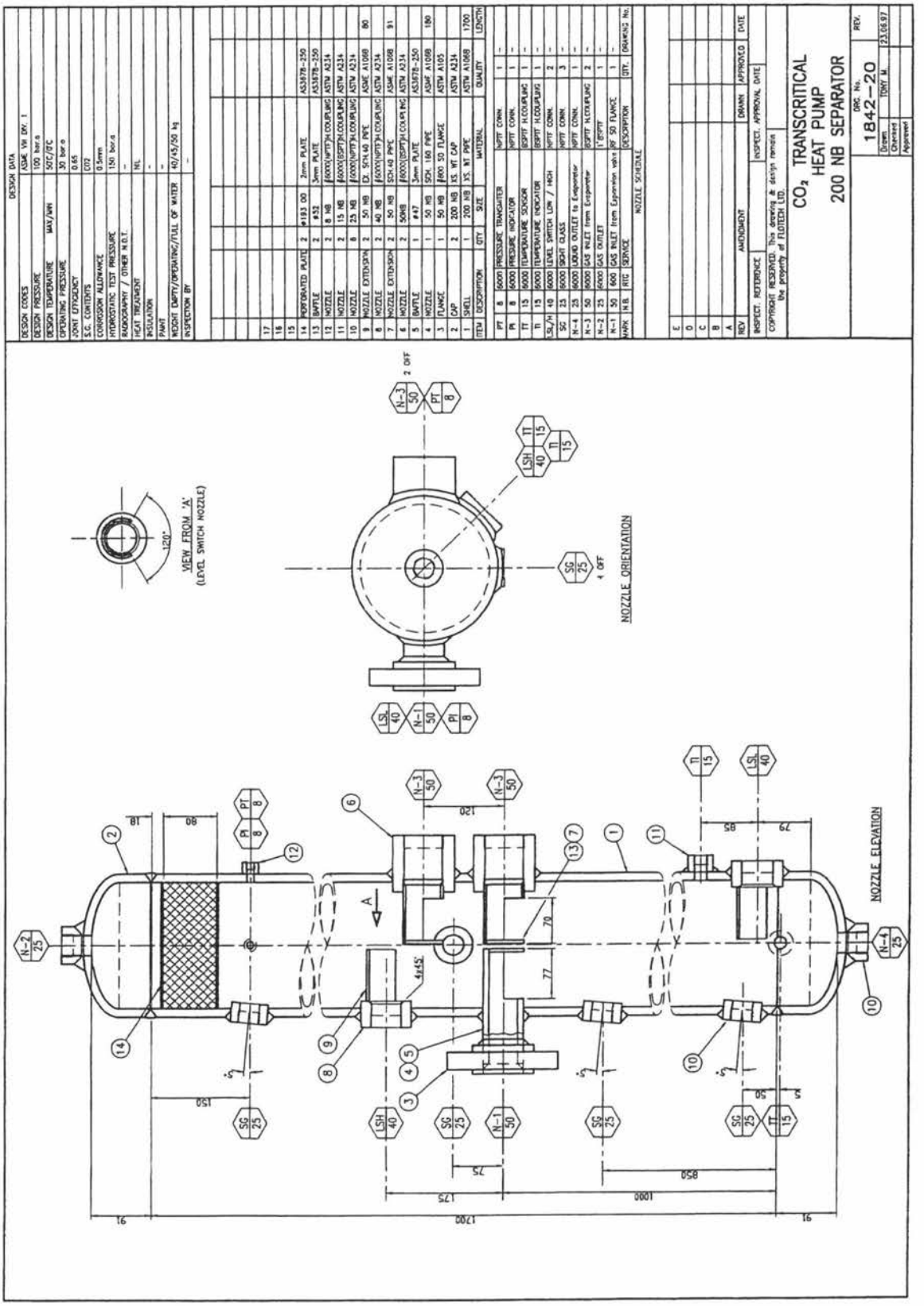

Figure 4.6: Mechanical Drawings for Separator

4.3.7 Piping

Pipe selection represented a compromise between higher pressure drops and hence lower energy efficiency with small pipe sizes, and higher capital cost with larger pipe sizes (especially as the wall thickness to cope with the high operating pressure increases with pipe size). The piping for CO_2 vapour was designed to give a 10 m/s maximum velocity except for the evaporator piping (discussed below). Due to the high pressure of the transcritical CO_2 system, higher pressure drops can be tolerated than for lower pressure systems. The water lines were designed for a maximum velocity of 2 m/s. The pipe specifications are given in Table 4.5.

Table 4.5: Pipe Sizes and Types

Location	Type	Size	Length	Bends
Compressor to Cooler 1	Stainless steel tube	19 mm (¾")	3300 mm	2 × 45° bend 4 × 90° bend 1 × 90° elbow
Cooler 1 to Cooler 2	Stainless steel tube	12.7 mm (½")	230 mm	2 × 90° bend
Cooler 2 to Cooler 3	Stainless steel tube	12.7 mm (½")	230 mm	2 × 90° bend
Cooler 3 to recuperator	Stainless steel tube	12.7 mm (½")	1770 mm	8 × 90° bend
Recuperator to Expansion Valve	Stainless steel tube	12.7 mm (½")	2030 mm	3 × 90° bend
Separator to Evaporator	Stainless steel tube	25 mm (1")	1730 mm	3 × 90° bend 1 × 90° elbow
Evaporator to Separator	Carbon steel pipe	48.3 mm (1½"/40 NB) 60.3 mm (2"/50 NB)	680 mm 2110 mm	2 × 90° elbow 1 × 90° elbow 1 × Tee
Separator to Recuperator	Carbon steel pipe	33.4 mm (1" / 25 NB)	3270 mm	4 × 90° elbow
Recuperator to Compressor inlet	Carbon steel pipe	33.4 mm (1"/25 NB)	2140 mm	5 × 90° elbow
Gas Cooler water	Galvanised steel pipe	33.4 mm (1"/25 NB)		
Evaporator water	Galvanised steel pipe	48.3 mm (1½"/40 NB)		

4.3.7.1 Thermosiphon

The only part of the system where liquid CO_2 should exist is in the separator, evaporator and connecting tubework. Circulation of CO_2 in this part of the system is by thermosiphon.

A thermosiphon is the natural recirculation of fluid. The driving force for the thermosiphon comes from the hydrostatic pressure difference between the liquid above the inlet to the evaporator and the liquid-vapour mixture in the evaporator exit line. The CO_2 flowrate adjusts so that the friction pressure drop caused by the fluid flowing through the pipe lines and fittings, as well as the heat exchanger, equal this hydrostatic pressure difference.

A spreadsheet was created to work out the pipe diameters that should be used for the thermosiphon using the Darcy and the Lockhart & Martinelli equations (Perry's Chemical Engineers' Handbook, 1984). The spreadsheet estimated the separator height required for given pipe diameters and liquid overfeed rates at design conditions.

It was decided to use 25 NB (1") tube for the inlet, 2 × 40 NB (1 ½") pipes for the outlet converging to a 50 NB (2") tee with a 50 NB pipe returning the fluid to the separator. Given that the separator liquid level was 1.2 m above the bottom of the evaporator in a fully charged condition, these pipe sizes were estimated to correspond to a liquid overfeed rate of 2 : 1 at the design conditions, if it is assumed that the pressure drop across the evaporator was constant. Appendix A.1 - Thermosiphon Calculation shows the calculations. This overfeed is slightly lower than generally recommended as optimum for promoting heat transfer (Stoeker, 1988), but would minimise the likelihood of liquid logging in the vertical return piping from the evaporator.

4.3.7.2 Oil Return System

For this system, the oil was returned via a 6.3 mm (¼") tube from the bottom of the evaporator to the compressor suction line, with the flowrate controlled by a needle valve. A 19 mm (¾") orifice plate was placed in the compressor suction line to create a slight pressure difference between the evaporator and compressor suction to promote flow through the oil return line.

4.3.8 Valves

Many valves had to be quite specialised due to the combination of high pressures and low temperatures used in the system. All isolation valves on the CO_2 and water sides were ball valves as they give low pressure drops when fully open, and can be opened and closed quickly. Full-bore ball valves were used for the thermosiphon lines to reduce frictional head loss. Needle valves were only used as vents to the atmosphere, and to isolate pressure gauges. Valve specifications are given in Table 4.6.

Table 4.6: Valve Types and Positions at Start-Up

Valve Location	Type	Size	Valve Position
Compressor discharge to suction bypass valve	Ball	12.7 mm (½")	Open until oil pressure established
Before expansion valve	Ball	12.7 mm (½")	Open
Separator outlet	Ball	25.4 mm (1")	Open
Vent at top of separator	Needle	12.7 mm (½")	Closed
Vent at bottom of separator	Needle	12.7 mm (½")	Closed
Charging valve on evaporator inlet line	Ball	12.7 mm (½")	Closed
Cold water inlet	Ball	38 mm (1 ½")	Open
Discharge pressure gauge	Needle	6.3 mm (¼")	Open
Expansion valve inlet gauge	Needle	6.3 mm (¼")	Open
Separator pressure gauge	Needle	12.7 mm (½")	Open

4.3.9 System Charge

The system volume was calculated to be 96 L based on the geometry for each component in the system. CO_2 densities were calculated for each of these sections from the nominal operating conditions and the CO_2 thermodynamic property calculations. For the evaporator it was assumed that 67% of the volume was liquid under normal operating conditions. Hence the mass of charge for each section was calculated, and summed to estimate that the total charge of the system was 39 kg. The likely liquid level fluctuation in the separator was estimated by using the likely maximum and minimum densities for the low and high side (minimum low side and maximum high side densities give lowest level and vice versa). It was shown that even under extreme variations in operating conditions, the fluctuation in separator liquid level would be less than 100 mm. The detailed calculations for the charge in the system are shown in Appendix A.2 - System Volume and Charge.

4.3.10 Compressor

A Knox Western TP 65 compressor (Figure 4.7) was chosen as it could operate at the desired pressure and was cost effective. It is an open crankcase compressor with a splash-lubricated crank. The compressor is double acting, ie. it compresses CO_2 on both the forward and backward strokes. This meant that a connecting rod and crosshead had to be used to connect the crank to the piston rod, along with a piston rod packing. The compressor had two suction and two discharge valves. Table 4.7 summarises the compressor specifications at design conditions.

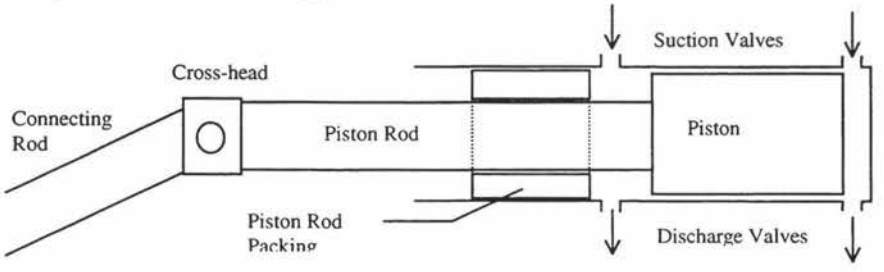

Figure 4.7: Schematic Diagram Showing the Knox Western TP65 Compressor

As the crankcase is effectively open to the atmosphere, an important issue was the seal obtained between the packing and piston rod. Because the compressor is to be used in a closed system, any leakage of the CO_2 charge will ultimately need to be replaced. The packing consisted of 3-piece graphite seals held in place by metal sleeves. Initially, the CO_2 side of the packing was operated oil free to eliminate the problem of oil accumulating in the lines and loss of heat transfer performance in the heat exchangers. Later, oil was added to the system in an attempt to improve the seal performance.

Lack of rod reversal was initially thought to be an issue because of the unusual conditions at start-up. Rod reversal occurs when the discharge pressure is significantly greater than the suction pressure, so the crosshead pin joining the connecting rod to the crosshead moves around the hole, thereby lubricating the pin. When the pressures are similar, the piston pushes against little resistance, so the crosshead pin is constantly on one side of the hole, and rod reversal doesn't occur. This means that oil cannot get completely round the pin, resulting in much greater wear on one side of the hole. This can ultimately lead to failure of the compressor. It was confirmed that rod reversal would not be a problem because a significant pressure difference would quickly establish on start-up.

With the early trials on start-up the discharge pressure tended to build up extremely quickly, which resulted in a large compression load being placed on the compressor and extremely high starting torque for the motor. This load proved to be excessive for the motor selected, preventing it from reaching normal operating speeds. To overcome this effect, a 12.7 mm (½") bypass line between the compressor suction and discharge was installed to reduce the load on the compressor during start-up. Once the compressor reached normal operating speed, the bypass line was isolated by a valve. A manual valve was used for all tests carried out, but for commercial purposes it was envisaged that a solenoid valve could be used to regulate the process air line to the expansion valve. Using the solenoid valve, the control system would leave the expansion valve fully open on start-up thus unloading the compressor, and allow the expansion valve to resume normal operation once the compressor was up to operating speed.

4.3.11 System Oil

The requirements of the oil were:

- Very low viscosity both at high and low temperatures to enable easy return of the oil from the evaporator
- Miscibility with CO_2 to assist in carry-through of oil through the systems
- Slightly greater density than CO_2 to assist in separation.
- Resistant to oxidation
- Resistant to thermal degradation

The specifications for the oil chosen for this application are given in

Table 4.8. This oil was developed specifically for refrigeration systems with flooded type evaporators. One of its main applications is with reciprocating compressor systems operating at very high temperatures and for systems with very low evaporator temperatures. For the trials with oil, 1.25 L of oil was added via the charging point at the high pressure inlet to the recuperator.

Table 4.7: Compressor Specifications

Knox Western TP 65

Bore Size	2.25" (57.15 mm)
Rod Diameter	1.125" (28.58 mm)
Stroke	4" (101.6 mm)
Swept Volume	0.513 L
Design flowrate	0.436 kg/s
Stages	1 (double acting)
Suction Pressure	30 bar
Discharge Pressure	130 bar
Pressure ratio	4.33 : 1
Suction Temperature	10°C
Discharge Temperature	141.6 °C
Suction Density	72 kg/m^3
Design (Maximum) Speed	1200 rpm
Minimum Speed	600 rpm
Power requirement	40.4 kW
Nominal Volumetric Efficiency	0.59
Nominal Isentropic Efficiency	0.73

Table 4.8: Lubrication Oil Specifications

Mobil Gargoyle	Arctic SHC 226E
Density at 15°C	830 kg/m^3
ISO grade	68
Viscosity	66 cSt @ 40°C 10 cSt @ 100°C
Pour point	<-45°C
Flash point	266°C

4.3.12 Motor and Drive

The compressor motor used was a Teco IP55. This was a 6 pole motor, with a 45 kW rating. It ran on 400V, 50 Hz, 3 phase supply, at a nominal speed of 970 rpm. The motor speed was controlled by a Vectron OMNI-Verter OD4-150 Variable Speed Drive. This had a 150% overload capacity, and was rated to 55 kW. The motor and compressor were coupled directly using a flexible disc type of coupling.

4.4 Control

Figure 4.8, the Process and Instrumentation Diagram (P&ID), shows the instrumentation and control for the CO_2 heat pump. As well as operating the heat pump automatically and safely, the control system must allow the system to be controlled as both a heat pump and a refrigeration system. Hot water storage is relatively inexpensive compared with storage of refrigeration, so the broad strategy was to control the refrigeration capacity first, and let the water heating capacity vary, but to ensure that any water heating satisfied a minimum water temperature criteria.

A Programmable Logic Controller (PLC) controlled all the general operating and safety functions, whilst there were separate control loops for each of the refrigeration and water heating functions.

4.4.1 Refrigeration Control

It was anticipated that the heat pump would be used to supply refrigeration to a wide range of applications, so a simple and universal control mechanism was sought. It was decided to control low side pressure (evaporation pressure). This type of control is commonly employed for large scale refrigeration systems with multiple applications. In addition, although it does not provide direct control of the application temperature (ie. chilled water temperature), such a scheme can be easily adapted to do so by using the application temperature as the control variable instead of pressure.

The pressure (and therefore temperature) on the low pressure side of the system was controlled by varying the compressor speed. The signal from the separator pressure transmitter (Table 4.17 give the specifications) goes to a PID controller (Watlow 965a-3kf0-00rg) which controls the variable speed drive. Increasing the compressor speed acts to decrease the compressor suction pressure and hence the low side pressure. Conversely, decreasing compressor speed acts to increase the low side pressure. Therefore if the low side pressure is below its set-point, the controller will decrease the compressor speed, and if above the set-point, it will increase the compressor speed. The PID constants could be set using an autotune function or set manually. During performance trials the compressor speed was manually controlled.

4.4.2 Water Heating Control

The heat pump discharges CO_2 as a supercritical vapour, so pressure and temperature are independent of each other. Also, the refrigeration control strategy may change the CO_2 flowrate through the system, and therefore the potential available heating capacity. This meant a two stage control of water heating was necessary. The first stage is discharge pressure control to ensure that the CO_2 discharge conditions are such that both the desired water temperature is thermodynamically feasible and the energy performance of the whole system is maximised. The second part is control of gas cooler water flowrate to give the desired hot water outlet temperature.

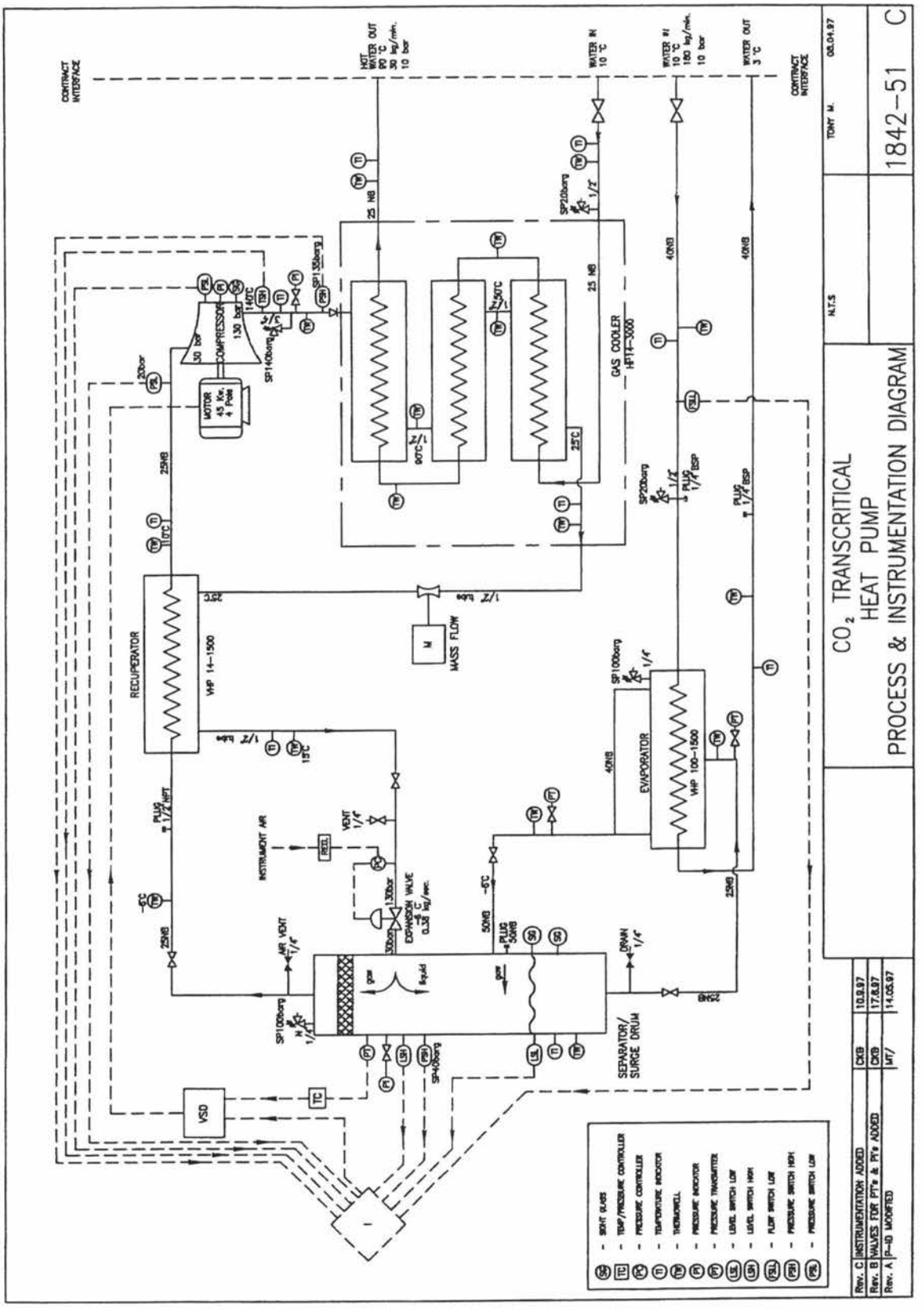

Figure 4.8: Process and Instrumentation Diagram (P&ID)

4.4.2.1 Discharge Pressure Control

Discharge pressure must be controlled to provide a sufficiently high CO_2 discharge temperature to allow the desired hot water temperatures to be reached, yet as low as possible to maximise energy efficiency. The discharge pressure was controlled by a standalone backpressure control loop (Table 4.9). This uses the signal from the discharge pressure transmitter to control the expansion valve actuated using compressed air via a Wizard Controller (high CO_2 pressure causing the valve to open and low CO_2 pressure causing valve to close). The design discharge pressure set-point was 130 bar. The set-point was manually adjusted for the prototype but it was envisaged that the set-point could be automatically adjusted if a more sophisticated controller was used. For example, a number of authors (Liao and Jakobsen, 1998; Lorentzen *et al*, 1991) describe how the optimal discharge pressure to maximise system efficiency can change with operating conditions.

The Wizard controller is an air actuated system. Essentially, it uses the CO_2 discharge line pressure to regulate the supply of air from a compressed air supply to the valve actuator. The expansion valve is fail close meaning that if the air supply to the valve is stopped the valve will close. Thus if the air supply was stopped, the valve would close, the discharge pressure would build up and the system would automatically stop due to the high discharge pressure trip.

Table 4.9: Discharge Pressure Control Equipment Specifications

Unit	Make	Model
Expansion Valve	Badger	807 – ½" (Fail Close)
Actuator	Badger	754 – ½"
Controller	Fisher	4160K Wizard Proportional plus Reset Controller

4.4.2.2 Water Temperature Control

The temperature of the outlet hot water from the gas cooler was controlled by adjusting the water flowrate. For the system performance trials, this was done using a manual needle valve. Ultimately automatic control would be desired so a thermostatic control valve (Honeywell Braukmann T100 R) was also installed, with the temperature sensor between the first and second gas coolers. Commissioning trials showed that this arrangement did not control the water outlet temperature adequately. To overcome this problem, the temperature sensor would need to be placed in the hot water discharge line to directly control the temperature. This was not implemented for the prototype because manual control was sufficient for the performance trials.

4.4.3 PLC and Safety Controls

4.4.3.1 Overview

A number of switches were installed to ensure the safe and efficient operation of the heat pump. All were connected to the PLC (Table 4.10). If any trip signal was received, the system was configured so that the fault indicator turned on, the compressor motor stopped and the expansion valve shut. Four indicator lights on the PLC indicated the fault type. Under trip conditions, the pressure in the system will naturally equilibrate as CO_2 leaks through the compressor, and as heat exchange with the surroundings occurs. Signals that initiated a system trip were:

- High compressor discharge pressure - this protects the compressor from overloading, as well as protecting the system from over pressurisation.
- Low compressor suction pressure - this protects the compressor from operating with an excessive pressure ratio and from being starved in case the manual valve in the suction line is closed.
- Low separator level - this ensures adequate head for the thermosiphon and safeguards against low CO_2 charge.
- High separator level - this protects the compressor from liquid slugs entering the suction line and overcharging with CO_2.
- High separator pressure - protects the separator from overpressurisation.
- Low evaporator water flow - this provides protection against water freezing in the evaporator.
- Low compressor oil pressure - ensures adequate lubrication of the crankcase side of the compressor.
- High compressor discharge temperature - protects the compressor and system from high temperatures.
- VSD fault - protects the compressor motor from overloading.

There was also an emergency stop button that disconnects power from the PLC. This results in the run signal to the VSD being stopped, thus stopping the motor and shutting down the whole system.

Table 4.10: Programmable Logic Controller and Expansion Unit Specifications

Make	Idec
Model	Micro-1
Type	FC1A E2A1E
Input	8 channels each for PLC and expansion unit (16 total). 24 VDC 5 mA
Output	6 channels each for PLC and expansion unit (12 total). 220 VAC/30VDC 2A

The PLC programme enabled starting and stopping, as well as the tripping of the system if faults occurred. The system was prevented from being restarted until it was reset if a fault occurred. The delays given in Table 4.11 were used for certain switches to prevent the system tripping on start-up, as well as to only trip the system after a fault had occurred for a certain period of time.

Table 4.11: Fault Delays Used by the PLC

	Delay from Start-up (s)	Delay on Trip (s)
High compressor discharge pressure	0	2
Low compressor suction pressure	0	5
Low separator level	0	5
High separator level	60	5
High separator pressure	60	10
Low cold water flow	0	5
Low compressor oil pressure	30	1
High compressor discharge temperature	0	2
Run fault	0	5
VSD fault	0	1

4.4.3.2 Switches

All switches were set to be fail safe, ie. they are closed during normal operation (sending a signal), and open during trip conditions or if there is a break in the line or power supply. The detailed specification of the pressure, level and flow switches and their set-points are given in Table 4.12.

The original level switches were rated to 1500 psi (100 bar), but the hollow stainless steel floats imploded under the combination of high pressure and low temperature. The level switches specified in Table 4.12 had solid plastic floats and were used for all performance testing trials.

Two types of power failure can occur with the system: single or 3 phase power failure. Single phase power failure results in the shut down of the PLC. Three phase power failure results in the compressor motor stopping. In either event, the control system and switches provided appropriate shut-down of the prototype.

4.4.3.3 Pressure Relief Valves

In addition to the PLC safety controls, independent pressure relief valves were installed to ensure the safety of the system even in the event of the PLC failing. Nupro pressure relief valves were used for all applications. The details of the pressure relief valves used are given in Table 4.13.

The compressor discharge pressure relief valve was a backup for the pressure switch, in case the switch failed, or the pressure increased too quickly. Separator and evaporator pressure relief valves were used to prevent the overpressurisation of these components if significant heating occurred when the system was not operating. The relief valves were designed to discharge CO_2 at a rate so that the pressure quickly dropped below the set-point. The valve would then reseat to prevent complete loss of CO_2 charge.

Table 4.12: Switch Specifications

		Make	Model	Range	Set-point	Switch Type
Pressure Switches	Compressor Discharge	Telemecanique	Nautilus	10 160 bar g	140 bar g	High Pressure
	Separator	Telemecanique	Nautilus	5 70 bar g	40 bar g	High Pressure
	Compressor Suction	Telemecanique	Nautilus	5 70 bar g	20 bar g	Low Pressure
	Oil Pressure	Telemecanique	XMJ-AO127	1 12 bar g	3 bar g	Low Pressure
Level Switches		Linc	471-02	5000 psi (350 bar.g)		High/Low Level
Flow Switch		Honsberg	Fluvatest CR25 V			Low Flow
Temperature Switch		Danfoss		70 150°C	145°C	High Temperature

Table 4.13: Pressure Relief Valve Specifications

Location	Model	Set-point
Compressor Discharge	R3A SS4R3A5 (1/4")	150 bar.g
Separator	R3A SS4R3A5 (1/4")	100 bar.g
Evaporator	R3A SS4R3A5 (1/4")	100 bar.g

4.5 Instrumentation and Data Acquisition

The prototype was fully instrumented so that the performance of each component and of the overall system could be accurately measured. Figure 4.9 shows the instrumentation and data acquisition system.

4.5.1 Temperature

Temperature indicators were used to give an indication of the process conditions to the operator, as indicated in Table 4.14. Teltherm 63 mm dial gauges (model 3CC) were used for all temperature indicator applications. These gauges had an accuracy of ± 1% of full scale. The temperature gauges were calibrated by placing them in an ice point, and zeroing the scales to 0°C.

During commissioning trials, type T thermocouples were also used at the locations indicated in Table 4.14. The thermocouples were calibrated using two points (0°C using ice water and 100°C using boiling water). Offset and scaling factors were then calculated for each thermocouple from the values recorded by the data logger. The accuracy of the thermocouples was estimated to be ± 0.3°C.

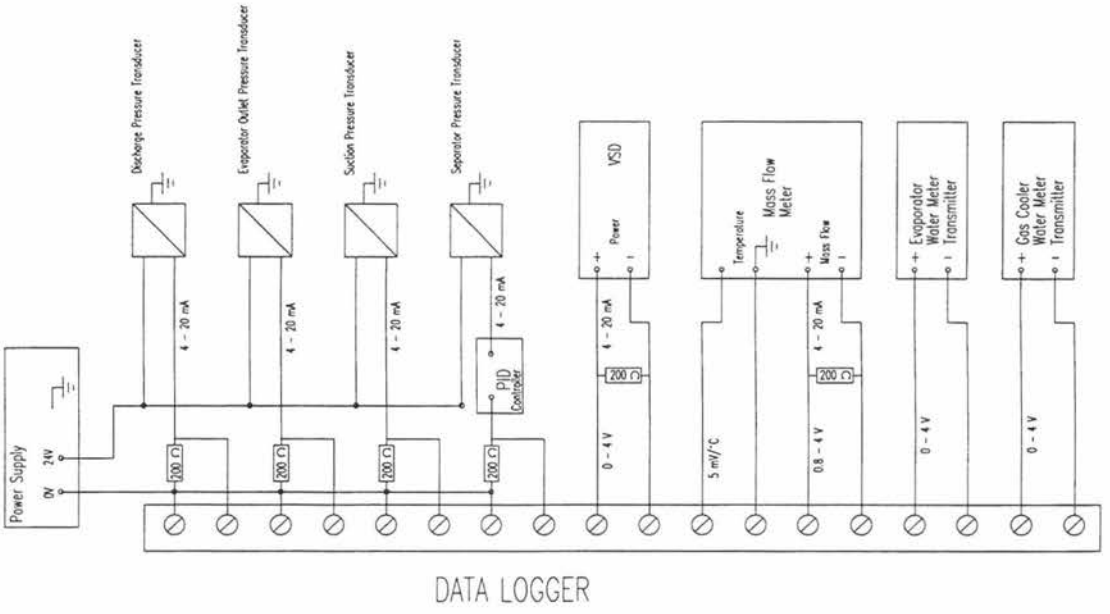

Figure 4.9: Data acquisition system

Table 4.14: Temperature Indicator Locations and Specifications

Location	Range	Accuracy (°C)
Compressor discharge	0 – 150°C	± 1.5
Pre expansion valve	0 – 50°C	± 0.5
Separator	-20 – 40°C	± 0.6
Cold water in	-20 – 40°C	± 0.6
Cold water out	-20 – 40°C	± 0.6
Hot water in	-20 – 40°C	± 0.6
Hot water out	0 – 120°C	± 1.2
Compressor suction	-20 – 40°C	± 0.6

To reduce measurement inaccuracy due to heat losses and poor contact between temperature sensors and the fluid being measured, thermowells were used for all temperature measurement. These consisted of a 6.4 mm (¼″) piece of tube inserted in plugs with 6.4 mm (¼″) holes drilled through. The thermocouple wire was inserted and the end of the tube sealed by crimping and soldering. These plugs (of various sizes) were then screwed in to the appropriate places on the heat pump. Where there was no fitting for the thermowell, a hole was drilled and a nut welded over the hole to provide a sensor holder.

4.5.2 CO_2 Flowrate

A mass flow meter was used to measure both the CO_2 flowrate and the temperature at the exit from the gas cooler. Table 4.15 gives the specifications. The mass flow meter, which was a coriolis type, consisted of a U-tube vibrated at its natural frequency. The coriolis effect from the fluid flowing through the tube imparts a twist on the tube. This twist is proportional to the mass flowrate. The temperature output signal was 5 mV per degree Celsius above 0°C, and it measured temperatures in the range –240 to 204°C.

The mass flow meter was placed on the high pressure side after the coolers. This was because the meter can only handle single phases and, at this point, only supercritical CO_2 existed. Also, after the coolers it would not be exposed to the high discharge temperature of the compressor.

The mass flow meter was calibrated by Micromotion using a standing start finish method using water. A calibration certificate was supplied with the mass flow meter. This indicated an error of 0.053% at 100% of full flow, 0.148% at 50% of full flow (close to the design flowrate for the heat pump) and 0.372% at 25% of full flow. Overall, the accuracy was taken as ± 0.2%

Table 4.15: Mass Flow Meter Specifications

Meter	Micromotion DH1000S-925-S-M
Transmitter	Micromotion RFT9712-2-P-N-M
Measured range	0-0.833 kg/s
Maximum CO_2 flowrate required	0.43 kg/s
Accuracy	0.2% of rate
Output signal range	4-20 mA
Maximum signal required	12.256 mA
Resistor nominal value	270 Ω
Voltage output (to max required)	1.080 - 3.309 V

4.5.3 Pressure

4.5.3.1 Pressure Indicators

Teltherm 63 mm 3025SS gauges were used for all pressure gauge applications as indicated Table 4.16. The accuracy of these gauges was ± 2% of full scale.

Table 4.16: Pressure Indicators

Location	Range	Accuracy (bar)
Compressor discharge	0 - 160 bar g	± 3.2
Pre expansion valve	0 - 160 bar g	± 3.2
Separator	0 - 100 bar g	± 2
Compressor oil	0 - 25 bar g	± 0.5

4.5.3.2 Pressure Transducers

Four pressure transducers were used on the heat pump as indicated in Figure 4.8. A Sensit transducer (Table 4.17) was used for all low pressure locations (on the separator, evaporator exit and compressor suction). The compressor discharge pressure transducer was a Kamstrup model (Table 4.18), and was placed after the coolers to lower the temperature the transducer experienced.

The pressure transducers were calibrated against a P-tronic calibrated pressure gauge by opening all valves in the system and letting the whole system equilibrate to various pressures (0 bar g plus 3 other pressures) without the compressor operating. The output signals from the pressure transducers were measured for each system pressure, and offset and scaling factors were calculated by linear regression. The accuracy of the transducers was estimated to be about ± 1 bar.

Differential pressure measurement between the evaporator and separator, and between the separator and compressor suction were carried out by connecting the voltage outputs together, with the resultant voltage being proportional to the pressure difference between the two transducers.

Table 4.17: Sensit Pressure Transducer

Model	M6420
Output	4 -20 mA
Compensated Temperature Range	-10°C to 80°C
Operating Temperature Range	-25°C to 100°C
Non linearity, Hysterisis and Repeatability	<±0.25% of span
Thermal zero shift	<±0.015% of span / °C
Thermal span shift	<±0.008% / °C
Measured range	0-100 bar g
Maximum pressure required	80 bar g
Output signal range	4-20 mA
Maximum signal required	16.8 mA
Resistor nominal value	220 Ω
Voltage output (to max required)	0.880 – 3.696 V

Table 4.18: Kamstrup - Metro Pressure Transmitter

Output	4 –20 mA
Operating Temperature Range	-25°C to 70°C
Accuracy	0.5%
Response Time	0.6 s
Hysterisis	<0.1% of span
Temperature Drift	<0.04% / °C
Measured range	0-160 bar
Maximum pressure required	145 bar
Output signal range	4-20 mA
Maximum signal required	18.5 mA
Resistor nominal value	220 Ω
Voltage output (to max required)	0.880 – 4.070 V

4.5.4 Power Consumption

Power, energy use and other electrical data for the electric motor was available from the VSD via two analogue output channels. The output channels could output any variable that could be recorded by the VSD, depending on what was selected in the VSD programme. Only one channel was used to measure the real output power from the VSD as given in Table 4.19.

Table 4.19: Power Consumption Monitoring

Analogue output	Power
Measured range	0-52 kW
Output signal range	4-20 mA
Resistor nominal value	180 Ω
Voltage output	0.720 – 3.600 V

4.5.5 Water Flowrate

Measurement of both the gas cooler (hot) and evaporator (cold) water flowrates was required to estimate the heating and cooling capacity of the prototype. Details of the flowmeters used are given in Table 4.20. Frequency transmitters (Table 4.21) converted the pulse rate from the meters to a voltage signal. The water flow meters were placed in the water lines on the water inlet side so they would not have to deal with extremes in temperature. They were calibrated by the timed collection of a measured mass of water. This value was compared to both the numerical reading from the water flow meters themselves, as well as the signal from the flow transmitters to provide calibration. Overall, the water flowrates were considered to be accurate to within ± 2%.

Table 4.20: Water Meter Specifications

	Gas Cooler Water	Evaporator Water
Make	Kent	Kent
Model	PSM Water Meter	Helix 3000 Cold Potable Water Meter
Size	25 mm	40 mm
Output	2 Pulses/litre	High Resolution Pulser (uses optical sensor) 1 Pulse/litre

Table 4.21: Frequency Transmitter Specifications

Make	Intech Instruments	Intech Instruments
Model	PI-F (Programmable Isolating Frequency Transmitter)	PI-F
Input	0 – 1 Hz	0 – 4 Hz
Output	0 – 4 V	0 – 4 V

4.5.6 Data Acquisition

The output signals from the instrumentation were all connected to a common termination block. For current signals, appropriate resistors were placed between connections on the termination block to convert mA signals to voltage. This voltage drop could then be measured by a data logger (Table 4.22) or manually with a voltmeter.

The data logger also allowed thermocouple scales as well as voltage. If these were selected, the data logger would automatically use the cold junction compensation to output a temperature in °C. Thermocouples were connected directly to the analogue to digital converter to avoid the effect of the dissimilar metal connections on the reading.

Table 4.22: Data Logger Specifications

Company:	Computer Instrumentation Ltd.
Series:	MiniPOD
Model:	Supreme
Channels	30 single analogue inputs 3 double analogue outputs 8 logic inputs 8 logic outputs

5 EXPERIMENTAL PROCEDURE

5.1 Commissioning and Preliminary Trials

5.1.1 Commissioning

The prototype was fully commissioned before performance measurement trials began. This involved:

(a) Leak Testing and Charging:
Once the pipework was put together, the system was pressured with water to find leaks. Leaks were fixed by tightening the pipework or tubework. The system was then run on air for two hours with the inlet to the compressor fitted with a filter to remove contaminants in the system. The heat pump was then purged with CO_2. The vents to atmosphere were opened, as was part of the tubing bypassing the compressor, and CO_2 from a standard bottle was discharged into the low pressure side of the system via the charging valve between the evaporator and separator. After a minute, the vents and tubing were closed and the CO_2 bottle shut. The system was evacuated overnight using a vacuum pump. The system was then charged to the bottle pressure (saturation pressure at ambient temperature) with vapour to provide a holding charge.

Full charging of the system involved running the system to reduce the pressure in the low-side of the prototype thus drawing in CO_2. The CO_2 bottles were connected to the system via a flexible hose to the charging valve on the evaporator inlet line. A number of different charging systems were tried. Charging using normal CO_2 bottles (drawing vapour off the top) was used, but this proved far too slow. The bottles were then used upside down to allow liquid CO_2 to enter the system. This lead to a good charging rate, but proved awkward when it came to changing bottles. Finally, CO_2 bottles with tubes running from the bottle valve to the bottom of the bottle (BOC GE type) were used. This was a convenient method which resulted in liquid CO_2 entering the low side, quickly filling the separator with liquid. Liquid charging was considered safe because the charging valve was in the thermosiphon loop, so the compressor was protected from liquid slugs by the separator.

The system was considered fully charged when the liquid level was about half way between the low level switch and evaporator return line in the separator, and the compressor was running with a discharge pressure above 100 bar.

After charging, CO_2 leaks were detected by spraying soapy water on all joints. All switches and pressure relief valves were then set to the required settings.

The system was initially run for about 10 hours before any measurements were taken to make sure the compressor packing was worn in to provide a good seal with the piston rod.

(b) Programmable Logic Controller:
The Programmable Logic Controller (PLC) was programmed using Ladder Logic. The programme was entered into a computer, then transferred to EPROM via a hand loader. The programme on the EPROM was put into a unit designed to test PLC programmes. This consisted of a test PLC with a bank of switches that simulated inputs to the PLC. By activating these inputs and checking the right outputs were achieved, the programme could be verified. After testing the programme, it was transferred back to the hand loader, and then to the PLC itself. The final version of the ladder logic code is provided in Appendix A.3 - PLC Ladder Logic Code.

(c) Control:
The auto-tune function of the Watlow proportional integral derivative (PID) controller was tuned to ensure fast and stable response of the VSD to low side pressure changes. Auto-tune activates the system using on/off control at 90% of the set-point, and determines the PID constants from the speed of the response of the system. A slow auto-tune function was used to ensure stability of the system. For a 32.5 bar set-point, the proportional constant was 4.8% of span, the integral constant was 1.6 min/repeat, and the derivative constant was 0.02 min.

The Variable Speed Drive (VSD) needed to be tuned to ensure smooth starting and stopping of the compressor. This was performed by an expert from Vectron.

The Fisher Wizard controller for discharge pressure was also tuned to give a fast and stable response. The set-point was set by a manual dial, and the proportional and the reset (integral action), was adjusted by trial and error during the initial operation of the system.

(d) Packing Leakage:
Leakage of CO_2 through the compressor (via the piston rod packing) was found to be a major issue. There was substantial leakage both when the compressor was at rest and when running. A total of three different styles of packing were used (including water cooled packing), but none lead to significant improvement of the leakage. The system had to be continually charged during trials to keep the liquid level in the separator at a high enough level.

The rate of CO_2 loss was quantified through four different methods. Firstly, the system was shut down and the high side isolated (only vapour present). The discharge pressure was measured over time, and this (along with the temperature) was used to calculate the density of the CO_2. The volume of the system could then be used to calculate the mass of CO_2 at different times, and therefore the rate of loss of CO_2. Secondly, the time between the liquid level in the separator dropping from the high level switch to the low level switch after shut down was measured. Thirdly a rotameter was attached to the breather holes on the compressor and the gas flowrate was measured both during operation and when the system was stopped. Lastly, as an overall check the mass of CO_2 added to the system to maintain the CO_2 charge was measured along with the system run hours, enabling an average leakage rate to be determined.

(e) Miscellaneous Aspects:
The original separator used was 100 NB diameter and about 1.1 m high. It had a design separation velocity of about 0.81 m/s. Commissioning trials showed that liquid separation performance was inadequate. Liquid was being carried over to the compressor and the compressor discharge temperature was substantially lower than expected for the apparent suction condition (saturated or slightly superheated vapour). The lower discharge temperature was attributed to liquid present in the suction gas which evaporated as the gas was compressed. Apart from the low discharge temperature, there were no other apparent signs of liquid entering the compressor. However, it was likely that the liquid droplets were very small and therefore did not affect the compression cycle. The final separator design had both reduced separation velocity and greater separation distance to overcome this separation problem.

5.1.2 Start-Up Procedures

Before the system was run for each commissioning or performance trial, a pre-startup inspection was carried out. Air supply to the expansion valve and power to the instrumentation and VSD were checked. The manual ball valves at the separator exit and inlet to the expansion valve were slowly opened, and the positions of the rest of the valves checked. Water flow was then established in the evaporator and condenser. This ensured that residual water would not freeze in the tubes of the evaporator. The bypass valve was opened to reduce the load on the compressor, enabling the compressor to gain momentum at start-up.

At this point, the motor was started by giving the start signal to the PLC, and the VSD ramped the motor speed up to the level set by the Watlow suction pressure controller. Once compressor oil pressure had been established (this required the compressor to be running as the oil pump ran off the compressor) the unloading valve could be closed. This resulted in the discharge pressure building up until it reached the expansion valve set-point. The expansion valve then opened, releasing the charge to the low side. Water flow through the gas cooler was then manually adjusted to obtain the desired hot water temperature.

For commercial applications, the start-up would need to be automated. A solenoid valve would be placed in the air supply line to the expansion valve, causing the expansion valve to be open for a fixed period of time on start-up, thus unloading the compressor.

For each standard data collection trial, after a set-point had been changed, measurements were only taken after the system had been running at steady-state for at least 5 minutes. The system generally took less than 5 minutes to reach a new steady-state condition.

5.1.3 Shut Down Procedures

In order to minimise leakage through the compressor, the shut down procedure involved CO_2 being pumped into the separator and evaporator by closing the ball valve on the separator exit and keeping the compressor running. The system eventually would trip

on low suction pressure, and the high and low sides would then be isolated by closing the ball valve on the inlet to the expansion valve.

To prevent water freezing, the cold water flow to the evaporator was only turned off when the separator and evaporator CO_2 temperature rose above 0°C.

5.2 Performance Trials

It was desired to test both the performance of the individual components and of the overall prototype over a range of operating conditions. The main variables affecting the performance were:

- The desired hot water exit temperature,
- Discharge pressure, and
- Suction pressure (evaporation pressure and temperature).

In addition, it was desired to investigate the effect of evaporator water temperature and evaporator water flowrate, as well as the effect of oil on the component and system performance.

The hot water exit temperature was set by adjusting the gas cooler water flowrate using the manual needle valve. The factory water supply temperature of about 21°C ± 1°C, was used for the gas cooler water inlet temperature for all runs. Trials were carried out for three hot water discharge temperatures: 90°C, 77.5°C, and 65°C. 90°C was used as this represents the desired temperature (allowing for heat losses) for processes such as in the meat industry where water greater than 82°C is required for sterilisation. 65°C represents more typical (eg. domestic) hot water temperature, while 77.5°C is the mid point between the two.

Discharge pressure was set directly using the Fisher controller (expansion valve). Discharge pressures were varied from 85 bar (lowest expected operating discharge pressure) to 130 bar (design conditions) in 5 to 10 bar steps.

In each set of trials, the discharge pressure was varied while keeping suction pressure constant. This was repeated for a number of suction pressures. To do this, it was necessary to choose suitable values for the suction pressure. The absolute minimum suction pressure is achieved with the highest discharge pressure and the highest compressor speed, and the absolute maximum at the lowest discharge pressure and lowest speed. While these suction pressures represent the extremes achievable with the equipment, these values could not be maintained for the full range of discharge pressures.

For trial purposes, suction pressures were chosen which were achievable over the entire range of other operating conditions. To obtain the highest suction pressure that could be used for the range of conditions, the compressor was operated at the lowest speed and highest discharge pressure. This allows the compressor speed to be increased to compensate for the increased suction pressure caused by lowering the discharge pressure. To obtain the lowest suction pressure, the compressor was run at the highest speed and lowest discharge pressure. A maximum suction pressure of 35.5 bar (0.7°C)

and a minimum of 29.6 bar (-6.1°C) were achieved in this manner, so these pressures, or the average of 31.6 bar (-2.5°C), were used for all trials.

The normal water supply temperature of about 21°C was also used as the evaporator water inlet temperature for most runs, but as the design inlet temperature was 10°C, it was decided that a lower temperature should also be used. This was achieved by mixing the factory supply with the evaporator outlet water in a tank and pumping the mixture through the evaporator. Figure 5.1 shows the modified evaporator water supply system. With this modified water supply system, the flowrate of the evaporator water was controlled by a manual valve in the inlet line for coarse adjustment, and by a manual valve controlling the water returned to the drum for fine adjustment. The temperature of the water was controlled by varying the amount of recirculation of the evaporator water. This set-up was only available after the first two sets of trials.

5.2.1 Constant Evaporator Water Flowrate Trials

The first set of trials was carried out with a constant evaporator water flowrate and the evaporator pressure was controlled by changing the compressor speed. These trials represent the case of operating with a particular process task (achieving hot water at a certain temperature for a fixed evaporator heat load).

The evaporator water flowrate and temperature was about 0.625 L/s and 20°C respectively. This flowrate was less than the design value because of pump limitations. The trials were carried out for the three suction pressures for the full range of discharge pressures.

A set of the above trials was carried out for each of the three hot water discharge temperatures. The full set of 63 trials including replicates is given in Table 5.1.

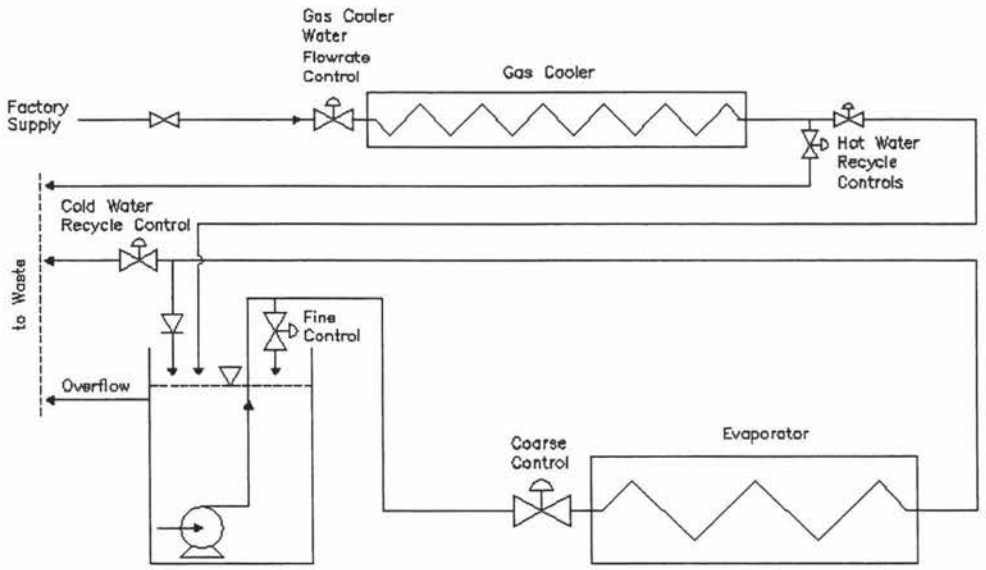

Figure 5.1: Evaporator Water Supply System

Table 5.1: Constant Evaporator Water Flowrate Trials

Trial No.	Order	Hot Water Temperature (°C)	Suction Pressure (bar g)	Discharge Pressure (bar g)
1	1	90	28.6	90
2	15	90	28.6	100
3	9	90	28.6	110
4	3	90	28.6	120
5	13, 25	90	28.6	130
6	7, 27	90	31.6	90
7	4, 17, 19, 21	90	31.6	100
8	10, 18, 24, 29	90	31.6	110
9	8, 16, 23	90	31.6	120
10	5, 28	90	31.6	130
11	6, 20, 22	90	34.5	90
12	14	90	34.5	100
13	12, 26	90	34.5	110
14	11	90	34.5	120
15	2	90	34.5	130
16	30	77.5	31.6	85
18	32	77.5	31.6	95
17	31	77.5	31.6	105
19	33	77.5	31.6	115
21	43	65	28.6	85
22	34	65	28.6	95
23	39	65	28.6	105
24	46	65	28.6	115
25	48	65	28.6	125
26	45, 55	65	31.6	85
27	35, 52	65	31.6	95
28	38, 51	65	31.6	105
29	44, 61	65	31.6	115
30	40, 54, 56, 63	65	31.6	125
31	50, 60	65	31.6	130
32	36, 53	65	33	85
33	41	65	33	95
34	49, 57	65	33	105
35	37, 62	65	33	115
36	42, 58	65	33	125
37	47, 59	65	33	130

The maximum suction pressure for runs with 65°C hot water was 33 bar.g. This was because the higher water flow required to achieve 65°C hot water cooled the high pressure refrigerant further compared with 90°C water, leading to a lower suction pressure, even at minimum compressor speed.

The trials were carried out in random order for each temperature. The replicates were carried out to assess experimental uncertainty and to check repeatability.

5.2.2 Constant Speed Trials

Constant speed trials were carried out to test the full load limits of the prototype. In these trials, the compressor speed was run at 100% of full speed, the discharge pressure set, and the desired suction pressure was achieved by varying the evaporator water flowrate. A larger pump was available for these trials, so higher evaporator water flows could be achieved than for the first set of trials (up to 1.5 L/s).

Trials were carried out in random order for the three hot water temperatures and the full range of discharge pressures. The full set of 37 trials, including replicates, is given in Table 5.2.

Table 5.2: Constant Speed Trials

Trial No.	Order	Hot Water Temperature (°C)	Suction Pressure (bar g)	Discharge Pressure (bar g)
38	6	90	28.6	90
39	11	90	28.6	100
40	4	90	28.6	110
41	8	90	28.6	120
42	9, 15	90	28.6	130
43	2, 16	90	31.6	95
44	7	90	31.6	100
45	5	90	31.6	110
46	14	90	31.6	120
47	10	90	31.6	130
48	1	90	34.5	100
49	13	90	34.5	110
50	3,17	90	34.5	120
51	12	90	34.5	130
52	18	77.5	28.6	85
53	20	77.5	28.6	95
54	21	77.5	28.6	105
55	30	77.5	28.6	110
56	24	77.5	28.6	120
57	22, 33	77.5	28.6	130
58	19	77.5	34.5	85
59	23, 29	77.5	34.5	95
60	27, 31	77.5	34.5	105
61	26, 32	77.5	34.5	110
62	28	77.5	34.5	120
63	25	77.5	34.5	130
64	35	65	28.6	80
65	34	65	28.6	90
66	36	65	28.6	100
67	38	65	28.6	115
68	37	65	28.6	125

5.2.3 Effect of Evaporator Water Flowrate and Inlet Temperature

These trials set out to assess the performance of the evaporator with different flowrates and temperatures.

A set of 12 trials was carried out varying the evaporator water inlet temperature along with the water flowrate to maintain constant suction conditions for a range of discharge pressures. Trials were carried out with evaporator inlet water at approximately 11°C and 15°C to supplement the earlier 20°C trials (Section 5.2.1). The evaporator water inlet temperature was first set, and the flowrate adjusted to achieve 34.5 bar g suction pressure at 130 bar g discharge pressure and the lowest compressor speed. This resulted in flowrates of 1.2 L/s for the 11°C water, and 0.9 L/s for the 15°C water compared with 0.625 L/s for the 20°C water. The compressor speed was varied to control variations in the suction pressure caused by changing the discharge pressure.

A hot water discharge temperature of 90°C was used for all trials. A 34.5 bar g suction pressure was only used as lower suction pressures led to the risk of the evaporator water freezing with the 11°C inlet water. The full set of trials plus replicates is given in Table 5.3.

5.2.4 Evaporator Design Condition Trials

None of the above trials were close to the design conditions because of evaporator water flowrate and temperature limitations. Nine trials were carried out as close to design conditions as possible to try to enable a closer comparison of the actual equipment performance to the design performance to be made.

The maximum evaporator flowrate that could be achieved with the water recirculation system was about 1.4 L/s when the temperature was 11°C, whereas the design conditions were 3 L/s and 10°C. Trials were conducted for hot water temperatures of 90°C and 65°C, with a suction pressure of 31.5 bar g achieved by varying the compressor speed. The full set of trials is given in Table 5.4.

Table 5.3: Effect of Evaporator Water Flowrate and Inlet Temperature Trials

Trial No.	Order	Evaporator Water Inlet Temperature (°C)	Hot Water Temperature (°C)	Suction Pressure (bar g)	Discharge Pressure (bar g)
69	3	11	90	34.5	95
70	2	11	90	34.5	105
71	5	11	90	34.5	115
72	4	11	90	34.5	125
73	1, 6	11	90	34.5	130
74	9	15	90	34.5	95
75	11	15	90	34.5	100
76	8	15	90	34.5	110
77	10, 12	15	90	34.5	120
78	7	15	90	34.5	130

Table 5.4: Design Condition Trials

Trial No.	Order	Hot Water Temperature (°C)	Suction Pressure (bar g)	Discharge Pressure (bar g)
79	3	90	31.5	95
80	1	90	31.5	110
81	2	90	31.5	120
82	4	90	31.5	130
83	5	65	31.5	85
84	7	65	31.5	95
85	6	65	31.5	105
86	9	65	31.5	115
87	8	65	31.5	125

Table 5.5: Performance Trials with Oil in System

Trial No.	Order	Hot Water Temp. (°C)	Suction Pressure (bar g)	Discharge Pressure (bar g)	Comp-ressor Speed	Evaporator Water Flow /Inlet Temp.	Comments
88	3	90	31.6	90	Variable	0.6 L/s 20°C	Constant Low load
89	1	90	31.6	100			
90	2	90	31.6	110			
91	5	90	31.6	120			
92	4	90	31.6	130			
93	6, 12	90	31.6	95	100%	Variable 20°C	High load with 90°C hot water
94	9	90	31.6	105			
95	13	90	31.6	110			
96	8, 10	90	31.6	120			
97	7, 11	90	31.6	130			
98	14, 17	65	28.6	85	100%	Variable 20°C	High load with 65°C hot water
99	15	65	28.6	95			
100	19	65	28.6	105			
101	18	65	28.6	115			
102	16	65	28.6	125			
103	23	90	31.6	90	Variable	1.4 L/s 11°C	As close to design conditions as possible
104	21	90	31.6	100			
105	22	90	31.6	110			
106	20	90	31.6	120			
107	24	90	31.6	130			
108	25	90	Variable	100	100%	1.6 L/s 20°C	Maximum load
109	26	90	Variable	120			
110	27	90	Variable	130			

5.2.5 Oil Trials

Due to the ongoing high rate of CO_2 leakage through the compressor packing, it was decided to investigate the effect of oil in the system. The oil was expected to enable the packing to obtain a better seal, as well as lubricate the compressor leading to less wear. The possible drawbacks of oil in the system are poorer heat transfer, especially in the evaporator (as the oil collects there), and difficulty in oil return, as the oil has to be taken from the evaporator and separator and transported back to the compressor.

Twenty-two trials were carried out with 1.25 L of oil in the system. The trial conditions were generally chosen to be the same as the oil free trials to enable a direct comparison to be made. The trial conditions are detailed in Table 5.5.

5.3 Data Analysis

The performance of the overall system and each component was determined by calculating heat balances using a spreadsheet. A separate sheet was used for each set of trials.

5.3.1 Thermodynamic and Transport Properties

Calculation of heat balances and estimation of heat transfer coefficients required both thermodynamic and transport properties for both CO_2 and water.

1. CO_2 Density: The Benedict Webb Ruben (BWR) equation of state (equation (5.1), Perry's Chemical Engineers' Handbook, 1984) was used to calculate the density of CO_2 in the vapour and liquid phases.

$$P = \rho RT + \left(B_0 RT - A_0 - \frac{C_0}{T^2} \right)\rho^2 + (bRT - a)\rho^3 + a\alpha\rho^6 + \frac{c}{T^2}\rho^3\left(1 + \gamma\rho^2\right)e^{-\gamma\rho^2} \qquad (5.1)$$

where:
P = Pressure (Pa)
T = temperature of fluid (K)
ρ = density of fluid (kg mol/m^3)
R = Gas constant (kg.m^2/kg mol.K.s^2)
A_0, B_0, C_0, a, b, c, α, γ = BWR constants (specific to fluid)

This equation of state was solved iteratively for density using a Microsoft Excel Macro (The source code is given in Appendix A.4 - BWR Macro).

A number of sets of constants have been published for CO_2, so predictions were compared with saturated CO_2 data given by ASHRAE (1993). The constants from Perry's Chemical Engineers' Handbook (1984) gave predictions that differed substantially from the ASHRAE data, with an average difference of 0.3% for vapour and 5% for liquid density. Similarly the constants of Reid *et al* (1977) gave predictions with an average difference of 0.3% for vapour and 5.1% for liquid. The constants given

by Bishnoi *et al* (1974) were chosen because they gave the closest match to the ASHRAE data (0.6% difference for vapour, 1.0% for liquid).

2. CO_2 Enthalpy: The BWR equation was manipulated (details are given in Appendix A.5 - Enthalpy Calculations) and substituted in the general equation for the deviation of the actual enthalpy from the enthalpy at standard pressure. This resulted in an explicit equation for the difference between actual enthalpy and the enthalpy at standard pressure as a function of pressure, density, and various constants specific to the substance involved.

$$H - H^0 = \Delta H' \tag{5.2}$$
$$= \left(2A_0 + \frac{4C_0}{T^2} - RTB_0\right)\rho + \left(\frac{3a}{2} - RTb\right)\rho^2 - \frac{6a\alpha}{5}\rho^5 + \left(\left(\frac{3}{\gamma} + \frac{\rho^2}{2} - \gamma\rho^4\right)e^{-\gamma\rho^2} - \frac{3}{\gamma}\right)\frac{c}{T^2}$$

where:
H = actual enthalpy (J/kg)
H^0 = enthalpy at standard pressure (J/kg)
$\Delta H'$ = difference between actual enthalpy and enthalpy at standard pressure (J/kg)

The ideal gas heat capacity equation (Reid *et al*, 1977) was integrated with respect to temperature to create an equation for change in enthalpy at standard temperatures and pressures.

$$H^0_2 - H^0_1 = \Delta H^0 = A(T_1 - T_2) + \frac{B\left(T_2^2 - T_1^2\right)}{2} + \frac{C\left(T_2^3 - T_1^3\right)}{3} + \frac{D\left(T_2^4 - T_1^4\right)}{4} \tag{5.3}$$

where:
H^0_1 = enthalpy at standard pressure for condition 1 (J/kg)
H^0_2 = enthalpy at standard pressure for condition 2 (J/kg)
ΔH^0 = difference between actual enthalpy and enthalpy at standard pressure (J/kg)
T_1 = temperature at condition 1 (°C)
T_2 = temperature at condition 2 (°C)
A, B, C, D = equation constants specific to fluid (from Reid *et al*, 1977)

To calculate the total enthalpy change from one temperature and pressure (condition 1) to another (condition 2), first the difference between the enthalpy at condition 1 (H_1) and the enthalpy at standard pressure (H'_1) was calculated ($\Delta H'_1$). The enthalpy change at standard pressure (ie. the ideal gas enthalpy change, $\Delta H°$) was then calculated, followed by the difference between the ideal gas enthalpy and the second condition ($\Delta H'_2$). The difference in enthalpies between conditions 1 and 2 can be expressed by:

$$H_2 - H_1 = \Delta H = \Delta H_1' + \Delta H^0 - \Delta H_2' \tag{5.4}$$

where:
ΔH = difference between enthalpy at condition 1 and enthalpy at condition 2 (J/kg)

This is illustrated in Figure 5.2.

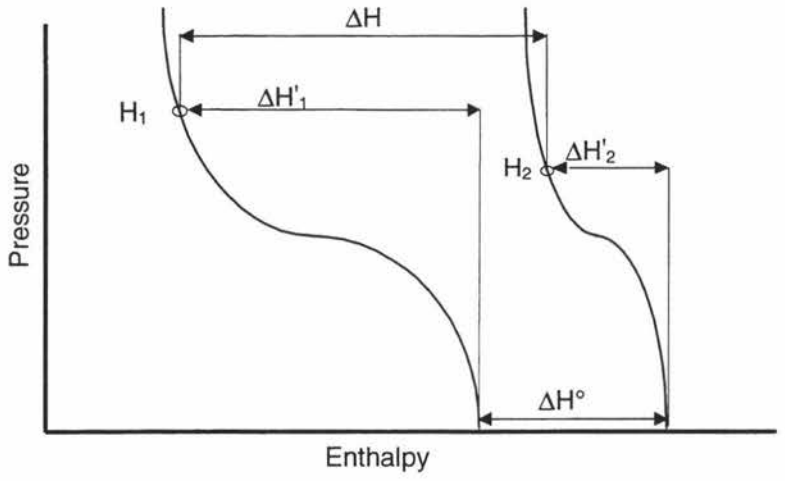

Figure 5.2: Calculation of Change in Enthalpy

All enthalpies were calculated relative to a datum of 0 kJ/kg for supercritical CO_2 at 15°C and 130 bar absolute. This is the point of lowest enthalpy at the design conditions (just before the expansion valve).

Trying to accurately predict the properties of CO_2 near the critical region is very difficult. This is due to the large change in many properties, as well as the lack of experimental data for CO_2 near the critical region. The lack of accurate data in this region means that there may be discrepancies between different data sources.

The simulation programme Hysis (Hyprotech, 1996 - version 1.1) was used to calculate enthalpies using other equations of state (Peng-Robinson and Soave Redlich-Kwong) to compare with the BWR method. Figure 5.3 shows the enthalpies predicted by the different equations of state over a range of operating temperatures at 130 bar. Predictions were not made between 40°C and 100°C because these temperatures lie between the gas cooler inlet and outlet temperatures and were not used in calculations for any trial. The BWR results were generally within 5 kJ/kg of the other equations of state at high temperatures, but tended to predict lower enthalpies by about 15 kJ/kg near the critical temperature. As there is no evidence in the literature that any of these equations of state are more accurate, the BWR method was retained, but the higher uncertainty near the critical temperature was noted.

3. CO_2 Specific Heat: The specific heat capacity for CO_2 was calculated by finding the enthalpy change for a 1°C increase in temperature.

4. CO_2 Viscosity and Thermal Conductivity: The viscosity and thermal conductivity were calculated using equations given by Vesovic *et al* (1990). These equations are given in Appendix A.6 - CO_2 Property Equations.

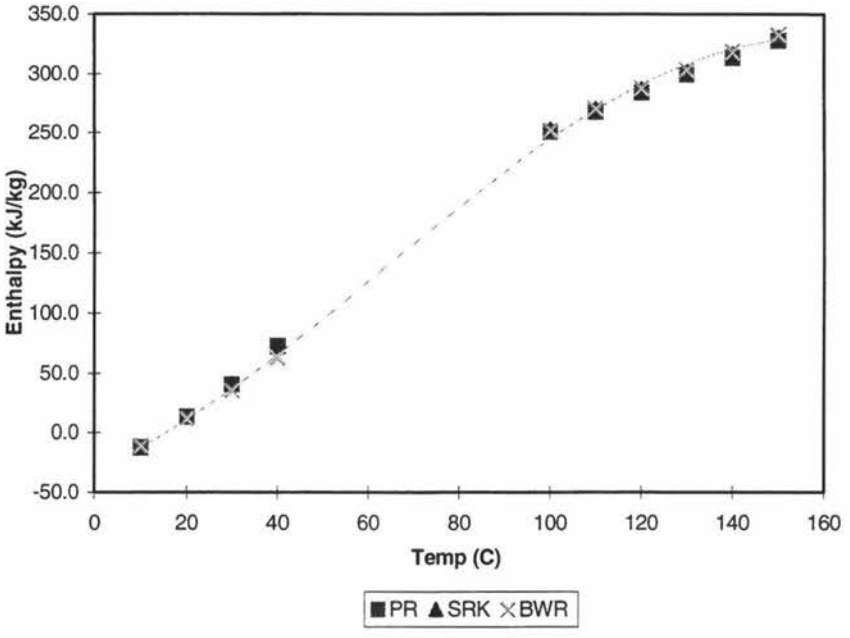

Figure 5.3: Comparison of Equations of State Enthalpy Predictions at 130 bar

5. CO_2 Saturated Pressure Temperature Relationship: This relationship was determined by a curve fit to the ASHRAE (1993) data.

$$T_{sat} = -81.76 + 6.72\left(\frac{P_{sat}}{10^6}\right) - 25.62\left(\frac{P_{sat}}{10^6}\right)^2 + 7.620\left(\frac{P_{sat}}{10^6}\right)^3 - 1.326\left(\frac{P_{sat}}{10^6}\right)^4 + 0.122\left(\frac{P_{sat}}{10^6}\right)^5 - 0.00453\left(\frac{P_{sat}}{10^6}\right)^6 \quad (5.5)$$

where:

T_{sat} = CO_2 saturation temperature at P_{sat} (°C)

P_{sat} = CO_2 saturation pressure (Pa)

6. Water: Enthalpy, specific heat, viscosity and thermal conductivity for water were calculated from measured temperature data using a curve-fit equations to the saturated water data from Cooper and Le Fevre (1975). These equations (Appendix A.7 - Saturated Water Equations) had R^2 values greater than 0.999 except for the specific heat equation which had an R^2 of 0.9985.

5.3.2 Gas Cooler Performance

5.3.2.1 Heat Transfer Rate

The rate of heat transfer in the gas cooler was estimated using both CO_2 and water side heat balances:

$$\phi_{cCO2} = m_{CO2}(H_{dis} - H_{co}) \tag{5.6}$$

and

$$\phi_{cw} = m_{cw}(H_{cwi} - H_{cwo}) \tag{5.7}$$

where:

ϕ_{cCO2} = total heat flow from CO_2 in the gas coolers (W)
m_{CO2} = mass flowrate of CO_2 (kg/s)
H_{dis} = CO_2 enthalpy at compressor discharge / gas cooler inlet conditions (J/kg)
H_{co} = CO_2 enthalpy at gas cooler outlet conditions (J/kg)
ϕ_{cw} = total heat flow to gas cooler water (W)
m_{cw} = mass flowrate of gas cooler water (kg/s)
H_{cwi} = water enthalpy at gas cooler inlet conditions (J/kg)
H_{cwo} = water enthalpy at gas cooler outlet conditions (J/kg)

The CO_2 mass flowrate was measured directly, whereas the water mass flowrate was calculated from the measured volumetric flowrate using:

$$m_{cw} = \frac{Q_{cw}}{1000}\rho_{cwi} \tag{5.8}$$

where:

m_{cw} = mass flowrate of gas cooler water (kg/s)
Q_{cw} = volumetric flowrate of gas cooler water (L/s)
ρ_{cwi} = density of gas cooler water at gas cooler inlet conditions (kg/m^3)

CO_2 and water properties were calculated from measured pressure and/or temperature data using the methods given in Section 5.3.1.

If heat losses are negligible, ϕ_{cCO2} and ϕ_{cw} should be equal. Differences were less than 6% for most trials, but the two values differed significantly for a few trials. There were quite large uncertainties associated with measurement of CO_2 mass flowrate, particularly because it was measured in a supercritical state. There was also some uncertainty in the estimation of CO_2 enthalpy because the CO_2 was near the critical region where rapid changes in properties occur with small changes in temperature and pressure. In contrast, water flowrate uncertainty was low, and the large temperature difference on the water-side meant that uncertainties arising from the measurement of temperature were relatively small. Therefore, it was decided to use ϕ_{cw} as the best estimate of the gas cooler heat transfer rate.

5.3.2.2 *Gas Cooler Heat Transfer Rating*

The overall heat transfer coefficient for the gas cooler was estimated using:

$$U_{c,o} = \frac{\phi_{cw}}{A_{c,o}\Delta\theta_{lm,c}} \tag{5.9}$$

where:

$U_{c,o}$ = overall heat transfer coefficient based on tube outside area (W/m^2°C)
$A_{c,o}$ = gas cooler surface area outside tube (m^2)
$\Delta\theta_{lm,c}$ = log mean temperature difference for gas coolers (°C)

The mean temperature difference between the CO_2 and water in the gas cooler was approximated by the log mean to keep calculations simple.

$$\Delta\theta_{lm,c} = \frac{(T_{dis} - T_{cwo}) - (T_{co} - T_{cwi})}{\ln\left(\frac{T_{dis} - T_{cwo}}{T_{co} - T_{cwi}}\right)} \tag{5.10}$$

where:

$\Delta\theta_{lm,c}$ = log mean temperature difference for gas coolers (°C or K)
T_{dis} = discharge/gas cooler CO_2 inlet temperature (°C)
T_{cwo} = gas cooler water outlet temperature (°C)
T_{co} = gas cooler CO_2 outlet temperature (°C)
T_{cwi} = gas cooler water inlet temperature (°C)

The true mean temperature difference for the gas cooler is not equal to the log mean because the specific heat capacity of CO_2 is not constant near the critical point. The true temperature difference is given by the following equation:

$$\Delta\theta_{m,c} = \frac{H_{co} - H_{ci}}{\int_{Hci}^{Hco} \frac{1}{(T_{CO_2} - T_w)} dH} \tag{5.11}$$

where:

$\Delta\theta_{m,c}$ = true mean temperature difference for gas coolers (°C)
T_{CO2} = CO_2 gas cooler temperature as function of enthalpy (°C)
T_w = gas cooler water temperature as function of enthalpy (°C)
H_{co} = gas cooler outlet enthalpy (J/kg)
H_{ci} = gas cooler inlet enthalpy (J/kg)

Using this equation is difficult as there is no explicit analytical equation for temperature as a function of enthalpy when using the Benedict Webb Ruben equation of state. A curve fit for each given pressure could be performed, but this would be very tedious. Figure 5.4 shows the non-linearity of the CO_2 temperature profile through the gas cooler for a number of discharge pressures. The temperature is plotted as a function of enthalpy using the CO_2 entry condition as the datum.

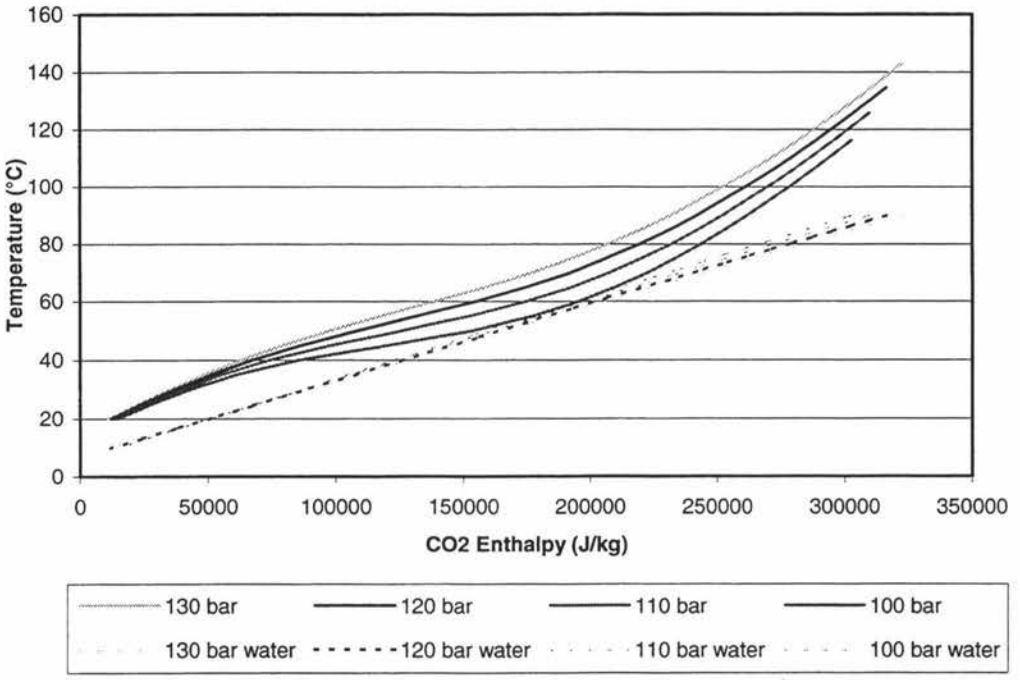

Figure 5.4: Temperature Profile in Gas Cooler

Using these profiles, $\Delta\theta_{lm,c}$ and $\Delta\theta_{m,c}$ were estimated for the case of water being heated from 10°C to 90°C with a temperature difference between the CO_2 and water at the water inlet of 10°C. Table 5.6 shows the ratios of the two temperature differences for discharge pressures that enabled 90°C hot water to be achieved. Pressures lower than 110 bar led to the pinch point near the critical region becoming limiting (less than 10°C temperature difference). The ratio between $\Delta\theta_{lm,c}$ and $\Delta\theta_{m,c}$ is reasonably constant if the discharge pressure is significantly above the critical pressure. For example, there is only a 10% change in the ratio from 130 to 120 bar. Many trials were carried out with such discharge pressure conditions. Therefore, as long as the same temperature difference basis is used for both measured and design conditions, it was considered that a valid comparison of heat transfer rating could be made for the gas cooler.

Table 5.6: Ratios of Log-Mean to True Mean Temperature Difference for the Gas Cooler with a 10°C Minimum Temperature Approach

Discharge Pressure (bar)	$\Delta\theta_{lm,c}$ / $\Delta\theta_{m,c}$
130	1.31
120	1.46
110	1.86
100	infeasible

The relationship between the overall heat transfer coefficient and the individual coefficients is given by:

$$\frac{1}{U_{c,o}A_{c,o}} = \frac{1}{h_{CO2}A_{c,o}} + \frac{x}{\lambda A_{mean}} + \frac{1}{h_w A_{c,i}} \tag{5.12}$$

where:

h_{CO2} = CO_2 side heat transfer coefficient based on outside tube area ($W/m^2°C$)
x = tube wall thickness (m)
λ = thermal conductivity of wall material ($W/m°C$)
A_{mean} = mean tube surface area (m^2)
h_w = water side heat transfer coefficient based on inside tube area ($W/m^2°C$)
$A_{c,i}$ = gas cooler surface area inside tube (m^2)

Taking the log mean area this equates to:

$$\frac{1}{U_{c,o}A_{c,o}} = \frac{1}{2\pi L_c n_{t,c}}\left(\frac{1}{h_{CO2}r_{c,o}} + \frac{\ln(r_{c,o}/r_{c,i})}{\lambda} + \frac{1}{h_w r_{c,i}}\right) \tag{5.13}$$

where:

L_c = length of gas cooler tubes (m)
$n_{t,c}$ = number of tube in gas cooler
$r_{c,o}$ = gas cooler outside tube radius (m)
$r_{c,i}$ = gas cooler inside tube radius (m)

The CO_2 side heat transfer coefficient was calculated by:

$$h_{CO2} = \frac{1}{r_{c,o}\left(\frac{2\pi L_c n_{t,c}}{U_o A_o} - \frac{1}{h_w r_{c,i}} - \frac{\ln(r_{c,o}/r_{c,i})}{\lambda}\right)} \tag{5.14}$$

The water side coefficient, h_w, was calculated using the method for forced convective heat transfer described in Perry's Chemical Engineers' Handbook (1984), equation (10-50).

5.3.3 Evaporator Performance

5.3.3.1 Heat Transfer Rate

The heat transferred to the CO_2 in the evaporator was calculated assuming that the vapour exiting the separator was saturated, and that heat losses or gains to the evaporator and separator were small.

$$\phi_{eCO2} = m_{CO2}(H_{vsep} - H_{TXi}) \tag{5.15}$$

where:

ϕ_{eCO2} = heat flow to CO_2 in evaporator (W)
H_{vsep} = CO_2 vapour enthalpy in separator (J/kg)
H_{TXi} = enthalpy at expansion valve inlet (J/kg)

The evaporator heat transfer was also calculated from the change in temperature of the water being cooled.

$$\phi_{ew} = m_{ew}\left(H_{ewi} - H_{ewo}\right) \tag{5.16}$$

where:

ϕ_{ew} = total heat flow from evaporator water (W)
m_{ew} = mass flowrate of evaporator water (kg/s)
H_{ewi} = water enthalpy at evaporator inlet (J/kg)
H_{ewo} = water enthalpy at evaporator outlet (J/kg)

The measured CO_2 mass flowrate was used, and water mass flowrate was calculated from the measured volumetric flowrate as for the gas coolers:

$$m_{ew} = \frac{Q_{ew}}{1000}\rho_{ew} \tag{5.17}$$

where:

m_{ew} = mass flowrate of evaporator water (kg/s)
Q_{ew} = volumetric flowrate of evaporator water (L/s)
ρ_{ewi} = density of gas cooler water at evaporator inlet (kg/m^3)

As for the gas coolers, the two heat flows ϕ_{eCO2} and ϕ_{ew} should agree, but the two values differed significantly for some trials although most discrepancies were less than 10%. In the case of the evaporator, the uncertainty in the water temperatures was larger than for the gas cooler because of the smaller temperature change of the water from the inlet to the outlet. Because of the uncertainty in both estimates of the evaporator heat flow, it was decided to use the average of the two heat flows as the best estimate of the heat transfer rate.

$$\phi_e = \frac{\left(\phi_{eCO2} + \phi_{ew}\right)}{2} \tag{5.18}$$

where:

ϕ_e = heat flow in evaporator (W)

5.3.3.2 Evaporator Rating

The overall heat transfer coefficient was also calculated for the evaporator.

$$U_{e,o} = \frac{\phi_e}{A_{e,o}\Delta\theta_{lm,e}} \tag{5.19}$$

where:

$U_{e,o}$ = overall heat transfer coefficient based on outside tube area (W/m^2°C)
$A_{e,o}$ = evaporator outside tube surface area (m^2)
$\Delta\theta_{lm,e}$ = log mean temperature difference for evaporator (°C or K)

For the evaporator, the mean temperature difference is equal to the log mean because the CO_2 is evaporated at constant temperature and pressure, and the heat capacity of the water is virtually constant.

$$\Delta\theta_{lm,e} = \frac{(T_{ewo} - T_{sep}) - (T_{ewi} - T_{sep})}{\ln\left(\frac{T_{ewo} - T_{sep}}{T_{ewi} - T_{sep}}\right)} \tag{5.20}$$

where:

T_{sep} = separator temperature (°C)
T_{ewi} = evaporator water inlet temperature (°C)
T_{ewo} = evaporator water outlet temperature (°C)

The CO_2 and water-side heat transfer coefficients for the evaporator were calculated using the same method as described in Section 5.3.2.2.

5.3.4 Recuperator Performance

5.3.4.1 Heat Transfer Rate

High pressure side and low pressure side heat balances for the recuperator heat transfer are:

$$\phi_{rh} = m_{CO2}(H_{co} - H_{TXi}) \tag{5.21}$$

and

$$\phi_{rc} = m_{CO2}(H_{vsep} - H_{suc}) \tag{5.22}$$

where:

ϕ_{rh} = total heat flow from CO_2 for the recuperator hot side (W)
ϕ_{rc} = total heat flow to CO_2 for the recuperator cold side (W)
H_{suc} = CO_2 enthalpy at compressor suction (recuperator cold side exit) (J/kg)

Any uncertainty in the measurement of the CO_2 mass flowrate will not affect the agreement between the heat balances because it affects both equally. On the high pressure side, there was considerable uncertainty in the estimation of the CO_2 enthalpy because it is in the critical region. On the low pressure side, uncertainty arose because the CO_2 may not be pure vapour if there was liquid carryover from the separator. Therefore, the average of the two heat flows was taken as the heat flow for the recuperator.

$$\phi_r = \frac{\phi_{rc} + \phi_{rh}}{2} \tag{5.23}$$

where:
ϕ_r = recuperator heat transfer (W)

5.3.4.2 *Recuperator Rating*

The rating for the recuperator was estimated using:

$$U_{r,o} = \frac{\phi_r}{A_{r,o}\Delta\theta_{lm,r}} \tag{5.24}$$

where:
$U_{r,o}$ = overall heat transfer coefficient based on tube outside area (W/m^2°C)
$A_{r,o}$ = recuperator surface area outside tube (m^2)
$\Delta\theta_{lm,r}$ = log mean temperature difference for recuperator (°C or K)

The mean temperature difference was approximated by the log mean, but as for the gas coolers, the true mean temperature difference is influenced by the changing specific heat of CO_2 in the supercritical region. This effect is not as strong for the recuperator as for the gas cooler as it operates further away from the critical region. This effect was ignored because it is difficult to quantify and it was felt that as adequate comparisons between the design and measured ratings could be achieved if they were estimated in a consistent manner.

$$\Delta\theta_{lm,r} = \frac{(T_{co} - T_{suc}) - (T_{TXi} - T_{sep})}{\ln\left(\frac{T_{co} - T_{suc}}{T_{TXi} - T_{sep}}\right)} \tag{5.25}$$

where:
T_{suc} = CO_2 temperature at compressor suction (recuperator cold side exit) (J/kg)
T_{Txi} = temperature at expansion valve inlet (recuperator hot side exit) (°C)

5.3.5 Variable Speed Drive (VSD) and Motor

The compressor speed was determined from the percentage speed data from the PID controller. The VSD assigned the nameplate motor speed of 970 rpm as 100% of speed. The PID controller output (nominally 4-20 mA) was calibrated to the PID input (in percent) using a least squares line fitted to the data. The minimum speed of the VSD was set to 62% (at 4 mA) and the maximum speed was 125% (at 20 mA). Hence, the actual percentage speed of the compressor is given by:

$$\omega_{comp}(\%) = (125 - 62) \times \frac{(0.166 \times ctrl_i(\%) + 3.889) - 4}{16} + 62 \tag{5.26}$$

where:
$\omega_{comp}(\%)$ = compressor speed as percentage of nameplate motor speed (%)
$ctrl_i(\%)$ = percentage value entered into PID controller

and the actual speed given by:

$$\omega_{comp} = \frac{\omega_{comp}(\%)}{100} \times 970 \tag{5.27}$$

where:
$\omega_{comp}(\%)$ = compressor speed as percentage of nameplate motor speed (%)
ω_{comp} = compressor speed (rpm)

The real input power of the VSD is given by:

$$E_{VSD,i} = \frac{E_{VSD,o}}{\varepsilon_{VSD}} \tag{5.28}$$

where:
$E_{VSD,i}$ = real input power for VSD (kW)
$E_{VSD,o}$ = real output power for VSD (kW)
ε_{VSD} = VSD efficiency

Based on the VSD manufacturer's data ε_{VSD} was taken to be 0.97 for all trials.

The compressor power requirement was calculated using:

$$\phi_{comp,i} = E_{VSD,o}\varepsilon_M \tag{5.29}$$

where:
$\phi_{comp,i}$ = motor output power / compressor inlet power (kW)
ε_M = motor efficiency

Based on motor manufacturer's data ε_M was taken as 0.929 for all trials.

5.3.6 Compressor Performance

The pressure ratio for the compressor was calculated by:

$$PR = \frac{P_{dis}}{P_{suc}} \tag{5.30}$$

where:
PR = compressor pressure ratio

The compressor volumetric and isentropic efficiencies are the main indicators of compressor performance.

Isentropic efficiency was estimated using:

$$\eta_i = \frac{\Delta H_{comp}}{\Delta H_{comp,isentropic}} \tag{5.31}$$

where:

η_i = compressor isentropic efficiency
ΔH_{comp} = actual enthalpy change in compressor (J/kg)
$\Delta H_{comp,isentropic}$ = enthalpy change in compressor if isentropic process (J/kg)

The actual compressor enthalpy change was given by:

$$\Delta H_{comp} = H_{dis} - H_{suc} \tag{5.32}$$

H_{dis} and H_{suc} were calculated from measured temperature and pressure data. The isentropic compressor enthalpy change was calculated through an iterative process that, for given suction conditions and discharge pressure, finds the discharge temperature that gives a zero entropy change, and then calculates the resulting enthalpy change. Appendix A.8 - Entropy Calculations gives details of the entropy change calculations.

The volumetric efficiency was estimated using:

$$\eta_v = \frac{Q_{comp,i}}{Q_{comp,i'}} \tag{5.33}$$

where:

η_v = compressor volumetric efficiency
$Q_{comp,i}$ = actual volumetric flowrate into compressor (m^3/s)
$Q_{comp,i'}$ = theoretical volumetric flowrate into compressor (m^3/s)

The actual volumetric flowrate into the compressor was given by:

$$Q_{comp,i} = \frac{m_{CO2}}{\rho_{suc}} \tag{5.34}$$

The theoretical volumetric flowrate into the compressor was given by:

$$Q_{comp,i'} = V_{comp} \frac{\omega_{comp}}{60} \tag{5.35}$$

where:

V_{comp} = compressor swept volume (m^3)

5.3.7 Overall System Performance

The energy efficiency of the system was represented by the heating, cooling and overall Coefficients of Performance. The Coefficient of Performance (COP) is the amount of heating or cooling achieved from the system for each unit of power the system uses.

$$COP_H = \frac{\phi_{cw}}{\phi_{comp,i}} \tag{5.36}$$

$$COP_C = \frac{\phi_e}{\phi_{comp,i}} \tag{5.37}$$

where:
COP_H = Heating Coefficient of Performance
COP_C = Cooling Coefficient of Performance

The overall COP is given by:

$$COP = \frac{\phi_{cw} + \phi_e}{\phi_{comp,i}} = COP_H + COP_C \tag{5.38}$$

From equations (5.38) and (5.42) it can be shown that the heating COP is related to the overall COP by:

$$COP_H = \frac{COP + 1}{2} \tag{5.39}$$

5.3.8 Heat Losses and Gains

Heat losses and gains were estimated for the system to determine whether they had a significant effect on the heat balances. This was done by first assuming a uniform surface temperature for different sections of the plant, then calculating the heat transfer coefficients for these sections using the correlation in Perry's Chemical Engineers' Handbook (1984) for natural convection (equation 10-32b). The heat transferred to or from each section was then calculated using:

$$\phi_{surf,n} = h_{surf,n} A_{surf,n} \left(T_{air} - T_{surf,n}\right) \tag{5.40}$$

where:
$h_{surf,n}$ = combined convective and radiative heat transfer coefficient for section (W/m^2K)
$A_{surf,n}$ = surface area of section (m^2)
T_{air} = air ambient temperature (°C)
$T_{surf,n}$ = surface temperature (°C)

The overall heat transfer from the plant was given by summing the heat transfer for the individual sections:

$$\phi_{surf} = \sum_{0}^{n} \phi_{surf,n} \tag{5.41}$$

where:

ϕ_{surf} = total heat transfer from plant surface (W)
$\phi_{surf,n}$ = heat transfer from surface of section (W)

Maximum and minimum values for both air and surface temperatures were used to give estimates of maximum and minimum heat losses and gains.

Appendix A.9 - Heat Loss Calculations gives details of these calculations. It was found that the maximum heat loss from the combined hot sections of the plant was about 1.2 kW, while the maximum heat gain to the cold sections was 1.1 kW. These are not considered significant compared to the gas cooler and evaporator heat transfer (about 90 kW and 60 kW respectively), and approximately cancel each other in terms of the overall energy balance for the prototype, so they were ignored.

5.3.9 Overall Heat Balance and Experimental Uncertainty

As well as a heat balance for each component, a heat balance over the whole system was also calculated as a guide to experimental uncertainty. Assuming negligible heat losses, the overall heat balance for the system can be given by:

$$\phi_{cw} = \phi_e + \phi_{comp,i} \tag{5.42}$$

Trials were eliminated from the data analysis if the balances disagreed by significantly more than 10%. Only five trials were omitted due to this reason and are not included in Table 5.1 to Table 5.5. The average absolute discrepancy between the measured gas cooler heat transfer rate and the right hand side of equation (5.42) for the remaining trials was 2.2 kW (3.2% based on gas cooler water heat transfer rate). The maximum absolute difference was 7 kW (9% of gas cooler heat transfer rate). In general, the gas cooler heat load tended to be slightly greater that the sum of the evaporator heat load and compressor power input. Given the difficulty in measuring CO_2 flowrates, CO_2 property and water temperature differences for the evaporator and the assumption that heat losses were negligible, this was considered to be acceptable agreement.

Alternatively an overall heat balance can also include the recuperator:

$$\phi_{cw} + \phi_{rh} = \phi_e + \phi_{comp,i} + \phi_{rc} \tag{5.43}$$

The average absolute discrepancy for this balance was 2.3 kW (3.3% based on gas cooler water heat transfer rate) again suggesting low experimental uncertainty.

As an additional check on experimental uncertainty, overall heat balances were calculated using equation (5.42) with a CO_2 flowrate that was back-calculated from the

gas cooler water-side heat balance instead of the measured values. For all but two sets of trials, this modified heat balance was within 1% of the original heat balance, indicating that the measured CO_2 flowrates were reasonable reliable. Therefore, including the CO_2 side heat transfer rate for the evaporator calculations was warranted given the uncertainty in the water-side balance. However, for the gas cooler, the higher water-side accuracy and the greater uncertainty in CO_2 properties meant that not using the CO_2 side heat transfer rate was justified.

Overall, the decisions to use the water heat load for the gas coolers and the average of the water and CO_2 heat loads for the evaporator was considered to give the best estimates of the actual heat transfer rates..

5.3.10 Process Simulation

The process was also modelled using Hysis (version 1.1). This is a commercial process engineering simulation programme from Hyprotech. It was used to solve the complete set of heat and mass balances around the transcritical cycle using user supplied heat exchanger performance ratings, compressor efficiencies and in-built CO_2 thermodynamic property prediction algorithms.

The process was modelled by selecting pro forma unit operations from the available list and connecting them together with process streams to represent the full system. Necessary input data and performance specifications were supplied for each unit.

The cycle was simulated with all the components shown in the process flow diagram (Figure 4.2). For the simulation, a mixer was used for the streams entering the evaporator, and recycle tear streams were put between the expansion valve and mixer, and between the gas cooler and recuperator to assist in calculations. These did not affect the results of the simulation, but allowed the calculation process to converge more easily for the closed cycle simulation.

Average UA values calculated from experimental data for the gas cooler and recuperator for each set of trials, high and low side pressures, and compressor polytropic efficiency were entered into the programme, along with the CO_2 mass flow. The inlet water temperatures for the gas cooler and evaporator, the required gas cooler outlet (hot) water temperature, and both the water and CO_2 mass flowrates through the evaporator were also entered. The Peng Robinson thermodynamic package was used to predict CO_2 properties. Hysis then calculated the temperatures and compositions of mixtures at all other points of the process. This simulated data could then be compared with the measured values.

6 RESULTS AND DISCUSSION

6.1 Commissioning and Preliminary Trials

Commissioning trials enabled the individual components of the prototype to be tested to assess their ability to perform their function.

6.1.1 Control Loop Performance

As expected, compressor speed had a large effect on low-side pressure. Using manual control, it was observed that a 1-2 % change on the Watlow controller (which equates to 6 – 12 rpm) changed the pressure by about 0.1 bar. On automatic control, the controller performed reasonably well, although it could take more than one minute to reach the set-point after start-up or a change in the set-point. This probably reflects the slow process dynamics, as the suction pressure took a long time to respond to compressor speed changes. Once steady-state was reached, the offset from the set-point was generally about 0.5 bar (but could be as much as 1 bar). The PID values the controller used were selected by its autotune function, so more appropriate values may be able to be found by selecting them manually. This was not pursued because manual control was adequate for the performance trials.

It was observed that the evaporator water flowrate also had a large effect on the low-side pressure. By comparison, the gas cooler water flowrate had a minor effect (of the order of 0.1 bar per 2°C change in hot water discharge temperature).

The backpressure control loop controlled the discharge pressure well. Usually it took less than 5 seconds for the discharge pressure to stabilise after a change in set-point. When there was an air line failure to the valve, the discharge pressure built up very quickly and the pressure relief valve occasionally released before the system tripped on high pressure. Therefore, a fail-open valve may be more appropriate in future designs.

6.1.2 Separator Performance

The 200 NB separator performed well, with no evidence of liquid carry over. It was difficult to assess whether the thermosiphon was giving adequate overfeed of CO_2 to be evaporated. Attempts were made to measure the thermosiphon flow using an ultrasonic and a Doppler flowmeter, but erroneous results were obtained. The thermosiphon appeared to work well, as frosting occurred uniformly on the return leg from the evaporator, indicating that overfeed was occurring, and considerable liquid was observed in the sight glasses coming from the return leg of the evaporator.

6.1.3 CO_2 Leakage

Several tests were performed with the original packing to estimate the rate of leakage from the compressor. By measuring high side pressure after shut down, leakage rates were found to be about 0.14 kg/min at 46 bar high side pressure, and 0.1 kg/min at 30 bar. The time between the liquid level in the separator dropping from the high level

switch to the low level switch after shut down gave a rate of loss of 0.18 kg/min. The flowrate measured through the compressor breather holes gave a loss of 0.18 kg/min. The leakage rate estimate based on the amount of CO_2 added per hour of operation was slightly greater, as this method did not take into account losses when the system was stopped.

The final packing that was used (water cooled) significantly improved the leakage rates. Using a rotameter to measure the leakage rates through the breathers on the compressor, the leakage was found to be greater when the plant was stopped (0.058 kg/min) than when it was running (0.022 kg/min), possibly due to the piston rod seal being more effective when active. When oil was added to the CO_2 in the system, the maximum leakage rate when stopped dropped slightly to 0.056 kg/min, but dropped significantly when running to 0.007 kg/min.

Although the addition of oil significantly reduced leakage, these rates are still too high for a commercial installation of the heat pump, so further effort will have to be put into developing more effective shaft seals for the compressor. For example, at the lowest leakage rate of 0.007 kg/min (when running), recharging would be required every 37 hours of operation. This would drop to just over eight hours if the system was run only half the time due to the higher leakage rate when the system was stopped.

6.1.4 Pressure Drop

It was found that the pressure drop between the separator and evaporator outlet, and between the separator and compressor suction were less than the accuracy of the transducer which was 0.5 to 1 bar. Therefore it was assumed that pressure drops were negligible and the evaporator pressure was assumed to be the same as the compressor suction.

6.1.5 Experimental Uncertainty

The 95% confidence interval for COP values for replicates was 2.8% (ie. the difference between COP values for replicates was seldom more than 3% from the mean). For the temperature measurements, the average absolute deviation of each replicate from the mean value for a set of replicates was 0.47°C. The average percentage deviations for the CO_2 mass flow, gas cooler water flow, evaporator water flow and compressor power consumption were 5%, 2%, 2%, and 2% respectively.

The saturation temperature calculated from the measured suction pressure data was compared to the measured temperature in the separator / receiver as a check. The difference for the majority of the trials was less than 0.5°C.

Combined with the good energy balances described in Section 5.3.9, it was felt that, in general, experimental uncertainty was less than 5% at the 95% level of confidence.

6.2 Component Performance

The raw data for all of the system and component performance trials are given in Appendix A.10 - Raw Data. All pressures are given as absolute pressures.

6.2.1 Gas Cooler

Figure 6.1 shows the overall heat transfer coefficient for the gas cooler as a function of water flowrate for the oil-free trials based on outside surface area. The range of overall heat transfer coefficients was from 550 W/m^{2}K to 1550 W/m^{2}K. Calculated water side heat transfer coefficients (based on inside surface area) ranged from 2850 W/m^{2}K to 5950 W/m^{2}K, giving CO_2 side film heat transfer coefficients of 700 W/m^{2}K to 3100 W/m^{2}K (based on outside surface area). These measured CO_2 side values are similar to the values reported by literature. Overall heat transfer coefficients with the CO_2 inside the tubes range from 250 to 3650 W/m^{2}K (Schönfeld and Krauss, 1997; Hwang and Radermacher, 1997). The CO_2 in the heat pump used in this project had the CO_2 flow on the outside of the tubes, and generally flowing perpendicular to the tubes, so a more precise comparison is difficult to make.

Figure 6.1 also shows that the design heat transfer coefficient for the gas cooler was slightly higher than the average of the experimental values. This indicates that the gas cooler heat exchanger may be performing slightly worse than expected based on correlations given by Perry's Chemical Engineer's Handbook (1984). Increasing the gas cooler size to compensate for the lower heat transfer coefficient could be beneficial for the trials with high compressor speed if the gas cooler performance started to constrain overall system performance.

Addition of oil had no discernible effect on gas cooler heat transfer performance, indicating that any oil fouling was minimal at the high temperature and pressure.

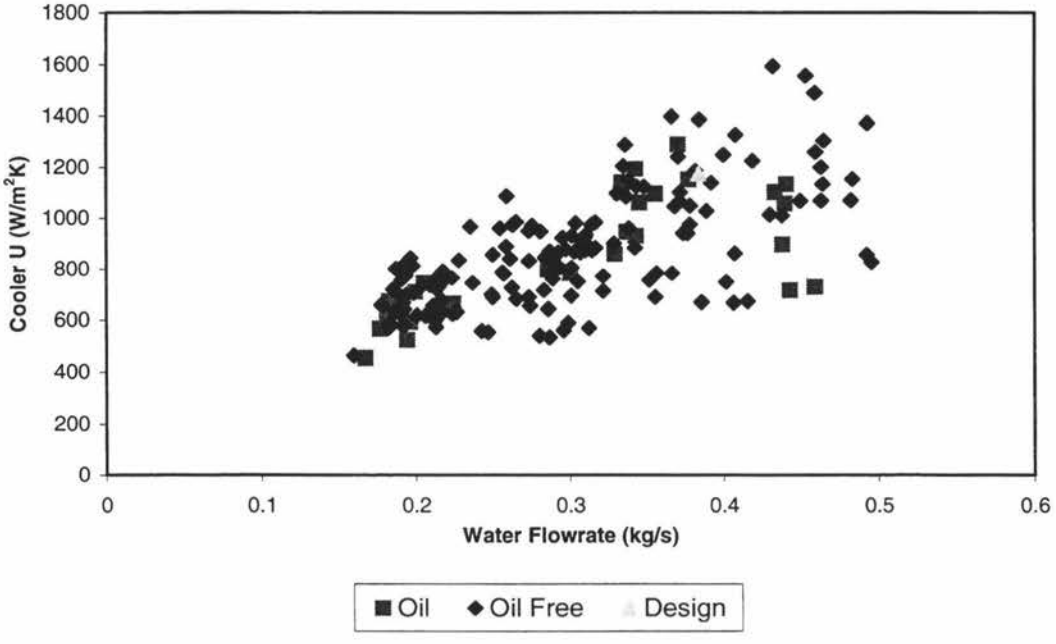

Figure 6.1: Gas Cooler heat transfer coefficient as a function of cooler water flowrate for trials with and without oil in the system.

6.2.2 Evaporator

Figure 6.2 to Figure 6.4 show the heat transfer performance of the evaporator. The range of overall heat transfer coefficients for oil-free operation was from 500 W/m^{2}K to 1300 W/m^{2}K for the evaporator. Calculated water side heat transfer coefficients ranged from 1300 W/m^{2}K to 2800 W/m^{2}K giving CO_2 side film heat transfer coefficients ranging from 700 W/m^{2}K to 1800 W/m^{2}K.

Heat transfer coefficients from literature for in-tube evaporation of CO_2 range from 2000 to 15000 W/m^{2}K for the evaporator (Bresden *et al*, 1997; Zhao *et al*, 1997). In general, these are higher than the values achieved in this study. However, direct comparison of the literature with the results achieved is not possible, as in the prototype the CO_2 was evaporated on the outside of the tube rather than the inside.

In all of the trials, the evaporator water flowrate was significantly lower than the design value, so a direct comparison of measured and design performance could not be made. However, the expected (design) performance of the evaporator was re-estimated using the actual water flowrate for the last set of trials. As Figure 6.2 shows, the adjusted design heat transfer coefficient was very similar to those measured for the evaporator without oil, suggesting that if the design water flowrate was used, the evaporator heat transfer performance would have been close to the original design value.

With oil added to the system, there was a significant decline in overall heat transfer coefficient due to oil fouling. This is further discussed in Section 6.3.5.

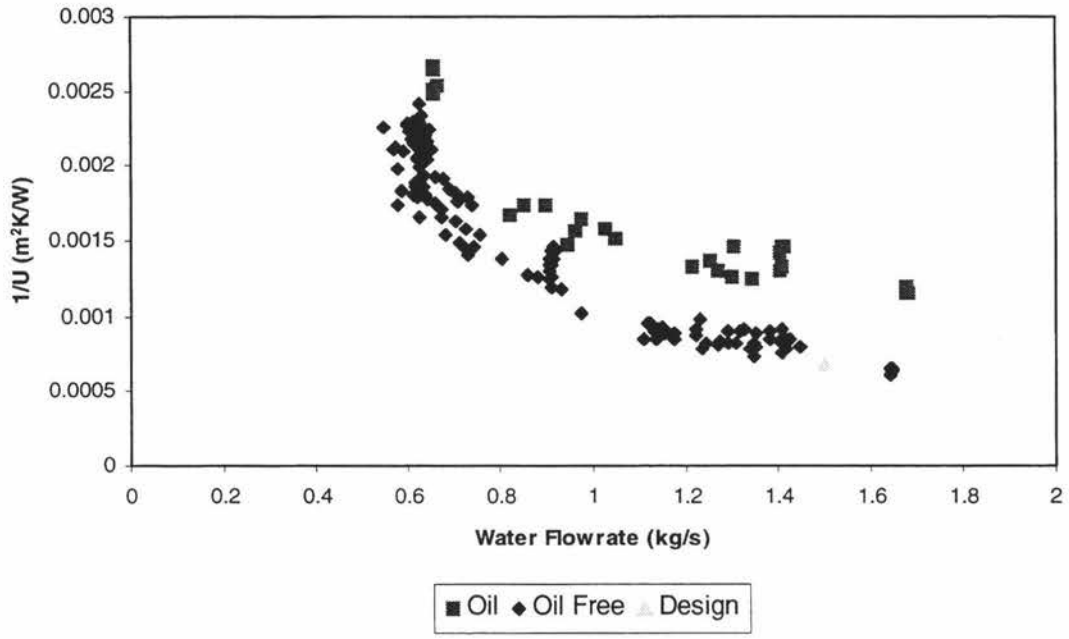

Figure 6.2: Evaporator heat transfer resistance as a function of evaporator water flowrate for trials with and without oil in the system.

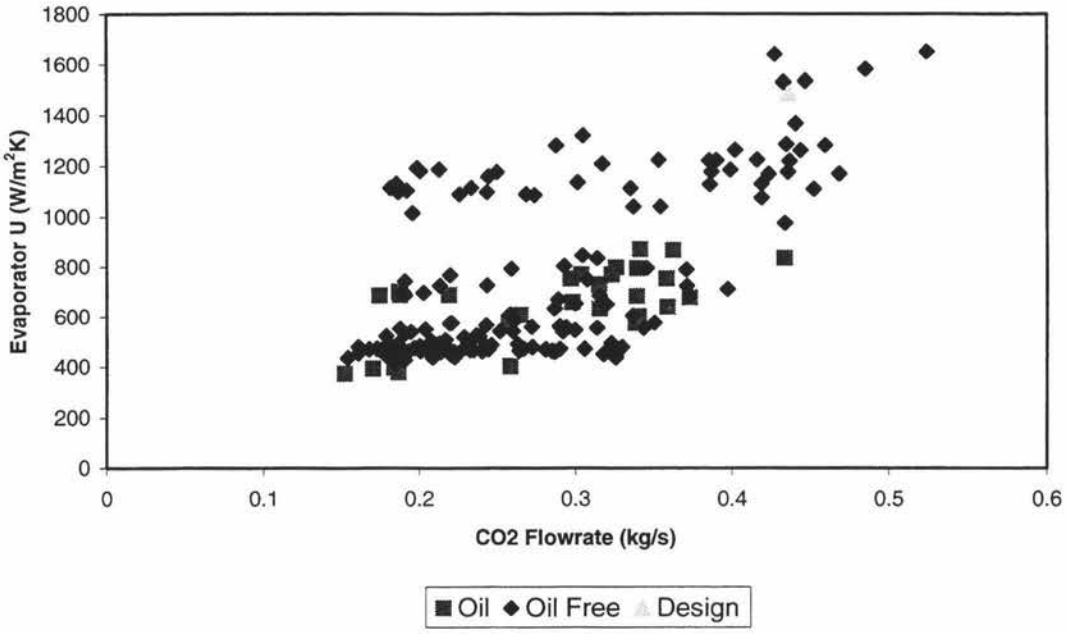

Figure 6.3: Evaporator heat transfer coefficient as a function of CO_2 mass flowrate for trials with and without oil in the system.

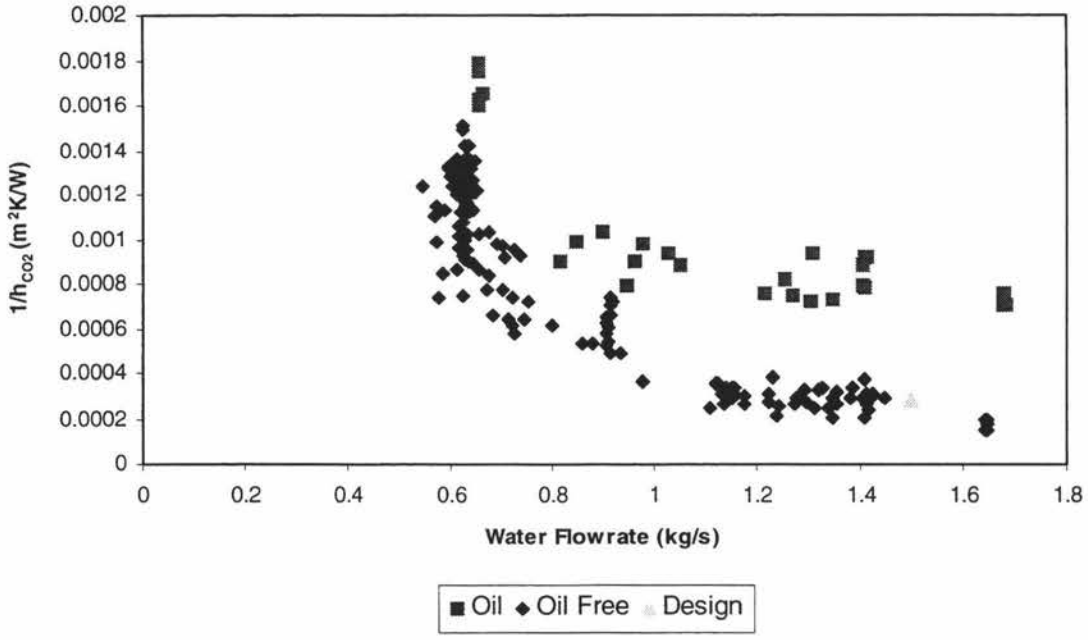

Figure 6.4: Evaporator CO_2 side heat transfer resistance as a function of evaporator water flowrate for trials with and without oil in the system.

6.2.3 Recuperator

The overall heat transfer coefficient for the recuperator was estimated to be between 600 W/m^2K and 1400 W/m^2K. The CO_2 mass flowrate appears to have a reasonably strong effect on heat transfer coefficient (Figure 6.5). At the design CO_2 flowrate, the heat transfer performance of the recuperator was about 30% greater than the expected design performance. The design heat transfer coefficient was similar to the measured values of the recuperator at lower CO_2 flowrates.

The addition of oil did not have a significant effect on the recuperator heat transfer coefficients.

6.2.4 Compressor

Figure 6.6 shows the isentropic and volumetric efficiencies for the compressor as a function of the pressure ratio for all trials conducted. There was a rapid decline in volumetric efficiency as the pressure ratio increased. The volumetric efficiency dropped from about 0.7 at a pressure ratio just over 2, to about 0.3 at a pressure ratio of almost 4.5. The isentropic efficiency does not seem to be greatly affected by the pressure ratio, and seems to be reasonable constant at a value of about 0.7.

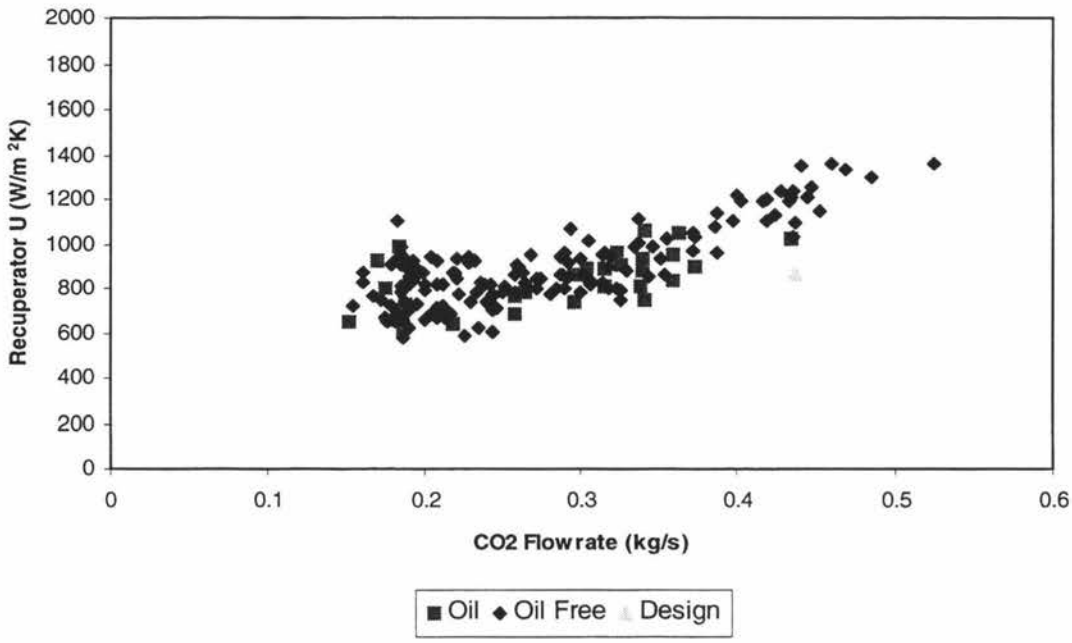

Figure 6.5: Recuperator heat transfer coefficient as a function of CO_2 mass flowrate for trials with and without oil in the system.

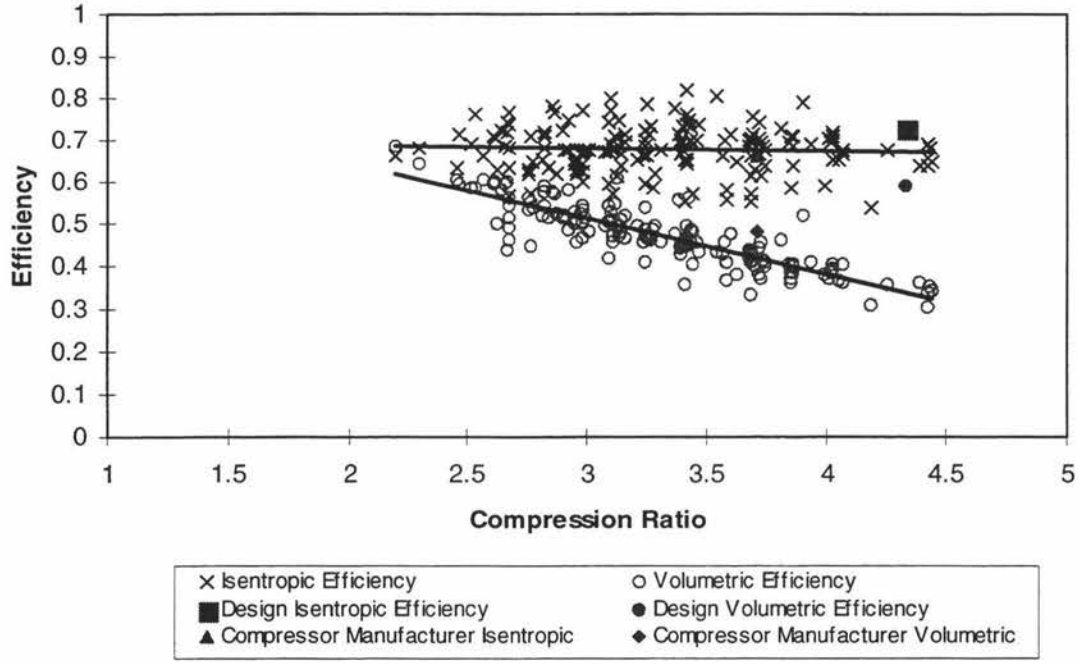

Figure 6.6: Compressor Efficiencies for All Trials

At the design pressure ratio of about 4.3, the measured volumetric efficiency was about 40% lower than design, and the measured isentropic efficiency is only slightly less than the nominal design value. The nominal design efficiencies were taken from manufactures data for a pressure ratio of 3.7 because, at that time, the data was not available for the full pressure ratio range. When comparing efficiencies obtained from the same pressure ratio as the manufacturer data, the measured volumetric efficiency was only 12% less, and the measured isentropic efficiency was slightly higher than the manufacturers data. Overall, although the isentropic efficiency was similar to that expected, the volumetric efficiency was significantly worse.

The volumetric efficiency is a measure of the actual swept volume compared to the theoretical (ideal) swept volume. If there is a large clearance volume (the volume left in the cylinder at the top of the piston stroke) compared to the cylinder volume, a large proportion of the gas will be left in the cylinder, and the compressor will have a low volumetric efficiency.

The isentropic efficiency is a measure of the actual energy taken to compress the gas relative to that if the compression was isentropic (the minimum energy requirement for a given pressure lift). The extra energy used in actual compression results in added heating (higher discharge temperature). If gas is left behind in the clearance volume, this will re-expand on the suction stroke, allowing less new gas to enter the cylinder. The expanded gas then has to be re-compressed, wasting some of the energy used to compress it in the first place. This contributes to a reduction in the isentropic efficiency of the compressor. However, the work expended on compressing the gas in the clearance volume is not completely wasted, as when it expands it performs work on the piston, thus reducing the energy consumption of the compressor on its suction stroke.

The compressor used had a small cylinder, so the clearance volume was relatively large. This explains both the reasonably low volumetric efficiencies and the observed rapid drop in efficiency with increasing pressure ratio. The isentropic efficiency remained reasonably constant over the range of pressure ratios. This was not expected, but could be explained by the experimental uncertainty.

Leakage of the gas past piston rings and piston rod packing also contribute to a loss in both volumetric and isentropic efficiency.

The isentropic efficiencies obtained were more constant and the volumetric efficiency was significantly lower than that obtained by Enkemann and Kruse (1997). Isentropic efficiencies from literature range from 0.5 to 0.79 (Enkemann and Kruse, 1997, Aarlien and Frivik, 1998; Yin *et al*, 1998), so the efficiencies obtained were quite comparable. However, the volumetric efficiencies in the literature tend to be much higher, with values generally between 0.5 and 0.85 (Fagerli, 1996; Nekså *et al*, 1997; Aarlien and Frivik, 1998; Yin *et al*, 1998). Optimisation of the clearance volume and valve design could significantly improve volumetric efficiency.

6.3 System Performance

Unless stated otherwise, the following results are presented in terms of overall COP, which is the sum of both heating and cooling COP.

6.3.1 Constant Evaporator Water Flowrate Trials

Figure 6.7 to Figure 6.13 summarise the results obtained from the prototype for the trials where the evaporator water flowrate was held constant, and the VSD was used to control suction pressure (refrigerant evaporation temperature).

Figure 6.7 shows the overall Coefficient Of Performance (COP) as a function of discharge pressure for the three suction pressures used, when the heat pump was producing 90°C hot water. For each suction pressure, the COP reached a maximum at a certain discharge pressure, as reported in the literature (eg. Nekså, 1994; Pettersen and Skaugen, 1994; Nekså *et al*, 1997; White *et al*, 1997; and Liao and Jakobsen, 1998). The optimum discharge pressure for each suction pressure was found by differentiating a cubic equation fitted to the data. The roots of the resultant quadratic equation gave an estimate of the optimum pressure, and the optimum COP was found by substituting this pressure back into the original equation. Table 6.1 illustrates the change in optimum conditions with changing suction pressure. The optimum COP increases with increasing suction pressure (about 1.7% per °C saturated suction temperature), while the optimum discharge pressure decreases slightly. This is consistent with the results of Pettersen and Skaugen (1994) who found that increasing the in evaporation temperature led to a very small decrease in the optimum discharge pressure.

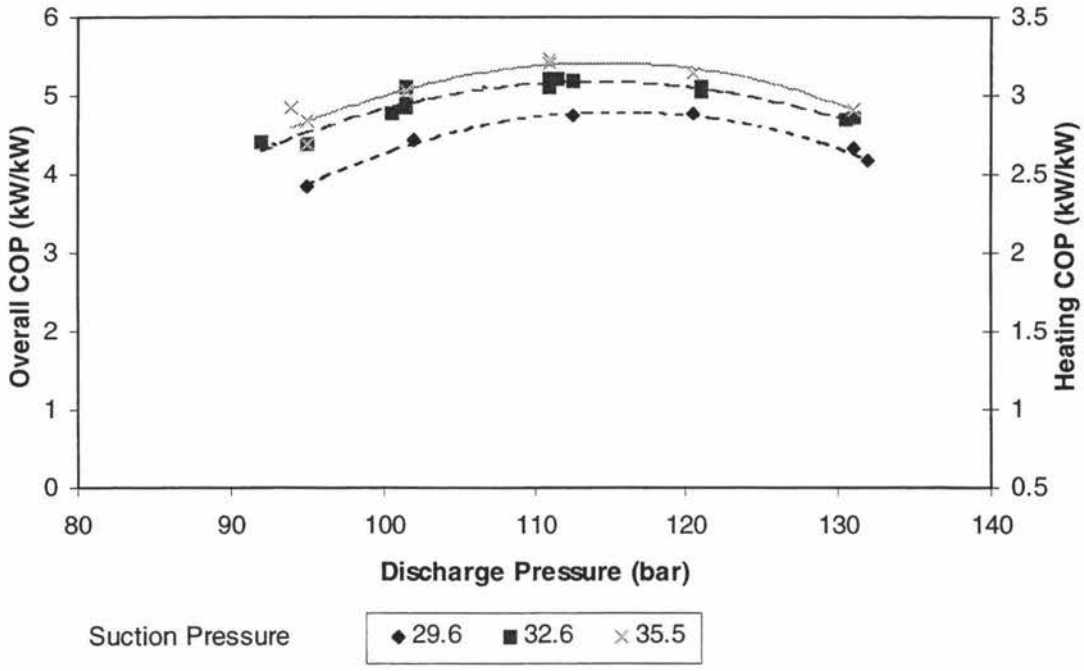

Figure 6.7: COP as a function of discharge pressure for various suction pressures, with constant evaporator water flowrate (90°C hot water).

Table 6.1: Optimum Discharge Pressure and COP for Constant Evaporator Water Flowrate Trials Producing 90°C Hot Water

Suction Pressure	Optimum Discharge Pressure	Optimum COP
29.6 bar (-6.1 °C)	116 bar	4.8
32.6 bar (-2.5 °C)	114 bar	5.2
35.5 bar (0.7 °C)	114 bar	5.4

The optimum discharge pressure (for maximum COP) is the result of a number of competing effects. Firstly, as discharge pressure increases, the compressor discharge temperature increases (Figure 6.8a), which leads to a higher temperature difference in the gas cooler and therefore a greater rate of heat transfer (Figure 6.10). This in turn leads to a lower enthalpy of the CO_2 at the inlet to the expansion valve (Figure 6.8b), which gives a higher fraction of liquid exiting the valve. Therefore more liquid can be evaporated which leads to a greater refrigeration effect for the same total CO_2 mass flowrate.

The benefit of increased refrigeration capacity is balanced by the increased work of compression per kilogram of CO_2. This is caused by both an increase in compression ratio and a reduction in compressor efficiency at high pressure ratios. Pettersen (1994) explains the maximum in the COP by suggesting that above the optimum discharge pressure, the extra refrigerating capacity no longer fully compensates for the additional compressor energy input.

(a)

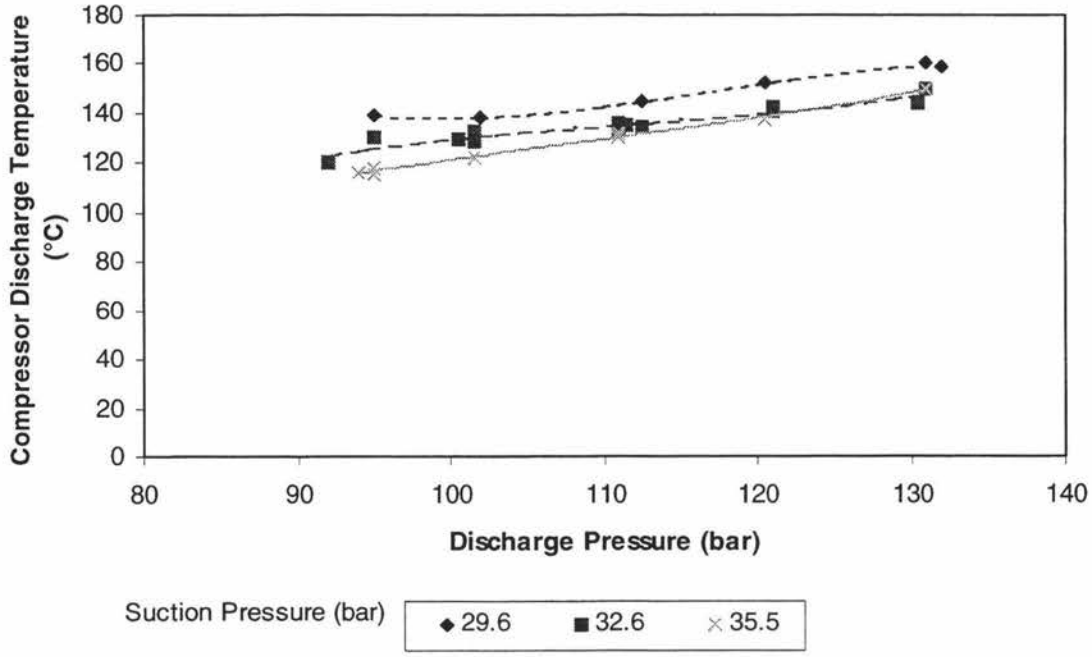

(b)

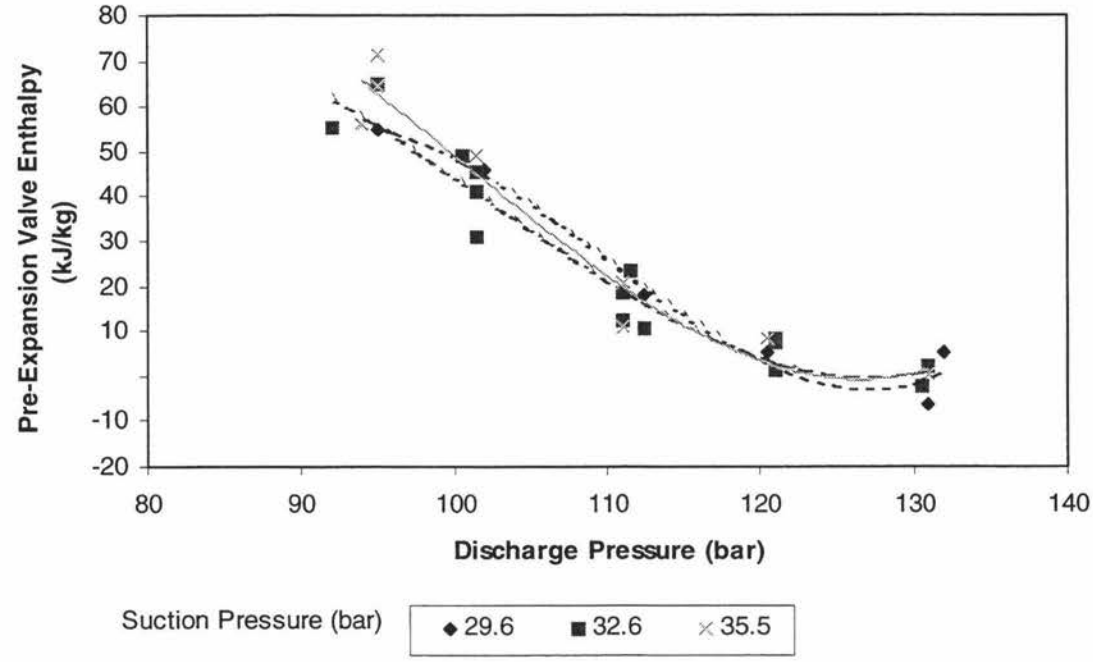

Figure 6.8: (a) Discharge Temperature, and (b) Enthalpy at inlet to expansion valve as a function of Discharge Pressure for various suction pressures, with constant evaporator water flowrate (90°C hot water).

(a)

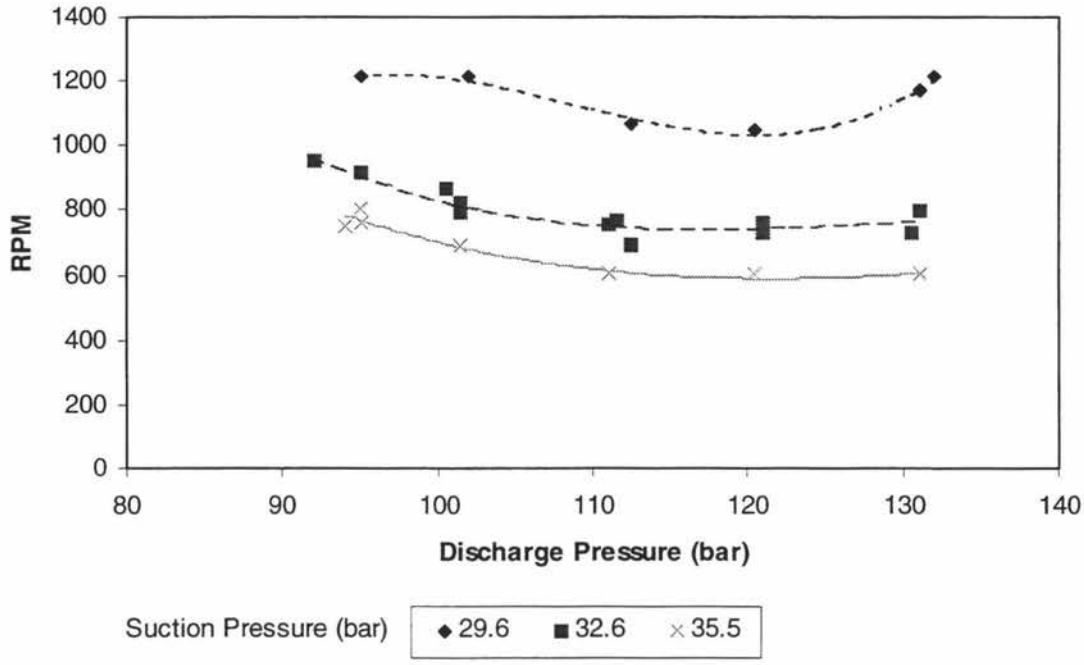

(b)

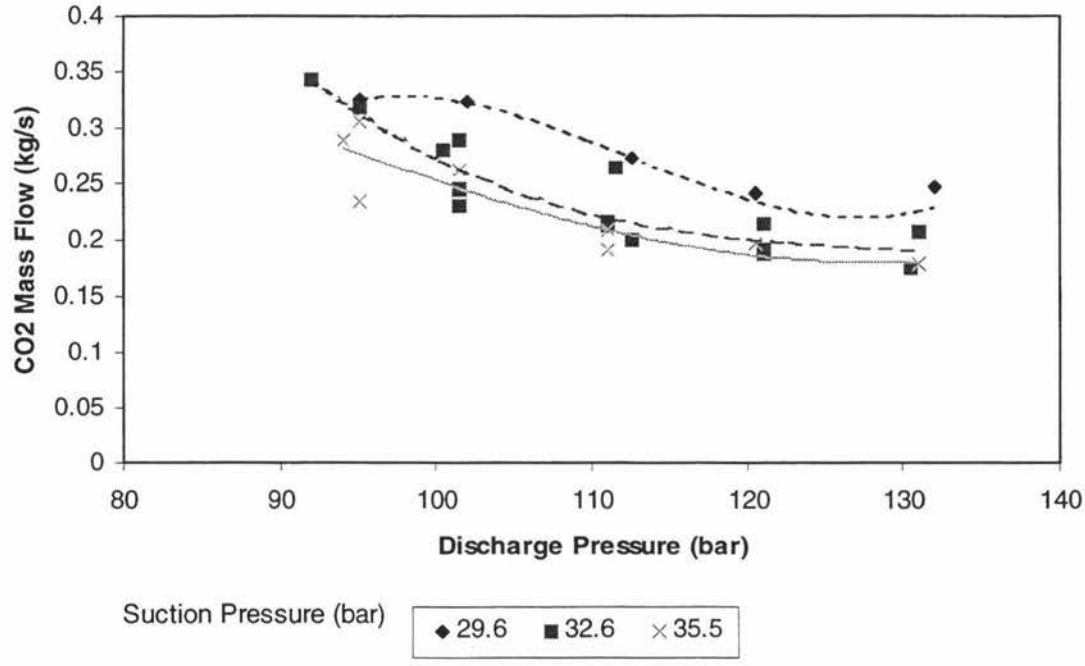

Figure 6.9: (a) Compressor speed, and (b) CO_2 mass flowrate as a function of discharge pressure for various suction pressures, with constant evaporator water flowrate (90°C hot water).

For these trials compressor speed (and hence CO_2 flowrate) was controlled to maintain a reasonably constant refrigeration load. As the discharge pressure increases, the increased refrigeration effect means that the evaporator water is cooled more, so the mean temperature difference across the evaporator reduces. To regain steady state at the same evaporation pressure means that the compressor speed has to be lowered to counteract this effect (Figure 6.9a) and the mass flowrate of CO_2 decreases (Figure 6.9a). Eventually, the increase in discharge pressure and pressure ratio also leads to significant drop in compressor volumetric efficiency, so that the speed has to be further increased to counteract this effect. Overall, this leads to the compressor speed and compressor power both going through a minimum (Figure 6.9a and Figure 6.10).

As the evaporator heat load for each suction pressure is relatively constant, and the gas cooler heat load is the sum of the evaporator load and the compressor load, the gas cooler heat load should follow a similar trend as the compressor power curve. In Figure 6.10, the compressor power curves go through a minimum, but the gas cooler heat loads were reasonably constant. However, there is enough uncertainty in the data that a minimum cannot be completely ruled out.

Higher suction pressures gave higher COPs for the entire range of discharge pressures (Figure 6.7). Nekså *et al* (1997), Hwang and Radermacher (1998) and Nekså *et al* (1998) reported the same effect. Higher COPs are achieved because higher suction pressures reduce the pressure ratio required to achieve the desired thermal lift, and compressor efficiency is also improved.

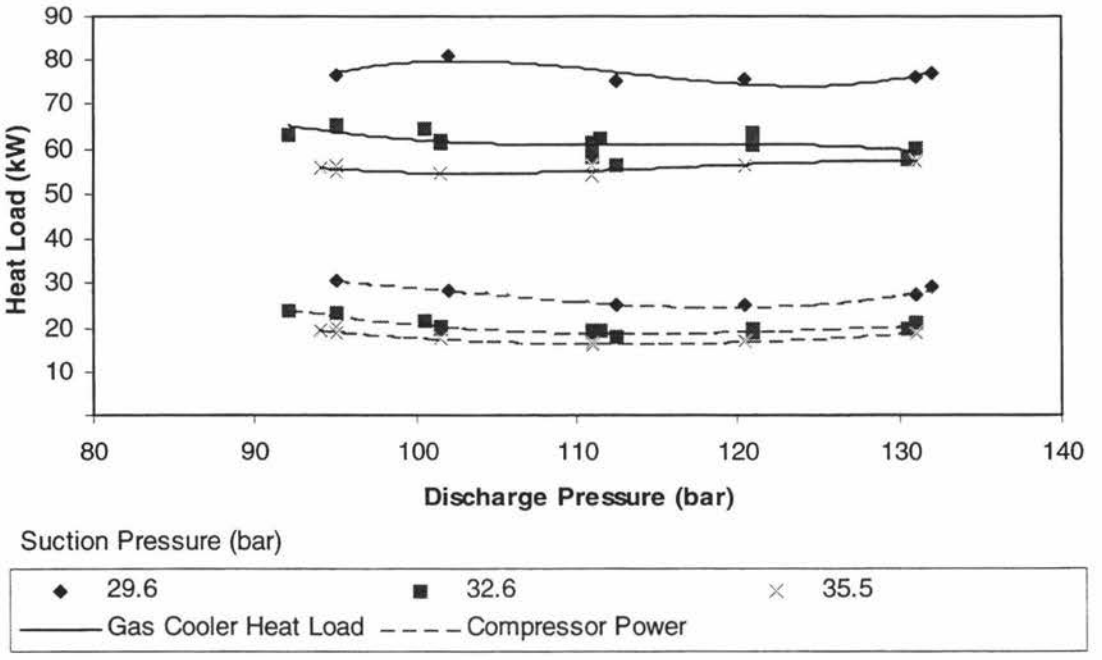

Figure 6.10: Gas cooler heat load and compressor power as a function of discharge pressure for various suction pressures, with constant evaporator water flowrate (90°C hot water).

Figure 6.11 and Table 6.2 summarise the results for the production of 65°C hot water. As expected, the optimum COP was greater (by about 20%) than for the production of 90°C hot water, due to the increase in thermodynamic efficiency as the heat sink temperature is reduced. This result has also been reported in the literature (Protsenko, 1992; Nekså, 1994; Halozan, 1996; White *et al*, 1997, Nekså *et al*, 1997; Hwang and Radermacher, 1998). Figure 6.12 shows system heating capacity against discharge pressure for the 65°C hot water trials. The compressor capacity is largely unchanged by shifting from 90°C to 65°C water. Hence, for the same suction and discharge pressure, the gas cooler heat load is similar to the 90°C trials, and the hot water flowrate must be increased to achieve a 65°C hot water discharge temperature. The increased water flowrate lowers the gas cooler CO_2 outlet temperature and therefore the approach temperature. Hence, for a given discharge pressure, the refrigeration effect per unit mass is greater, but the compressor power consumption will be largely unchanged. The result is a higher COP when producing 65°C hot water.

The optimum discharge pressure was about 17 bar lower because heat transfer in the gas cooler is less constrained. This was also found in other studies (Nekså, 1994 and Nekså *et al*, 1997). As the gas cooler size is fixed and the gas cooler heat load is similar, the limiting approach temperature is reached at a lower discharge pressure than for the 90°C trials, resulting in a lower optimum discharge pressure. The lower optimum discharge pressure also contributed to a higher optimum COP for the 65°C water compared with the 90°C water. The difference between optimum discharge pressures for different suction pressures remains quite small.

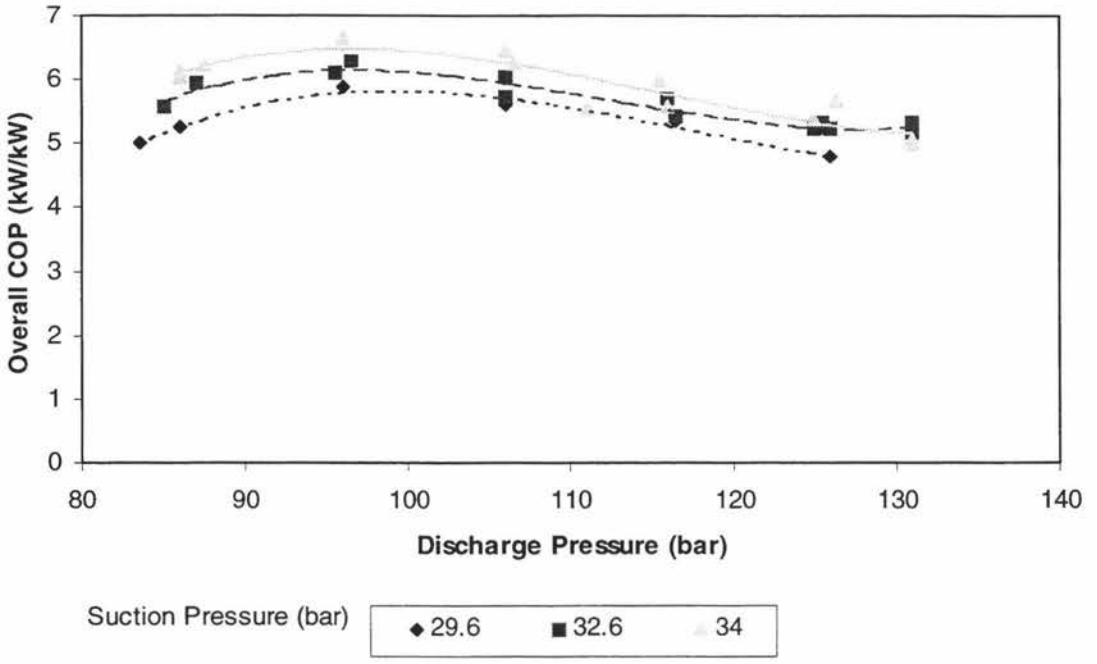

Figure 6.11: COP as a function of discharge pressure for various suction pressures, with constant evaporator water flowrate (65°C hot water).

Table 6.2: Optimum discharge pressure and COP for constant evaporator flowrate trials producing 65°C hot water

Suction Pressure	Optimum Discharge Pressure	Optimum COP
29.6 bar (-6.1 °C)	99.1 bar	5.8
32.6 bar (-2.5 °C)	96.7 bar	6.2
34 bar (-1.0 °C)	96.4 bar	6.5

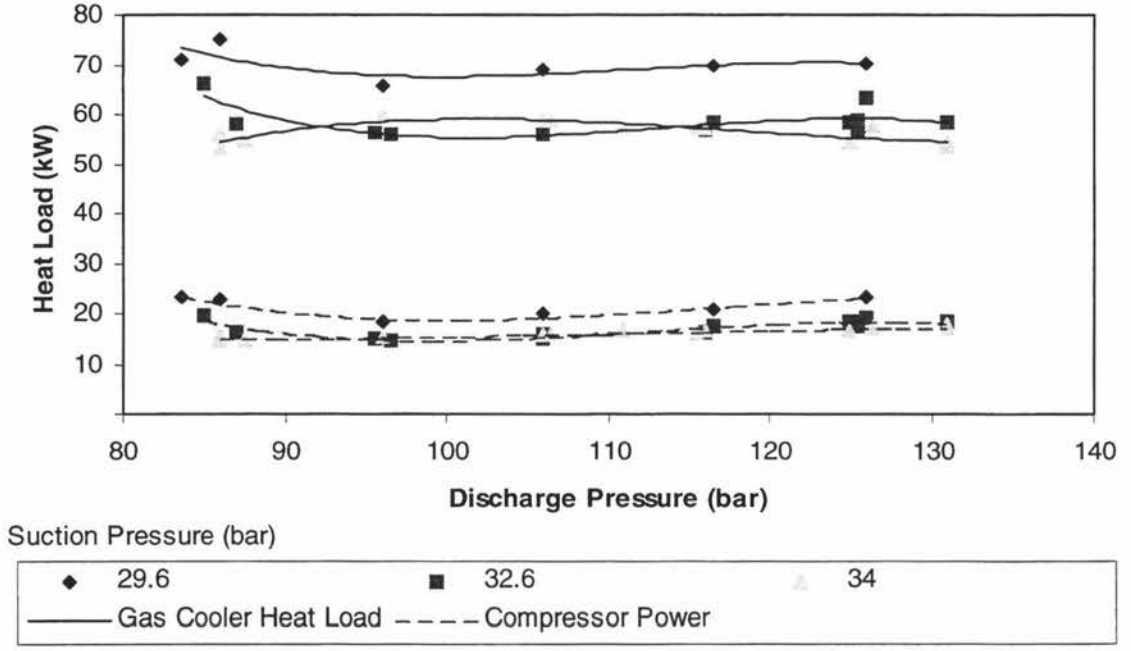

Figure 6.12: Gas Cooler Heat Load and Compressor power as a function of discharge pressure for various suction pressures, with constant evaporator water flowrate (65°C hot water).

The other trends for the 65°C hot water trial are very similar to those at 90°C.

Trials for 77.5°C hot water were only carried out for one suction pressure. In general, the results from these trials were similar (but intermediate) to the 65°C and 90°C trials, so the full results are not given.

The effect of discharge pressure on COP for different hot water discharge temperatures is given in Figure 6.13 for a suction pressure of 32.6 bar. The decrease in COP and increase in optimum discharge pressure with increasing hot water temperature is clear. At high discharge pressure, there is very little difference in COP for the different hot water temperatures, as the gas cooler heat transfer is not the constraint on overall system performance. Nekså *et al* (1997) observed very similar trends.

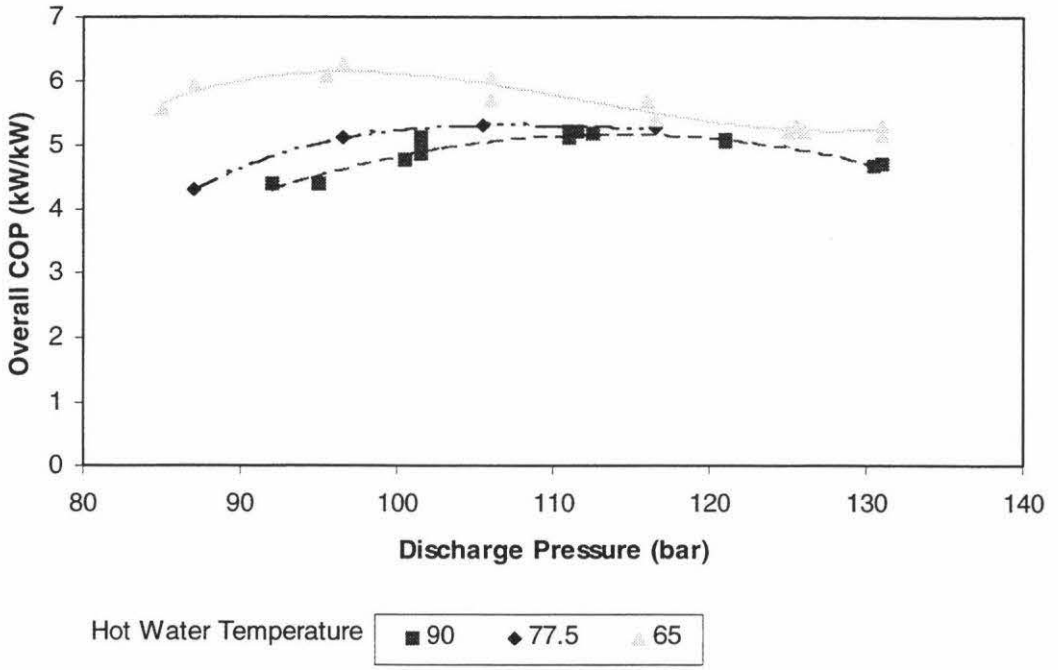

Figure 6.13: COP as a function of discharge pressure for various hot water temperatures, with constant evaporator water flowrate (32.6 bar suction pressure).

For all trials, the COPs obtained were consistent with those found in the literature for both simulated and experimental studies. The overall COP ranged from about 4 to 6.5, which equates to a heating COP of 2.5 to 3.8. Heating COP values in literature range from 3.3 to 4.7, but many of these use lower gas cooler water inlet temperature or higher evaporation temperature, both of which act to increase COP. For example, for water heating from 20°C to 65°C with an evaporation temperature of 0°C (35 bar) an optimum heating COP of 3.7 was obtained whereas a simulation by Protsenko *et al* (1992) gave 3.6. Interpolating the results from Nekså *et al* (1997), a heating COP of 4.1 (11% higher than the prototype) was achieved when heating water from 8°C to 65°C with a 0°C evaporating temperature. This difference can be explained by both the difference in compressor isentropic efficiency and the lower gas cooler inlet water temperature. The compressor used by Nekså *et al* (1997) had an efficiency greater than 80% whereas the efficiency of the prototype was only about 70%. For water heating to 77.5°C a COP of 3.2 was obtained compared to 3.3 from Protsenko *et al* (1992) and 3.6 for Nekså *et al* (1997), both of whom heated water to 80°C. Again, the differences can largely be explained by differences in compressor efficiency.

6.3.2 Constant Speed Trials

Figure 6.14 and Table 6.3 show the results of the trials where the compressor was run at full speed (1200 rpm) with 90°C hot water produced, and the suction pressure was controlled by varying the evaporator water flowrate. Compared with the variable speed trials, the compressor speed and hence the heating and cooling capacity was 0% to 35% greater for the same suction pressure conditions. The COPs are slightly lower than those for the constant evaporator water flowrate trials, and the optimum discharge pressure is higher and increased with increasing suction pressure.

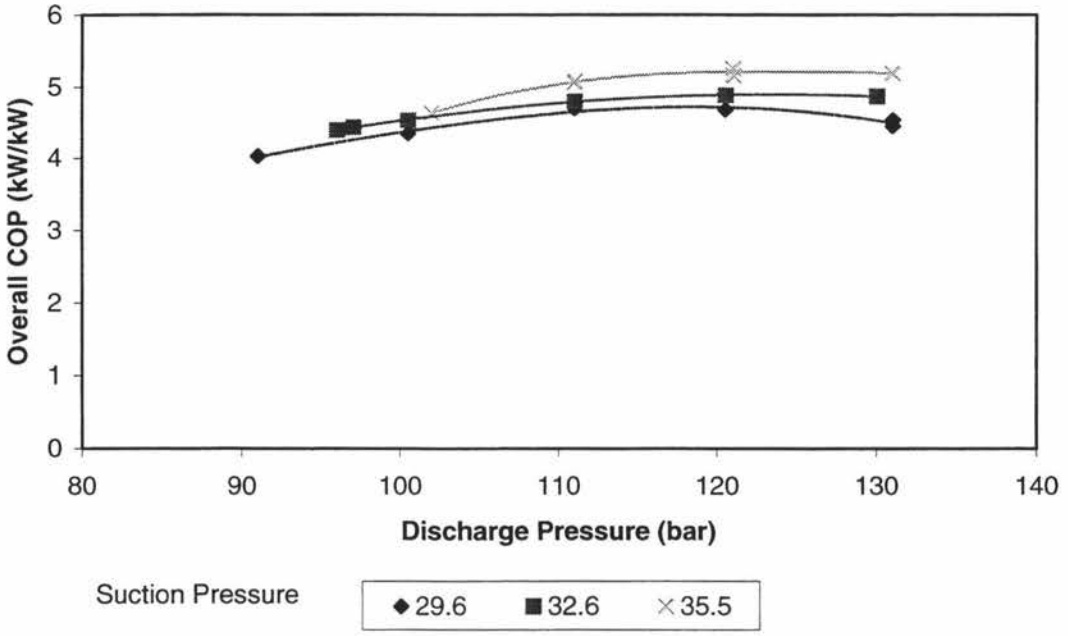

Figure 6.14: COP as a function of discharge pressure for various suction pressures, with constant compressor speed (90°C hot water).

Table 6.3: Optimum Discharge Pressure and COP for Constant Compressor Speed Trials Producing 90°C Hot Water

Suction Pressure	Optimum Discharge Pressure	Optimum COP
29.6 bar (-6.1 °C)	119 bar	4.7
32.6 bar (-2.5 °C)	123 bar	4.9
35.5 bar (0.7 °C)	123 bar	5.2

The lower COP and higher optimum discharge pressure were expected because with the compressor at full speed, the compressor capacity (CO_2 mass flowrate) is greater than the variable speed trials, and therefore the gas cooler heat transfer becomes more limiting. The higher system heating capacity requires a higher temperature difference in the gas cooler and hence higher discharge pressure, but this leads to lower energy efficiency. The same COPs and optimum discharge pressures as for the variable speed trials could have been achieved if the gas cooler heat transfer area was increased by 0 - 35%, thereby maintaining the same relative capacity compared with the compressor.

Figure 6.15 shows the change in gas cooler heat load and compressor power consumption with respect to discharge pressure for the 90°C hot water constant speed trials. The compressor power remains relatively constant for each suction pressure throughout the range of discharge pressures. As discussed previously, as the discharge pressure is increased, the discharge temperature increases which leads to greater heat transfer in the coolers. However, at high discharge pressures, the heat load reduces because the CO_2 mass flowrate decreases due to the drop-off in the volumetric efficiency of the compressor with increasing pressure ratio. This drop in mass flowrate

compensates for the increased work per unit mass caused by the increased pressure ratio, leading to almost constant compressor power consumption. The system heating capacity (gas cooler heat load) increased with discharge pressure across most of the range with the 29.6 bar trials reaching a maximum at about 120 bar. For the 32.6 bar trials, the capacity reached a maximum near the end of the pressure range, and the 35.5 bar trials did not quite reach a maximum.

Table 6.4 gives the maximum attainable heating and cooling loads for the prototype when achieving 90°C hot water. The heat loads are significantly lower than design conditions (129 kW of heating for the gas cooler, and 88 kW of cooling for the evaporator at a saturated suction temperature of –5°C).

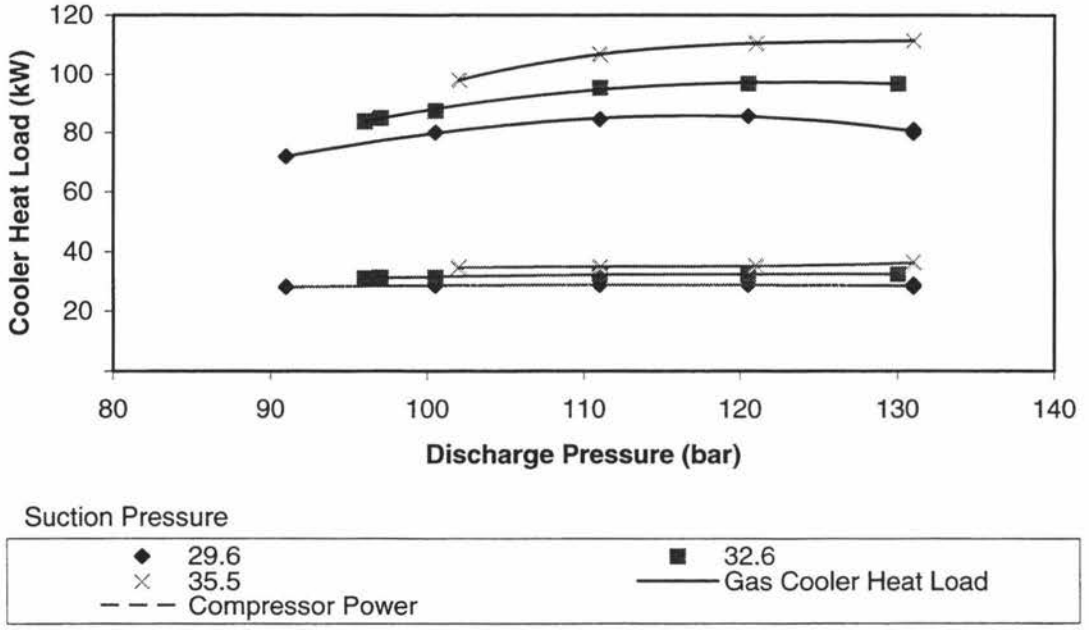

Figure 6.15: Gas cooler heat load and compressor power as a function of discharge pressure for various suction pressures, with constant compressor speed (90°C hot water).

Table 6.4: Maximum Heating and Cooling Capacity for Constant Compressor Speed Trials Producing 90°C Hot Water

Suction Pressure (bar)	Heating Capacity (kW)	Optimum Discharge Pressure for Heating (bar)	Cooling Capacity (kW)	Optimum Discharge Pressure for Cooling (bar)
29.6 (-6.1°C)	86	117	55	120
35.5 (0.7°C)	111	>131	77	>131

As expected, heating capacity increased significantly at higher suction pressures. The higher suction pressure gives a higher CO_2 density which leads to a higher mass flowrate, if the volumetric flowrate through the compressor is constant. Also, at high suction pressures the pressure ratio is lower, so the volumetric efficiency is higher and the volumetric flowrate through the compressor also increases. Overall, this leads to an increased CO_2 mass flowrate and gas cooler heat load.

The results for the full speed trials with 65°C hot water being produced are given in Figure 6.16 for a 29.6 bar suction pressure only. The optimum discharge pressure was 100 bar (19 bar less than the 90°C trials) and the optimum COP was 5.1 (9% higher than for the 90°C). The increase in COP at 65°C compared with 90°C is less for the variable speed trials because the gas cooler heat transfer performance is limiting overall system performance.

Figure 6.17 shows the system heating capacity and compressor power as a function of discharge pressure for 65°C hot water. There is a higher maximum heating capacity, and a lower optimum discharge pressure for heating capacity, but the compressor power is about the same as for the 90°C trials. The higher heating capacity is due to the increase in CO_2 mass flowrate caused by the reduced pressure ratio and higher volumetric efficiency.

As for the 90°C hot water trials, as the discharge pressure is increased, the CO_2 mass flowrate drops off due to deteriorating compressor volumetric efficiency. As the mass flowrate decreases, the gas cooler becomes less constrained, leading to lower optimum discharge pressure for heating capacity.

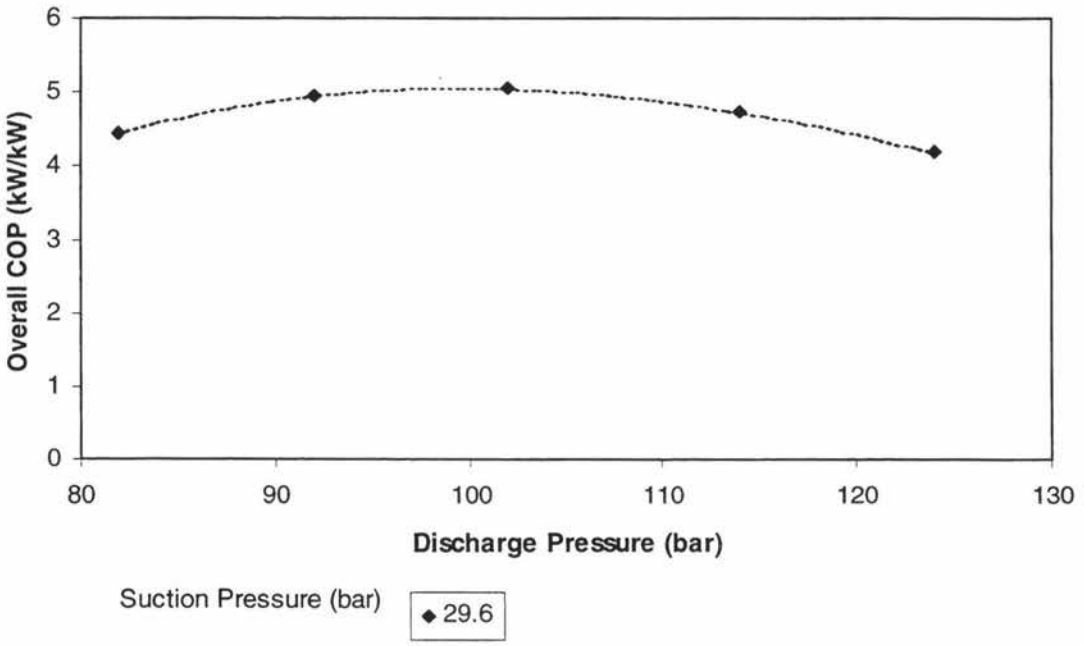

Figure 6.16: COP as a function of discharge pressure for a 29.6 bar suction pressure, with constant compressor speed (65°C hot water).

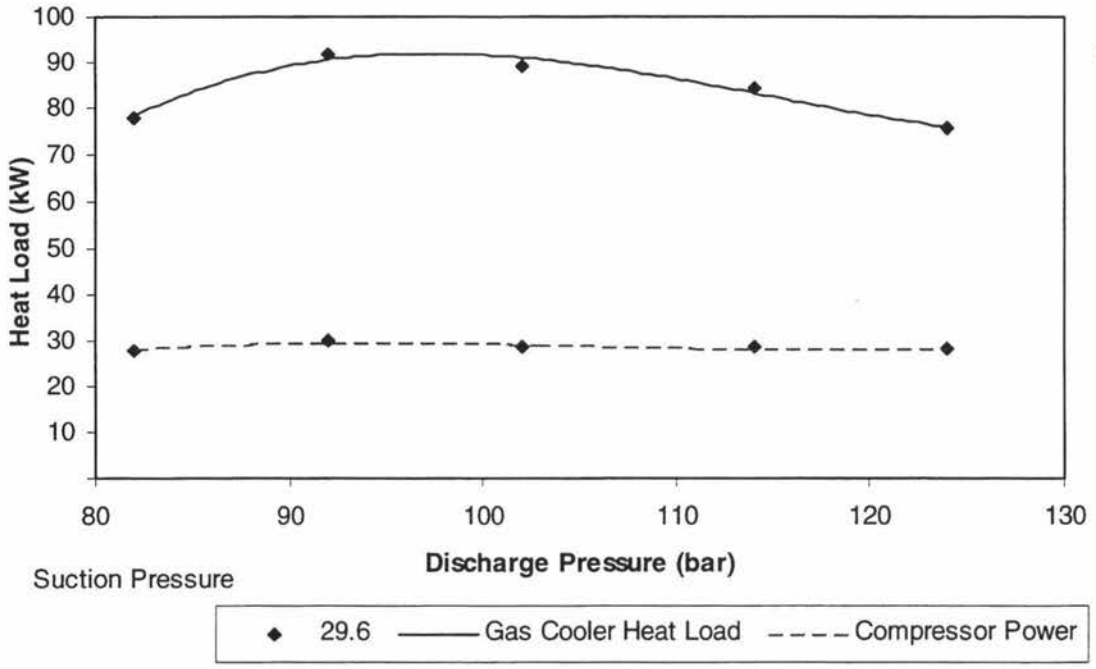

Figure 6.17: Gas Cooler Heat Load and Compressor power as a function of discharge pressure for various suction pressures, with constant compressor speed (65°C hot water).

The constant speed, 65°C hot water trials were carried out only with a 29.6 bar (-6.1 °C) suction pressure. The maximum heating capacity for was 92 kW at a discharge pressure of 97 bar. The maximum cooling capacity was 57 kW at a discharge pressure of 98 bar. These heat loads are the maximum heat loads obtained for the system for the given suction pressure.

6.3.3 Effect of Evaporator Water Flowrate and Inlet Temperature

In the third set of trials, the evaporator water inlet temperature was varied along with the water flowrate to maintain constant suction conditions. Because suction conditions are constant, it was expected that compressor and gas cooler performance would be largely unchanged but that evaporator performance might change.

Figure 6.18 and Table 6.5 show the effect of discharge pressure on COP for different suction pressures for three evaporator water inlet temperature and evaporator water flowrate combinations. As expected, the COPs were generally quite similar to each other.

At lower water temperatures there is a reduced thermal driving force for heat transfer in the evaporator. Consequently, the evaporation rate of CO_2 is reduced. The reduced flowrate of CO_2 means that the CO_2 outlet temperature from the gas cooler is lower, leading to an increase in COP. This increase is not dramatic because the effect of reduced thermal driving force in the evaporator was offset, to a large extent, by an increase in heat transfer coefficient. The extent of the increase in overall heat transfer

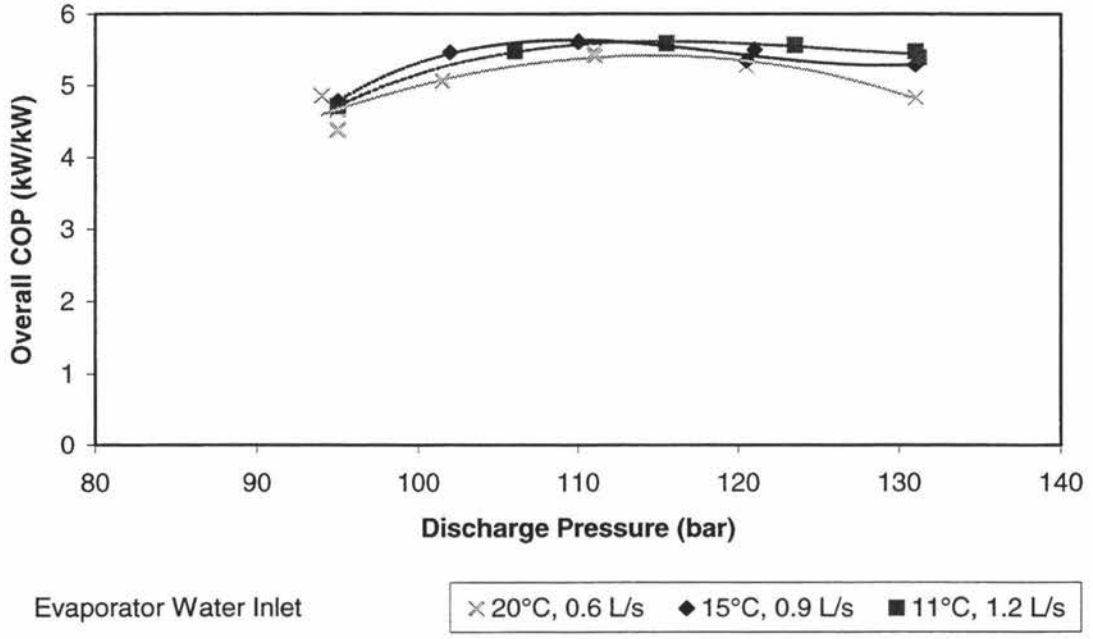

Figure 6.18: COP as a function of discharge pressure for various evaporator water inlet temperatures (35.5 bar suction pressure).

Table 6.5: Optimum Discharge Pressure, Optimum COP and Evaporator Heat Transfer Coefficient for Evaporator Water Inlet Temperature Trials (35.5 bar suction pressure).

Temperature and Flowrate	Optimum Discharge Pressure	Optimum COP	Evaporator Heat Transfer Coefficient (W/m^2K)
11 °C, 1.2 L/s	115 bar	5.6	1016 – 1137
15 °C, 0.9 L/s	109 bar	5.6	686 – 804
20 °C, 0.6 L/s	114 bar	5.4	428 – 561

6.3.4 Performance at Design Conditions

Figure 6.19 shows the results of the trials with 11°C evaporator water at as high a flowrate as could be achieved with the water supply system, for 90°C and 65°C hot water. This was the closest that the prototype could be operated to design conditions due to water flowrate limitations. The maximum COP for the 90°C hot water trials was 5.5 (at 114 bar discharge pressure), which was 0.3 higher than the maximum COP obtained in the constant evaporator water flowrate trials. The maximum for the 65°C trials was 6.6 (at 102 bar) which was 0.4 higher than for the constant evaporator water flowrate trials. The maximum heating and cooling capacities were 85 kW and 54 kW respectively for 90°C hot water which were still considerably lower than the design values.

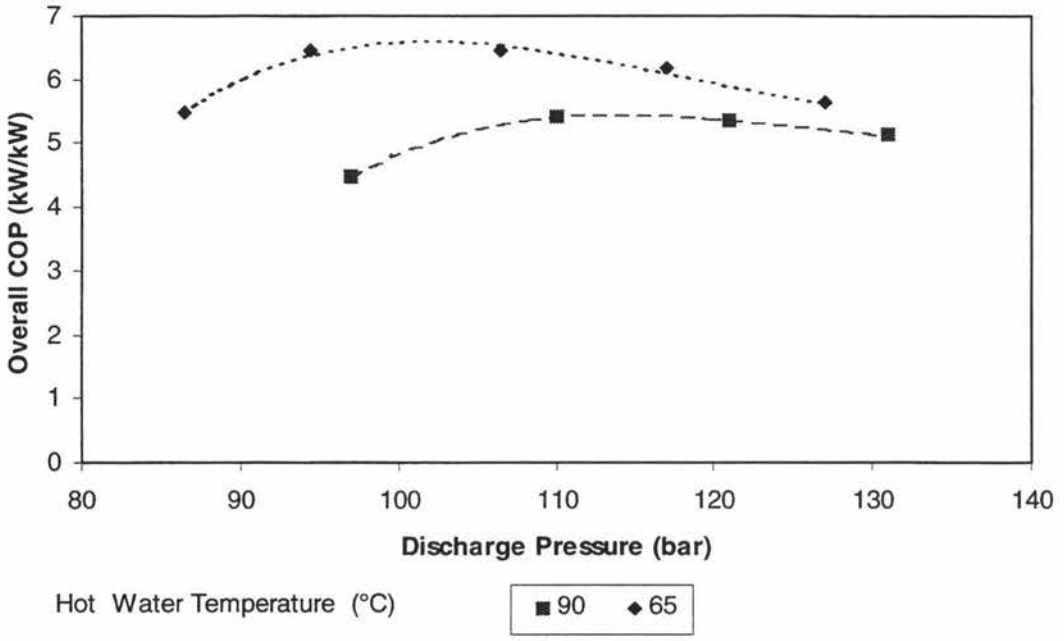

Figure 6.19: COP as a function of discharge pressure for various hot water temperatures, for evaporator water conditions close to design conditions (32.6 bar suction pressure).

As the increased evaporator flow lead to improved evaporator performance, if the evaporator water flowrate was at actual design conditions the performance of the system would be improved even further. Overall, the slightly lower COPs and lower capacities than design were attributed to the compressor performance being slightly lower than anticipated at the design stage, and the higher than design gas cooler water inlet temperature.

6.3.5 Oil Trials

Oil was added to the system to try to improve the leakage rate past the piston rod packing. Figure 6.1 to Figure 6.5 show the difference between the performance of the gas cooler and evaporator with and without oil in the system. The heat transfer coefficient (U) was plotted against water flowrate. This was done to allow comparison of heat transfer coefficient values, as water flowrate has an effect on the water-side heat transfer coefficient (higher flowrates lead to higher heat transfer coefficient).

As can be seen, oil seems to have little or no effect on the gas cooler performance (Figure 6.1), but a significant effect on the performance of the evaporator (Figure 6.2). In the gas coolers the oil would have been relatively hot with a low viscosity, so there would have been little fouling caused by the oil.

Figure 6.2 shows that there is a reasonably constant difference between the overall heat transfer resistance (1/U) with and without oil in the system. The difference in the resistance was about 0.00055 m^2K/W irrespective of water flowrate (which corresponds to a heat transfer coefficient of about 1800 W/m^2K). This resistance was attributed to

the oil fouling in the evaporator, which would only occur on the CO_2 side. The fouling caused by the oil was expected, as the oil in the system would tend to accumulate in the bottom of the evaporator, being physically the lowest part of the system. Also, the oil in the evaporator would be quite cold, thus increasing its viscosity and the thickness of the film on the heat transfer surfaces. This observation is consistent with the effect of oil fouling in heat exchangers for other refrigerants (Stoeker, 1988).

Figure 6.5 shows the heat transfer coefficient for the recuperator with and without oil in the system. This indicates that oil did not have a significant effect on the performance of the recuperator. This is reasonable, because the CO_2 gas on the hot side would still be warm, and thus the viscosity of the oil would be low. In addition, oil would not tend to accumulate in the cold side of the recuperator as it was located after the separator, which would remove most of the oil from the vapour.

Figure 6.20 and Figure 6.25 show the difference in overall system performance for the constant evaporator water flowrate trials with and without oil in the system. As can be seen, at low discharge pressures the performances are quite similar, but at higher discharge pressures the performance of the system with oil declines. Figure 6.21 shows that the compressor isentropic efficiency for the system with oil is worse than for the system without oil, especially at high discharge pressures. This loss in efficiency accounts for the drop off in COP. It is unlikely the loss in efficiency is caused by wear, as only three days elapsed between the oil-free and oil trials for the 90°C hot water with 1.4 L/s 11°C evaporator water flowrate trials. Such a loss in isentropic efficiency due to the presence of oil was not expected and should be further investigated with the compressor manufacturer.

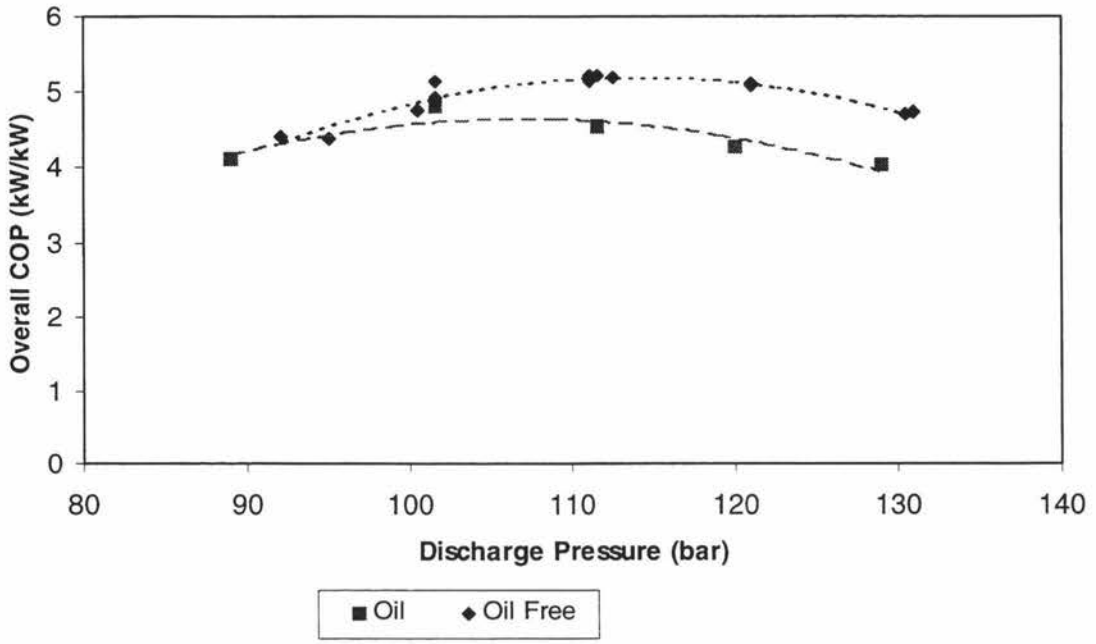

Figure 6.20: COP as a function of discharge pressure, with 0.6 L/s evaporator water flowrate at 21°C and 32.6 bar suction pressure, producing 90°C hot water, with and without oil in the system.

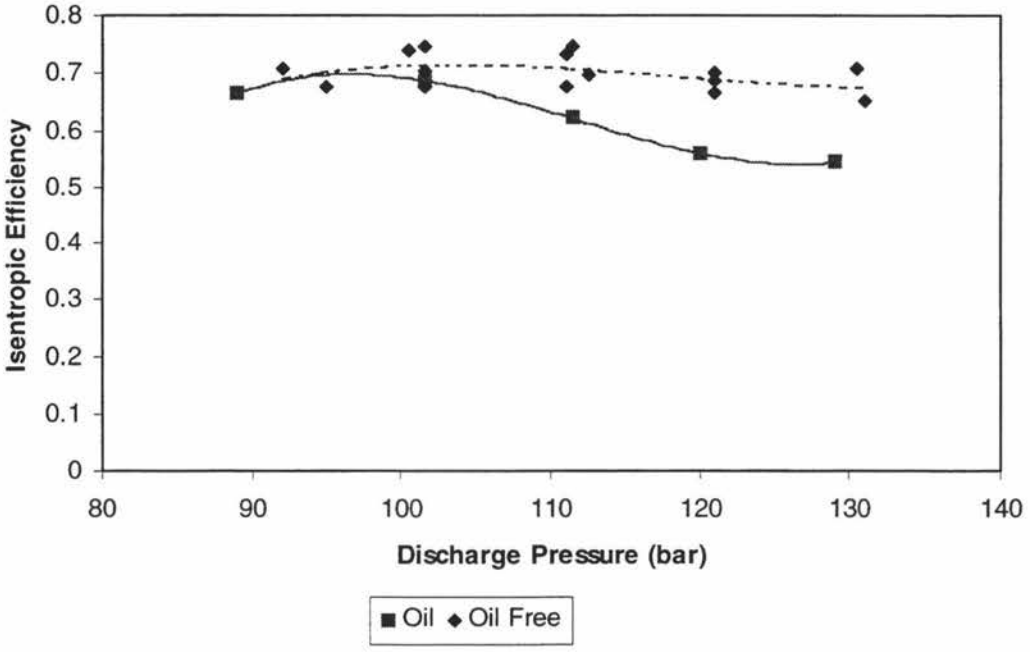

Figure 6.21: Isentropic efficiency as a function of discharge pressure, for trials with 0.6 L/s evaporator water flowrate at 21°C and 32.6 bar suction pressure, producing 90°C hot water, with and without oil in the system.

For the constant speed trials (Figure 6.22 and Figure 6.24), the difference in COP between the oil and oil-free systems is very small, with the oil-free system having slightly better performance. For the middle of the pressure range where the heat loads were the greatest, the water flows required to achieve 65°C hot water could not be achieved due to water supply limitations at the time of testing. This meant higher water temperatures (up to 73°C) were obtained which led to slightly poorer performance for those trials. Figure 6.23 shows that for the 90°C constant speed trials the compressor isentropic efficiencies for both systems were very similar, and hence the overall COPs were also very similar.

Paired t-tests were used to determine if there were statistical differences between the performance with oil and without oil. Overall, oil had a statistically significant detrimental effect on evaporator heat transfer performance at the 95% level of confidence for all trials except the constant speed trials with 65°C hot water. Both the 20°C and 11°C evaporator water inlet temperature trials with constant evaporator water flow and 90°C hot water had a statistically significant difference in isentropic efficiency. Hence, for these trials the performance of the oil and oil-free systems were different, but for all other trials, for the same suction and discharge pressures, there was no evidence that prototype performance was affected by oil.

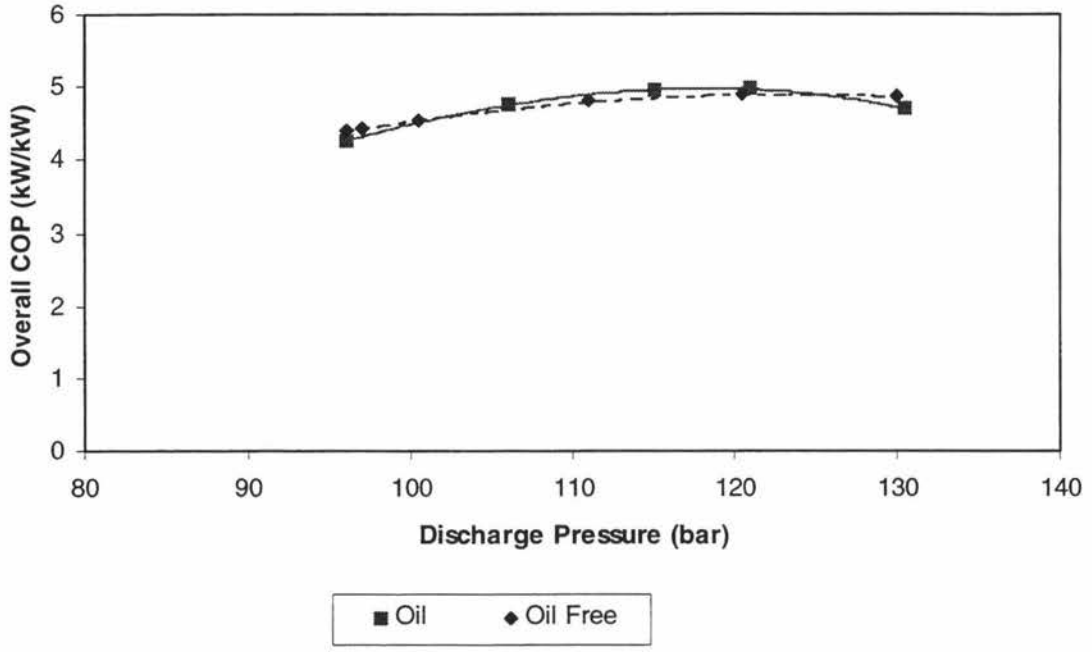

Figure 6.22: COP as a function of discharge pressure, with constant compressor speed and 32.6 bar suction pressure, producing 90°C hot water, with and without oil in the system.

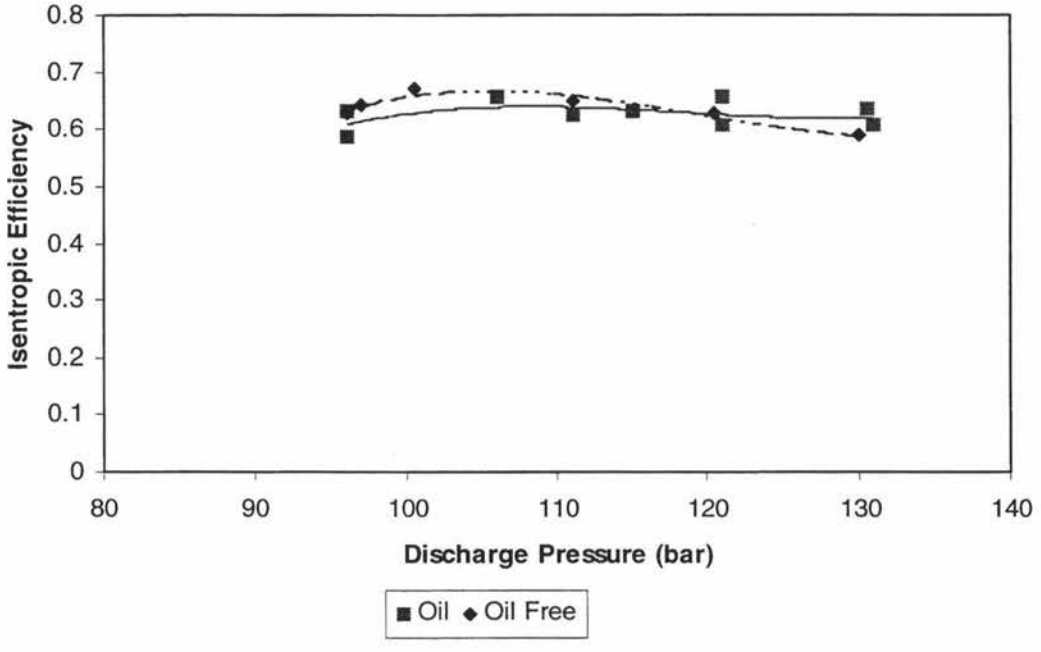

Figure 6.23: Isentropic efficiency as a function of discharge pressure, with constant compressor speed and 32.6 bar suction pressure, producing 90°C hot water, with and without oil in the system.

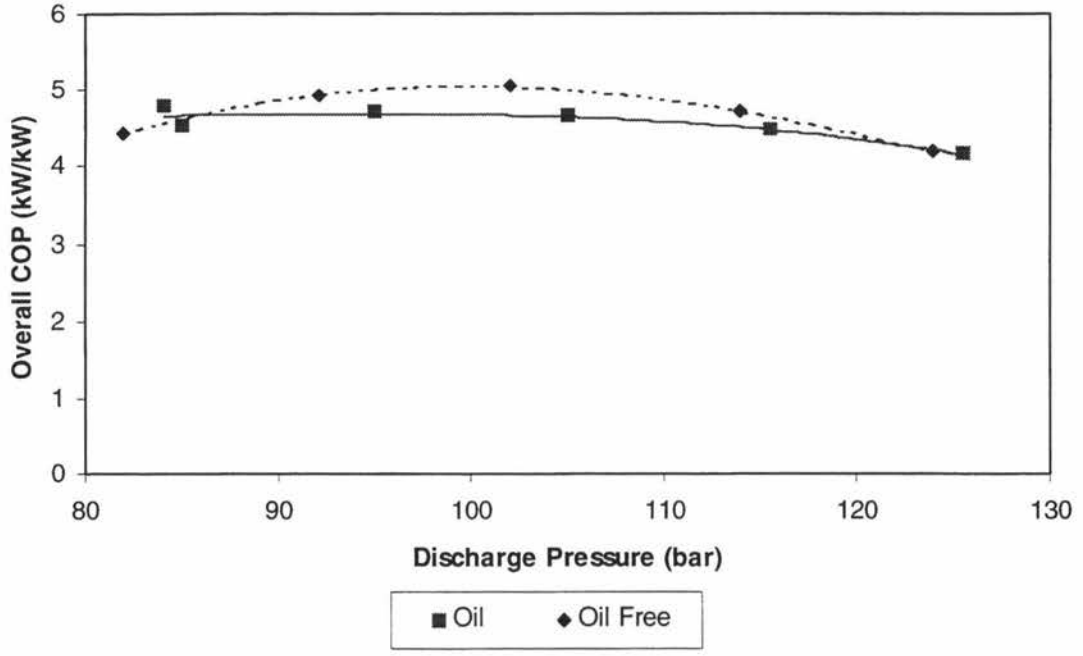

Figure 6.24: COP as a function of discharge pressure, with constant compressor speed and 29.6 bar suction pressure, producing 65°C hot water, with and without oil in the system.

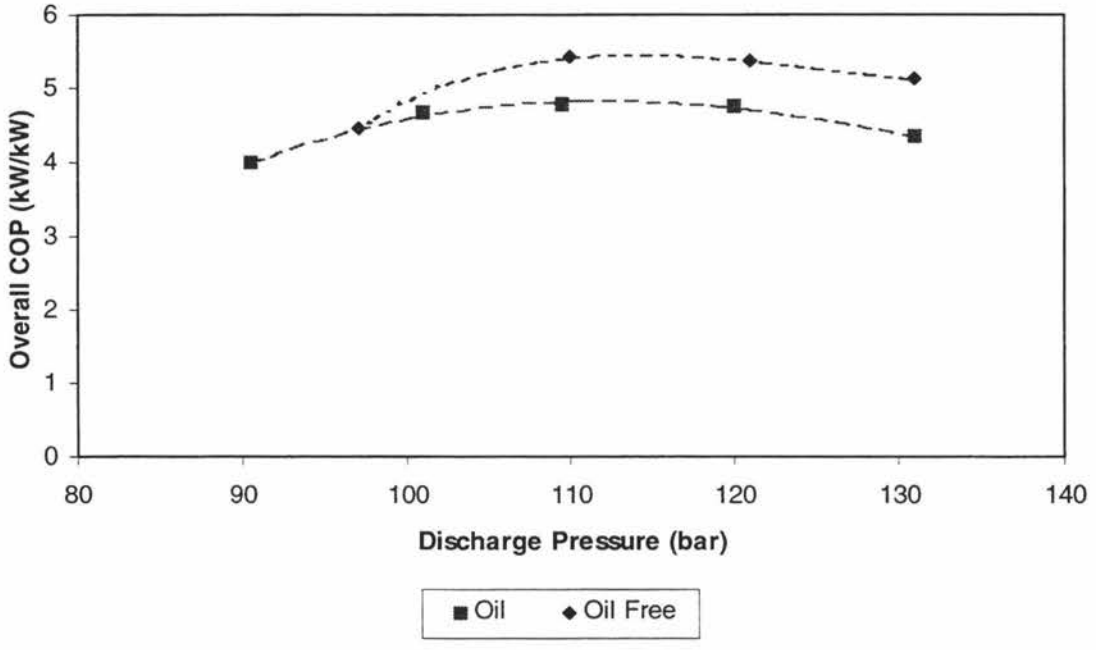

Figure 6.25: COP as a function of discharge pressure, with 1.4 L/s evaporator water flowrate at 11°C and 32.6 bar suction pressure, producing 90°C hot water, with and without oil in the system.

6.4 Process Simulations

6.4.1 System Performance

The constant evaporator water flowrate trials in Section 6.3.1 were simulated for 65°C and 90°C hot water production. Figure 6.26 and Figure 6.27 show the results of the Hysis simulations for 90°C and 65°C hot water being produced with a constant evaporator water flowrate of 0.625 L/s and constant water inlet temperatures of 20°C. The experimental CO_2 flowrate data and *UA* values were used. A compressor polytropic efficiency of 70% was assumed for all calculations.

Figure 6.28 and Figure 6.29 show the results for simulations carried out with a fixed CO_2 mass flowrate for 90°C hot water production. The COP curves have an optimum, with the highest suction pressures leading to the highest COPs. The reason the COP reaches a maximum is clearly illustrated, as the compressor power increases in a linear fashion, while the gas cooler heat load increases rapidly at first, then levels off slightly as discharge pressure increases.

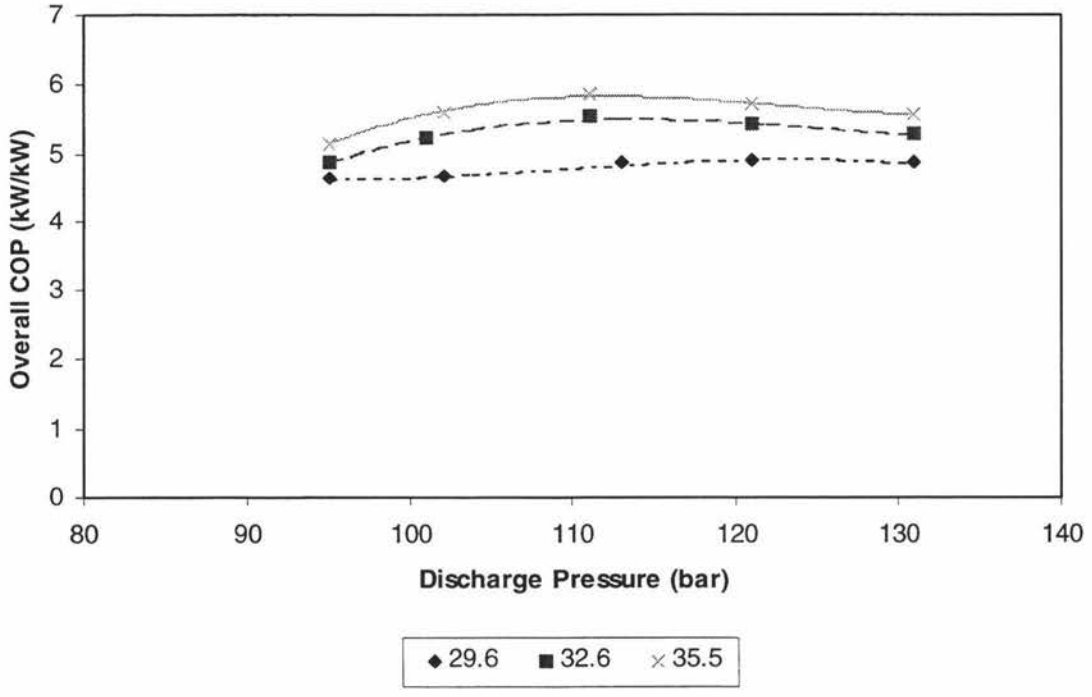

Figure 6.26: Simulated COP as a function of discharge pressure for various suction pressures, with constant evaporator water flowrate (90°C hot water).

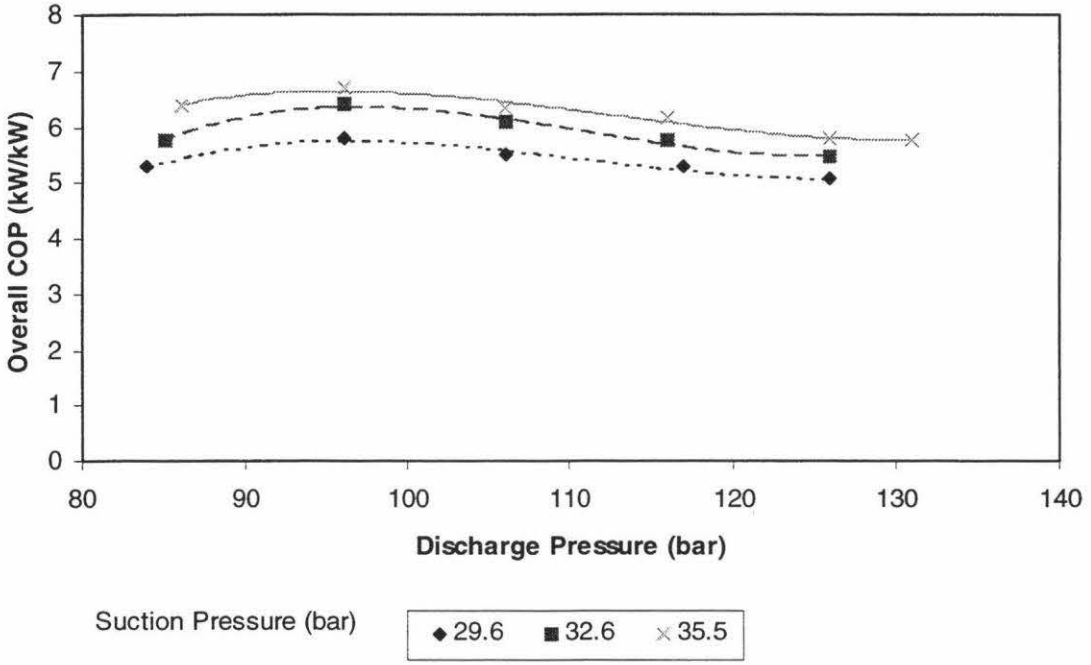

Figure 6.27: Simulated COP as a function of discharge pressure for various suction pressures, with constant evaporator water flowrate (65°C hot water).

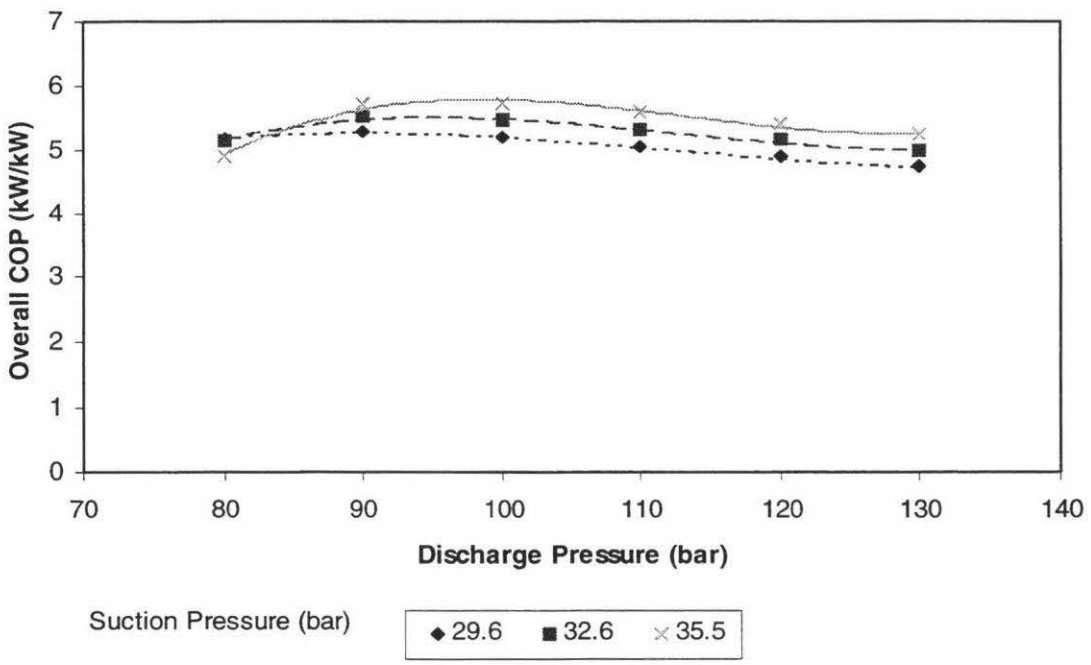

Figure 6.28: Simulated COP as a function of discharge pressure for various suction pressures, with constant evaporator water flowrate with constant CO_2 mass flowrate (90°C hot water).

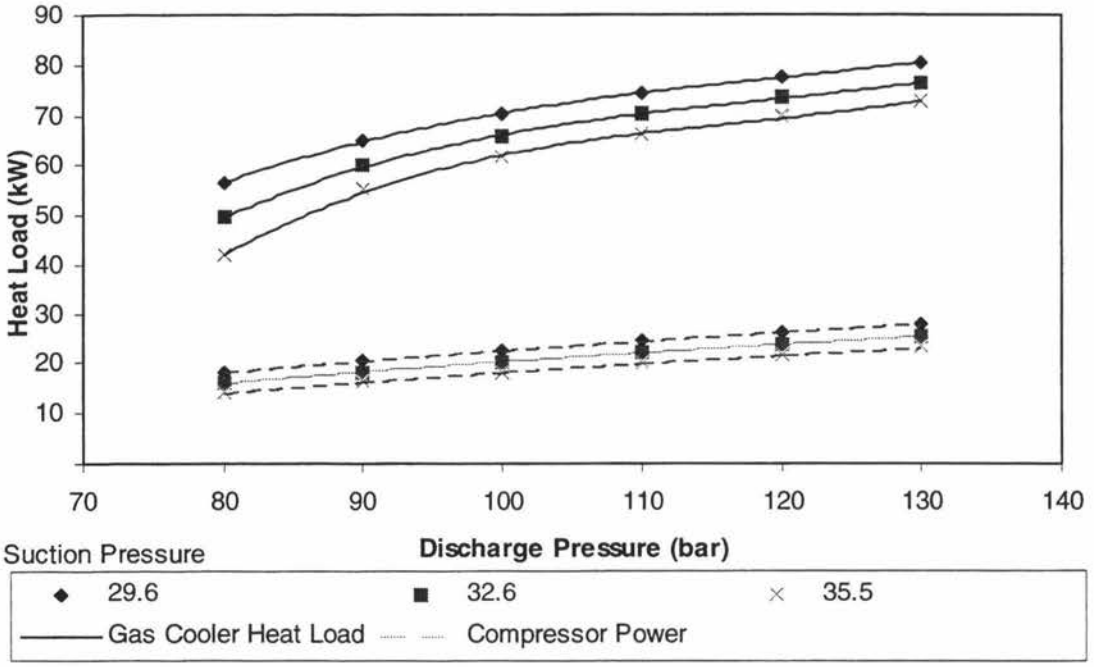

Figure 6.29: Simulated gas cooler and compressor heat load as a function of discharge pressure for various suction pressures, with constant compressor speed with constant CO_2 mass flowrate (90°C hot water).

Overall, the simulations predicted very similar performance trends to those measured for the prototype.

6.4.2 Gas Cooler Temperature Profile

In the experimental trials, it was shown that the gas cooler size limited overall system performance under some conditions. The gas cooler temperature profile simulation was undertaken to quantify whether the prototype gas cooler was significantly affecting overall system performance. This was done by comparing actual performance with the performance that would be achieved if the gas cooler was large enough to achieve a 1°C approach temperature between the CO_2 and the water. The temperature profile was modelled for a number of different discharge pressures with the compressor suction conditions fixed at 30 bar and 10°C and the isentropic efficiency fixed at 70%. For a given discharge pressure, this led to a fixed discharge temperature. The water inlet temperature was set to 20°C, and the outlet temperature set to 90°C. A constant CO_2 mass flowrate of 0.4 kg/s was used for all discharge pressures. This was considered reasonable, as apart from the effect of pressure ratio on volumetric efficiency, the suction pressures have the largest bearing on mass flowrate. The water mass flowrate was then set to give a minimum approach temperature difference between the CO_2 and water of 1°C. The predicted temperature profiles through the gas coolers are shown in Figure 6.30 for different discharge pressures.

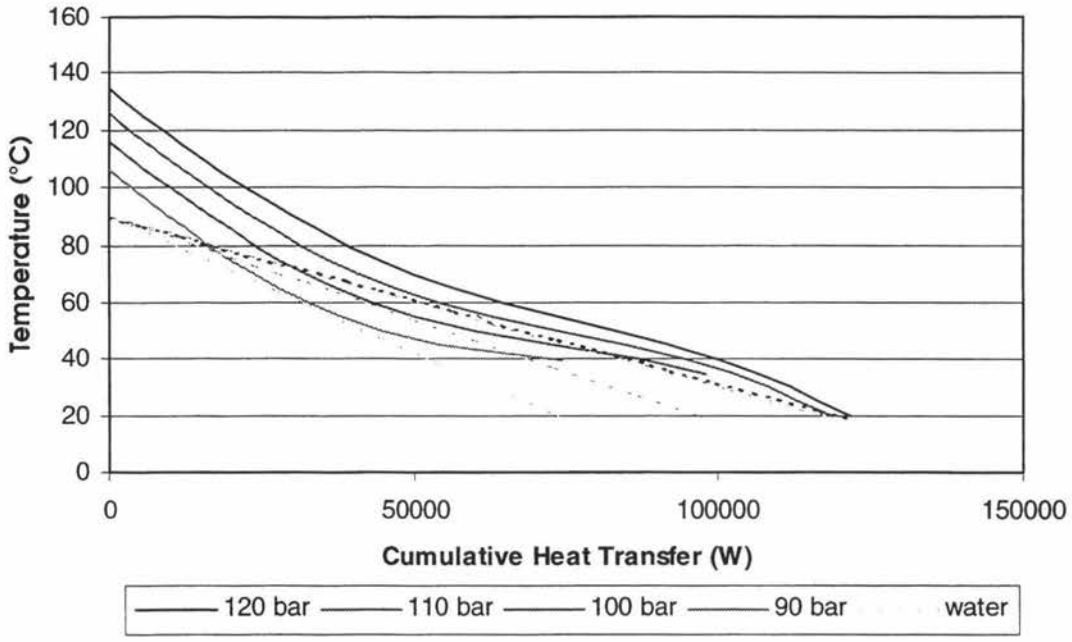

Figure 6.30: Gas Cooler Temperature Profile

As can be seen, the lower the pressure, the lower the amount of heat transfer that can take place (shown by the distance of the curves to the right). Also, lower pressures lead to higher CO_2 gas cooler exit temperatures. For the lowest two pressures, the heat transfer becomes limited by the pinch effect of the CO_2 curve rather than the approach at the water inlet. As the pressure is increased, the pinch point has less of an effect. For the 110 bar curve, the CO_2 temperature approaches the water temperature around the pinch in the middle of the gas cooler, but the actual limiting factor is the approach temperature at the water inlet. For the 120 bar curve, the pinch point temperature difference becomes quite large and the overall heat exchange is only constrained by the water entry approach temperature.

Figure 6.31 shows the resulting COPs from the temperature profile calculations.

The optimum COP can be seen to occur at around 114 bar, which agrees with the experimental data. The optimum COP is about 3.6, which equates to an overall COP of 6.2 which is higher than the experimental COP of 5.4 (15% higher). This suggests that there could be some benefit if the prototype gas cooler was increased in size.

Overall, these curves are similar in shape to the constant CO_2 mass flowrate simulations using Hysis.

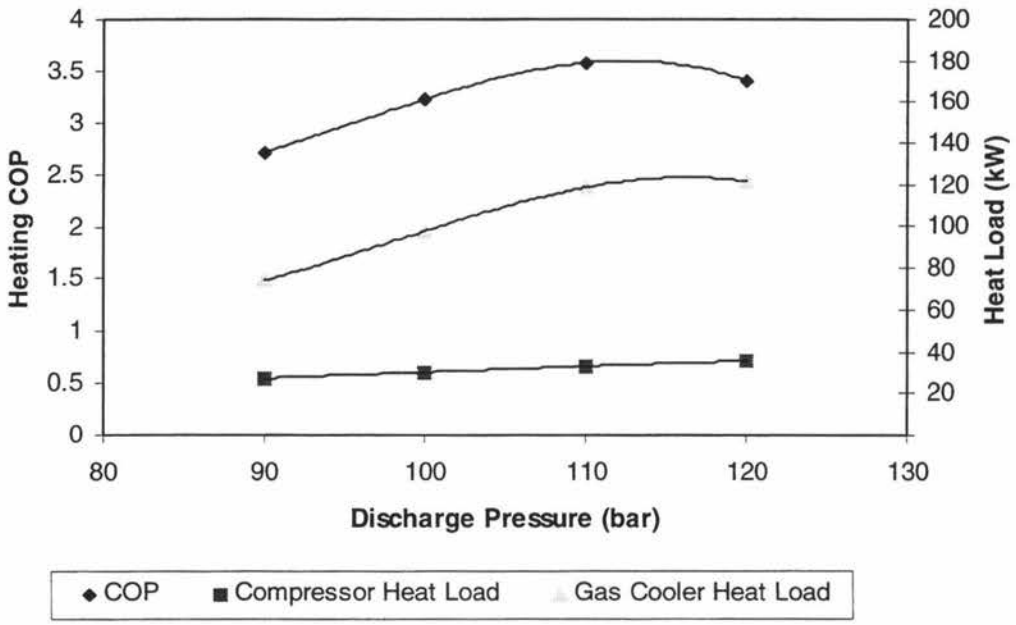

Figure 6.31: COP as a function of discharge pressure for temperature profile

6.5 Economic Viability

Fleming (1996) calculated the potential savings for using a CO_2 transcritical heat pump instead of separate refrigeration and hot water systems. The separate systems were sized for 430 kW of cooling at –5°C and 600 kW of heating to 90°C. An ammonia unit was used for refrigeration, with an assumed COP of 4.2. It had an estimated capital cost of about $200,000. Assuming 4000 hours of operation per year and a 90% motor efficiency, this leads to a 1638 GJ net annual energy use. The boiler for water heating would use 12343 GJ per year assuming 70% efficiency, and would have a capital cost of about $20,000. The CO_2 heat pump examined assumed a combined COP of 6. This gave an overall electricity use of 2733 GJ per year which equates to savings of $56,830 per year assuming costs of 9.7 ¢/kWh for electricity and $7/GJ for natural gas.

An experimental COP of 5.4 was achieved when heating water from 20°C to 90°C, so the analysis was repeated for this lower value. The net annual energy use increased to 3052 GJ, but this still leads to energy savings of 10929 GJ/year if all the hot water is utilised. Assuming costs of 9.7 ¢/kWh for electricity and $7/GJ for natural gas, this equates to annual savings of $48,229.

The estimated capital cost for a CO_2 heat pump of 600 kW heating capacity was between $121,000 and $133,000. This is lower than the capital for the traditional systems, but does no include a hot water storage system that might be required if the refrigeration and hot water demand are not concurrent. However, for a new facility it is likely that the heat pump has both lower capital and lower operating costs, and is obviously a better option. For the case where the heat pump could replace an existing system, the extra capital expenditure for the heat pump must be compared with the ongoing energy savings.

Figure 6.32 shows the internal rate of return (average return over ten years) for the CO_2 heat pump (with a COP of 5.4), for different capital costs and operating hours. The longer the CO_2 heat pump is operated the greater the rate of return. If the capital is between \$121,000 and \$133,000, this gives an internal rate of return greater than 34% for 4000 hours of operation per year. Clearly, even with slightly lower COP than assumed by Fleming (1996), the heat pump looks economically attractive, but further refinements of the capital cost need to be made.

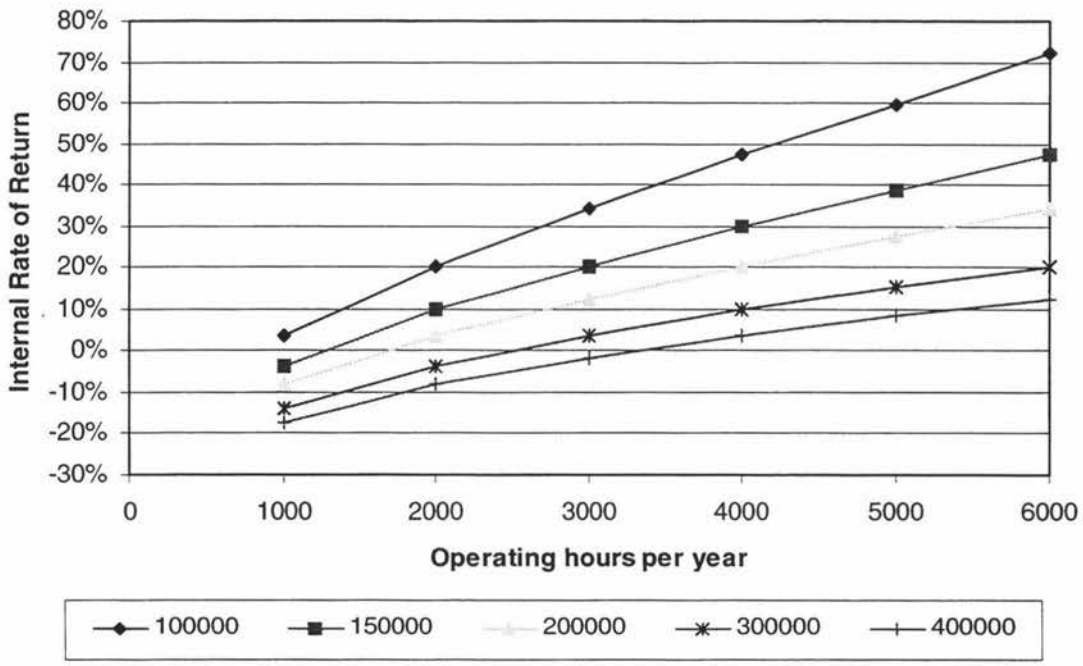

Figure 6.32: Internal rate of return

7 CONCLUSION

The components of the prototype transcritical carbon dioxide heat pump were sized using standard heat transfer and thermodynamic relationships, and were mainly selected from standard high pressure heat transfer equipment used by the gas processing industry. Commissioning of the heat pump showed that CO_2 leakage past the compressor piston rod packing was a significant problem that prevented prolonged operation of the prototype without recharging. The use of compressor speed to control refrigeration capacity, and a combination of discharge pressure and gas cooler water flowrate to control heating capacity and hot water outlet temperatures proved to be effective.

Testing of the heat transfer performance of the heat exchangers was limited by water flowrate restrictions. The heat transfer performance of each of the gas cooler, recuperator, and evaporator were very similar to the design values, if adjusted for the difference between design and experimental water and CO_2 flowrates. The compressor volumetric efficiency was lower than expected, especially when the prototype was operated with high pressure ratios. The compressor isentropic efficiency was slightly lower than both the nominal design value and efficiencies for other compressors reported in the literature.

The maximum overall system COP when producing 90°C water and refrigeration at 1°C (35.5 bar suction pressure) was 5.4 at a discharge pressure of 114 bar. Lowering the suction pressure to 29.6 (-6°C) bar reduced the optimum COP to 4.8 and increased the optimum discharge pressure to 116 bar. Lower hot water outlet temperature resulted in a decrease in the optimum discharge pressure and an increase in maximum COP (eg. the maximum COP was 6.5 for 65°C water). There was some evidence that the overall system COP could be significantly improved if a slightly larger gas cooler was used, especially when the compressor operated at full speed with a high suction pressure (maximum heating capacity). The decline in COP when moving away from the optimum discharge pressure was not large, so the use of a fixed discharge pressure (about 110 bar) would be adequate for most industrial applications.

The maximum measured system heat capacity was 13% less than design. Because the system was operated at fixed suction pressure and the gas cooler and recuperator heat transfer performance were close to design levels, this lower capacity was attributed to the lower than expected volumetric efficiency for the compressor.

The addition of oil to the system did not have a significant effect on the CO_2 leakage rate. The performance of the compressor, gas cooler and recuperator were not significantly affected by the oil, but the evaporator performance was significantly poorer due to oil fouling.

The performance obtained experimentally was very close to the predictions made using Hysis, as well as to those from the literature. Therefore, process simulations may provide a cost-effective way to optimise component designs and sizes for future systems.

Compared with traditional refrigeration and heating technologies, the CO_2 heat pump was shown to give a high return on the capital investment. An internal rate of return of greater than 34% was estimated if capital costs were less than $133,000 for a system heating capacity of 600 kW and producing 90°C water. Further developments that are required before the transcritical CO_2 heat pump can become commercially viable include improving the compressor efficiency, elimination of CO_2 leakage, and the automation of the start-up and of the hot water temperature control systems.

8 REFERENCES

Aarlien R., Frivik P.E. (1998). Comparison of Practical Performance Between CO_2 and R-22 Reversible Heat Pumps for Residential Use. Natural Working Fluids '98 – IIR Gustav Lorentzen Conference: Proceedings of the Conference of International Institute of Refrigeration Sections B and E. Oslo. pp 341-350.

Aarlien R., Pettersen J., Skaugen G., Nekså P. (1996). Residential Air Conditioning with CO_2 – Preliminary Results. Applications for Natural Refrigerants: Proceedings of the Conference of International Institute of Refrigeration Commissions B1, B2, E1 & E2. Aarhus, Denmark.

American Society of Heating, Refrigerating and Air conditioning Engineers. (1993). ASHRAE Handbook - Fundamentals, SI edition. American Society of Heating, Refrigerating and Air conditioning Engineers, Atlanta.

Angelino G., Invernizzi C. (1994). Supercritical Heat Pump Cycles. International Journal of Refrigeration. Vol. 17: No. 8, pp 543-554.

Berghmans J. (1996). Safety Aspects of CO_2 Supercritical Processes. Seminar on the Use of CO_2 as Working Fluid for Heat Pumping Systems. Hannover.

Bishnoi P.R., Miranda R.D., Robinson D.B. (1974). BWR Applied to NG/SNG Needs. Hydrocarbon Processing. November 74 pp 197-201

Bouma J.W.J. (1995). International Heat Pump Assessment. Proceedings of the 19th International Congress of Refrigeration. Vol. IVb.

Bredesen A.M., Hafner A., Pettersen J., Nekså P., Aflekt K. (1997). Heat Transfer and Pressure Drop for In-Tube Evaporation of CO_2. Proceedings of the Conference of International Institute of Refrigeration Commissions B1 with E1 & E2. College Park, USA.

Chumak I.G., Onistchenko V.P., Zagoruchenko N.V., Kustovsky V.G., Kurbatov A.V. (1996). Thermodynamical Appraisal of Heat Pumps with CO_2 Refrigerant. Applications for Natural Refrigerants: Proceedings of the Conference of International Institute of Refrigeration Commissions B1, B2, E1 & E2. Aarhus, Denmark.

Cooper J.R., Le Fevre E.J. (1975). Thermophysical Properties of Water Substance: Students Tables in S.I. Units. Edward Arnold, London.

Edwards B., Kallu R. (1997). High Temperature Ammonia Heat Pump Installation – A Case Study. The Australian Institute of Refrigeration Air Conditioning and Heating: International Air Conditioning and Refrigeration Conference. Hobart, Australia.

Eggen G., Aflekt K. (1998). Commercial Refrigeration with Ammonia and CO_2 as Working Fluids. Natural Working Fluids '98 – IIR Gustav Lorentzen Conference: Proceedings of the Conference of International Institute of Refrigeration Sections B and E. Oslo. pp 237-246.

Eggen G., Røsvik S. (1995). Commercial Refrigeration with Ammonia and CO_2 as Working Fluids. Compression Systems with Natural Working Fluids - Applications, Experience and Developments: Workshop Proceedings. Trondheim, Norway. pp 189-199.

Enkemann T., Kruse H. (1997). Operation Control of a CO_2 Heat Pump for Application in Existing Heating Systems. Proceedings of the Conference of International Institute of Refrigeration Commissions E2, with E1 and B2, Linz. Austria.

Fagerli B.E. (1996). An Investigation of Possibilities for CO_2 Compression in a Hermetic Compressor. Applications for Natural Refrigerants: Proceedings of the Conference of International Institute of Refrigeration Commissions B1, B2, E1 & E2. Aarhus, Denmark.

Fagerli B.E. (1998). Theoretical Analysis of Compressing CO_2 in Scroll Compressors. Natural Working Fluids '98 – IIR Gustav Lorentzen Conference: Proceedings of the Conference of International Institute of Refrigeration Sections B and E. Oslo. pp 204-213.

Fleming A.K. (1996). Economics of 600 kW CO_2 Heat Pump. ECNZ internal document. Wellington.

Gentner H. (1998). Passenger Car Air Conditioning using Carbon Dioxide as Refrigerant. Natural Working Fluids '98 – IIR Gustav Lorentzen Conference: Proceedings of the Conference of International Institute of Refrigeration Sections B and E. Oslo. pp 259-268.

Hafner A., Pettersen J., Skaugen G., Nekså P. (1998). An Automobile HVAC System with CO_2 as the Refrigerant. Natural Working Fluids '98 – IIR Gustav Lorentzen Conference: Proceedings of the Conference of International Institute of Refrigeration Sections B and E. Oslo. pp 289-298.

Halozan H. (1996). Natural Refrigerants - An Option for Heat Pumps?. Refrigeration, Climate Control and Energy Conservation: Proceedings of the Conference of International Institute of Refrigeration Commissions E2, E1, B1 & B2. Melbourne, Australia.

Hesse U., Kruse H. (1993). Alternatives for CFC's and H-CFC 22 Based on CO_2. Energy Efficiency in Refrigeration and Global Warming Impact: Proceedings of Meetings of International Institute of Refrigeration Commissions B1/2. pp 317-341.

Hewitt G.F., Shires G.L., Polezhaev Y.V. editors. (1997). International Encyclopedia of Heat & Mass Transfer. CRC Press, Boca Raton, New York.

Heyl P., Kraus W.E., Quack H. (1998). Expander-Compressor for a More Efficient Use of CO_2 as Refrigerant. Natural Working Fluids '98 – IIR Gustav Lorentzen Conference: Proceedings of the Conference of International Institute of Refrigeration Sections B and E. Oslo. pp 195-203.

Hwang Y., Kim B.H., Radermacher R. (1997). Boiling Heat Transfer Correlation for Carbon Dioxide. Proceedings of the Conference of International Institute of Refrigeration Commissions B1 with E1 & E2. College Park, USA.

Hwang Y., Radermacher R. (1997). Evaluation of Carbon Dioxide Heat Exchanger. Proceedings of the Conference of International Institute of Refrigeration Commissions B1 with E1 & E2. College Park, USA.

Hwang Y., Radermacher R. (1998). Experimental Evaluation of CO_2 Water Heater. Natural Working Fluids '98 – IIR Gustav Lorentzen Conference: Proceedings of the Conference of International Institute of Refrigeration Sections B and E. Oslo. pp 321-328.

Kaiser H. (1996). Verdichter für Natürliche Kältemittel in Nutzfahrzeugen und Omnibussen. Ki Luft- und Kältetechnik. 8/1996, pp 353-358.

Kallu R.D.S., Cleland D.J. (1996). Heat Recovery in Food Processing. The Institute of Refrigeration Heating and Air Conditioning Engineers of New Zealand: Technical Conference Proceedings. Napier, New Zealand.

Kristensen A.P.R. (1993). R717 High Pressure Heat Pump – Application for Food Refrigeration Systems. Proceedings of the Conference of International Institute of Refrigeration Commissions B1, B2, D1, D2/3. Palmerston North, New Zealand.

Liao S., Jakobsen A. (1998). Optimal Heat Rejection Pressure in Transcritical Carbon Dioxide Air Conditioning and Heat Pump Systems. Natural Working Fluids '98 – IIR Gustav Lorentzen Conference: Proceedings of the Conference of International Institute of Refrigeration Sections B and E. Oslo. pp 301-310.

Lorentzen G. (1993). Application of "Natural" Refrigerants. Energy Efficiency in Refrigeration and Global Warming Impact: Proceedings of Meetings of International Institute of Refrigeration Commissions B1/2. pp 55-64.

Lorentzen G. (1994). Natural Refrigerants, A Complete Solution. CFC's, The Day After: Proceedings of Meetings of International Institute of Refrigeration Commissions B1, B2, E1, E2. Padova. pp 317-328.

Lorentzen G. (1994). Revival of Carbon Dioxide as a Refrigerant. International Journal of Refrigeration. Vol. 17: No. 5, pp 292-301.

Lorentzen G. (1994). Use of CO_2 in Commercial Refrigeration - An Energy Efficient Solution. New Applications of Natural Working Fluids in Refrigeration and Air Conditioning - A Contribution to Reduced Global Warming and Energy Consumption:

Proceedings of the Conference of International Institute of Refrigeration Commission B2. Hannover. pp 703-709.

Lorentzen G. (1995). The Use of Natural Refrigerants: A Complete Solution to the CFC/HCFC Predicament. International Journal of Refrigeration. Vol. 18: No. 3, pp 190-197.

Lorentzen G., Pettersen J. (1993). A New, Efficient and Environmentally Benign System for Car Air-Conditioning. International Journal of Refrigeration. Vol. 16: No. 1, pp 4-12.

Lorentzen G., Pettersen J., Bang R.R. (1991). Method and Device for High Side Pressure Regulation in Transcritical Vapor Compression Cycle. United States Patent.

Lucas L. (1993). A New Challenge: From the Ozone Layer to the Greenhouse Effect. Energy Efficiency in Refrigeration and Global Warming Impact: Proceedings of Meetings of International Institute of Refrigeration Commissions B1/2. pp 31-43.

Lunde H., Lorentzen G. (1994). Accidents and Critical Situations due to the Unintentional Escape of Refrigerants: A Survey of Cases in Norway Over the Last Two Decades. International Journal of Refrigeration. Vol. 17: No. 6, pp 371-373.

Manzione J.A. (1998). Development of Carbon Dioxide Environmental Control Unit for the US Army. Natural Working Fluids '98 – IIR Gustav Lorentzen Conference: Proceedings of the Conference of International Institute of Refrigeration Sections B and E. Oslo. pp 251-256.

Nekså P. (1994). Trans-critical Vapour Compression Heat Pumps. New Applications of Natural Working Fluids in Refrigeration and Air Conditioning - A Contribution to Reduced Global Warming and Energy Consumption: Proceedings of the Conference of International Institute of Refrigeration Commission B2. Hannover. pp 395-404.

Nekså P., Grirotto S., Schiefloe P.A. (1998). Commercial Refrigeration Using CO_2 as Refrigerant – System Design and Experimental Results. Natural Working Fluids '98 – IIR Gustav Lorentzen Conference: Proceedings of the Conference of International Institute of Refrigeration Sections B and E. Oslo. pp 227-236.

Nekså P., Rekstad H., Zakeri G. (1997). CO_2 Prototype Hot Water Heat Pump Characteristics, System Design and Experimental Results. Proceedings of the Conference of International Institute of Refrigeration Commissions E2, with E1 and B2. Linz, Austria.

Pearson S.F. (1993). Development of Improved Secondary Refrigerants. Proceedings of the Institute of Refrigeration. pp 65-80.

Perry's Chemical Engineers' Handbook, 6th ed. (1984). McGraw Hill.

Pettersen J. (1994). An Efficient New Automobile Air-Conditioning System Based on CO_2 Vapor Compression. ASHRAE Transaction: Symposia. Vol. 100: No. 2, pp 657-665.

Pettersen J. (1995). Refrigerating, Air Conditioning and Heat Pump Systems Based on CO_2. Compression Systems with Natural Working Fluids - Applications, Experience and Developments: Workshop Proceedings. Trondheim, Norway. pp 163-180.

Pettersen J., Skaugen G. (1994). Operation of Trans-critical CO_2 Vapour Compression Circuits in Vehicle Air Conditioning. New Applications of Natural Working Fluids in Refrigeration and Air Conditioning - A Contribution to Reduced Global Warming and Energy Consumption: Proceedings of the Conference of International Institute of Refrigeration Commission B2. Hannover. pp 495-504.

Protsenko V.P., Zaitsev A.A., Starshinin V.N. (1990). Heat Pump Plant with Working Medium at Supercritical Parameters. Thermal Engineering. Vol. 37: No. 6, pp. 50-53.

Protsenko V.P., Zaitsev A.A., Starshinin V.N. (1992). Ozone-Safe Working Fluid for Compression Heat Pumps. Heat Recovery Systems & CHP. Vol. 12: No. 3, pp. 241-245.

Reid R.C., Prausnitz J.M., Sherwood T.K. (1977). The Properties of Gases and Liquids, Third edition. McGraw-Hill.

Riffat S.B., Afonso C.F., Oliveira A.C., Reay D.A. (1997). Natural Refrigerants for Refrigeration and Air-Conditioning Systems. Applied Thermal Engineering. Vol. 17: No. 1, pp 33-42.

Robinson D.M., Groll E.A. (1998). Efficiencies of Transcritical CO_2 Cycles With and Without and Expansion Turbine. International Journal of Refrigeration. Vol. 21: No. 7, pp 577-589.

Schönfeld H., Krauss W.E. (1997). Calculation and Simulation of a Heat Exchanger: Supercritical Carbon Dioxide – Water. Proceedings of the Conference of International Institute of Refrigeration Commissions B1 with E1 & E2. College Park, USA.

Skaugen G., Svensson M.C. (1998). Dynamical Modelling and Simulation of a Transcritical CO_2 Heat Pump Unit. Natural Working Fluids '98 – IIR Gustav Lorentzen Conference: Proceedings of the Conference of International Institute of Refrigeration Sections B and E. Oslo. pp 183-192.

Stene J. (1996). International Status Report on Compression Systems with Natural Working Fluids. IEA Heat Pump Centre, Sittard, The Netherlands.

Stoeker W.F. (1988). Industrial Refrigeration. Business News Publishing.

Süß J., Kruse H. (1998). Heat Transfer Phenomena Inside the Cylinder of CO_2–Compressors and the Influence on Their Efficiency. Natural Working Fluids '98 – IIR

Gustav Lorentzen Conference: Proceedings of the Conference of International Institute of Refrigeration Sections B and E. Oslo. pp 214-222.

Taniguchi H., Kudo K., Giedt W.H., Park I., Kumazawa S. (1988). Analytical and Experimental Investigation of Two-Phase Flow Screw Expanders for Power Generation. Journal of Engineering for Gas Turbines and Power. Vol. 110, pp 628-635.

Vesovic V., Wakeham W.A., Olchowy G.A., Sengers J.V., Watson J.T.R., Millat J. (1990). The Transport Properties of Carbon Dioxide. Journal of Physical and Chemical Reference Data. Vol. 19: No. 3, pp 763-808.

White S.D., Cleland D.J., Cotter S.D., Stephenson R.A., Kallu R.D.S., Fleming A.K. (1997). A Heat Pump for Simultaneous Refrigeration and Water Heating. IPENZ Transactions. Vol. 24: No. 1, pp 36-43.

Yin J., Park Y.C., Boewe D., McEnaney R., Beaver A., Bullard C.W., Hrnjak P.S. (1998). Experimental and Model Comparison of Transcritical CO_2 Versus R134A and R410 System Performance. Natural Working Fluids '98 – IIR Gustav Lorentzen Conference: Proceedings of the Conference of International Institute of Refrigeration Sections B and E. Oslo. pp 331-340.

Zhao Y., Ohadi M.M., Dessiatoun S.V., Schuster A., McNair A., Radermacher R., Darabi J. (1997). Evaporation Heat Transfer Coefficients of Ammonia and CO_2 Inside a Smooth Tube. Proceedings of the Conference of International Institute of Refrigeration Commissions B1 with E1 & E2. College Park, USA.

9 NOMENCLATURE

A	Area	m^2
COP	Coefficient of Performance	
$cos\ \phi$	Power Factor	
c_p	Specific Heat Capacity	J/kgK
E	Energy Rate (Power)	W
H	Enthalpy	J/kg
h	Individual Heat Transfer Coefficient	W/m^2K
H^0	Enthalpy at standard pressure	J/kg
H_{lv}	Enthalpy of Vaporisation	J/kg
m	Mass Flowrate	kg/s
P	Pressure	Pa
PR	Pressure Ratio	
Q	Volumetric Flowrate	m^3/s
R	Gas Constant	$Pa.m^3/kg\ mol.K$
r	radius	m
S	Entropy	J/kgK
T	Temperature	K
U	Overall Heat Transfer Coefficient	W/m^2K
UA	Sensible Capacity Rating	W/K
v	Velocity	m/s
V	Volume	m3
x	Wall Thickness	m
Z	Gas Compressibility	
$\Delta\theta_{lm}$ *or LMTD*	Log Mean Temperature Difference	K or °C
ε	Efficiency	
ϕ	Heat Flow	W or J/s
η_i	Compressor Isentropic Efficiency	
η_v	Compressor Volumetric Efficiency	
λ	Thermal Conductivity	W/mK
μ	Viscosity	Pa.s
ρ	Density	kg/m^3 or $kg\ mol/m^3$
ω	Frequency	rpm

9.1 Subscripts

c	Gas Cooler
C	Cooling
comp	Compressor
dis	Compressor discharge (Cooler inlet)
e	Evaporator
H	Heating
i	inlet
l	Liquid
lm	Log mean
M	Motor
m	mean
o	outlet
r	Recuperator
sat	Saturation
sep	Separator
suc	Compressor suction (Recuperator cold side outlet)
surf	surface
TXi	Expansion Valve inlet
v	Vapour
VSD	Variable Speed Drive
w	Water

10 APPENDICES

A.1 - Thermosiphon Calculation

General Circuit

Temperature		-6	°C		
		Liquid	Vapour	2 phase	
Density	ρ	913.3	80.8	142.3	kg/m^3
Viscosity	μ	0.000116	1.41E-05	2.41E-05	Pa.s
Latent Heat of Vaporisation	Hv	247730	J/kg		
Heat Transfer in evaporator		88000	W		
Rate of CO2 evaporation		0.355225	kg/s		
Overfeed Rate		1.9	times evaporation rate		
Mass flow	m	0.674928	kg/s		

Evaporator Inlet Pipe Pressure Loss

Total length	L	1.73	m	
Tube Diameter	d	25	mm	
Tube inside diameter	D	0.02664	m	
Surface roughness	ε	1.52E-06	m	
Flow rate	q	0.000739	m^3/s	
Fluid velocity	V	1.325824	m/s	
Reynolds Number	Re	277366.4		
Fannings friction factor assuming turbulent (N_{Re} > 3000) flow and isothermal conditions	f	0.003813		
	F	0.870608		
Straight Pipe losses		795.1	Pa	Darcy equation (Perry's Chemical Engineers' Handbook, 1984)
K value (90° bend)		0.81		
K value (Reducer)		0.466434		
Fittings losses		2325.0	Pa	
Total Head Loss	ΔP	3120.1	Pa	

Evaporator Outlet Pipe Pressure Loss

Half flow (two pipes exiting evaporator)

Tube Diameter	d	40	mm		
Tube inside diameter	D	0.04094	m		
Surface roughness	ε	4.57E-05	m		
Total length for 1/2 flow	L	0.68	m		
		Liquid Fraction		Vapour Fraction	
Mass flow	m	0.159851		0.177613	kg/s
Flow rate	q	0.000175		0.002197	m^3/s
Fluid velocity	V	0.080914		1.015711	m/s
Reynolds Number	Re	33346.72		305829.5	
Fannings friction factor assuming turbulent (N_{Re} > 3000) flow and isothermal conditions	f	0.006449		0.00526	
	F	0.003787		0.486749	
Individual fraction pressure drop	ΔP	3.5		39.3	Pa
K value (90° Bend)		0.63			
K value (reducer)		0.21			
Fittings losses		5.0		70.0	Pa

		8.5		109.4	Pa
	X	0.278435			
	YL	78.01385			
Overall Pressure drop	ΔP	661.4574	Pa	Lockhart & Martinelli eqn (Perry's Chemical Engineers' Handbook, 1984)	
Full Flow					
Tube Diameter	d	50	mm		
Tube inside diameter	D	0.05248	m		
Surface roughness	ε	4.57E-05	m		
Total length for full flow	L	2.11	m		
		Liquid Fraction		Vapour Fraction	
Mass flow	m	0.319703		0.355225	kg/s
Flow rate	q	0.00035		0.004394	m^3/s
Fluid velocity	V	0.161829		2.031422	m/s
Reynolds Number	Re	66693.45		611659	
Fannings friction factor assuming turbulent (N_{Re} > 3000) flow and isothermal conditions	f	0.00569		0.004882	
	F	0.012		1.620	Pa
Pipe Pressure loss		10.9		131.0	Pa
K value (90° Bend)		0.63			
K value (Ball valve)		0.06			
K value (Tee)		1.26			
		30.9		430.3	Pa
Individual fraction pressure drop	ΔP	41.79753		561.3	Pa
	X	0.272884			
	YL	79.3641			
Overall Pressure drop	ΔP	3317.2	Pa	Lockhart & Martinelli eqn	
Total Pressure drop	ΔP	3978.7	Pa		

Evaporator Pressure Loss

		Liquid Fraction		Vapour Fraction	
Individual fraction pressure drop	ΔP	100		2400	Pa
	from heat exchanger ΔP data				
	X	0.204124			
	YL	97.88843			
2 phase pressure drop	ΔP	9788.8	Pa	Lockhart & Martinelli eqn	
Evaporator Pressure Drop	ΔP	2000	Pa	average of liquid and 2 phase	

Total Pressure Loss

	ΔP	9098.8	Pa	

Separator Height

Height from separator liquid level to bottom of evaporator inlet nozzle		1.234	m

A.2 - System Volume and Charge

Gas Cooler

		Shell (65NB sch. 80)	Tubes (3/8")	Baffle
OD	mm	73	9.525	
wt	mm	7.01	1.2	
ID	mm	58.98	7.125	57
A (ID)	m^2	0.002732	3.99E-05	0.001002
A (OD)	m^2		7.13E-05	
L	mm	2958	3000	3
Number		1	14	28
V (ID)	m^3	0.008082	0.001675	8.42E-05
V (OD)	m^3		0.002951	

ID = inside diameter
OD = outside diameter
wt = wall thickness

Hot side (shell)
Volume = Shell Volume - OD tube volume - baffle volume
Volume of 1 cooler 0.005047 m^3

Cooler 1	Density	289.0	kg/m^3
		1.458	kg
Cooler 2	Density	622.9	kg/m^3
		3.144	kg
Cooler 3	Density	897.0	kg/m^3
		4.527	kg
Total	**9.129**	**kg**	

Recuperator

		Shell (65NB sch. 80)	Tubes (3/8")	Baffle	Header	Pipe in HE (25 NB)
OD	mm	73	9.525			33.4
wt	mm	7.01	1.2			4.55
ID	mm	58.98	7.125	57	24.5	24.3
A (ID)	m^2	0.002732	0.000040	0.001002	0.000471	0.000464
A (OD)	m^2		0.000071			
L	mm	1460	1500	3	22	30
Number		1	14	14	2	2
V (ID)	m^3	0.003989	0.000837	0.000042	0.000021	0.000028
V (OD)	m^3		0.001456			

Hot side (shell)
Volume = Shell Volume - OD tube volume - baffle volume

Volume	0.00249	m^3
Density	949.8	kg/m^3
	2.365	kg

Cold side (tubes)
Volume = ID tube volume + Header volume + Volume of pipe in HE

Volume	0.000886	m^3
Density	107.2	kg/m^3
	0.095	kg
Total	**2.460**	**kg**

Evaporator

		Shell (65NB sch. 80)	Tubes (3/8")
OD	mm	168.3	9.525
wt	mm	10.97	0.9
ID	mm	146.36	7.725
A (ID)	m^2	0.016824	0.000047
A (OD)	m^2		0.000071
L	mm	1446	1500
Number		1	109
V (ID)	m^3	0.024328	0.007663
V (OD)	m^3		0.011231

Cold, CO2 side (shell)
Volume = Shell Volume - OD tube volume
Volume 0.013097 m^3

Assume 67% w/w full of liquid
Density 278.7 kg/m^3
3.650 **kg**

Separator

Total Volume

		Separator (200NB xs wt)
OD	mm	219.1
wt	mm	12.7
ID	mm	193.7
A (ID)	m^2	0.029468
L	mm	1861
V (ID)	m^3	0.05484

Assuming liquid level half way between LSL and evaporator return for normal operating conditions
Liquid
L mm 612
V (ID) m3 0.018034

Volume 0.018034 m^3
Density 890.3 kg/m^3
16.057 kg

Vapour
L mm 1249
V (ID) m^3 0.036805

Volume 0.036805 m^3
Density 116.4 kg/m^3
4.284 kg

Total **20.341** **kg**

Pipework

	Pipe size	OD mm	wt mm	ID mm	A (ID) m2	L mm	V m^3	ρ kg/m^3	M kg	ρ kg/m^3	M kg	ρ kg/m^3	M kg
								minimum level		Nominal level		Maximum level	
Compressor							0.000356	142.9	0.051	139.1	0.050	134.9	0.048
	3/4"	19.05	1.65	15.75	0.000195	3299	0.000643	187.8	0.121	206.7	0.133	210.7	0.135
Cooler 1							0.005047	289.0	1.458	253.0	1.277	248.2	1.253
	1/2"	12.7	1.24	10.22	0.000082	233	0.000019	390.2	0.007	299.3	0.006	285.7	0.005
Cooler 2							0.005047	622.9	3.144	468.2	2.363	410.7	2.072
	1/2"	12.7	1.24	10.22	0.000082	233	0.000019	855.6	0.016	637.1	0.012	535.6	0.010
Cooler 3							0.005047	897.0	4.527	746.4	3.767	666.2	3.362
	1/2"	12.7	1.24	10.22	0.000082	1766	0.000145	938.4	0.136	855.7	0.124	796.7	0.115
Recuperator							0.002490	949.8	2.365	882.3	2.197	828.6	2.064
	1/2"	12.7	1.24	10.22	0.000082	2030	0.000167	961.3	0.160	908.9	0.151	860.5	0.143
Separator	liquid						0.018034	890.3		961.0	17.332	996.4	
	25NB	33.4	4.55	24.3	0.000464	1730	0.000802	890.3	0.714	961.0	0.771	996.4	0.799
Evaporator							0.013097	584.5	7.656	585.3	7.665	587.1	7.690
	40NB	48.3	5.08	38.14	0.001142	680	0.000777	278.7	0.217	209.5	0.163	177.9	0.138
	50NB	60.3	3.91	52.48	0.002163	2110	0.004564	278.7	1.272	209.5	0.956	177.9	0.812
Separator	vapour						0.036805	116.4		80.9	2.979	66.7	
	25NB	33.4	4.55	24.3	0.000464	3270	0.001517	116.4	0.177	80.9	0.123	66.7	0.101
Recuperator							0.000886	107.2	0.095	76.3	0.068	62.9	0.056
	25NB	33.4	4.55	24.3	0.000464	2137	0.000991	98.0	0.097	71.6	0.071	59.1	0.059
Compressor													

Total Volume	L	96.452		
		minimum level	Nominal level	maximum level
High Side Charge	kg	11.985	10.079	9.208
Low Side Charge	kg	10.227	30.127	9.655
Total Charge	kg		**40.206**	System Charge
Charge Less Separator	kg	**22.213**	**19.895**	**18.863**
Separator Fluctuation from nominal	kg	-2.317		1.032
Separator Charge	kg	17.994	20.311	21.343
Liquid volume fraction		0.274	0.329	0.347
Liquid Volume	m^3	0.015002	0.018034	0.019024
Separator Fluctuation	m^3	-0.003032		0.00099
	mm	-102.9		33.6

A.3 PLC Ladder Logic Code

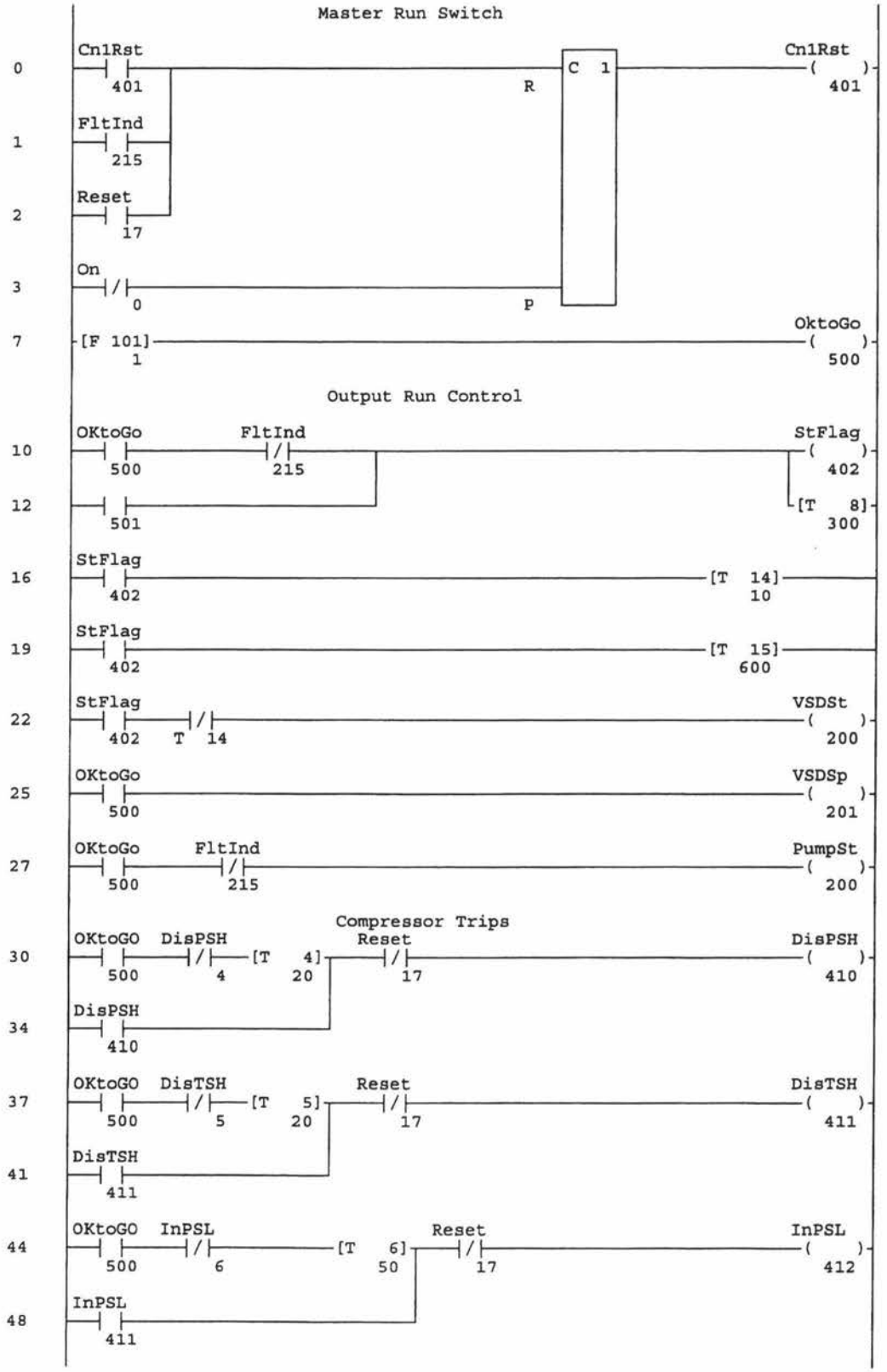

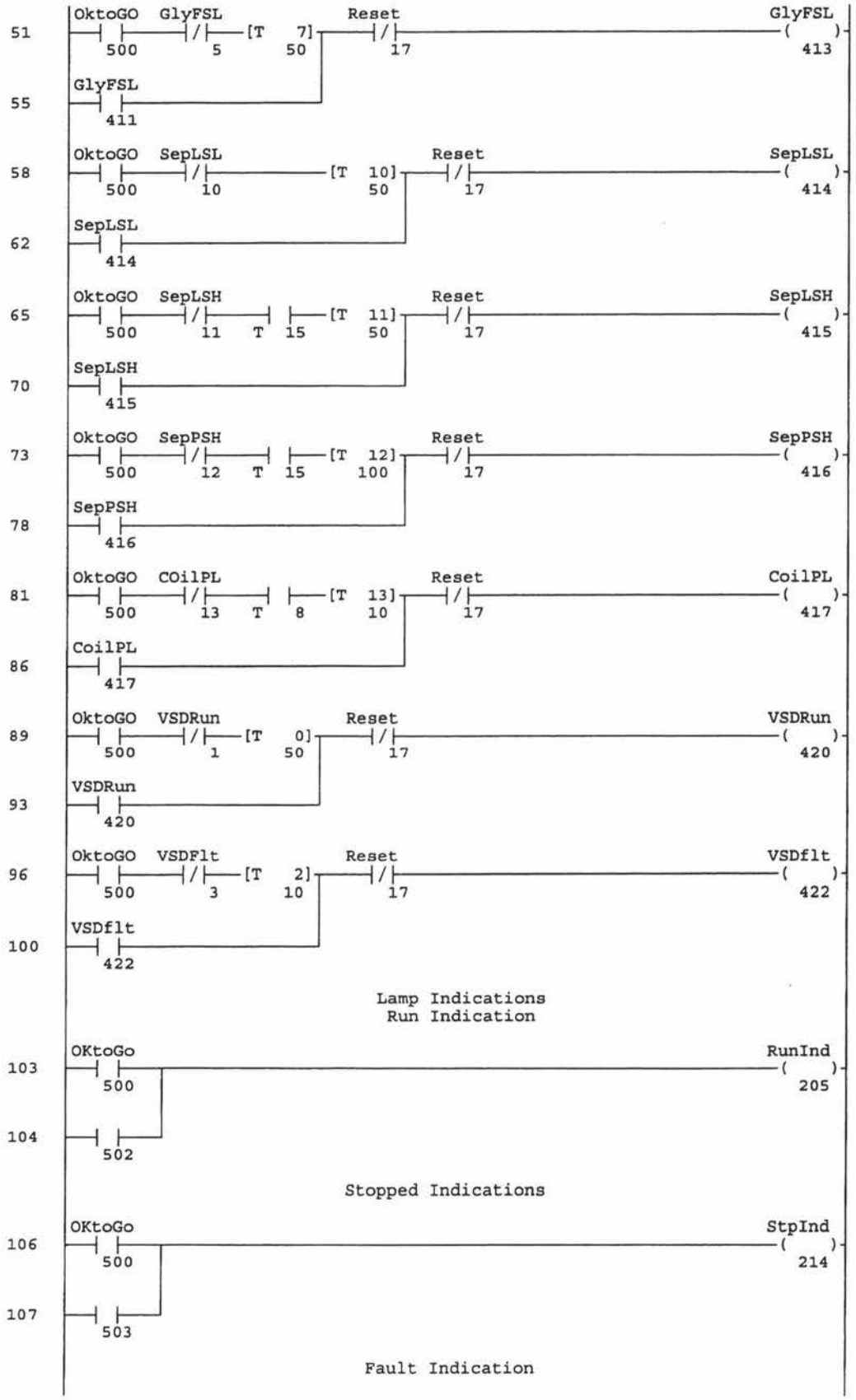
51
OktoGO 500
GlyFSL 5
[T 7] 50
Reset 17
GlyFSL 413
55
GlyFSL 411
58
OktoGO 500
SepLSL 10
[T 10] 50
Reset 17
SepLSL 414
62
SepLSL 414
65
OktoGO 500
SepLSH 11
T 15
[T 11] 50
Reset 17
SepLSH 415
70
SepLSH 415
73
OktoGO 500
SepPSH 12
T 15
[T 12] 100
Reset 17
SepPSH 416
78
SepPSH 416
81
OktoGO 500
COilPL 13
T 8
[T 13] 10
Reset 17
CoilPL 417
86
CoilPL 417
89
OktoGO 500
VSDRun 1
[T 0] 50
Reset 17
VSDRun 420
93
VSDRun 420
96
OktoGO 500
VSDFlt 3
[T 2] 10
Reset 17
VSDflt 422
100
VSDflt 422
Lamp Indications
Run Indication
103
OKtoGo 500
RunInd 205
104
502
Stopped Indications
106
OKtoGo 500
StpInd 214
107
503
Fault Indication

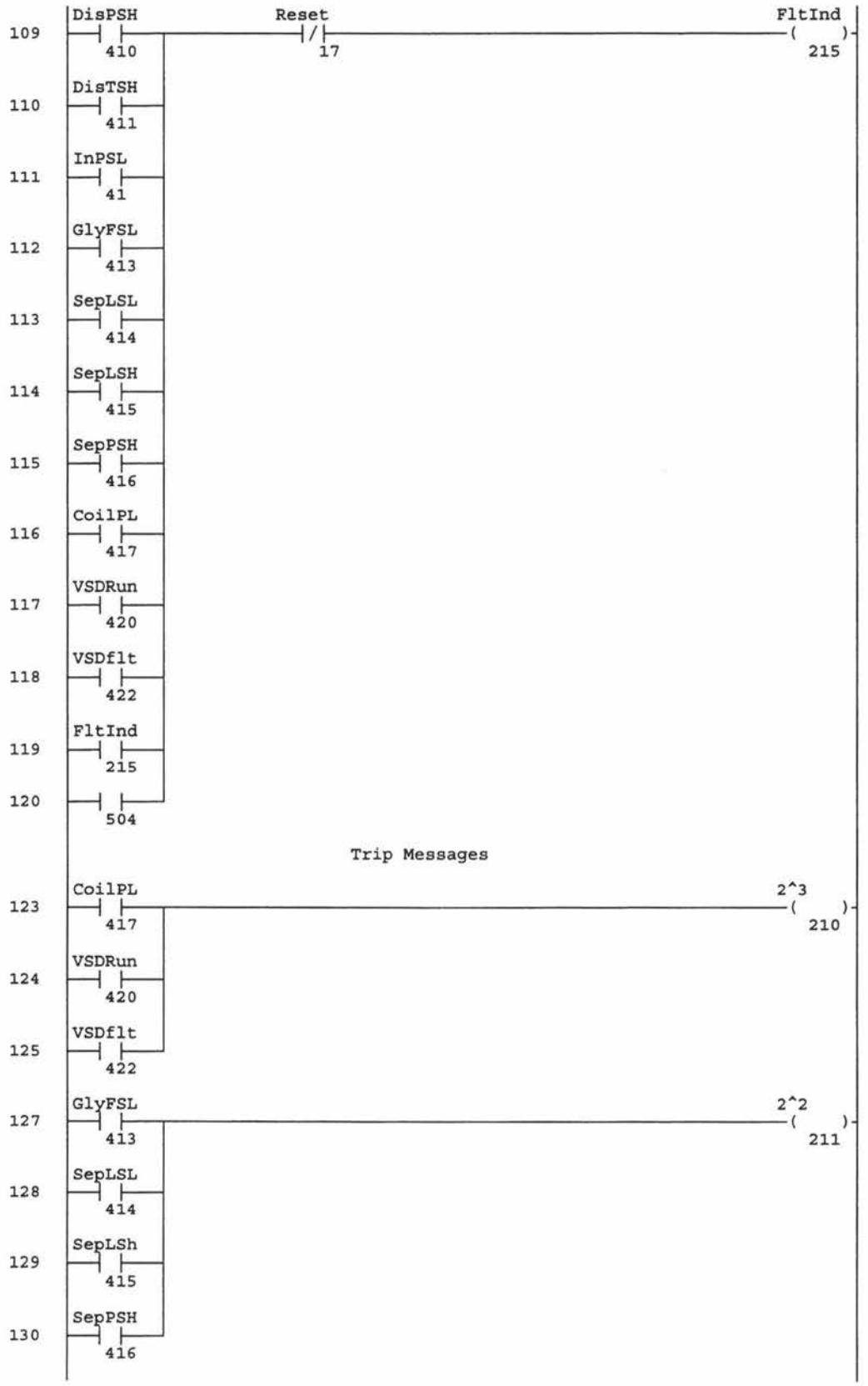
DisPSH
410
Reset
17
FltInd
215
109
DisTSH
411
110
InPSL
41
111
GlyFSL
413
112
SepLSL
414
113
SepLSH
415
114
SepPSH
416
115
CoilPL
417
116
VSDRun
420
117
VSDflt
422
118
FltInd
215
119
504
120
Trip Messages
CoilPL
417
2^3
210
123
VSDRun
420
124
VSDflt
422
125
GlyFSL
413
2^2
211
127
SepLSL
414
128
SepLSh
415
129
SepPSH
416
130

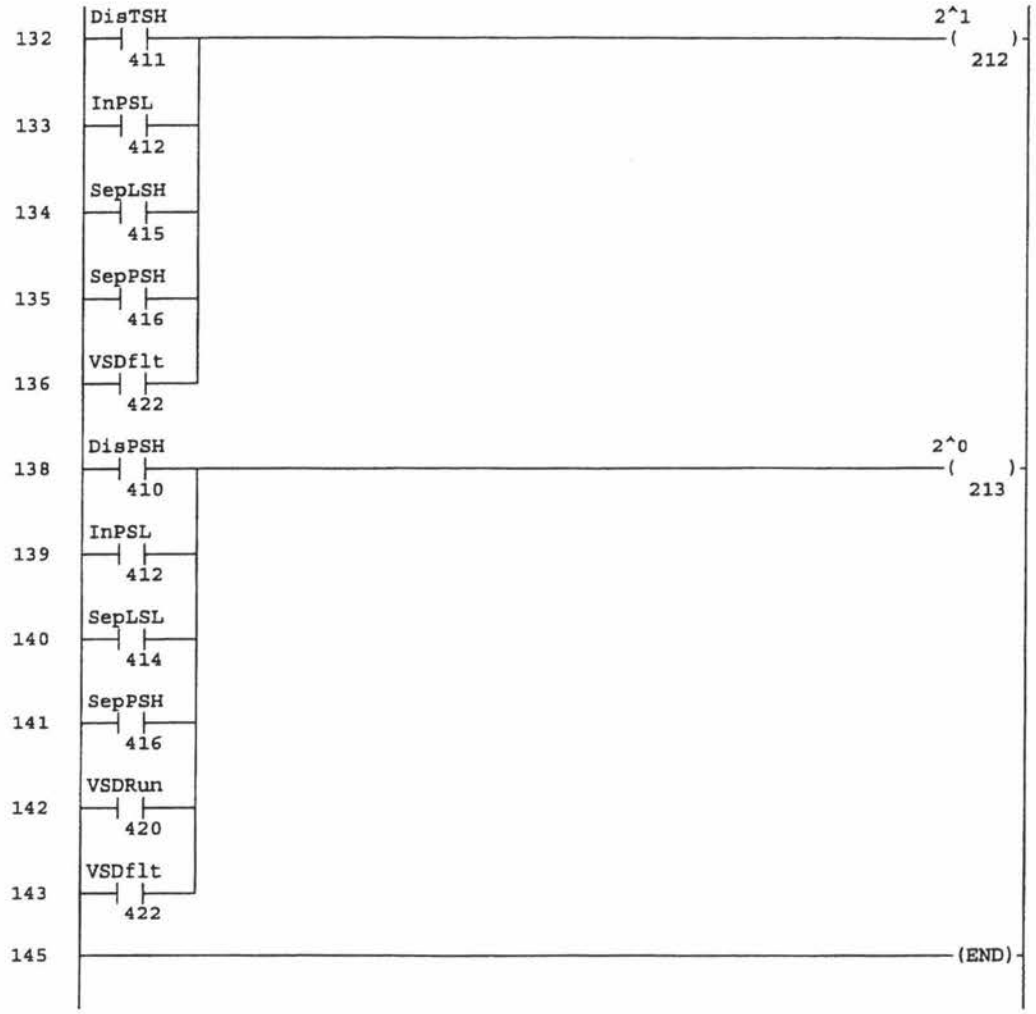
132
DisTSH
411
2^1
212
133
InPSL
412
134
SepLSH
415
135
SepPSH
416
136
VSDflt
422
138
DisPSH
410
2^0
213
139
InPSL
412
140
SepLSL
414
141
SepPSH
416
142
VSDRun
420
143
VSDflt
422
145
(END)

A.4 - BWR Macro

```
' BWR Macro
' Macro recorded 26/03/97 by Mike Yarrall
'
Public rho, dH, root1, root2, root3, root4, root5, root6 As Double
Public T, P, R, M, precision, increment, rhostart, rhoend, rhovap, rholiq, A0, B0, C0, a, b, c, gamma,
alpha As Single

Sub BWR()

'read in values
Sheets("enthalpy").Select
precision = Range("precision").Value
increment = Range("increment").Value
rhostart = Range("rhostart").Value
rhoend = Range("rhoend").Value

R = Range("gasconst").Value
M = Range("M").Value

T = 0
P = 0

'set BWR constants
A0 = Range("A0").Value
B0 = Range("B0").Value
C0 = Range("C0").Value
a = Range("a").Value
b = Range("b").Value
c = Range("c_").Value
alpha = Range("alpha").Value
gamma = Range("gamma").Value

'read in temp and pressure 1
T = Range("temp1")
P = Range("press1")

density 'run sub density

'output data
Range("rhovap1").Value = rhovap
Range("rholiq1").Value = rholiq

'read in temp and pressure
T = Range("temp2")
P = Range("press2")

density 'run sub density with second set of P and T values

'output data
Range("rhovap2").Value = rhovap
Range("rholiq2").Value = rholiq

End Sub
```

```
Sub density()

'setting initial values
root1 = 0
root2 = 0
root3 = 0
root4 = 0
root5 = 0
root6 = 0

rootn = 1
Pcalc = 0
Ptest = 0
rho = rhostart

'first iteration to give Pcalc a value
Pcalc = R * T * rho + (B0 * R * T - A0 - C0 / T ^ 2) * rho ^ 2 + (b * R * T - a) * rho ^ 3 _
 + a * alpha * rho ^ 6 + (c * rho ^ 3 / T ^ 2) * (1 + gamma * rho ^ 2) * Exp(-gamma * rho ^ 2)
Ptest = Pcalc

Do While rho < rhoend
   'quickly (at 10*increment) goes till the difference between the calculated and actual P
   'values starts to decrease and Pcalc is within 10% of P
   Do Until Abs(Pcalc - P) < Abs(Ptest - P) And Abs(Pcalc - P) < 0.1 * P
      If rho > rhoend Then
      finishdensity
      Exit Sub
      End If
      Ptest = Pcalc
      rho = rho + 10 * increment
      Pcalc = R * T * rho + (B0 * R * T - A0 - C0 / T ^ 2) * rho ^ 2 + (b * R * T - a) * rho ^ 3 _
       + a * alpha * rho ^ 6 + (c * rho ^ 3 / T ^ 2) * (1 + gamma * rho ^ 2) * Exp(-gamma * rho ^ 2)
   Loop

   'repeats until the difference between the calculated and actual P values increases
   '-this should give as close to an agreement between the two as possible
   Do Until Abs(Pcalc - P) > Abs(Ptest - P)
      If rho > rhoend Then
         finishdensity
         Exit Sub
      End If
      Ptest = Pcalc
      If Abs(Pcalc - P) > 10 * precision Then
         rho = rho + 10 * increment
         Else: rho = rho + increment
      End If
      Pcalc = R * T * rho + (B0 * R * T - A0 - C0 / T ^ 2) * rho ^ 2 + (b * R * T - a) * rho ^ 3 _
       + a * alpha * rho ^ 6 + (c * rho ^ 3 / T ^ 2) * (1 + gamma * rho ^ 2) * Exp(-gamma * rho ^ 2)
   Loop
```

```
'Puts the value of rho where Pcalc and P are closest and within "precision" Pa into storage
If Abs(Ptest - P) < precision Then
If rootn = 1 Then root1 = (rho - increment)
If rootn = 2 Then root2 = (rho - increment)
If rootn = 3 Then root3 = (rho - increment)
If rootn = 4 Then root4 = (rho - increment)
If rootn = 5 Then root5 = (rho - increment)
If rootn = 6 Then root6 = (rho - increment)
rootn = rootn + 1
End If

Loop

finishdensity

End Sub


Sub finishdensity()

'puts the lowest and highest roots as the vapour and liquid densities respectively
rhovap = root1

rholiq = root1
If root2 > rholiq Then rholiq = root2
If root3 > rholiq Then rholiq = root3
If root4 > rholiq Then rholiq = root4
If root5 > rholiq Then rholiq = root5
If root6 > rholiq Then rholiq = root6

End Sub
```

A.5 - Enthalpy Calculations

Calculation of enthalpy change between two points:

$$H_2 - H_1 = \Delta H = \Delta H_1' + \Delta H^0 - \Delta H_2' \tag{A.1}$$

Derivation of equation for difference between actual enthalpy and enthalpy at standard pressures

General equation for difference between actual enthalpy and enthalpy at standard pressures (equation (4-279b), Perry's Chemical Engineers' Handbook, 1984)

$$\Delta H' = RT^2 \int_0^{\rho} \left(\frac{\partial Z}{\partial T}\right)_{\rho} \frac{\partial \rho}{\rho} - RT(Z-1) \tag{A.2}$$

$\Delta H'$ = difference between actual enthalpy and enthalpy at standard pressures (J/kg)
R = Gas Constant (kg.m^2/kgmol.K.s^2)
Z = Compressibility
T = Temperature (K)
ρ = Density (kgmol/m^3)

Benedict Webb Ruben Equation (equation (3-51), Perry's Chemical Engineers' Handbook, 1984):

$$P = \rho RT + \left(B_0 RT - A_0 - \frac{C_0}{T^2}\right)\rho^2 + (bRT - a)\rho^3 + a\alpha\rho^6 + \frac{c}{T^2}\rho^3\left(1+\gamma\rho^2\right)e^{-\gamma\rho^2} \tag{A.3}$$

P = Pressure (Pa)
A_0, B_0, C_0, a, b, c, α, γ = BWR constants (specific to fluid)

As

$$Z = \frac{PV}{nRT} = \frac{P}{\rho RT} \tag{A.4}$$

Dividing equation (A.3) by ρRT

$$Z = 1 + \left(B_0 - \frac{A_0}{RT} - \frac{C_0}{RT^3}\right)\rho + \left(b - \frac{a}{RT}\right)\rho^2 + \frac{a\alpha}{RT}\rho^5 + \frac{c}{RT^3}\rho^2\left(1+\gamma\rho^2\right)e^{-\gamma\rho^2} \tag{A.5}$$

Differentiating equation (A.5) with respect to temperature with constant density

$$\left(\frac{\partial Z}{\partial T}\right)_{\rho} = \frac{A_0}{RT^2}\rho + \frac{3C_0}{RT^4}\rho + \frac{a}{RT^2}\rho^2 - \frac{a\alpha}{RT^2}\rho^5 - \frac{3c}{RT^4}\rho^2 e^{-\gamma\rho^2} - \frac{3c}{RT^4}\rho^4\gamma e^{-\gamma\rho^2} \tag{A.6}$$

Dividing by ρ:

$$\left(\frac{\partial Z}{\partial T}\right)_{\rho}\frac{1}{\rho} = \frac{A_0}{RT^2} + \frac{3C_0}{RT^4} + \frac{a}{RT^2}\rho - \frac{a\alpha}{RT^2}\rho^4 - \frac{3c}{RT^4}\rho e^{-\gamma\rho^2} - \frac{3c}{RT^4}\rho^3\gamma e^{-\gamma\rho^2} \tag{A.7}$$

Integrating with respect to ρ:

The integration of the last term is done as follows:

$$\int_0^{\rho} \frac{3c}{RT^4}\rho^3\gamma e^{-\gamma\rho^2}d\rho = \frac{3c}{RT^4}\int_0^{\rho}\rho^3\gamma e^{-\gamma\rho^2}d\rho$$

Integration by parts:

$$dv = \gamma\rho e^{-\gamma\rho^2}d\rho$$

$$v = -\frac{e^{-\gamma\rho^2}}{2}$$

$$u = \rho^2$$

$$du = 2\rho d\rho$$

$$\int udv = uv - \int vdu$$

$$\int_0^{\rho}\left(\rho^2 \times \gamma\rho e^{-\gamma\rho^2}\right)d\rho = -\rho^2 \times \frac{e^{-\gamma\rho^2}}{2} - \int_0^{\rho}\frac{-e^{-\gamma\rho^2}}{2}\times 2\rho d\rho$$

$$= -\frac{\rho e^{-\gamma\rho^2}}{2} - \frac{e^{-\gamma\rho^2}}{2\gamma}\Bigg]_0^{\rho}$$

$$= -\frac{\left(\rho^2 + \frac{1}{\gamma}\right)e^{-\gamma\rho^2}\Big]_0^{\rho}}{2}$$

$$\int_0^{\rho}\left(\frac{\partial Z}{\partial T}\right)_{\rho}\frac{d\rho}{\rho} = \left(\frac{A_0}{RT^2}\rho + \frac{3C_0}{RT^4}\rho + \frac{a}{2RT^2}\rho^2 - \frac{a\alpha}{5RT^2}\rho^5 - \frac{3c}{2\gamma RT^4}e^{-\gamma\rho^2} - \frac{3c}{2\gamma RT^4}\left(\rho^2 + \frac{1}{\gamma}\right)\gamma e^{-\gamma\rho^2}\right)\Bigg]_0^{\rho}$$

$$= \left[\left(\frac{A_0}{RT^2} + \frac{3C_0}{RT^4}\right)\rho + \frac{a}{2RT^2}\rho^2 - \frac{a\alpha}{5RT^2}\rho^5 + \frac{3c}{RT^4}\left(\frac{1}{\gamma} + \frac{\rho^2}{2}\right)e^{-\gamma\rho^2}\right]$$

$$-\left[0 + 0 - 0 + \frac{3c}{RT^4}\left(\frac{1}{\gamma} + 0\right)e^{-\gamma\times 0^2}\right]$$

$$\int_0^{\rho}\left(\frac{\partial Z}{\partial T}\right)_{\rho}\frac{d\rho}{\rho} = \left(\frac{A_0}{RT^2} + \frac{3C_0}{RT^4}\right)\rho + \frac{a}{2RT^2}\rho^2 - \frac{a\alpha}{5RT^2}\rho^5 + \frac{3c}{RT^4}\left(\frac{1}{\gamma} + \frac{\rho^2}{2}\right)e^{-\gamma\rho^2} - \frac{3c}{\gamma RT^4} \qquad \text{(A.8)}$$

Multiply by RT^2:

$$RT^2\int_0^{\rho}\left(\frac{\partial Z}{\partial T}\right)_{\rho}\frac{d\rho}{\rho} = \left(A_0 + \frac{3C_0}{T^2}\right)\rho + \frac{a}{2}\rho^2 - \frac{a\alpha}{5}\rho^5 + \frac{3c}{T^2}\left(\frac{1}{\gamma} + \frac{\rho^2}{2}\right)e^{-\gamma\rho^2} - \frac{3c}{\gamma T^2} \qquad \text{(A.9)}$$

Rearranging equation (A.5):

$$RT(Z-1) = \left(RTB_0 - A_0 - \frac{C_0}{T^2}\right)\rho + (RTb - a)\rho^2 + a\alpha\rho^5 + \frac{c}{T^2}\rho^2\left(1 + \gamma\rho^2\right)e^{-\gamma\rho^2} \qquad \text{(A.10)}$$

Substituting equations (A.9) and (A.10) into (A.2):

$$\Delta H' = RT^2 \int_0^{\rho} \left(\frac{\partial Z}{\partial T}\right)_{\rho} \frac{\partial \rho}{\rho} - RT(Z-1)$$

$$= \left(A_0 + \frac{3C_0}{T^2}\right)\rho + \frac{a}{2}\rho^2 - \frac{a\alpha}{5}\rho^5 + \frac{3c}{T^2}\left(\frac{1}{\gamma} + \frac{\rho^2}{2}\right)e^{-\gamma\rho^2} - \frac{3c}{\gamma T^2}$$

$$-\left(RTB_0 - A_0 - \frac{C_0}{T^2}\right)\rho + (RTb - a)\rho^2 + a\alpha\rho 5 + \frac{c}{T^2}\rho^2\left(1 + \gamma\rho^2\right)e^{-\gamma\rho^2} \qquad \text{(A.11)}$$

Rearranging:

$$\Delta H' = \left(2A_0 + \frac{4C_0}{T^2} - RTB_0\right)\rho + \left(\frac{3a}{2} - RTb\right)\rho^2 - \frac{6a\alpha}{5}\rho^5 + \left(\left(\frac{3}{\gamma} + \frac{\rho^2}{2} - \gamma\rho^4\right)e^{-\gamma\rho^2} - \frac{3}{\gamma}\right)\frac{c}{T^2} \qquad \text{(A.12)}$$

Derivation of equation for change in enthalpy at standard pressures

Specific heat capacity equation for ideal gas:

$$c_p = A + BT + CT^2 + DT^3 \qquad \text{(A.13)}$$

c_p = specific heat capacity (J/kgK)
A,B,C,D = constants specific to fluid.

$$c_p = \frac{dH}{dT} \qquad \text{(A.14)}$$

Substituting equation (A.14) into (A.13):

$$\frac{dH}{dT} = A + BT + CT^2 + DT^3 \qquad \text{(A.15)}$$

$$\int_{H_1^0}^{H_2^0} dH = \int_{T_1}^{T_2} \left(A + BT + CT^2 + DT^3\right)dT \qquad \text{(A.16)}$$

Integrating:

$$H_2^0 - H_1^0 = \Delta H^0 = A(T_1 - T_2) + \frac{B\left(T_2^2 - T_1^2\right)}{2} + \frac{C\left(T_2^3 - T_1^3\right)}{3} + \frac{D\left(T_2^4 - T_1^4\right)}{4} \qquad \text{(A.17)}$$

A.6 - CO_2 Property Equations

Viscosity and Thermal Conductivity equations from Vesovic *et al* (1990)

Viscosity

$$\mu^0 = \frac{1.00697T^{1/2}}{\varsigma_\mu^*} \tag{A.18}$$

$$\varsigma_\mu^* = 0.235156 - 0.491266(\ln T^*) + 5.211155\times10^{-2}(\ln T^*)^2 + 5.347906\times10^{-2}(\ln T^*)^3 - 1.537102\times10^{-2}(\ln T^*)^4 \tag{A.19}$$

$$T^* = kT/\varepsilon \tag{A.20}$$

$$\Delta\mu_g = 3.6350734\times10^{-3}\rho + 7.209997\times10^{-5}\rho^2 + 3.00306\times10^{-20}\rho^7 \tag{A.21}$$

$$\Delta\mu_l = \frac{1}{B\left[\frac{1}{\rho} - V_0\right]} \tag{A.22}$$

$$B = 18.56 + 0.014T \tag{A.23}$$

$$V_0 = 7.41\times10^{-4} - 3.3\times10^{-7}T \tag{A.24}$$

$$\mu_g = \mu^0 + \Delta\mu_g \tag{A.25}$$

$$\mu_l = \mu^0 + \Delta\mu_l \tag{A.26}$$

Where:

μ_g = gas viscosity (μPa.s)
μ_l = liquid viscosity (μPa.s)
μ^0 = viscosity at zero density (μPa.s)
$\Delta\mu_g$ = deviation from zero density for gas (μPa.s)
$\Delta\mu_l$ = deviation from zero density for liquid (μPa.s)

Thermal Conductivity

$$\lambda^0 = \frac{0.475598T^{1/2}(1+r^2)}{\varsigma_\lambda^*} \tag{A.27}$$

$$\varsigma_\lambda^* = 0.4226159 - 0.6280115(\ln T^*) - 0.5387661(\ln T^*)^2 + 0.6735941(\ln T^*)^3 - 0.4362677(\ln T^*)^6 + 0.2255388(\ln T^*)^7 \tag{A.28}$$

$$r = \left(\frac{2c_{\text{int}}}{5k}\right)^{1/2} \tag{A.29}$$

$$\frac{c_{\text{int}}}{k} = 1 + \exp(-183.5/T)(2.387869\times10^{-2}(T/100) + 4.350794 - 10.33404(T/100)^{-1} + 7.981590(T/100)^{-2} - 1.940558(T/100)^{-3}) \tag{A.30}$$

$$\Delta\lambda = 2.447164\times10^{-2}\rho + 8.705605\times10^{-5}\rho^2 - 6.5479506\times10^{-8}\rho^3 + 6.594919\times10^{-11}\rho^4 \tag{A.31}$$

$$\lambda = \lambda^0 + \Delta\lambda \tag{A.32}$$

Where:

λ = thermal conductivity (mW/m.K)
λ^0 = thermal conductivity at zero density (mW/m.K)
$\Delta\lambda$ = deviation from zero density (mW/m.K)

A.7 - Saturated Water Equations

$$P = -6.65E\text{-}09 \times T^6 + 4.56E\text{-}06 \times T^5 + 9.67E\text{-}05 \times T^4 + 0.0348 \times T^3 + 1.27 \times T^2 + 45.5 \times T + 610 \quad \text{(A.33)}$$

where:
P saturated pressure (Pa)
T saturation tempeature (°C)

Density:

$$\rho_l = 4.53E\text{-}12 \times T^6 - 2.32E\text{-}09 \times T^5 + 2.56E\text{-}07 \times T^4 + 1.28E\text{-}05 \times T^3 - 0.00652 \times T^2 + 0.0343 \times T + 1000 \quad \text{(A.34)}$$

$$\rho_v = -3.26E\text{-}14 \times T^6 + 1.79E\text{-}11 \times T^5 + 1.21E\text{-}09 \times T^4 + 1.94E\text{-}07 \times T^3 + 9.77E\text{-}06 \times T^2 + 3.37E\text{-}04 \times T + 0.00484 \quad \text{(A.35)}$$

where:
ρ_l liquid density (kg/m^3)
ρ_v vapour density (kg/m^3)

Viscosity:

$$\mu_l = 3.26E\text{-}15 \times T^6 - 1.26E\text{-}12 \times T^5 + 2.09E\text{-}10 \times T^4 - 1.97E\text{-}08 \times T^3 + 1.24E\text{-}06 \times T^2 - 5.59E\text{-}05 \times T + 0.00175E\text{-}03 \quad \text{(A.36)}$$

$$\mu_v = -2.84E\text{-}19 \times T^6 + 3.06E\text{-}17 \times T^5 + 2.09E\text{-}15 \times T^4 - 4.07E\text{-}13 \times T^3 + 1.15E\text{-}11 \times T^2 + 4.05E\text{-}08 \times T + 8.04E\text{-}06 \quad \text{(A.37)}$$

where:
μ_l liquid viscosity (Pa.s)
μ_v vapour viscosity (Pa.s)

Specific Heat Capacity:

$$c_{pl} = 6.55E\text{-}10 \times T^6 - 2.69E\text{-}07 \times T^5 + 4.42E\text{-}05 \times T^4 - 0.00370 \times T^3 + 0.176 \times T^2 - 4.44 \times T + 4220 \quad \text{(A.38)}$$

$$c_{pv} = 3.70E\text{-}07 \times T^4 + 6.71E\text{-}06 \times T^3 + 0.00923 \times T^2 + 0.345 \times T + 1860 \quad \text{(A.39)}$$

where:
C_{pl} liquid viscosity (J/kgK)
C_{pv} vapour viscosity (J/kgK)

Thermal Conductivity:

$$\lambda_l = 7.91E\text{-}09 \times T^3 - 8.57E\text{-}06 \times T^2 + 0.00190 \times T + 0.569 \quad \text{(A.40)}$$

$$\lambda_v = 1.31E\text{-}07 \times T^2 + 5.66E\text{-}05 \times T + 0.0176 \quad \text{(A.41)}$$

where:
λ_l liquid thermal conductivity (W/mK)
λ_v vapour thermal conductivity (W/mK)

Enthalpy:

$$H_l = 8.23E\text{-}07 \times T^5 - 2.36E\text{-}04 \times T^4 + 0.0286 \times T^3 - 1.59 \times T^2 + 4220 \times T - 31.8 \quad \text{(A.42)}$$

$$H_v = -1.27 \times T^2 + 1890 \times T + 2500000 \quad \text{(A.43)}$$

$$\Delta H_{lv} = -1.36 \times T^2 - 2290 \times T + 2500000 \quad \text{(A.44)}$$

where:
H_l liquid enthalpy (J/kg)
H_v vapour enthalpy (J/kg)
ΔH_{lv} enthalpy of vaporisation (J/kg)

A.8 - Entropy Calculations

Calculation of entropy change between two points (Perry's Chemical Engineers' Handbook, 1984):

$$S_2 - S_1 = \Delta S = \Delta S_1' + \Delta S^0 - \Delta S_2' \quad \text{(A.45)}$$

Derivation of equation for difference between actual Gibb's energy and Gibb's energy at standard pressures

General equation for difference between actual Gibb's energy and Gibb's energy at standard pressures (derived from equation (4-278b), Perry's Chemical Engineers' Handbook, 1984)

$$\Delta G' = RT\left[\int_0^{\rho} (Z-1)\frac{d\rho}{\rho} + Z - 1 - \ln Z\right] \quad \text{(A.46)}$$

$\Delta G'$ = difference between actual Gibb's energy and Gibb's energy at standard pressures (J/kg)
R = Gas Constant (kg.m^2/kgmol.K.s^2)
Z = Compressibility
T = Temperature (K)
ρ = Density (kgmol/m^3)

Subtracting 1, diving by ρ and integrating equation (A.5) with respect to density

$$\int_0^\rho \frac{Z-1}{\rho}d\rho = \left[\left(B_0 - \frac{A_0}{RT} - \frac{C_0}{RT^3}\right)\rho + \left(b - \frac{a}{RT}\right)\frac{\rho^2}{2} + \frac{a\alpha}{RT}\frac{\rho^5}{5} - \frac{c}{RT^3}\left(\frac{\rho^2 e^{-\gamma\rho^2}}{2} + \frac{e^{-\gamma\rho^2}}{\gamma}\right)\right]_0^\rho$$

$$= \left(B_0 - \frac{A_0}{RT} - \frac{C_0}{RT^3}\right)\rho + \left(b - \frac{a}{RT}\right)\frac{\rho^2}{2} + \frac{a\alpha}{RT}\frac{\rho^5}{5} - \frac{c}{RT^3}\left(\frac{\rho^2 e^{-\gamma\rho^2}}{2} + \frac{e^{-\gamma\rho^2}}{\gamma} - \frac{1}{\gamma}\right) \quad \text{(A.47)}$$

Rearranging and substituting equation (A.5) and equation (A.48) into equation (A.46).

$$\Delta G' = RT\left[\begin{array}{l}\left(B_0 - \frac{A_0}{RT} - \frac{C_0}{RT^3}\right)\rho + \left(b - \frac{a}{RT}\right)\frac{\rho^2}{2} + \frac{a\alpha}{RT}\frac{\rho^5}{5} - \frac{c}{RT^3}\left(\frac{\rho^2 e^{-\gamma\rho^2}}{2} + \frac{e^{-\gamma\rho^2}}{\gamma} - \frac{1}{\gamma}\right) \\ -\left(B_0 - \frac{A_0}{RT} - \frac{C_0}{RT^3}\right)\rho - \left(b - \frac{a}{RT}\right)\rho^2 - \frac{a\alpha}{RT}\rho^5 - \frac{c}{RT^3}\rho^2\left(1+\gamma\rho^2\right)e^{-\gamma\rho^2} - \\ -\ln\left[1 + \left(B_0 - \frac{A_0}{RT} - \frac{C_0}{RT^3}\right)\rho + \left(b - \frac{a}{RT}\right)\rho^2 + \frac{a\alpha}{RT}\rho^5 + \frac{c}{RT^3}\rho^2\left(1+\gamma\rho^2\right)e^{-\gamma\rho^2}\right]\end{array}\right] \quad \text{(A.48)}$$

From Perry's Chemical Engineers' Handbook, 1984

$$TS' = H' - G' \quad \text{(A.49)}$$

Therefore:

$$S' = \frac{H' - G'}{T} \quad \text{(A.50)}$$

Thus S' can be calculated using the formulae for G' (as calculated above), and H' (as calculated previously).

<u>Derivation of equation for change in entropy at standard pressures</u>

$$c_p = \frac{dH}{dT} = T\frac{dS}{dT} \quad \text{(A.51)}$$

Substituting equation (A.51) into (A.13):

$$\frac{dS}{dT} = \frac{A + BT + CT^2 + DT^3}{T} \quad \text{(A.52)}$$

$$\int_{S_1^0}^{S_2^0} dS = \int_{T_1}^{T_2}\left(\frac{A}{T} + B + CT + DT^2\right)dT \quad \text{(A.53)}$$

Integrating:

$$S_2^0 - S_1^0 = \Delta S^0 = \ln\left(\frac{T_2}{T_1}\right) + B(T_2 - T_1) + \frac{C\left(T_2^2 - T_1^2\right)}{2}\frac{D\left(T_2^3 - T_1^3\right)}{3} \quad \text{(A.54)}$$

A.9 - Heat Loss Calculations

Component Surface Areas

	Fluid	No.	OD (mm)	L_H (mm)	A_H (m^2)
Gas Cooler					
Shell (65 NB sch. 80)	CO2	1	73	2956	0.677918
Header	water	2	90	32	0.018096
Bonnet	water	2	90	16	0.009048
					0.027143
Recuperator					
Shell (65 NB sch. 80)	Hot CO2	1	73	1456	0.333914
Header	Cold CO2	2	90	70	0.039584
Evaporator					
Shell (150 NB sch. 80)	CO2	1	168.3	1450	0.766659
Header	Water	2	234	45	0.066162
		2	168.3	80	0.084597
					0.150759

Separator	Fluid	No.	OD (mm)	L_V (mm)	A_V (m^2)
200NB xs wt	CO2	1	219.1	1700	1.170149

Pipework Surface Area

	Pipe size	OD (mm)	L_V (mm)	L_H (mm)	A_V (m^2)	A_H (m^2)
Compressor						
	3/4"	19.05	621	2951	0.037148	0.176599
Cooler 1						
	1/2"	12.7	193	39	0.007715	0.001543
Cooler 2						
	1/2"	12.7	193	39	0.007715	0.001543
Cooler 3						
	1/2"	12.7	193	1576	0.007715	0.062878
Recuperator						
	1/2"	12.7	1350	680	0.053863	0.027131
Separator						
	25NB	33.4	670	1060	0.070303	0.111225
Evaporator						
	40NB	48.3	480	200	0.072835	0.030348
	50NB	60.3	1220	890	0.231114	0.1686
Separator						
	25NB	33.4	2330	940	0.244485	0.098633
Recuperator						
	25NB	33.4	290	2137	0.030435	0.224206
Compressor						

Ambient Air Temperature (°C)	Max	Avg	Min
	30	20	10

	LV	AV	OD	AH	Surface Temperature (°C)			Temperature Difference (°C)			Heat Transfer Coefficient (W/m^{2}K)						Heat Flow (W)		
											Vertical			Horizontal			Max gain scenario	Average scenario	Max loss scenario
	m	m2	m	m2	Min	Avg	Max												
Compress																			
	0.621	0.037	0.019	0.177	130	140	145	-100	-120	-135	5.73	5.96	5.77	10.16	10.64	10.26	-201	-252	-274
Cooler 1			0.073	0.678	105	115	122.5	-75	-95	-112.5	1.57	1.58	1.58	4.58	4.80	4.54	-233	-309	-346
	0.193	0.008	0.013	0.002	80	90	100	-50	-70	-90	4.11	4.39	4.62	6.16	6.63	7.02	-2	-3	-4
Cooler 2			0.073	0.678	60	70	80	-30	-50	-70	1.27	1.27	1.28	5.40	6.01	6.48	-110	-204	-307
	0.193	0.008	0.013	0.002	40	50	60	-10	-30	-50	4.59	5.72	6.40	7.18	9.16	10.33	0	-2	-3
Cooler 3			0.073	0.678	27.5	37.5	47.5	2.5	-17.5	-37.5	1.08	1.08	1.08	4.11	6.04	7.14	7	-72	-182
	0.193	0.008	0.013	0.063	15	25	35	15	-5	-25	5.53	4.48	6.24	8.93	7.08	10.16	9	-2	-17
Recuperat			0.073	0.334	10	20	30	20	0	-20	0.99	0.00	0.99	6.63	0.00	6.73	44	0	-45
	1.350	0.054	0.013	0.027	5	15	25	25	5	-15	5.86	3.86	5.19	10.43	7.35	9.44	15	2	-8
Separator	1.700	1.170			-12.1	-5.6	5.4	42.1	25.6	4.6	7.36	6.53	4.09	0.89	0.87	0.87	362	196	22
	0.670	0.070	0.033	0.111	-12.1	-5.6	5.4	42.1	25.6	4.6	7.36	6.53	3.74	10.00	9.09	6.26	69	38	4
Evaporator			0.168	0.767	-12.1	-5.6	5.4	42.1	25.6	4.6	0.89	0.87	0.87	6.97	6.36	4.47	225	125	16
	0.480	0.073	0.048	0.030	-12.1	-5.6	5.4	42.1	25.6	4.6	6.16	5.63	3.99	9.19	8.37	5.79	31	17	2
	1.220	0.231	0.060	0.169	-12.1	-5.6	5.4	42.1	25.6	4.6	7.36	6.53	4.09	8.74	7.96	5.52	134	73	9
Separator																			
	2.330	0.244	0.033	0.099	-12.1	-5.6	5.4	42.1	25.6	4.6	7.36	6.53	4.09	10.00	9.09	6.26	117	64	8
Recuperat			0.090	0.020	-12.1	-5.6	5.4	42.1	25.6	4.6	0.89	0.87	0.87	8.00	7.29	5.08	7	4	0
			0.090	0.020	0	10	20	30	10	-10	0.94	0.94	0.94	7.15	5.70	5.74	4	1	-1
	0.290	0.030	0.033	0.224	0	10	20	30	10	-10	6.17	4.95	4.98	8.90	7.04	7.09	66	17	-17
Compress																			
TOTAL		1.933	m2	4.077	m2									gain in cool side			1089	536	61
														loss from hot side			-546	-844	-1205

+ is gain, - is loss

A.10 - Raw Data

20°C - 90°C Hot Water; 20°C, 0.6 l/s Cold Water In

RAW DATA

VARIABLE	UNITS	SYMBOL	1	15	9	3	25	13	27	7	17	4	19	21	24	18	10	29	8	16
CO_2 LINE			TX full open					min Psuc		TX full open										
High Side Pressure	Bar g		94	101	111.5	119.5	130	131	91	94	99.5	100.5	100.5	100.5	110	110	110.5	111.5	120	120
	Bar a	P_H	95	102	113	121	131	132	92	95	101	102	102	102	111	111	112	113	121	121
Low Side Pressure	Bar g		28.6	28.7	28.5	28.6	28.6	28.8	31.6	31.5	31.5	31.5	31.4	31.6	31.6	31.6	31.5	31.5	31.4	31.5
	Bar a	P_L	29.6	29.7	29.5	29.6	29.6	29.8	32.6	32.5	32.5	32.5	32.4	32.6	32.6	32.6	32.5	32.5	32.4	32.5
CO_2 Mass Flow	kg/s	m_{CO2}	0.326	0.323	0.273	0.240	0.208	0.246	0.344	0.318	0.281	0.290	0.244	0.230	0.213	0.216	0.264	0.200	0.191	0.214
Compressor Suction/Recuperator Cold Side Exit Temp	°C	T_{suc}	24.9	25.3	21.6	17.9	14.9	17.4	25.2	27.9	26.8	26.3	25.6	24.5	21	22.2	23.9	20	19.4	19.6
Compressor Discharge/Cooler 1 Inlet Temperature	°C	T_{dis}	139	138.5	144.5	152	160	159	120	130.1	129	132.2	128.3	131.5	135.8	132.7	134.8	134	142	140.5
Cooler 3 Exit/Recuperator Hot Side Inlet Temperature	°C	T_{co}	37.6	38.6	32.9	27.2	23.7	25.4	37.0	39.2	39.6	39.1	39.1	37.6	32.4	34.2	34.8	30.3	28.2	28.2
Pre-Expansion Valve/Recuperator Hot Side Exit Temp	°C	T_{TXi}	32.7	31.2	22	17	12.2	17.4	32.3	35	31.9	31	29.7	26.2	19.7	22.2	24.1	19	18.1	18.3
Separator/Recuperator Cold Side Inlet Temperature	°C	T_{sep}	-6.4	-6.3	-6.6	-6.7	-6.9	-6.1	-3.1	-3.1	-3.1	-3.1	-2.9	-3.1	-3	-2.9	-3.1	-3.1	-3.1	-3.1
HOT WATER LINE																				
Inlet Temperature	°C	T_{cwi}	21.2	21.6	21.6	21.2	21	20.6	19.9	21.3	21.2	21.1	21	20.9	21	21	21.6	20.1	21.5	21.2
Outlet Temperature	°C	T_{cwo}	90	90	90	90.4	90	88	90	90.2	90	90	90	90	90	90.3	90	89.8	89.3	90
Flowrate	L/s	Q_{cw}	0.266	0.284	0.263	0.262	0.264	0.274	0.215	0.227	0.224	0.214	0.213	0.213	0.212	0.201	0.217	0.193	0.214	0.220
COLD WATER LINE																				
Inlet Temperature	°C	T_{ewi}	20.5	21.2	21	21	21	21.1	20.1	20.9	21.1	20.9	21	20.9	21	21	21.1	20.6	20.9	21.1
Outlet Temperature	°C	T_{ewo}	7.1	6	6.1	6.2	4.8	5.9	7	8.6	8	8.3	7	6.95	7.1	6.1	8.9	6.8	8.2	8
Flowrate	L/s	Q_{ew}	0.615	0.631	0.629	0.645	0.613	0.621	0.638	0.620	0.625	0.620	0.574	0.636	0.639	0.577	0.624	0.629	0.630	0.623
VSD/MOTOR																				
VSD Output/Motor Input Real Power	kW	f_{VSDo}	32.9	30.7	27.3	26.9	29.5	31.3	25.8	25.3	23.3	21.1	21.7	21.9	20.6	20.2	21.0	19.4	20.2	21.3
Motor/Compressor Speed	%		125%	125%	110%	108%	120%	125%	98%	94%	89%	81%	84%	82%	78%	78%	79%	71%	75%	79%
	RPM	w_{comp}	1212.5	1212.5	1065.8	1046.8	1167.1	1212.5	951.8	913.8	863.3	787.1	818.8	799.8	755.5	755.5	768.1	692.1	730.1	761.5

CALCULATIONS

VARIABLE	UNITS	SYMBOL																		
COOLERS																				
Total Heat Transfer from CO2	**W**	ϕ_c	**83740**	**82754**	**78133**	**74630**	**67744**	**78954**	**79818**	**74581**	**66854**	**71168**	**58659**	**57990**	**58830**	**57779**	**70675**	**56022**	**56053**	**62351**
Hot Water Mass Flow	kg/s	m_{cw}	0.265	0.283	0.263	0.261	0.263	0.273	0.215	0.227	0.224	0.213	0.212	0.212	0.211	0.201	0.216	0.192	0.214	0.220
Total Heat Transfer to Hot Water	**W**	ϕ_{cw}	**76478**	**81152**	**75235**	**75705**	**76004**	**77173**	**63114**	**65379**	**64465**	**61481**	**61392**	**61443**	**60999**	**58214**	**61919**	**56133**	**60621**	**63273**
Overall Cooler Water Line LMTD	°C	$\Delta\theta_{lm,c}$	29.8	30.1	27.5	23.9	20.7	24.6	22.9	27.4	27.4	28.4	26.9	27.3	24.7	25.0	25.9	23.2	22.3	22.0
Cooler Overall Heat Transfer Coefficient	W/m²°C	U_c	681	716	726	842	976	832	730	632	624	574	605	598	655	618	635	642	721	764
Water Side Heat Transfer Coefficient	W/m²°C	hw	3830	4041	3803	3785	3799	3892	3220	3378	3341	3211	3203	3200	3186	3061	3255	2946	3215	3291

CO2 Side Heat Transfer Coefficient	$W/m^2°C$	hco2	969	1021	1065	1336	1704	1296	1151	909	897	808	869	856	980	914	928	983	1129	1226
Cooler Heat Load	**kW**	ϕ_c	**76478**	**81152**	**75235**	**75705**	**76004**	**77173**	**63114**	**65379**	**64465**	**61481**	**61392**	**61443**	**60999**	**58214**	**61919**	**56133**	**60621**	**63273**
Heating COP	**kW/kW**	COP_H	**2.50**	**2.84**	**2.97**	**3.03**	**2.78**	**2.66**	**2.63**	**2.78**	**2.98**	**3.13**	**3.05**	**3.02**	**3.19**	**3.10**	**3.18**	**3.11**	**3.22**	**3.19**
EVAPORATOR																				
Heat Transfer to CO_2	**W**	ϕ_e	**48370**	**50794**	**50557**	**47516**	**43325**	**48798**	**50184**	**43460**	**42951**	**45319**	**39364**	**39292**	**40209**	**39672**	**47139**	**38253**	**37068**	**41342**
Cold Water Mass Flow	kg/s	m_{ew}	0.614	0.630	0.628	0.644	0.611	0.619	0.636	0.619	0.624	0.619	0.572	0.635	0.638	0.576	0.623	0.627	0.629	0.622
Heat Transfer from Cold Water	**W**	ϕ_{ew}	**34462**	**40127**	**39189**	**39919**	**41512**	**39457**	**34934**	**31877**	**34240**	**32657**	**33572**	**37113**	**37126**	**35948**	**31830**	**36282**	**33447**	**34141**
Log Mean Temperature Difference	°C	$\Delta\theta_m$	19.4	18.9	19.2	19.4	18.6	18.6	15.8	17.1	16.8	16.9	15.9	16.0	16.1	15.3	17.4	15.8	16.9	16.8
Evaporator Overall Heat Transfer Coefficient	$W/m^2°C$	U_e	436	492	478	462	465	486	553	450	470	471	469	487	492	507	464	482	428	459
Water Side Heat Transfer Coefficient	$W/m^2°C$	hw	1409	1435	1430	1460	1390	1414	1446	1432	1438	1430	1335	1449	1456	1335	1443	1432	1447	1435
CO2 Side Heat Transfer Coefficient	$W/m^2°C$	hco2	737	901	857	794	834	890	1118	770	827	835	874	879	892	1013	808	869	702	796
Evaporator Heat Load	**kW**	ϕ_e	**41416**	**45461**	**44873**	**43718**	**42418**	**44127**	**42559**	**37669**	**38596**	**38988**	**36468**	**38202**	**38667**	**37810**	**39484**	**37268**	**35258**	**37741**
Cooling COP	**kW/kW**	COP_L	**1.36**	**1.59**	**1.77**	**1.75**	**1.55**	**1.52**	**1.77**	**1.60**	**1.78**	**1.98**	**1.81**	**1.88**	**2.02**	**2.01**	**2.03**	**2.07**	**1.88**	**1.91**
Overall COP	**kW/kW**	**COP**	**3.86**	**4.44**	**4.74**	**4.77**	**4.33**	**4.18**	**4.40**	**4.38**	**4.76**	**5.11**	**4.86**	**4.91**	**5.21**	**5.11**	**5.21**	**5.18**	**5.10**	**5.10**
RECUPERATOR																				
HOT SIDE Heat Transfer from Hot CO_2	W	ϕ_{rH}	7874	9483	8080	5892	5374	4540	8690	7923	9308	9498	9017	9244	7187	7212	8068	5844	4684	5113
COLD SIDE Heat Transfer to superheat cold CO_2 vapour	W	ϕ_{rL}	14039	14059	10689	8391	6536	8260	14240	14231	12204	12401	10097	9337	7585	8032	10459	6884	6379	7231
Log Mean Temperature Difference	°C	$\Delta\theta_m$	23.5	23.4	18.7	15.4	13.3	14.4	21.5	22.1	22.0	21.7	21.7	20.2	16.4	17.7	17.8	15.5	14.1	14.0
Recuperator Overall Heat Transfer Coefficient	$W/m^2°C$	U_r	743	802	801	739	713	708	850	800	777	802	702	734	718	685	827	655	624	701
Recuperator Heat Load	**kW**	ϕ_e	10956	11771	9385	7141	5955	6400	11465	11077	10756	10949	9557	9290	7386	7622	9264	6364	5532	6172
POWER																				
Motor Output/Comp. Input Power	**kW**	$\phi_{comp,i}$	**30.6**	**28.5**	**25.3**	**25.0**	**27.4**	**29.0**	**24.0**	**23.5**	**21.7**	**19.6**	**20.1**	**20.3**	**19.1**	**18.8**	**19.5**	**18.0**	**18.8**	**19.8**
COMPRESSOR																				
Enthalpy Change	J/kg	ΔH_{comp}	89674	84858	91604	102429	112052	107348	70103	78090	74757	79140	74564	80753	85744	79847	80056	83593	90673	88480
Isentropic Compression Enthalpy Change	J/kg	$\Delta H_{comp,\Delta S=0}$	58373	62367	66775	68506	71582	72992	49642	52705	55371	55697	55616	54664	57884	58494	59840	58342	62284	62148
Isentropic Efficiency		$\varepsilon_{comp,\Delta S=0}$	**0.651**	**0.735**	**0.729**	**0.669**	**0.639**	**0.680**	**0.708**	**0.675**	**0.741**	**0.704**	**0.746**	**0.677**	**0.675**	**0.733**	**0.747**	**0.698**	**0.687**	**0.702**
Theoretical Volumetric Flow into Compressor	m3/s	$Q_{comp,i}'$	0.01037	0.01037	0.00911	0.00895	0.00998	0.01037	0.00814	0.00781	0.00738	0.00673	0.00700	0.00684	0.00646	0.00646	0.00657	0.00592	0.00624	0.00651
Actual Volumetric Flow into Compressor	m3/s	$Q_{comp,i}$	0.00511	0.00506	0.00420	0.00360	0.00305	0.00365	0.00481	0.00456	0.00401	0.00412	0.00346	0.00321	0.00288	0.00296	0.00368	0.00270	0.00258	0.00288
Volumetric Efficiency		$\varepsilon_{comp,V}$	**0.493**	**0.488**	**0.461**	**0.402**	**0.306**	**0.352**	**0.591**	**0.583**	**0.543**	**0.611**	**0.495**	**0.469**	**0.446**	**0.459**	**0.560**	**0.457**	**0.413**	**0.442**

20°C - 77.5°C Hot Water; 20°C, 0.6 l/s Cold Water In

RAW DATA

VARIABLE	UNITS	SYMBOL	23	28	5	22	6	20	14	12	26	11	2	1	3	2	4
CO_2 LINE							TX full open			max Psuc		max Psuc		TX f o			
High Side Pressure	Bar g		120	129.5	130	93	94	94	100.5	110	110	119.5	130	86	95.5	104.5	115.5
	Bar a	P_H	121	131	131	94	95	95	102	111	111	121	131	87	97	106	117
Low Side Pressure	Bar g		31.5	31.5	31.5	34.6	34.6	34.6	34.5	34.1	34.1	34.0	34.5	31.5	31.6	31.5	31.5
	Bar a	P_L	32.5	32.5	32.5	35.6	35.6	35.6	35.5	35.1	35.1	35.0	35.5	32.5	32.6	32.5	32.5
CO_2 Mass Flow	kg/s	m_{CO2}	0.187	0.175	0.208	0.290	0.306	0.234	0.263	0.209	0.191	0.197	0.179	0.267	0.222	0.201	0.193
Compressor Suction/Recuperator Cold Side Exit Temp	°C	T_{suc}	17.9	17	17.2	28.9	29	27.8	29.7	26.1	24	23	18.1	26.3	23.3	19.3	17.4
Compressor Discharge/Cooler 1 Inlet Temperature	°C	T_{dis}	141.3	144	150.1	116.5	118	115	121.7	131.6	130	137.8	149.5	122.5	130	136.5	149
Cooler 3 Exit/Recuperator Hot Side Inlet Temperature	°C	T_{co}	26.9	23.3	25.7	39.3	40.4	39.6	40.4	34.9	32.4	28.7	24.0	34.7	33.7	26.5	23.3
Pre-Expansion Valve/Recuperator Hot Side Exit Temp	°C	T_{TXi}	15.2	14	16	32.8	36.2	34.9	32.1	23.1	19.1	18.3	15.1	30.0	22.7	15.5	12.9
Separator/Recuperator Cold Side Inlet Temperature	°C	T_{sep}	-3.1	-3.1	-3.1	0.3	0.1	0.2	0.1	-0.1	-0.2	-0.5	-0.05	-3	-3.2	-3.2	-3.1
HOT WATER LINE																	
Inlet Temperature	°C	T_{cwi}	20.9	20	21.1	20.9	21.2	21	21.6	20.4	21	21.8	21.2	20.7	20.7	20.7	20.7
Outlet Temperature	°C	T_{cwo}	90	90.1	89.5	90.2	90	90.5	89.5	90	90.2	89.7	90	77.7	77.7	77.5	77.8
Flowrate	L/s	Q_{cw}	0.218	0.197	0.210	0.192	0.191	0.194	0.192	0.193	0.187	0.199	0.198	0.275	0.248	0.251	0.257
COLD WATER LINE																	
Inlet Temperature	°C	T_{ewi}	20.9	20.6	20.9	20.9	20.9	21	21.2	21.1	20.9	20.6	20.8	21	20.9	20.9	20.9
Outlet Temperature	°C	T_{ewo}	7.1	6.9	7.2	8.7	10.1	9	9.6	9.6	7.8	9.1	8.1	7.7	7.6	7.5	7.6
Flowrate	L/s	Q_{ew}	0.645	0.634	0.630	0.645	0.635	0.638	0.620	0.633	0.618	0.624	0.630	0.633	0.623	0.623	0.620
VSD/MOTOR																	
VSD Output/Motor Input Real Power	kW	f_{VSDo}	21.3	21.5	22.6	20.6	20.5	21.7	19.0	17.9	17.5	18.4	20.4	25.8	20.2	19.6	20.1
Motor/Compressor Speed	%		79%	75%	82%	77%	79%	82%	71%	62%	62%	62%	62%	99%	80%	79%	84%
	RPM	w_{comp}	761.5	730.1	793.5	749.1	761.8	799.8	692.1	601.4	601.4	601.4	601.4	958.1	780.8	768.1	818.8

CALCULATIONS

VARIABLE	UNITS	SYMBOL															
COOLERS																	
Total Heat Transfer from CO2	**W**	ϕ_c	**55345**	**53484**	**63929**	**61856**	**63936**	**49536**	**58923**	**54851**	**51226**	**56414**	**55602**	**65385**	**58934**	**59470**	**61299**
Hot Water Mass Flow	kg/s	m_{cw}	0.218	0.196	0.210	0.192	0.190	0.194	0.191	0.192	0.187	0.198	0.198	0.274	0.247	0.250	0.257
Total Heat Transfer to Hot Water	**W**	ϕ_{cw}	**62955**	**57658**	**60026**	**55654**	**54806**	**56349**	**54394**	**56072**	**54080**	**56381**	**57046**	**65385**	**58934**	**59470**	**61299**
Overall Cooler Water Line LMTD	°C	$\Delta\theta_{lm,c}$	21.1	18.1	21.7	22.1	23.3	21.4	24.9	25.7	22.7	21.3	18.6	26.5	28.2	22.9	20.6
Cooler Overall Heat Transfer Coefficient	W/m²°C	U_c	792	845	735	667	624	698	580	579	632	704	813	655	554	688	788
Water Side Heat Transfer Coefficient	W/m²°C	hw	3263	2997	3165	2951	2934	2977	2947	2952	2889	3037	3029	**3786**	3484	3517	3592

CO2 Side Heat Transfer Coefficient	W/m²°C	hco2	1306	1535	1175	1042	942	1115	844	842	968	1118	1423	920	748	1013	1234
Cooler Heat Load	**kW**	ϕ_c	**62955**	**57658**	**60026**	**55654**	**54806**	**56349**	**54394**	**56072**	**54080**	**56381**	**57046**	**65385**	**58934**	**59470**	**61299**
Heating COP	**kW/kW**	COP_H	**3.18**	**2.89**	**2.86**	**2.91**	**2.88**	**2.80**	**3.09**	**3.37**	**3.32**	**3.29**	**3.01**	**2.72**	**3.13**	**3.27**	**3.29**
EVAPORATOR																	
Heat Transfer to CO_2	**W**	ϕ_e	**37475**	**35755**	**41424**	**41691**	**39260**	**31682**	**39623**	**37467**	**36099**	**37722**	**35616**	**40739**	**39709**	**39851**	**39667**
Cold Water Mass Flow	kg/s	m_{ew}	0.644	0.633	0.629	0.644	0.634	0.636	0.619	0.632	0.617	0.623	0.629	0.631	0.621	0.622	0.618
Heat Transfer from Cold Water	**W**	ϕ_{ew}	**37210**	**36329**	**36088**	**32887**	**28660**	**31982**	**30072**	**30418**	**33838**	**29997**	**33449**	**35174**	**34623**	**34924**	**34448**
Log Mean Temperature Difference	°C	$\Delta\theta_m$	16.1	15.9	16.2	13.6	14.7	14.0	14.5	14.7	13.5	14.6	13.5	16.5	16.6	16.5	16.5
Evaporator Overall Heat Transfer Coefficient	W/m²°C	U_e	474	464	489	561	471	467	490	472	529	474	522	471	459	463	460
Water Side Heat Transfer Coefficient	W/m²°C	hw	1466	1443	1440	1478	1471	1468	1442	1465	1422	1441	1446	**1449**	1429	1430	1423
CO2 Side Heat Transfer Coefficient	W/m²°C	hco2	828	808	889	1127	818	806	891	823	1042	840	1001	828	797	811	804
Evaporator Heat Load	**kW**	ϕ_e	**37343**	**36042**	**38756**	**37289**	**33960**	**31832**	**34848**	**33942**	**34968**	**33859**	**34533**	**37956**	**37166**	**37387**	**37057**
Cooling COP	**kW/kW**	COP_L	**1.88**	**1.80**	**1.85**	**1.95**	**1.78**	**1.58**	**1.98**	**2.04**	**2.15**	**1.98**	**1.82**	**1.58**	**1.98**	**2.05**	**1.99**
Overall COP	**kW/kW**	**COP**	**5.06**	**4.69**	**4.71**	**4.86**	**4.66**	**4.38**	**5.06**	**5.42**	**5.47**	**5.27**	**4.83**	**4.30**	**5.11**	**5.32**	**5.28**
RECUPERATOR																	
HOT SIDE Heat Transfer from Hot CO_2	W	ϕ_{rH}	5182	3689	4603	10874	8622	6662	9512	6968	6747	5015	3634	6713	7924	5582	4684
COLD SIDE Heat Transfer to superheat cold CO_2 vapour	W	ϕ_{rL}	5897	5324	6360	12646	13501	9943	11805	8333	7133	7184	5244	11363	8682	6754	5964
Log Mean Temperature Difference	°C	$\Delta\theta_m$	13.1	10.8	13.1	19.4	21.4	21.2	19.4	14.8	13.1	11.0	9.8	18.0	17.0	12.0	10.1
Recuperator Overall Heat Transfer Coefficient	W/m²°C	U_r	674	663	668	964	822	623	873	821	843	882	719	800	778	815	840
Recuperator Heat Load	**kW**	ϕ_e	5540	4506	5481	11760	11061	8302	10659	7651	6940	6099	4439	9038	8303	6168	5324
POWER																	
Motor Output/Comp. Input Power	**kW**	$\phi_{comp,i}$	**19.8**	**20.0**	**21.0**	**19.1**	**19.1**	**20.1**	**17.6**	**16.6**	**16.3**	**17.1**	**19.0**	**24.0**	**18.8**	**18.2**	**18.6**
COMPRESSOR																	
Enthalpy Change	J/kg	ΔH_{comp}	91877	91805	99969	63438	64733	62140	64631	76807	77306	84024	102786	74935	83222	91916	105481
Isentropic Compression Enthalpy Change	J/kg	$\Delta H_{comp,\Delta S=0}$	61199	64858	65194	45992	46598	46119	50621	54729	53723	57901	58500	47295	51411	54535	58846
Isentropic Efficiency		$e_{comp,\Delta S=0}$	**0.666**	**0.706**	**0.652**	**0.725**	**0.720**	**0.742**	**0.783**	**0.713**	**0.695**	**0.689**	**0.569**	**0.631**	**0.618**	**0.593**	**0.558**
Theoretical Volumetric Flow into Compressor	m3/s	$Q_{comp,i}'$	0.00651	0.00624	0.00679	0.00641	0.00651	0.00684	0.00592	0.00514	0.00514	0.00514	0.00514	0.00819	0.00668	0.00657	0.00700
Actual Volumetric Flow into Compressor	m3/s	$Q_{comp,i}$	0.00248	0.00232	0.00275	0.00372	0.00392	0.00299	0.00340	0.00267	0.00241	0.00248	0.00212	0.00379	0.00306	0.00270	0.00256
Volumetric Efficiency		$e_{comp,V}$	**0.381**	**0.371**	**0.405**	**0.580**	**0.602**	**0.437**	**0.574**	**0.519**	**0.469**	**0.482**	**0.412**	**0.462**	**0.459**	**0.411**	**0.365**

20°C - 65°C Hot Water; 20°C, 0.6 l/s Cold Water In

RAW DATA

VARIABLE	UNITS	SYMBOL	34	36	35	37	39	25	38	26	33	29	32	30	52	1	45	47	54	48
CO_2 LINE																				
High Side Pressure	Bar g		85	95	105	115.5	125	84	86	94.5	95.5	105	105	115	115.5	124	124.5	124.5	125	130
	Bar a	P_H	86	96	106	117	126	85	87	96	97	106	106	116	117	125	126	126	126	131
Low Side Pressure	Bar g		28.6	28.6	28.6	28.6	28.6	31.5	31.5	31.4	31.3	31.5	31.8	31.5	31.5	31.5	31.5	31.5	31.6	31.5
	Bar a	P_L	29.6	29.6	29.6	29.6	29.6	32.5	32.5	32.4	32.3	32.5	32.8	32.5	32.5	32.5	32.5	32.5	32.6	32.5
CO_2 Mass Flow	kg/s	m_{CO2}	0.287	0.222	0.220	0.209	0.209	0.314	0.242	0.191	0.191	0.185	0.179	0.182	0.187	0.186	0.185	0.179	0.185	0.181
Compressor Suction/Recuperator Cold Side Exit Temp	°C	T_{suc}	22.7	16.9	15.7	15.5	15.2	23.9	23.2	19	19	18.5	17.8	14.5	11.6	14.1	16.1	14.5	16	14.5
Compressor Discharge/Cooler 1 Inlet Temperature	°C	T_{dis}	123	124	132	142.5	152	111	114	120	120	124.5	126.5	132	136	136.2	138.2	138	145	141
Cooler 3 Exit/Recuperator Hot Side Inlet Temperature	°C	T_{co}	33.6	26.2	23.3	22.3	22.1	33.3	33.4	26.3	25.1	23.0	22.8	21.2	22.1	21.1	21.9	21.1	22.1	21.1
Pre-Expansion Valve/Recuperator Hot Side Exit Temp	°C	T_{TXi}	26.0	14.8	12.1	11.5	11	29	24.6	14.8	13.9	12.5	12	11.9	11.3	12	12	12.1	11.4	12.2
Separator/Recuperator Cold Side Inlet Temperature	°C	T_{sep}	-6.9	-6.8	-6.8	-6.7	-6.6	-3.1	-3.1	-3.1	-3.2	-3.1	-2.9	-3.1	-3.1	-3.1	-3.1	-3.2	-3.1	-3.1
HOT WATER LINE																				
Inlet Temperature	°C	T_{cwi}	20.9	20.9	20.9	20.9	20.9	20.9	20.7	20.7	20.9	20.9	21	20.1	20.8	20.1	20.6	20	20.8	20
Outlet Temperature	°C	T_{cwo}	65	65	65	65	65.5	65.4	65	65.5	64.7	65	65	65	65	65	65.2	65.3	65	65
Flowrate	L/s	Q_{cw}	0.407	0.357	0.375	0.379	0.378	0.356	0.313	0.301	0.306	0.304	0.307	0.302	0.317	0.311	0.315	0.298	0.343	0.311
COLD WATER LINE																				
Inlet Temperature	°C	T_{ewi}	21.7	21.4	21.6	21.3	21.2	21.2	20.9	20.9	21	21.2	21	20.4	21	20.5	21	20.8	21	20.9
Outlet Temperature	°C	T_{ewo}	5.9	5.9	5.9	5.9	6	6.6	7.5	7.6	7.8	8.8	8	6.8	7.9	6.8	7	7.1	8	7.1
Flowrate	L/s	Q_{ew}	0.608	0.600	0.604	0.601	0.599	0.613	0.635	0.635	0.640	0.626	0.649	0.631	0.624	0.644	0.629	0.642	0.637	0.636
VSD/MOTOR																				
VSD Output/Motor Input Real Power	kW	f_{VSDo}	24.4	19.7	21.5	22.4	25.1	21.1	17.5	16.4	15.9	17.2	16.4	17.7	19.0	19.9	20.0	19.1	20.6	19.3
Motor/Compressor Speed	%		103%	82%	86%	91%	103%	88%	72%	62%	62%	64%	62%	66%	70%	71%	72%	70%	75%	72%
	RPM	w_{comp}	996.1	799.8	837.8	882.1	1002.4	850.5	698.5	601.4	601.4	616.2	601.4	641.5	679.5	692.1	698.5	679.5	730.1	698.5

CALCULATIONS

VARIABLE	UNITS	SYMBOL																		
COOLERS																				
Total Heat Transfer from CO2	**W**	ϕ_c	**72285**	**63082**	**65830**	**64910**	**66974**	**74388**	**58640**	**52969**	**53609**	**53386**	**52236**	**54552**	**56489**	**56127**	**55837**	**54480**	**57512**	**55248**
Hot Water Mass Flow	kg/s	m_{cw}	0.407	0.357	0.374	0.378	0.377	0.356	0.313	0.301	0.305	0.303	0.306	0.301	0.317	0.311	0.315	0.297	0.342	0.310
Total Heat Transfer to Hot Water	**W**	ϕ_{cw}	**74967**	**65753**	**68943**	**69766**	**70279**	**66170**	**57895**	**56369**	**55899**	**55889**	**56309**	**56578**	**58560**	**58334**	**58660**	**56349**	**63303**	**58334**
Overall Cooler Water Line LMTD	°C	$\Delta\theta_{lm,c}$	29.8	22.2	19.4	19.0	19.8	25.5	26.9	21.5	19.8	17.1	17.0	16.1	17.5	16.5	17.8	17.0	19.0	17.7
Cooler Overall Heat Transfer Coefficient	W/m²°C	U_c	667	785	943	977	942	689	571	695	749	868	881	933	886	937	875	879	886	875
Water Side Heat Transfer Coefficient	W/m²°C	hw	**4989**	4492	4666	4711	4703	4489	4040	3925	3963	3945	3977	3914	4086	4011	4061	3876	4348	4002

CO2 Side Heat Transfer Coefficient	$W/m^2°C$	hco2	873	1124	1454	1529	1448	937	749	987	1098	1377	1405	1552	1398	1543	1374	1415	1360	1385
Cooler Heat Load	**kW**	ϕ_c	**74967**	**65753**	**68943**	**69766**	**70279**	**66170**	**57895**	**56369**	**55899**	**55889**	**56309**	**56578**	**58560**	**58334**	**58660**	**56349**	**63303**	**58334**
Heating COP	**kW/kW**	COP_H	**3.31**	**3.59**	**3.45**	**3.36**	**3.01**	**3.37**	**3.55**	**3.69**	**3.78**	**3.50**	**3.69**	**3.44**	**3.32**	**3.16**	**3.16**	**3.18**	**3.31**	**3.25**
EVAPORATOR																				
Heat Transfer to CO_2	**W**	ϕ_e	**48066**	**44595**	**45786**	**43771**	**44139**	**48712**	**41569**	**38089**	**38545**	**38015**	**36903**	**37872**	**39056**	**38748**	**38439**	**37234**	**38635**	**37586**
Cold Water Mass Flow	kg/s	m_{ew}	0.607	0.599	0.602	0.600	0.597	0.612	0.634	0.634	0.638	0.625	0.647	0.630	0.623	0.643	0.628	0.641	0.636	0.634
Heat Transfer from Cold Water	**W**	ϕ_{ew}	**40158**	**38880**	**39616**	**38691**	**38048**	**37443**	**35582**	**35336**	**35295**	**32440**	**35243**	**35903**	**34185**	**36883**	**36815**	**36782**	**34622**	**36671**
Log Mean Temperature Difference	°C	$\Delta\theta_{lm}$	19.7	19.4	19.5	19.3	19.2	15.9	16.4	16.5	16.7	17.4	16.6	15.7	16.7	15.8	16.1	16.2	16.8	16.1
Evaporator Overall Heat Transfer Coefficient	$W/m^2°C$	U_e	459	439	448	437	438	554	481	456	451	415	446	479	448	490	478	467	447	471
Water Side Heat Transfer Coefficient	$W/m^2°C$	hw	**1395**	1378	1386	1379	1375	1407	1451	1453	1462	1446	1480	1435	1435	1459	1437	1460	1459	1449
CO2 Side Heat Transfer Coefficient	$W/m^2°C$	hco2	812	758	780	751	754	1155	857	780	762	668	741	859	764	884	854	811	751	826
Evaporator Heat Load	**kW**	ϕ_e	**44112**	**41737**	**42701**	**41231**	**41093**	**43078**	**38576**	**36713**	**36920**	**35228**	**36073**	**36888**	**36621**	**37816**	**37627**	**37008**	**36629**	**37129**
Cooling COP	**kW/kW**	COP_L	**1.95**	**2.28**	**2.14**	**1.98**	**1.76**	**2.19**	**2.37**	**2.40**	**2.50**	**2.21**	**2.36**	**2.24**	**2.08**	**2.05**	**2.03**	**2.09**	**1.91**	**2.07**
Overall COP	**kW/kW**	**COP**	**5.25**	**5.87**	**5.59**	**5.34**	**4.77**	**5.56**	**5.92**	**6.09**	**6.28**	**5.71**	**6.05**	**5.68**	**5.40**	**5.21**	**5.19**	**5.26**	**5.22**	**5.31**
RECUPERATOR																				
HOT SIDE Heat Transfer from Hot CO_2	W	ϕ_{rH}	9679	6670	5973	5225	5206	6861	8703	5837	5514	4674	4664	3933	4689	3841	4138	3637	4450	3589
COLD SIDE Heat Transfer to superheat cold CO_2 vapour	W	ϕ_{rL}	11838	7526	7126	6652	6537	12424	9369	6277	6285	5983	5630	4918	4300	4924	5386	4871	5387	4878
Log Mean Temperature Difference	°C	$\Delta\theta_{lm}$	19.9	14.6	12.4	11.6	11.4	18.5	17.5	11.8	10.7	8.9	9.1	10.3	12.4	10.5	9.7	10.3	9.7	10.3
Recuperator Overall Heat Transfer Coefficient	$W/m^2°C$	U_r	860	776	841	817	820	831	820	814	882	954	902	683	579	662	780	656	810	651
Recuperator Heat Load	**kW**	ϕ_e	10759	7098	6550	5939	5872	9643	9036	6057	5900	5329	5147	4425	4494	4382	4762	4254	4919	4234
POWER																				
Motor Output/Comp. Input Power	**kW**	$\phi_{comp,i}$	**22.7**	**18.3**	**20.0**	**20.8**	**23.3**	**19.6**	**16.3**	**15.3**	**14.8**	**16.0**	**15.3**	**16.5**	**17.6**	**18.5**	**18.6**	**17.7**	**19.1**	**18.0**
COMPRESSOR																				
Enthalpy Change	J/kg	ΔH_{comp}	76875	79259	85688	94519	103112	64104	67702	75723	74953	76117	80362	86113	95448	87511	87430	89314	97112	90584
Isentropic Compression Enthalpy Change	J/kg	$\Delta H_{comp,\Delta S=0}$	51926	55351	60096	65229	69511	45169	46119	49402	50165	54396	53341	57012	55549	60740	62163	61197	62070	63543
Isentropic Efficiency		$e_{comp,\Delta S=0}$	**0.675**	**0.698**	**0.701**	**0.690**	**0.674**	**0.705**	**0.681**	**0.652**	**0.669**	**0.715**	**0.664**	**0.662**	**0.582**	**0.694**	**0.711**	**0.685**	**0.639**	**0.701**
Theoretical Volumetric Flow into Compressor	m3/s	$Q_{comp,i}'$	0.00852	0.00684	0.00716	0.00754	0.00857	0.00727	0.00597	0.00514	0.00514	0.00527	0.00514	0.00549	0.00581	0.00592	0.00597	0.00581	0.00624	0.00597
Actual Volumetric Flow into Compressor	m3/s	$Q_{comp,i}$	0.00444	0.00331	0.00326	0.00308	0.00307	0.00437	0.00336	0.00257	0.00258	0.00247	0.00235	0.00236	0.00237	0.00241	0.00242	0.00232	0.00241	0.00234
Volumetric Efficiency		$e_{comp,V}$	**0.521**	**0.485**	**0.455**	**0.408**	**0.359**	**0.601**	**0.562**	**0.499**	**0.501**	**0.468**	**0.457**	**0.431**	**0.408**	**0.407**	**0.406**	**0.400**	**0.386**	**0.392**

RAW DATA

VARIABLE	UNITS	SYMBOL	51	27	44	42	40	41	28	53	43	49	46	50
CO_2 LINE														
High Side Pressure	Bar g		130	85	85	95	105	105.5	114.5	115	124	125.3	130	130
	Bar a	P_H	131	86	86	96	106	107	116	116	125	126	131	131
Low Side Pressure	Bar g		31.6	33.2	33	33	33	33	33	32.9	33	32.9	33	33
	Bar a	P_L	32.6	34.2	34.0	34.0	34.0	34.0	34.0	33.9	34.0	33.9	34.0	34.0
CO_2 Mass Flow	kg/s	m_{CO2}	0.176	0.228	0.260	0.219	0.220	0.195	0.188	0.185	0.173	0.204	0.154	0.168
Compressor Suction/Recuperator Cold Side Exit Temp	°C	T_{suc}	14.5	26.1	25.5	19.5	16	16.7	15.2	17.8	16	16.8	16.4	16.3
Compressor Discharge/Cooler 1 Inlet Temperature	°C	T_{de}	141	110.5	106	111	116.5	119.5	125	133	134.5	136.4	138	138
Cooler 3 Exit/Recuperator Hot Side Inlet Temperature	°C	T_{co}	20.9	34.3	34.6	27.4	22.5	22.6	21.4	22.2	21.2	22.0	21.1	21.1
Pre-Expansion Valve/Recuperator Hot Side Exit Temp	°C	T_{TXi}	12	26	28	16.7	12.5	12.9	12.5	11.9	12.3	12.2	12	12.1
Separator/Recuperator Cold Side Inlet Temperature	°C	T_{sep}	-3.1	-1.4	-1.7	-1.7	-1.8	-1.7	-1.7	-1.8	-1.7	-1.8	-1.8	-1.6
HOT WATER LINE														
Inlet Temperature	°C	T_{cwi}	20.1	20.9	20.6	20.6	20.2	20.6	20.1	20.9	20	20.6	20.1	20.1
Outlet Temperature	°C	T_{cwo}	65	65	65.2	65	64.8	65	65	65	64.8	65.5	65	65.4
Flowrate	L/s	Q_{cw}	0.311	0.287	0.299	0.323	0.315	0.317	0.304	0.311	0.291	0.308	0.284	0.288
COLD WATER LINE														
Inlet Temperature	°C	T_{ewi}	20.4	20.9	21	22.1	21	22	20.6	20.9	20.9	21	20.8	20.4
Outlet Temperature	°C	T_{ewo}	6.9	8.6	7.1	7	7.8	7.1	7.1	8.3	8	7	8	7.7
Flowrate	L/s	Q_{ew}	0.633	0.652	0.626	0.659	0.738	0.636	0.703	0.648	0.644	0.630	0.624	0.622
VSD/MOTOR														
VSD Output/Motor Input Real Power	kW	f_{VSDo}	19.7	15.8	16.6	16.5	17.0	17.0	17.4	18.1	17.9	18.4	18.3	19.2
Motor/Compressor Speed	%		71%	62%	71%	62%	60%	62%	62%	62%	62%	67%	64%	65%
	RPM	w_{comp}	692.1	601.4	685.8	601.4	582.0	601.4	601.4	601.4	601.4	654.1	622.5	635.2

CALCULATIONS

VARIABLE	UNITS	SYMBOL												
COOLERS														
Total Heat Transfer from CO2	**W**	ϕ_c	**53858**	**52683**	**57733**	**57428**	**61409**	**55012**	**54221**	**55127**	**51606**	**60942**	**46391**	**50585**
Hot Water Mass Flow	kg/s	m_{cw}	0.310	0.287	0.299	0.322	0.314	0.317	0.304	0.310	0.290	0.307	0.284	0.287
Total Heat Transfer to Hot Water	**W**	ϕ_{cw}	**58223**	**52886**	**55732**	**59777**	**58614**	**58818**	**57052**	**57227**	**54393**	**57652**	**53296**	**54365**
Overall Cooler Water Line LMTD	°C	$\Delta\theta_{lm,c}$	16.7	26.2	25.1	20.5	15.9	15.8	15.4	16.8	17.0	17.6	16.7	16.6
Cooler Overall Heat Transfer Coefficient	W/m²°C	U_c	926	535	590	773	975	985	981	904	850	867	847	871
Water Side Heat Transfer Coefficient	W/m²°C	hw	4005	3774	3898	4135	4047	4082	3940	4020	3795	3988	3731	3769

CO2 Side Heat Transfer Coefficient	$W/m^2°C$	h_{co2}	1516	700	790	1131	1644	1664	1685	1456	1354	1366	1358	1415
Cooler Heat Load	**kW**	ϕ_c	**58223**	**52886**	**55732**	**59777**	**58614**	**58818**	**57052**	**57227**	**54393**	**57652**	**53296**	**54365**
Heating COP	**kW/kW**	COP_H	**3.18**	**3.60**	**3.61**	**3.90**	**3.71**	**3.73**	**3.54**	**3.41**	**3.27**	**3.37**	**3.14**	**3.05**
EVAPORATOR														
Heat Transfer to CO_2	**W**	ϕ_e	**36619**	**37733**	**41146**	**42427**	**44989**	**39586**	**38459**	**38116**	**35580**	**42028**	**31816**	**34711**
Cold Water Mass Flow	kg/s	m_{ew}	0.632	0.650	0.624	0.657	0.737	0.634	0.702	0.647	0.643	0.629	0.623	0.621
Heat Transfer from Cold Water	**W**	ϕ_{ew}	**35760**	**33510**	**36360**	**41585**	**40750**	**39591**	**39711**	**34125**	**34753**	**36871**	**33400**	**33036**
Log Mean Temperature Difference	°C	$\Delta\theta_m$	15.8	15.3	14.7	15.0	15.3	15.0	14.5	15.6	15.3	14.7	15.3	14.7
Evaporator Overall Heat Transfer Coefficient	$W/m^2°C$	U_e	468	475	540	573	574	538	551	475	472	549	435	470
Water Side Heat Transfer Coefficient	$W/m^2°C$	h_w	1440	1490	1432	1499	1641	1457	1569	1481	1472	1439	1434	1425
CO2 Side Heat Transfer Coefficient	$W/m^2°C$	h_{co2}	822	823	1079	1160	1079	1054	1033	826	819	1107	727	832
Evaporator Heat Load	**kW**	ϕ_e	**36190**	**35622**	**38753**	**42006**	**42869**	**39589**	**39085**	**36121**	**35166**	**39450**	**32608**	**33874**
Cooling COP	**kW/kW**	COP_L	**1.98**	**2.42**	**2.51**	**2.74**	**2.72**	**2.51**	**2.42**	**2.15**	**2.12**	**2.30**	**1.92**	**1.90**
Overall COP	**kW/kW**	**COP**	**5.16**	**6.02**	**6.12**	**6.64**	**6.43**	**6.24**	**5.96**	**5.56**	**5.39**	**5.67**	**5.07**	**4.96**
RECUPERATOR														
HOT SIDE Heat Transfer from Hot CO_2	W	ϕ_{rH}	3507	8760	8837	6399	5340	4547	3903	4415	3499	4510	3117	3354
COLD SIDE Heat Transfer to superheat cold CO_2 vapour	W	ϕ_{rL}	4775	9452	10649	7251	6273	5705	5085	5699	4886	6015	4472	4790
Log Mean Temperature Difference	°C	$\Delta\theta_m$	10.2	15.9	17.4	12.4	9.9	9.6	9.7	8.2	8.9	8.9	8.4	8.5
Recuperator Overall Heat Transfer Coefficient	$W/m^2°C$	U_r	649	912	890	874	932	851	739	985	749	945	716	767
Recuperator Heat Load	**kW**	ϕ_e	4141	9106	9743	6825	5806	5126	4494	5057	4192	5262	3795	4072
POWER														
Motor Output/Comp. Input Power	**kW**	$\phi_{comp,i}$	**18.3**	**14.7**	**15.4**	**15.3**	**15.8**	**15.8**	**16.1**	**16.8**	**16.6**	**17.1**	**17.0**	**17.8**
COMPRESSOR														
Enthalpy Change	J/kg	ΔH_{comp}	90739	62422	56791	64469	70245	73299	77674	85136	84706	85425	85866	86014
Isentropic Compression Enthalpy Change	J/kg	$\Delta H_{comp,\Delta S=0}$	63292	43089	43271	46441	49741	50337	53654	55556	58248	59517	61021	60959
Isentropic Efficiency		$e_{comp,\Delta S=0}$	**0.698**	**0.690**	**0.762**	**0.720**	**0.708**	**0.687**	**0.691**	**0.653**	**0.688**	**0.697**	**0.711**	**0.709**
Theoretical Volumetric Flow into Compressor	m3/s	$Q_{comp,i}'$	0.00592	0.00514	0.00586	0.00514	0.00498	0.00514	0.00514	0.00514	0.00514	0.00559	0.00532	0.00543
Actual Volumetric Flow into Compressor	m3/s	$Q_{comp,i}$	0.00227	0.00302	0.00345	0.00279	0.00274	0.00243	0.00231	0.00233	0.00214	0.00256	0.00192	0.00209
Volumetric Efficiency		$e_{comp,v}$	**0.384**	**0.587**	**0.588**	**0.543**	**0.550**	**0.473**	**0.449**	**0.454**	**0.417**	**0.457**	**0.360**	**0.385**

20°C - 90°C Hot Water; 20°C Cold Water In, Full speed

RAW DATA

VARIABLE	UNITS	SYMBOL	16	11	4	8	9	15	6	2	7	5	14	17	1	13	3	10	12
CO_2 LINE																			
High Side Pressure	Bar g		90	99.5	110	119.5	130	130	95	96	99.5	110	119.5	129	101	110	120	120	130
	Bar a	P_H	91	101	111	121	131	131	96	97	101	111	121	130	102	111	121	121	131
Low Side Pressure	Bar g		28.6	28.6	28.6	28.6	28.5	28.6	31.4	31.5	31.5	31.5	31.5	31.5	34.5	34.5	34.5	34.4	34.5
	Bar a	P_L	29.6	29.6	29.6	29.6	29.5	29.6	32.4	32.5	32.5	32.5	32.5	32.5	35.5	35.5	35.5	35.4	35.5
CO_2 Mass Flow	kg/s	m_{CO2}	0.326	0.285	0.272	0.252	0.238	0.236	0.373	0.397	0.371	0.346	0.314	0.304	0.434	0.419	0.399	0.386	0.390
Compressor Suction/Recuperator Cold Side Exit Temp	°C	T_{suc}	25.1	23.8	19.9	17.1	15.4	15.8	25.3	25.6	25.2	21.3	17.2	14.6	25.2	22	20	19.5	16.4
Compressor Discharge/Cooler 1 Inlet Temperature	°C	T_{dis}	132.5	141.5	145.7	150	160	159	132	132	132.5	139	143.5	152.5	128	132.5	135	135.5	141.5
Cooler 3 Exit/Recuperator Hot Side Inlet Temperature	°C	T_{co}	36.9	37.6	31.8	27.7	24.5	24.2	38.7	38.6	39.1	34.9	28.5	25.6	39.3	36.7	32.5	32.5	26.9
Pre-Expansion Valve/Recuperator Hot Side Exit Temp	°C	T_{TXi}	32.3	27.5	19.3	15.5	12.6	12.9	31.2	31	31.2	23.2	17.1	15.4	30.5	25	20.6	20.7	11.3
Separator/Recuperator Cold Side Inlet Temperature	°C	T_{sep}	-6.4	-6.9	-6.7	-6.8	-6.7	-6.7	-3.1	-3	-3.1	-3.1	-3.2	-3.1	-0.1	-0.05	0	-0.1	0
HOT WATER LINE																			
Inlet Temperature	°C	T_{cwi}	20.8	20.7	20.8	20.8	20.8	20.8	20.8	20.8	20.8	20.8	20.9	20.1	20.9	20.8	20.8	20.8	20.8
Outlet Temperature	°C	T_{cwo}	89.7	90.6	89.5	90	89.5	90	90	90.5	90	90	89.5	90	90	90	90	90	90
Flowrate	L/s	Q_{cw}	0.250	0.274	0.294	0.296	0.282	0.276	0.290	0.292	0.302	0.330	0.338	0.332	0.339	0.369	0.383	0.382	0.385
COLD WATER LINE																			
Inlet Temperature	°C	T_{ewi}	20.9	21	21	21	21	21	21	21	21.1	21.1	20.9	20.7	21.2	20.9	21.1	21	21
Outlet Temperature	°C	T_{ewo}	6.1	6	4.9	4.7	4.9	4.9	6.1	6.1	5.9	5.8	5.2	5.2	7.2	6.9	7.1	6.9	7.1
Flowrate	L/s	Q_{ew}	0.548	0.641	0.728	0.692	0.659	0.679	0.745	0.729	0.803	0.881	0.914	0.935	0.977	1.155	1.280	1.176	1.246
VSD/MOTOR																			
VSD Output/Motor Input Real Power	kW	f_{VSDo}	30.2	30.7	30.9	30.9	30.9	30.2	33.2	33.6	33.6	34.7	34.7	34.9	37.2	37.6	37.9	37.8	39.0
Motor/Compressor Speed	%		125%	125%	125%	125%	125%	125%	125%	125%	125%	125%	125%	125%	125%	125%	125%	125%	125%
	RPM	w_{comp}	1212.5	1212.5	1212.5	1212.5	1212.5	1212.5	1212.5	1212.5	1212.5	1212.5	1212.5	1212.5	1212.5	1212.5	1212.5	1212.5	1212.5

CALCULATIONS

VARIABLE	UNITS	SYMBOL																	
COOLERS																			
Total Heat Transfer from CO2	**W**	ϕ_c	**80775**	**75372**	**79405**	**77162**	**77361**	**76526**	**90391**	**96936**	**91096**	**94394**	**92727**	**94937**	**103687**	**108142**	**108719**	**105548**	**114170**
Hot Water Mass Flow	kg/s	m_{cw}	0.249	0.273	0.294	0.295	0.281	0.276	0.289	0.291	0.301	0.329	0.337	0.331	0.339	0.368	0.382	0.381	0.384
Total Heat Transfer to Hot Water	**W**	ϕ_{cw}	**71915**	**79998**	**84443**	**85577**	**80875**	**79903**	**83743**	**84941**	**87282**	**95322**	**96787**	**96870**	**97976**	**106778**	**110659**	**110448**	**111405**
Overall Cooler Water Line LMTD	°C	$\Delta\theta_{m,c}$	27.3	30.9	27.7	24.6	22.6	21.8	28.3	28.0	28.7	28.0	23.6	23.4	27.0	27.0	24.8	24.9	21.3
Cooler Overall Heat Transfer Coefficient	W/m²°C	U_c	699	688	808	925	950	972	786	805	807	903	1086	1099	962	1048	1186	1179	1386
Water Side Heat Transfer Coefficient	W/m²°C	hw	**3633**	3919	4139	4165	3998	3942	4093	4122	4231	4540	4623	4550	4648	4972	5116	5108	5143

CO2 Side Heat Transfer Coefficient	$W/m^2°C$	hco2	1024	974	1206	1484	1582	1656	1164	1203	1196	1376	1835	1887	1503	1670	2020	1998	2666
Cooler Heat Load	**kW**	ϕ_c	**71915**	**79998**	**84443**	**85577**	**80875**	**79903**	**83743**	**84941**	**87282**	**95322**	**96787**	**96870**	**97976**	**106778**	**110659**	**110448**	**111405**
Heating COP	**kW/kW**	COP_H	**2.57**	**2.80**	**2.94**	**2.98**	**2.82**	**2.85**	**2.71**	**2.72**	**2.80**	**2.96**	**3.00**	**2.99**	**2.83**	**3.06**	**3.14**	**3.15**	**3.07**
EVAPORATOR																			
Heat Transfer to CO_2	**W**	ϕ_e	**47971**	**47772**	**52082**	**50584**	**49692**	**49055**	**57280**	**61366**	**57639**	**62425**	**61546**	**61123**	**67534**	**72781**	**74243**	**71793**	**81020**
Cold Water Mass Flow	kg/s	m_{ew}	0.547	0.639	0.727	0.690	0.657	0.677	0.744	0.728	0.801	0.879	0.912	0.933	0.975	1.153	1.277	1.174	1.243
Heat Transfer from Cold Water	**W**	ϕ_{ew}	**33939**	**40191**	**49049**	**47166**	**44352**	**45709**	**46448**	**45429**	**51015**	**56384**	**60005**	**60617**	**57192**	**67629**	**74905**	**69332**	**72393**
Log Mean Temperature Difference	°C	$\Delta\theta_m$	18.9	19.4	18.5	18.5	18.5	18.5	15.5	15.4	15.4	15.3	14.9	14.7	13.1	12.7	12.9	12.8	12.8
Evaporator Overall Heat Transfer Coefficient	$W/m^2°C$	U_e	442	463	559	541	520	524	685	711	723	794	834	846	975	1132	1186	1129	1224
Water Side Heat Transfer Coefficient	$W/m^2°C$	hw	**1281**	1451	1598	1532	1474	1510	1638	1609	1737	1871	1918	1951	2048	2335	2539	2369	2484
CO2 Side Heat Transfer Coefficient	$W/m^2°C$	hco2	808	800	1048	1020	976	971	1554	1729	1637	1860	2028	2051	2772	3411	3392	3303	3873
Evaporator Heat Load	**kW**	ϕ_e	**40955**	**43981**	**50566**	**48875**	**47022**	**47382**	**51864**	**53397**	**54327**	**59405**	**60776**	**60870**	**62363**	**70205**	**74574**	**70563**	**76706**
Cooling COP	**kW/kW**	COP_L	**1.46**	**1.54**	**1.76**	**1.70**	**1.64**	**1.69**	**1.68**	**1.71**	**1.74**	**1.84**	**1.89**	**1.88**	**1.80**	**2.01**	**2.12**	**2.01**	**2.12**
Overall COP	**kW/kW**	**COP**	**4.03**	**4.34**	**4.70**	**4.68**	**4.46**	**4.54**	**4.39**	**4.43**	**4.54**	**4.80**	**4.89**	**4.87**	**4.64**	**5.07**	**5.25**	**5.16**	**5.19**
RECUPERATOR																			
HOT SIDE Heat Transfer from Hot CO_2	W	ϕ_{rH}	8452	10581	9033	7354	6389	6047	13373	13693	12161	11479	8657	7101	15173	14536	12108	11561	13882
COLD SIDE Heat Transfer to superheat cold CO_2 vapour	W	ϕ_{rL}	14119	12145	10181	8579	7536	7628	15423	16544	15343	12487	9672	8253	17124	14637	12759	12096	10445
Log Mean Temperature Difference	°C	$\Delta\theta_m$	22.6	22.6	18.1	15.7	13.5	13.2	22.3	21.8	22.6	19.3	15.4	14.4	21.3	19.4	16.2	16.6	10.9
Recuperator Overall Heat Transfer Coefficient	$W/m^2°C$	U_r	793	801	847	806	819	823	1030	1102	971	991	951	849	1208	1197	1219	1136	1774
Recuperator Heat Load	**kW**	ϕ_e	11286	11363	9607	7967	6962	6838	14398	15118	13752	11983	9165	7677	16149	14586	12434	11829	12164
POWER																			
Motor Output/Comp. Input Power	**kW**	$\phi_{comp,i}$	**28.0**	**28.5**	**28.7**	**28.7**	**28.7**	**28.0**	**30.9**	**31.2**	**31.2**	**32.2**	**32.2**	**32.4**	**34.6**	**34.9**	**35.3**	**35.1**	**36.3**
COMPRESSOR																			
Enthalpy Change	J/kg	ΔH_{comp}	83326	91362	96206	100722	111281	109544	83203	82386	81534	89604	96141	107323	78832	84157	84749	86013	93769
Isentropic Compression Enthalpy Change	J/kg	$\Delta H_{comp,\Delta S=0}$	56006	61079	64852	68048	72169	72132	52429	52902	54662	58275	60574	63179	48950	51891	55372	55319	57463
Isentropic Efficiency		$\varepsilon_{comp,\Delta S=0}$	**0.672**	**0.669**	**0.674**	**0.676**	**0.649**	**0.658**	**0.630**	**0.642**	**0.670**	**0.650**	**0.630**	**0.589**	**0.621**	**0.617**	**0.653**	**0.643**	**0.613**
Theoretical Volumetric Flow into Compressor	m3/s	$Q_{comp,i}'$	0.01037	0.01037	0.01037	0.01037	0.01037	0.01037	0.01037	0.01037	0.01037	0.01037	0.01037	0.01037	0.01037	0.01037	0.01037	0.01037	0.01037
Actual Volumetric Flow into Compressor	m3/s	$Q_{comp,i}$	0.00512	0.00444	0.00413	0.00375	0.00353	0.00350	0.00528	0.00561	0.00523	0.00472	0.00415	0.00395	0.00545	0.00513	0.00481	0.00465	0.00456
Volumetric Efficiency		$\varepsilon_{comp,V}$	**0.494**	**0.428**	**0.398**	**0.362**	**0.340**	**0.337**	**0.509**	**0.541**	**0.504**	**0.455**	**0.400**	**0.381**	**0.526**	**0.495**	**0.463**	**0.448**	**0.439**

20°C - 77.5°C Hot Water; 20°C Cold Water In, Full speed

RAW DATA

VARIABLE	UNITS	SYMBOL	6	8	9	18	12	10	21	11	16	15	19	14	20	17	13
CO_2 LINE			TX f o														
High Side Pressure	Bar g		86	95	104	110	119	129.5	130	96.5	97.5	105	105	110	110.5	121	130
	Bar a	P_H	87	96	105	111	120	131	131	98	99	106	106	111	112	122	131
Low Side Pressure	Bar g		28.5	28.5	28.6	28.6	28.6	28.7	28.6	34.4	34.5	34.5	34.5	34.3	34.5	34.5	34.5
	Bar a	P_L	29.5	29.5	29.6	29.6	29.6	29.7	29.6	35.4	35.5	35.5	35.5	35.3	35.5	35.5	35.5
CO_2 Mass Flow	kg/s	m_{CO2}	0.350	0.320	0.300	0.289	0.258	0.258	0.243	0.469	0.452	0.460	0.437	0.416	0.444	0.402	0.386
Compressor Suction/Recuperator Cold Side Exit Temp	°C	T_{suc}	23.4	20.2	17.9	14.8	14.5	12.8	13	23.1	22.8	20.1	19.3	19	19	17.5	14.7
Compressor Discharge/Cooler 1 Inlet Temperature	°C	T_{dis}	128.5	132.5	126.3	142	148	156	151	120.5	118.5	126	122.5	126.5	124	128	134
Cooler 3 Exit/Recuperator Hot Side Inlet Temperature	°C	T_{co}	34.6	33.5	28.8	25.7	23.3	21.7	21.8	36.5	36.7	32.9	33.8	32.1	31.6	26.9	24.5
Pre-Expansion Valve/Recuperator Hot Side Exit Temp	°C	T_{TXi}	28.9	22.2	17.3	14.5	12.5	12.1	12.3	27.5	29	22	24.2	21	21.6	18.1	15.8
Separator/Recuperator Cold Side Inlet Temperature	°C	T_{sep}	-6.6	-6.7	-6.8	-6.7	-6.8	-6.7	-6.7	0.1	0	0.1	0	0.1	0	-0.1	0
HOT WATER LINE																	
Inlet Temperature	°C	T_{cwi}	20.2	20.3	20.4	20.4	20.5	20.1	20.1	20.2	20	20.4	20.1	20.6	20	20	20
Outlet Temperature	°C	T_{cwo}	77.8	77	77.7	77	77	77.5	78	77.5	77.5	77.5	77.8	79.5	80	81	81
Flowrate	L/s	Q_{cw}	0.323	0.367	0.379	0.390	0.373	0.349	0.339	0.439	0.431	0.484	0.465	0.464	0.460	0.460	0.454
COLD WATER LINE																	
Inlet Temperature	°C	T_{ewi}	20.9	20.9	20.9	21	21	20.7	20.7	20.9	20.9	20.9	20.8	21	20.9	20.9	20.9
Outlet Temperature	°C	T_{ewo}	3.5	3.1	3.7	3	3.5	3.5	4.3	6.8	7.1	6.8	7	7	7.2	7.2	7.2
Flowrate	L/s	Q_{ew}	0.577	0.685	0.755	0.715	0.704	0.674	0.707	1.113	1.157	1.240	1.297	1.274	1.358	1.452	1.350
VSD/MOTOR																	
VSD Output/Motor Input Real Power	kW	f_{VSDo}	30.7	30.9	31.3	31.4	31.1	31.6	31.6	36.1	35.1	38.7	35.6	35.8	36.7	37.0	37.2
Motor/Compressor Speed	%		125%	125%	125%	125%	125%	125%	125%	125%	125%	125%	125%	125%	125%	125%	125%
	RPM	w_{comp}	1212.5	1212.5	1212.5	1212.5	1212.5	1212.5	1212.5	1212.5	1212.5	1212.5	1212.5	1212.5	1212.5	1212.5	1212.5

CALCULATIONS

VARIABLE	UNITS	SYMBOL															
COOLERS																	
Total Heat Transfer from CO2	**W**	ϕ_c	**88739**	**86243**	**82723**	**87895**	**81296**	**84082**	**77299**	**112585**	**107195**	**120652**	**111172**	**110043**	**116381**	**111267**	**110799**
Hot Water Mass Flow	kg/s	m_{cw}	0.322	0.367	0.379	0.389	0.372	0.348	0.338	0.438	0.430	0.483	0.464	0.463	0.460	0.459	0.453
Total Heat Transfer to Hot Water	**W**	ϕ_{cw}	**77589**	**86959**	**90747**	**92133**	**87925**	**83675**	**81974**	**105029**	**103454**	**115478**	**112087**	**114152**	**115409**	**117267**	**115740**
Overall Cooler Water Line LMTD	°C	$\Delta\theta_{lm,c}$	28.9	29.5	22.9	23.8	21.2	19.8	18.9	27.6	27.1	26.6	26.2	25.2	24.3	20.9	19.7
Cooler Overall Heat Transfer Coefficient	W/m²°C	U_c	713	784	1050	1029	1102	1124	1151	1012	1015	1154	1134	1201	1260	1491	1558
Water Side Heat Transfer Coefficient	W/m²°C	hw	**4298**	4759	4895	4993	4819	4573	4474	5495	5409	5949	5759	5788	5748	5762	5702

CO2 Side Heat Transfer Coefficient	$W/m^2°C$	h_{co2}	995	1100	1686	1619	1839	1958	2066	1518	1534	1799	1775	1942	2107	2837	3114
Cooler Heat Load	**kW**	ϕ_o	**77589**	**86959**	**90747**	**92133**	**87925**	**83675**	**81974**	**105029**	**103454**	**115478**	**112087**	**114152**	**115409**	**117267**	**115740**
Heating COP	**kW/kW**	COP_H	**2.72**	**3.03**	**3.12**	**3.16**	**3.05**	**2.85**	**2.79**	**3.13**	**3.18**	**3.21**	**3.39**	**3.43**	**3.39**	**3.41**	**3.35**
EVAPORATOR																	
Heat Transfer to CO_2	**W**	ϕ_e	**55537**	**58231**	**58594**	**58573**	**53617**	**53952**	**50711**	**76940**	**72066**	**83155**	**76449**	**76846**	**80985**	**77092**	**76285**
Cold Water Mass Flow	kg/s	m_{ew}	0.576	0.683	0.754	0.713	0.703	0.673	0.706	1.111	1.155	1.238	1.294	1.271	1.355	1.449	1.347
Heat Transfer from Cold Water	**W**	ϕ_{ew}	**42036**	**50992**	**54355**	**53848**	**51565**	**48506**	**48543**	**65619**	**66773**	**73113**	**74843**	**74568**	**77786**	**83155**	**77335**
Log Mean Temperature Difference	°C	$\Delta\theta_m$	17.4	17.2	17.7	17.2	17.6	17.4	18.0	12.4	12.8	12.4	12.7	12.6	12.9	13.0	12.9
Evaporator Overall Heat Transfer Coefficient	$W/m^2°C$	U_e	574	650	651	670	610	602	565	1171	1111	1284	1221	1226	1263	1264	1222
Water Side Heat Transfer Coefficient	$W/m^2°C$	hw	**1316**	1505	1633	1558	1544	1488	1554	2265	2340	2469	2561	2527	2661	2807	2649
CO2 Side Heat Transfer Coefficient	$W/m^2°C$	hco2	1348	1521	1393	1566	1286	1298	1093	4048	3215	4603	3632	3765	3757	3453	3442
Evaporator Heat Load	**kW**	ϕ_e	**48787**	**54612**	**56474**	**56211**	**52591**	**51229**	**49627**	**71280**	**69419**	**78134**	**75646**	**75707**	**79386**	**80123**	**76810**
Cooling COP	**kW/kW**	COP_L	**1.71**	**1.90**	**1.94**	**1.93**	**1.82**	**1.74**	**1.69**	**2.13**	**2.13**	**2.17**	**2.29**	**2.28**	**2.33**	**2.33**	**2.22**
Overall COP	**kW/kW**	**COP**	**4.43**	**4.93**	**5.07**	**5.09**	**4.87**	**4.59**	**4.48**	**5.26**	**5.31**	**5.39**	**5.68**	**5.71**	**5.72**	**5.74**	**5.57**
RECUPERATOR																	
HOT SIDE Heat Transfer from Hot CO_2	W	ϕ_{rH}	10194	11644	9075	7864	6482	5546	5149	15953	13319	14296	12418	12420	11890	8467	7697
COLD SIDE Heat Transfer to superheat cold CO_2 vapour	W	ϕ_{rL}	14529	12036	10522	8961	7954	7391	6977	16903	16269	14668	13525	12503	13549	11486	9370
Log Mean Temperature Difference	°C	$\Delta\theta_m$	21.1	20.1	16.7	15.5	13.4	13.2	13.2	19.6	20.5	17.0	18.9	16.7	16.7	13.3	12.6
Recuperator Overall Heat Transfer Coefficient	$W/m^2°C$	U_r	933	938	936	867	858	778	729	1335	1147	1360	1090	1188	1213	1194	1080
Recuperator Heat Load	**kW**	ϕ_e	12361	11840	9799	8412	7218	6468	6063	16428	14794	14482	12972	12461	12719	9977	8533
POWER																	
Motor Output/Comp. Input Power	**kW**	$\phi_{comp,i}$	**28.5**	**28.7**	**29.0**	**29.1**	**28.9**	**29.4**	**29.4**	**33.5**	**32.6**	**36.0**	**33.1**	**33.2**	**34.1**	**34.4**	**34.6**
COMPRESSOR																	
Enthalpy Change	J/kg	ΔH_{comp}	82359	86383	75639	97678	101509	109567	101977	74038	71159	80765	76952	79603	76022	77484	85140
Isentropic Compression Enthalpy Change	J/kg	$\Delta H_{comp,\Delta S=0}$	53078	57109	60710	62146	66313	69779	70403	45925	46100	48572	48184	50784	50586	54392	56407
Isentropic Efficiency		$\epsilon_{comp,\Delta S=0}$	**0.644**	**0.661**	**0.803**	**0.636**	**0.653**	**0.637**	**0.690**	**0.620**	**0.648**	**0.601**	**0.626**	**0.638**	**0.665**	**0.702**	**0.663**
Theoretical Volumetric Flow into Compressor	m3/s	$Q_{comp,i}'$	0.01037	0.01037	0.01037	0.01037	0.01037	0.01037	0.01037	0.01037	0.01037	0.01037	0.01037	0.01037	0.01037	0.01037	0.01037
Actual Volumetric Flow into Compressor	m3/s	$Q_{comp,i}$	0.00547	0.00489	0.00450	0.00425	0.00379	0.00373	0.00353	0.00582	0.00558	0.00554	0.00523	0.00501	0.00530	0.00474	0.00444
Volumetric Efficiency		$\epsilon_{comp,V}$	**0.528**	**0.471**	**0.434**	**0.410**	**0.365**	**0.360**	**0.340**	**0.562**	**0.538**	**0.534**	**0.504**	**0.483**	**0.511**	**0.457**	**0.428**

RAW DATA

VARIABLE	UNITS	SYMBOL	20°C - 65°C Hot Water; 20°C, Full speed					20°C - 90°C Hot Water; 11°C, 1.4 l/s (max recirculation flow) Cold Water In				20°C - 65°C Hot Water; 11°C, 1.4 l/s Cold Water In				
			2	1	3	5	4	3	1	2	4	1	3	2	5	4
CO_2 LINE			TXf o					txfo				txfo				
High Side Pressure	Bar g		81	91	101	113	123	96	109	120	130	85.5	93.5	105.5	116	126
	Bar a	P_H	82	92	102	114	124	97	110	121	131	87	95	107	117	127
Low Side Pressure	Bar g		28.6	28.6	28.6	28.6	28.6	31.6	31.5	31.5	31.5	31.5	31.6	31.6	31.5	31.5
	Bar a	P_L	29.6	29.6	29.6	29.6	29.6	32.6	32.5	32.5	32.5	32.5	32.6	32.6	32.5	32.5
CO_2 Mass Flow	kg/s	m_{CO2}	0.300	0.315	0.287	0.261	0.218	0.387	0.317	0.243	0.233	0.353	0.244	0.225	0.250	0.305
Compressor Suction/Recuperator Cold Side Exit Temp	°C	T_{suc}	22.2	17.9	15.1	14.4	15.6	25	20.5	18.9	16.8	22.3	18.3	14.7	13.6	13.8
Compressor Discharge/Cooler 1 Inlet Temperature	°C	T_{dis}	128	134.3	141	150.5	170	128.5	131	136	143	112	112	118	127	130
Cooler 3 Exit/Recuperator Hot Side Inlet Temperature	°C	T_{co}	32.6	28.4	23.5	22.3	21.9	38.5	34.2	29.0	25.1	33.4	29.7	23.0	21.9	21.6
Pre-Expansion Valve/Recuperator Hot Side Exit Temp	°C	T_{TXi}	27.8	18.3	13.7	12.1	11.3	32.2	22.6	18	15	28.6	19.8	13.8	13	12.4
Separator/Recuperator Cold Side Inlet Temperature	°C	T_{sep}	-6.7	-6.6	-6.7	-6.8	-6.8	-3.1	-3.1	-3.1	-3	-3.1	-3	-3	-3.1	-3.1
HOT WATER LINE																
Inlet Temperature	°C	T_{cwi}	20.5	20.4	20.7	20.7	20.7	20	20	20	20	20	20	20	20	20
Outlet Temperature	°C	T_{cwo}	65.4	65	65	65.5	65	90	89.5	90	89.2	65	65.5	65	65	65
Flowrate	L/s	Q_{cw}	0.416	0.493	0.483	0.451	0.408	0.291	0.258	0.251	0.266	0.402	0.353	0.372	0.393	0.420
COLD WATER LINE																
Inlet Temperature	°C	T_{ewi}	21	21	20.9	21	21	11.1	11.1	11.1	11	10.8	10.5	11	10.9	10.5
Outlet Temperature	°C	T_{ewo}	3.1	3.1	3.9	4	4.5	2.6	2.2	2.2	2.3	2.2	2.1	2.6	2.2	2.1
Flowrate	L/s	Q_{ew}	0.588	0.723	0.726	0.676	0.570	1.384	1.312	1.330	1.386	1.413	1.413	1.411	1.417	1.409
VSD/MOTOR																
VSD Output/Motor Input Real Power	kW	f_{VSDo}	30.2	32.5	30.7	30.9	30.4	33.4	25.5	24.4	26.4	25.3	19.3	19.7	21.9	25.8
Motor/Compressor Speed	%		125%	125%	125%	125%	125%	124%	93%	89%	94%	98%	76%	76%	81%	92%
	RPM	w_{comp}	1212.5	1212.5	1212.5	1212.5	1212.5	1205.1	901.1	863.1	913.8	951.8	736.5	736.5	787.1	888.5

CALCULATIONS

VARIABLE	UNITS	SYMBOL														
COOLERS																
Total Heat Transfer from CO2	**W**	**ϕ_c**	**78003**	**91820**	**89331**	**84312**	**75448**	**92975**	**83901**	**68952**	**69722**	**84536**	**62563**	**62976**	**72468**	**88442**
Hot Water Mass Flow	kg/s	m_{cw}	0.415	0.492	0.482	0.450	0.407	0.290	0.257	0.250	0.265	0.402	0.352	0.372	0.392	0.419
Total Heat Transfer to Hot Water	**W**	**ϕ_{cw}**	**78003**	**91820**	**89331**	**84312**	**75448**	**85045**	**74918**	**73351**	**76883**	**75588**	**66958**	**69918**	**73793**	**78812**
Overall Cooler Water Line LMTD	°C	$\Delta\theta_{lm,c}$	30.7	28.4	22.1	20.9	23.2	27.3	25.5	22.7	20.7	26.8	23.5	17.4	17.2	17.1
Cooler Overall Heat Transfer Coefficient	W/m²°C	U_c	674	858	1071	1069	863	827	781	858	987	749	756	1068	1139	1226
Water Side Heat Transfer Coefficient	W/m²°C	hw	**5075**	5804	5715	5417	4993	**4094**	3715	3637	3803	**4924**	4437	4626	4830	5091

CO2 Side Heat Transfer Coefficient	W/m²°C	hco2	881	1179	1631	1660	1242	1257	1198	1406	1739	1024	1070	1782	1942	2142
Cooler Heat Load	**kW**	ϕ_c	**78003**	**91820**	**89331**	**84312**	**75448**	**85045**	**74918**	**73351**	**76883**	**75588**	**66958**	**69918**	**73793**	**78812**
Heating COP	**kW/kW**	COP_H	**2.78**	**3.04**	**3.13**	**2.94**	**2.68**	**2.74**	**3.17**	**3.24**	**3.14**	**3.22**	**3.73**	**3.81**	**3.63**	**3.28**
EVAPORATOR																
Heat Transfer to CO_2	**W**	ϕ_e	**47748**	**60426**	**58418**	**54332**	**45870**	**57963**	**57748**	**47276**	**47068**	**55743**	**48023**	**47930**	**51331**	**63191**
Cold Water Mass Flow	kg/s	m_{ew}	0.587	0.722	0.724	0.675	0.569	1.383	1.312	1.329	1.386	1.413	1.412	1.410	1.416	1.408
Heat Transfer from Cold Water	**W**	ϕ_{ew}	**44022**	**54190**	**51616**	**48075**	**39321**	**49392**	**49054**	**49707**	**50651**	**51057**	**49859**	**49773**	**51775**	**49715**
Log Mean Temperature Difference	°C	$\Delta\theta_m$	17.2	17.1	17.8	18.0	18.3	9.3	9.0	9.0	9.0	8.9	8.6	9.2	9.0	8.7
Evaporator Overall Heat Transfer Coefficient	W/m²°C	U_e	545	685	633	582	475	1179	1209	1098	1116	1224	1160	1090	1177	1321
Water Side Heat Transfer Coefficient	W/m²°C	hw	**1333**	1574	1584	1498	1310	**2501**	2391	2417	2498	**2533**	2527	2538	2540	2521
CO2 Side Heat Transfer Coefficient	W/m²°C	hco2	1179	1627	1355	1203	909	3415	4018	2958	2937	3736	3207	2706	3315	4871
Evaporator Heat Load	**kW**	ϕ_e	**45885**	**57308**	**55017**	**51204**	**42595**	**53678**	**53401**	**48491**	**48860**	**53400**	**48941**	**48851**	**51553**	**56453**
Cooling COP	**kW/kW**	COP_L	**1.64**	**1.90**	**1.93**	**1.78**	**1.51**	**1.73**	**2.26**	**2.14**	**1.99**	**2.27**	**2.72**	**2.66**	**2.54**	**2.35**
Overall COP	**kW/kW**	**COP**	**4.42**	**4.94**	**5.06**	**4.72**	**4.19**	**4.47**	**5.42**	**5.38**	**5.13**	**5.49**	**6.45**	**6.48**	**6.17**	**5.63**
RECUPERATOR																
HOT SIDE Heat Transfer from Hot CO_2	W	ϕ_{rH}	7664	9216	6955	6222	5240	11388	10401	6525	5374	7969	7124	5029	5159	6316
COLD SIDE Heat Transfer to superheat cold CO_2 vapour	W	ϕ_{rL}	12069	10956	8997	8006	7015	15948	11126	8011	6970	13245	5415	3901	6438	7935
Log Mean Temperature Difference	°C	$\Delta\theta_m$	20.1	16.7	13.5	12.6	11.2	22.7	19.1	14.9	12.5	19.6	16.5	12.0	11.8	11.2
Recuperator Overall Heat Transfer Coefficient	W/m²°C	U_r	782	963	940	899	873	960	898	775	784	860	607	590	785	1013
Recuperator Heat Load	**kW**	ϕ_e	9866	10086	7976	7114	6127	13668	10764	7268	6172	10607	6270	4465	5798	7126
POWER																
Motor Output/Comp. Input Power	**kW**	$\phi_{comp,i}$	**28.0**	**30.2**	**28.5**	**28.7**	**28.2**	**31.1**	**23.7**	**22.7**	**24.5**	**23.5**	**18.0**	**18.3**	**20.3**	**24.0**
COMPRESSOR																
Enthalpy Change	J/kg	ΔH_{comp}	86279	94030	100740	108052	127619	78644	80156	82989	90361	66534	66517	71747	79463	77525
Isentropic Compression Enthalpy Change	J/kg	$\Delta H_{comp,\Delta S=0}$	49137	53516	57721	63397	68827	52427	57376	61763	64951	45472	48105	52449	56937	61410
Isentropic Efficiency		$\varepsilon_{comp,\Delta S=0}$	**0.570**	**0.569**	**0.573**	**0.587**	**0.539**	**0.667**	**0.716**	**0.744**	**0.719**	**0.683**	**0.723**	**0.731**	**0.717**	**0.792**
Theoretical Volumetric Flow into Compressor	m3/s	$Q_{comp,i}'$	0.01037	0.01037	0.01037	0.01037	0.01037	0.01031	0.00771	0.00738	0.00781	0.00814	0.00630	0.00630	0.00673	0.00760
Actual Volumetric Flow into Compressor	m3/s	$Q_{comp,i}$	0.00462	0.00473	0.00422	0.00383	0.00322	0.00542	0.00430	0.00326	0.00307	0.00486	0.00325	0.00292	0.00322	0.00393
Volumetric Efficiency		$\varepsilon_{comp,V}$	**0.445**	**0.456**	**0.407**	**0.369**	**0.310**	**0.525**	**0.558**	**0.442**	**0.393**	**0.597**	**0.515**	**0.463**	**0.478**	**0.518**

RAW DATA

VARIABLE	UNITS	SYMBOL	20°C - 90°C Hot Water; 11°C, 1.2 l/s Cold Water In						20°C - 90°C Hot Water; 15°C, 0.9 l/s Cold Water In					
			3	2	5	6	1	4	3	5	2	4	6	1
CO_2 LINE														
High Side Pressure	Bar g		94	105	114.5	122.5	130	130.2	94	101	109	119.5	120	130
	Bar a	P_H	95	106	116	124	131	131	95	102	110	121	121	131
Low Side Pressure	Bar g		34.5	34.5	34.5	34.6	34.5	34.5	34.5	34.6	34.5	34.5	34.4	34.6
	Bar a	P_L	35.5	35.5	35.5	35.6	35.5	35.5	35.5	35.6	35.5	35.5	35.4	35.6
CO_2 Mass Flow	kg/s	m_{CO2}	0.301	0.196	0.192	0.185	0.187	0.182	0.293	0.259	0.219	0.190	0.191	0.191
Compressor Suction/Recuperator Cold Side Exit Temp	°C	T_{suc}	27.9	27.2	24.4	20.9	19.2	19.5	27.3	27.5	25.7	19	23	18.5
Compressor Discharge/Cooler 1 Inlet Temperature	°C	T_{dis}	114	123.3	127	131.5	138.2	137.5	115	120	125	129	128	136.5
Cooler 3 Exit/Recuperator Hot Side Inlet Temperature	°C	T_{co}	39.6	38.1	31.3	27.4	25.1	25.0	39.4	40.2	36.1	27.8	29.9	24.9
Pre-Expansion Valve/Recuperator Hot Side Exit Temp	°C	T_{TXi}	34.0	26	18.5	15	13.4	13.6	33.2	29	23	16.7	18	13.2
Separator/Recuperator Cold Side Inlet Temperature	°C	T_{sep}	0.1	0.1	0.1	0.2	0.1	0	0.1	0	0	0	-0.1	0.1
HOT WATER LINE														
Inlet Temperature	°C	T_{cwi}	20.5	20.5	20.5	20.5	20.5	20.5	20.4	20.4	20.4	20	20.4	20.4
Outlet Temperature	°C	T_{cwo}	90	90	90	90	90	90.5	90	90.3	90	89.7	91	89.5
Flowrate	L/s	Q_{cw}	0.204	0.183	0.191	0.194	0.192	0.188	0.211	0.183	0.184	0.191	0.186	0.192
COLD WATER LINE														
Inlet Temperature	°C	T_{ewi}	11.4	11.4	11.2	11.1	11.5	10.9	15.4	15.2	15.2	15.3	15.3	15.2
Outlet Temperature	°C	T_{ewo}	4.2	4.2	4.1	4.2	4.1	4	6	6	6	6.6	5.9	7
Flowrate	L/s	Q_{ew}	1.223	1.231	1.294	1.356	1.222	1.321	0.908	0.911	0.908	0.920	0.908	0.916
VSD/MOTOR														
VSD Output/Motor Input Real Power	kW	f_{VSDo}	22.6	17.4	17.9	18.3	18.4	18.4	22.6	18.1	17.4	18.3	17.8	18.4
Motor/Compressor Speed	%		86%	64%	62%	62%	62%	62%	87%	69%	63%	62%	62%	62%
	RPM	w_{comp}	831.5	622.5	601.4	601.4	601.4	601.4	844.1	673.1	609.8	601.4	601.4	601.4

CALCULATIONS

VARIABLE	UNITS	SYMBOL												
COOLERS														
Total Heat Transfer from CO2	**W**	ϕ_c	**63255**	**46852**	**51143**	**51904**	**54564**	**52869**	**62155**	**57819**	**54749**	**52533**	**51363**	**55328**
Hot Water Mass Flow	kg/s	m_{cw}	0.204	0.182	0.190	0.193	0.192	0.187	0.211	0.183	0.183	0.191	0.185	0.192
Total Heat Transfer to Hot Water	**W**	ϕ_{cw}	**59390**	**53094**	**55371**	**56283**	**55893**	**54883**	**61449**	**53474**	**53393**	**55635**	**54811**	**55438**
Overall Cooler Water Line LMTD	°C	$\Delta\theta_{lm,c}$	21.5	24.6	21.3	19.3	18.5	18.2	21.9	24.4	24.1	19.5	20.2	18.1
Cooler Overall Heat Transfer Coefficient	W/m²°C	U_c	735	572	691	775	800	802	745	581	588	758	719	812
Water Side Heat Transfer Coefficient	W/m²°C	hw	**3095**	2830	2927	2965	2949	2893	**3176**	2834	2838	2923	2873	2938

CO2 Side Heat Transfer Coefficient	W/m²°C	hco2	1186	841	1105	1327	1409	1431	1198	860	875	1289	1192	1450
Cooler Heat Load	**kW**	ϕ_c	**59390**	**53094**	**55371**	**56283**	**55893**	**54883**	**61449**	**53474**	**53393**	**55635**	**54811**	**55438**
Heating COP	**kW/kW**	COP_H	**2.83**	**3.29**	**3.33**	**3.32**	**3.26**	**3.20**	**2.93**	**3.18**	**3.31**	**3.27**	**3.31**	**3.24**
EVAPORATOR														
Heat Transfer to CO_2	**W**	ϕ_e	**42008**	**33348**	**36627**	**36927**	**37947**	**36787**	**41762**	**41528**	**39236**	**37041**	**36646**	**38785**
Cold Water Mass Flow	kg/s	m_{ew}	1.223	1.231	1.293	1.355	1.222	1.320	0.908	0.911	0.908	0.919	0.908	0.915
Heat Transfer from Cold Water	**W**	ϕ_{ew}	**36962**	**37208**	**38565**	**39262**	**37970**	**38266**	**35779**	**35135**	**35020**	**33542**	**35781**	**31458**
Log Mean Temperature Difference	°C	$\Delta\theta_{lm}$	7.1	7.1	7.0	6.9	7.1	6.9	9.9	9.9	9.9	10.3	10.0	10.5
Evaporator Overall Heat Transfer Coefficient	W/m²°C	U_e	1137	1016	1105	1132	1099	1115	804	792	767	697	743	686
Water Side Heat Transfer Coefficient	W/m²°C	hw	**2290**	2302	2392	2482	2289	2426	**1863**	1866	1862	1888	1861	1884
CO2 Side Heat Transfer Coefficient	W/m²°C	hco2	3588	2588	3060	3083	3234	3065	1923	1853	1728	1392	1608	1350
Evaporator Heat Load	**kW**	ϕ_e	**39485**	**35278**	**37596**	**38094**	**37959**	**37526**	**38770**	**38331**	**37128**	**35291**	**36213**	**35121**
Cooling COP	**kW/kW**	COP_L	**1.88**	**2.19**	**2.26**	**2.25**	**2.22**	**2.19**	**1.85**	**2.28**	**2.30**	**2.07**	**2.19**	**2.05**
Overall COP	**kW/kW**	**COP**	**4.71**	**5.48**	**5.59**	**5.57**	**5.48**	**5.40**	**4.78**	**5.47**	**5.62**	**5.34**	**5.50**	**5.29**
RECUPERATOR														
HOT SIDE Heat Transfer from Hot CO_2	W	ϕ_{rH}	9808	7798	6281	5427	4953	4717	10160	11520	8401	5080	5568	5061
COLD SIDE Heat Transfer to superheat cold CO_2 vapour	W	ϕ_{rL}	12828	8151	7308	6116	5716	5673	12222	10994	8760	5799	6928	5671
Log Mean Temperature Difference	°C	$\Delta\theta_{lm}$	20.9	17.3	11.7	10.1	9.1	9.0	20.9	19.7	15.9	12.3	11.6	9.4
Recuperator Overall Heat Transfer Coefficient	W/m²°C	U_r	864	732	923	911	934	922	853	908	859	702	857	914
Recuperator Heat Load	**kW**	ϕ_e	11318	7975	6794	5772	5334	5195	11191	11257	8581	5439	6248	5366
POWER														
Motor Output/Comp. Input Power	**kW**	$\phi_{comp,i}$	**21.0**	**16.1**	**16.6**	**17.0**	**17.1**	**17.1**	**21.0**	**16.8**	**16.1**	**17.0**	**16.5**	**17.1**
COMPRESSOR														
Enthalpy Change	J/kg	ΔH_{comp}	60462	67200	70199	77064	84919	83320	62660	64888	69050	77775	70045	83554
Isentropic Compression Enthalpy Change	J/kg	$\Delta H_{comp,\Delta S=0}$	46361	51885	55201	56747	59165	59428	46118	49755	53192	54602	57227	58513
Isentropic Efficiency		$\varepsilon_{comp,\Delta S=0}$	**0.767**	**0.772**	**0.786**	**0.736**	**0.697**	**0.713**	**0.736**	**0.767**	**0.770**	**0.702**	**0.817**	**0.700**
Theoretical Volumetric Flow into Compressor	m3/s	$Q_{comp,i}'$	0.00711	0.00532	0.00514	0.00514	0.00514	0.00514	0.00722	0.00576	0.00522	0.00514	0.00514	0.00514
Actual Volumetric Flow into Compressor	m3/s	$Q_{comp,i}$	0.00385	0.00249	0.00240	0.00224	0.00223	0.00218	0.00373	0.00329	0.00277	0.00227	0.00237	0.00226
Volumetric Efficiency		$\varepsilon_{comp,V}$	**0.542**	**0.468**	**0.467**	**0.436**	**0.434**	**0.423**	**0.516**	**0.572**	**0.531**	**0.441**	**0.460**	**0.439**

OIL: 20°C -90°C Hot Water; 20°C, 0.6 l/s Cold Water In

OIL: 20°C - 90°C Hot Water; 20°C Cold Water In, Max speed

RAW DATA

VARIABLE	UNITS	SYMBOL	3	1	2	5	4	1	7	4	8	9	3	5	2	6
CO_2 LINE								txfo	txfo							
High Side Pressure	Bar g		88	100.5	110.5	119	128	95	95	105	110	114	120	120	130	129.5
	Bar a	P_H	89	102	112	120	129	96	96	106	111	115	121	121	131	131
Low Side Pressure	Bar g		31.6	31.5	31.4	31.5	31.5	31.5	31.5	31.6	31.5	31.5	31.6	31.6	31.5	31.5
	Bar a	P_L	32.6	32.5	32.4	32.5	32.5	32.5	32.5	32.6	32.5	32.5	32.6	32.6	32.5	32.5
CO_2 Mass Flow	kg/s	m_{CO2}	0.259	0.186	0.184	0.170	0.152	0.359	0.373	0.358	0.339	0.339	0.323	0.326	0.315	0.303
Compressor Suction/Recuperator Cold Side Exit Temp	°C	T_{suc}	26.2	27.3	24	20.8	18	25	25	22.9	20.8	18.9	17.7	18	16.5	16.2
Compressor Discharge/Cooler 1 Inlet Temperature	°C	T_{dis}	121.5	135	147	158	164	136	131	135.5	141	141	147	142	154	150
Cooler 3 Exit/Recuperator Hot Side Inlet Temperature	°C	T_{co}	37.0	36.8	27.9	24.2	22.8	38.0	38.2	37.0	34.0	32.8	27.9	29.7	24.7	25.7
Pre-Expansion Valve/Recuperator Hot Side Exit Temp	°C	T_{TXO}	33	25.6	17	14.3	14	32.8	32.6	27.1	23.2	22	17.8	19.3	17.1	16.3
Separator/Recuperator Cold Side Inlet Temperature	°C	T_{sep}	-3	-3.1	-3.4	-3.1	-3	-3.1	-3.1	-3.1	-3.1	-3.1	-3	-3.1	-3.1	-3.1
HOT WATER LINE																
Inlet Temperature	°C	T_{cwi}	20	20	20	20	20	20	20	20	20	19.9	19.9	20	19.9	20
Outlet Temperature	°C	T_{cwo}	90.5	90	91	90	91	90	90.3	89	90	90	89.5	89.8	91	90.5
Flowrate	L/s	Q_{cw}	0.190	0.168	0.177	0.181	0.183	0.301	0.286	0.330	0.344	0.338	0.356	0.346	0.343	0.335
COLD WATER LINE																
Inlet Temperature	°C	T_{ewi}	20.1	20.1	20.1	20.1	20.1	20.2	20	20	20.3	20	20.1	20	20.2	20
Outlet Temperature	°C	T_{ewo}	9	8.9	8.8	8.9	8.9	7.9	7.3	8.1	9.9	8.1	9.1	8.2	8.9	8.1
Flowrate	L/s	Q_{ew}	0.656	0.658	0.658	0.664	0.658	0.963	0.947	1.215	1.309	1.306	1.409	1.349	1.254	1.272
VSD/MOTOR																
VSD Output/Motor Input Real Power	kW		23.5	18.1	20.4	21.7	22.8	37.2	34.5	35.2	37.2	35.3	39.8	35.8	41.2	36.7
Motor/Compressor Speed	%		89%	65%	62%	65%	65%	125%	125%	125%	125%	125%	125%	125%	125%	125%
	RPM		863.1	628.8	601.4	628.8	628.8	1212.5	1212.5	1212.5	1212.5	1212.5	1212.5	1212.5	1212.5	1212.5

CALCULATIONS

VARIABLE	UNITS	SYMBOL	3	1	2	5	4	1	7	4	8	9	3	5	2	6
COOLERS																
Total Heat Transfer from CO2	W	ϕ_c	**59052**	**48516**	**55969**	**55456**	**50829**	**90482**	**91151**	**93496**	**94586**	**95611**	**97448**	**94477**	**99422**	**93425**
Hot Water Mass Flow	kg/s	m_{cw}	0.190	0.167	0.177	0.181	0.183	0.300	0.286	0.329	0.343	0.337	0.356	0.345	0.343	0.334
Total Heat Transfer to Hot Water	W	ϕ_{cw}	**56133**	**49036**	**52587**	**53083**	**54269**	**87999**	**84159**	**95148**	**100565**	**98993**	**103677**	**100953**	**102068**	**98643**
Overall Cooler Water Line LMTD	°C	$\Delta\theta_{lm,c}$	23.3	28.6	24.6	22.9	21.4	29.8	28.0	29.3	28.6	27.7	25.1	25.2	22.7	22.9
Cooler Overall Heat Transfer Coefficient	W/m²°C	U_c	639	455	568	615	672	783	799	862	933	948	1097	1063	1195	1141
Water Side Heat Transfer Coefficient	W/m²°C	hw	2924	2635	2763	2808	2833	**4207**	**4049**	**4518**	**4681**	**4616**	**4811**	**4704**	**4689**	**4590**

CO2 Side Heat Transfer Coefficient	W/m²°C	hco2	979	624	840	940	1074	1146	1197	1286	1428	1473	1828	1753	2150	2006
Cooler Heat Load	**kW**	ϕ_c	**56133**	**49036**	**52587**	**53083**	**54269**	**87999**	**84159**	**95148**	**100565**	**98993**	**103677**	**100953**	**102068**	**98643**
Heating COP	**kW/kW**	COP_H	**2.57**	**2.92**	**2.77**	**2.63**	**2.57**	**2.54**	**2.62**	**2.91**	**2.91**	**3.02**	**2.81**	**3.04**	**2.67**	**2.89**
EVAPORATOR																
Heat Transfer to CO_2	**W**	ϕ_e	**36291**	**32154**	**35921**	**34445**	**30992**	**52790**	**55210**	**60562**	**61277**	**62508**	**62861**	**62188**	**62095**	**60335**
Cold Water Mass Flow	kg/s	m_{ew}	0.655	0.656	0.657	0.663	0.657	0.962	0.945	1.213	1.306	1.303	1.407	1.347	1.252	1.270
Heat Transfer from Cold Water	**W**	ϕ_{ew}	**30455**	**30794**	**31105**	**31096**	**30830**	**49555**	**50308**	**60469**	**56892**	**64967**	**64822**	**66584**	**59242**	**63311**
Log Mean Temperature Difference	°C	$\Delta\theta_{lm}$	16.9	17.0	17.2	17.0	16.9	16.4	15.9	16.4	17.7	16.4	17.0	16.5	17.0	16.4
Evaporator Overall Heat Transfer Coefficient	W/m²°C	U_e	403	379	398	394	374	639	678	753	683	793	767	798	729	769
Water Side Heat Transfer Coefficient	W/m²°C	hw	1496	1497	1498	1509	1499	**2023**	**1987**	**2436**	**2613**	**2579**	**2758**	**2650**	**2511**	**2527**
CO2 Side Heat Transfer Coefficient	W/m²°C	hco2	626	570	614	604	560	1119	1263	1316	1075	1387	1260	1378	1221	1334
Evaporator Heat Load	**kW**	ϕ_e	**33373**	**31474**	**33513**	**32771**	**30911**	**51172**	**52759**	**60515**	**59084**	**63737**	**63841**	**64386**	**60668**	**61823**
Cooling COP	**kW/kW**	COP_L	**1.53**	**1.87**	**1.77**	**1.63**	**1.46**	**1.48**	**1.65**	**1.85**	**1.71**	**1.94**	**1.73**	**1.94**	**1.59**	**1.81**
Overall COP	**kW/kW**	COP	**4.10**	**4.80**	**4.54**	**4.26**	**4.03**	**4.02**	**4.27**	**4.76**	**4.62**	**4.96**	**4.54**	**4.97**	**4.25**	**4.71**
RECUPERATOR																
HOT SIDE																
Heat Transfer from Hot CO_2	W	ϕ_{rH}	7023	7051	5032	3939	3015	8967	10174	11491	10274	9751	7873	8321	5525	6564
COLD SIDE																
Heat Transfer to superheat cold CO_2 vapour	W	ϕ_{rL}	11008	8212	7378	6029	4788	14733	15327	13755	12031	11173	10097	10372	9354	8886
Log Mean Temperature Difference	°C	$\Delta\theta_{lm}$	20.9	17.3	10.0	8.6	9.6	22.5	22.6	21.1	19.0	19.0	14.9	16.4	13.3	13.9
Recuperator Overall Heat Transfer Coefficient	W/m²°C	U_r	685	701	989	925	646	838	898	952	935	879	963	905	888	887
Recuperator Heat Load	**kW**	ϕ_e	9016	7632	6205	4984	3902	11850	12751	12623	11152	10462	8985	9347	7439	7725
POWER																
Motor Output/Comp. Input Power	**kW**	$\phi_{comp,i}$	**21.8**	**16.8**	**19.0**	**20.1**	**21.2**	**34.6**	**32.1**	**32.7**	**34.6**	**32.8**	**36.9**	**33.2**	**38.3**	**34.1**
COMPRESSOR																
Enthalpy Change	J/kg	ΔH_{comp}	72631	81563	96357	111319	118949	88964	82466	85635	93029	93362	100216	92875	106344	101421
Isentropic Compression Enthalpy Change	J/kg	$\Delta H_{comp,\Delta S=0}$	48261	56140	60127	62337	64817	52080	52080	56296	58020	58965	60837	61009	64768	64371
Isentropic Efficiency		$\varepsilon_{comp,\Delta S=0}$	**0.664**	**0.688**	**0.624**	**0.560**	**0.545**	**0.585**	**0.632**	**0.657**	**0.624**	**0.632**	**0.607**	**0.657**	**0.609**	**0.635**
Theoretical Volumetric Flow into Compressor	m3/s	$Q_{comp,i}'$	0.00738	0.00538	0.00514	0.00538	0.00538	0.01037	0.01037	0.01037	0.01037	0.01037	0.01037	0.01037	0.01037	0.01037
Actual Volumetric Flow into Compressor	m3/s	$Q_{comp,i}$	0.00365	0.00267	0.00257	0.00231	0.00202	0.00504	0.00525	0.00493	0.00461	0.00455	0.00427	0.00432	0.00415	0.00398
Volumetric Efficiency		$\varepsilon_{comp,V}$	**0.494**	**0.496**	**0.500**	**0.430**	**0.376**	**0.486**	**0.506**	**0.475**	**0.445**	**0.439**	**0.412**	**0.416**	**0.400**	**0.384**

RAW DATA

VARIABLE	UNITS	SYMBOL	OIL: 20°C - 65°C Hot Water; 20°C Cold Water In, Max speed						OIL: 20°C - 90°C Hot Water;11°C, 1.4 l/s (max flow) Cold Water In					OIL: 20°C - 90°C Hot Water; 20°C, 1.6 l/s (max flow), Cold Water In, max speed		
			1	4	2	6	5	3	4	2	3	1	5	1	2	3
CO_2 LINE			txfo	txfo					txfo					txfo		
High Side Pressure	Bar g		83	84	94	104	114.5	124.5	89.5	100	108.5	119	130	103	120	129
	Bar a	P_H	84	85	95	105	116	126	91	101	110	120	131	104	121	130
Low Side Pressure	Bar g		28.6	28.5	28.6	28.6	28.5	28.5	31.5	31.5	31.5	31.5	31.5	34.9	32.8	33
	Bar a	P_L	29.6	29.5	29.6	29.6	29.5	29.5	32.5	32.5	32.5	32.5	32.5	35.9	33.8	34.0
CO_2 Mass Flow	kg/s	m_{CO2}	0.339	0.340	0.315	0.298	0.265	0.257	0.297	0.219	0.188	0.187	0.174	0.433	0.362	0.341
Compressor Suction/Recuperator Cold Side Exit Temp	°C	T_{suc}	21.5	20.5	17.8	15.3	13.4	13.1	26.3	25.1	22.1	18.1	18.9	25.2	18.3	18.1
Compressor Discharge/Cooler 1 Inlet Temperature	°C	T_{dis}	125	130	130.3	141	154	158	129	133.5	142	147	158	118	141.5	141
Cooler 3 Exit/Recuperator Hot Side Inlet Temperature	°C	T_{co}	32.6	32.5	30.6	25.0	22.0	21.2	36.7	37.7	30.1	25.3	23.2	39.6	29.8	27.2
Pre-Expansion Valve/Recuperator Hot Side Exit Temp	°C	T_{TXi}	27.9	27.9	21.5	15.6	13.2	12.6	33	28.3	18.7	17.1	14	32.9	19.3	17.8
Separator/Recuperator Cold Side Inlet Temperature	°C	T_{sep}	-6.8	-6.5	-6.8	-6.5	-6.8	-6.8	-3	-3.1	-3.1	-3	-3.1	0.6	-1.8	-1.1
HOT WATER LINE																
Inlet Temperature	°C	T_{cwi}	19.7	19.7	19.7	19.7	19.7	19.7	19.9	19.9	19.9	19.9	19.9	20	20	20
Outlet Temperature	°C	T_{cwo}	64	66	72	73	71.5	69	90	90	90	90	90	90	89.5	90
Flowrate	L/s	Q_{cw}	0.460	0.444	0.439	0.441	0.442	0.434	0.225	0.194	0.196	0.200	0.205	0.334	0.378	0.371
COLD WATER LINE																
Inlet Temperature	°C	T_{ewi}	20.1	19.9	19.9	19.9	19.9	20	11.1	11.1	11.1	11.1	11.1	20.3	20.1	20.1
Outlet Temperature	°C	T_{ewo}	6.1	5.1	6.1	6.1	5.9	5.5	4.9	4.9	4.9	4.9	4.9	11.9	10.1	10.4
Flowrate	L/s	Q_{ew}	0.899	0.819	1.028	1.051	0.979	0.850	1.408	1.410	1.412	1.408	1.415	1.681	1.681	1.686
VSD/MOTOR																
VSD Output/Motor Input Real Power	kW		31.1	32.9	35.2	36.5	36.5	36.7	28.4	21.5	21.1	21.5	23.9	38.8	39.4	39.4
Motor/Compressor Speed	%		125%	125%	125%	125%	125%	125%	96%	75%	69%	70%	75%	125%	125%	125%
	RPM		1212.5	1212.5	1212.5	1212.5	1212.5	1212.5	926.4	730.1	673.1	679.5	723.8	1212.5	1212.5	1212.5

CALCULATIONS

VARIABLE	UNITS	SYMBOL	1	4	2	6	5	3	4	2	3	1	5	1	2	3
COOLERS																
Total Heat Transfer from CO2	**W**	**ϕ_c**	**87707**	**90857**	**87623**	**91266**	**86862**	**85279**	**72454**	**55474**	**54842**	**57716**	**56598**	**97308**	**104756**	**99511**
Hot Water Mass Flow	kg/s	m_{cw}	0.459	0.443	0.438	0.440	0.441	0.433	0.224	0.194	0.196	0.199	0.205	0.334	0.377	0.371
Total Heat Transfer to Hot Water	**W**	**ϕ_{cw}**	**85020**	**85779**	**95847**	**98079**	**95526**	**89356**	**65810**	**56974**	**57530**	**58534**	**60193**	**97793**	**109814**	**108630**
Overall Cooler Water Line LMTD	°C	$\Delta\theta_{lm,c}$	31.0	31.8	28.3	24.6	22.4	21.5	26.3	28.8	25.7	21.9	21.5	23.6	25.3	22.3
Cooler Overall Heat Transfer Coefficient	W/m²°C	U_c	729	716	899	1058	1134	1103	663	526	594	709	745	1102	1153	1291
Water Side Heat Transfer Coefficient	W/m²°C	hw	**5453**	**5337**	**5392**	**5427**	**5411**	**5295**	**3330**	**2967**	**2990**	**3032**	**3100**	**4578**	**5045**	**4979**

CO2 Side Heat Transfer Coefficient	W/m²°C	hco2	961	943	1286	1633	1824	1762	980	732	870	1131	1211	1890	1937	2383
Cooler Heat Load	**kW**	ϕ_c	**85020**	**85779**	**95847**	**98079**	**95526**	**89356**	**65810**	**56974**	**57530**	**58534**	**60193**	**97793**	**109814**	**108630**
Heating COP	**kW/kW**	COP_H	**2.94**	**2.81**	**2.93**	**2.89**	**2.82**	**2.62**	**2.50**	**2.85**	**2.93**	**2.93**	**2.72**	**2.71**	**3.00**	**2.97**
EVAPORATOR																
Heat Transfer to CO_2	**W**	ϕ_e	**54153**	**54903**	**57827**	**59526**	**54591**	**53525**	**42173**	**35967**	**35945**	**36746**	**35557**	**64484**	**68876**	**66522**
Cold Water Mass Flow	kg/s	m_{ew}	0.898	0.818	1.026	1.049	0.977	0.849	1.408	1.410	1.412	1.407	1.415	1.678	1.678	1.682
Heat Transfer from Cold Water	**W**	ϕ_{ew}	**52677**	**50742**	**59362**	**60666**	**57344**	**51575**	**36647**	**36701**	**36745**	**36634**	**36827**	**59019**	**70285**	**68340**
Log Mean Temperature Difference	°C	$\Delta\theta_{lm}$	19.1	18.0	19.0	18.7	18.8	18.6	10.7	10.8	10.8	10.7	10.8	15.1	16.4	15.9
Evaporator Overall Heat Transfer Coefficient	W/m²°C	U_e	573	600	632	659	607	577	753	688	688	701	685	836	868	870
Water Side Heat Transfer Coefficient	W/m²°C	hw	**1895**	**1748**	**2107**	**2144**	**2024**	**1805**	**2570**	**2573**	**2575**	**2569**	**2580**	**3226**	**3193**	**3204**
CO2 Side Heat Transfer Coefficient	W/m²°C	hco2	970	1113	1069	1136	1026	1013	1273	1096	1096	1131	1088	1329	1421	1423
Evaporator Heat Load	**kW**	ϕ_e	**53415**	**52823**	**58595**	**60096**	**55968**	**52550**	**39410**	**36334**	**36345**	**36690**	**36192**	**61751**	**69580**	**67431**
Cooling COP	**kW/kW**	COP_L	**1.85**	**1.73**	**1.79**	**1.77**	**1.65**	**1.54**	**1.50**	**1.82**	**1.85**	**1.84**	**1.63**	**1.71**	**1.90**	**1.84**
Overall COP	**kW/kW**	**COP**	**4.79**	**4.54**	**4.72**	**4.66**	**4.47**	**4.16**	**3.99**	**4.67**	**4.78**	**4.77**	**4.35**	**4.42**	**4.90**	**4.81**
RECUPERATOR																
HOT SIDE Heat Transfer from Hot CO_2	W	ϕ_{rH}	7671	7189	8731	7025	5436	5020	6467	7571	5612	3664	3639	11716	9394	7452
COLD SIDE Heat Transfer to superheat cold CO_2 vapour	W	ϕ_{rL}	13401	12820	11027	9316	7751	7431	12631	9001	6982	5922	5739	16758	11377	10268
Log Mean Temperature Difference	°C	$\Delta\theta_{lm}$	20.7	21.3	19.5	15.1	13.5	13.0	20.6	20.6	13.8	12.6	9.3	22.2	15.8	13.4
Recuperator Overall Heat Transfer Coefficient	W/m²°C	U_r	810	749	805	863	778	765	738	641	727	607	802	1023	1046	1054
Recuperator Heat Load	**kW**	ϕ_e	10536	10004	9879	8170	6593	6225	9549	8286	6297	4793	4689	14237	10386	8860
POWER																
Motor Output/Comp. Input Power	**kW**	$\phi_{comp,i}$	**28.9**	**30.6**	**32.7**	**33.9**	**33.9**	**34.1**	**26.4**	**20.0**	**19.6**	**20.0**	**22.2**	**36.1**	**36.6**	**36.6**
COMPRESSOR																
Enthalpy Change	J/kg	ΔH_{comp}	82191	89110	87199	98928	113097	114054	81306	82721	93399	100057	108660	64101	93555	88461
Isentropic Compression Enthalpy Change	J/kg	$\Delta H_{comp,\Delta S=0}$	50171	50651	55194	59373	63833	68289	49426	54890	57940	60857	66221	49152	58301	61622
Isentropic Efficiency		$\epsilon_{comp,\Delta S=0}$	**0.610**	**0.568**	**0.633**	**0.600**	**0.564**	**0.599**	**0.608**	**0.664**	**0.620**	**0.608**	**0.609**	**0.767**	**0.623**	**0.697**
Theoretical Volumetric Flow into Compressor	m3/s	$Q_{comp,i}'$	0.01037	0.01037	0.01037	0.01037	0.01037	0.01037	0.00792	0.00624	0.00576	0.00581	0.00619	0.01037	0.01037	0.01037
Actual Volumetric Flow into Compressor	m3/s	$Q_{comp,i}$	0.00519	0.00521	0.00473	0.00439	0.00387	0.00376	0.00421	0.00307	0.00258	0.00249	0.00234	0.00537	0.00461	0.00430
Volumetric Efficiency		$\epsilon_{comp,V}$	**0.501**	**0.502**	**0.456**	**0.423**	**0.374**	**0.362**	**0.531**	**0.492**	**0.448**	**0.429**	**0.377**	**0.518**	**0.444**	**0.415**